28

COMPOSITION OF FINE AND ULTRA-FINE PARTICLES AND SOURCE IDENTIFICATION BY STABLE ISOTOPE RATIOS

by

Jec-Kong Gone

M.S., Department of Nuclear Science
National Tsing-Hua University, Taiwan, 1989

SUBMITTED TO THE DEPARTMENT OF NUCLEAR ENGINEERING IN PARTIAL FULFILLMENT OF THE REQUIREMENTS FOR THE DEGREE OF DOCTOR OF PHILOSOPHY IN ~~ENVIRONMENTAL RESEARCH AND RADIOCHEMISTRY~~ NUCLEAR ENGINEERING AT THE

MASSACHUSETTS INSTITUTE OF TECHNOLOGY

JUNE 1998

Signature of Author: .....
Department of Nuclear Engineering, May 15, 1998

Certified by : .....
Ilhan Olmez
Principal Research Scientist, Nuclear Reactor Laboratory, Thesis Supervisor

Accepted by : .....
Glen R. Cass
Professor of Environmental Engineering Science, California Institute of Technology
Thesis Reader

Accepted by : .....
Kevin W. Wenzel
Assistant Professor of Nuclear Engineering, Thesis Reader

Accepted by : ....
Lawrence M. Lidsky
Chairman, Departmental Committee on Graduate Students

COMPOSITION OF FINE AND ULTRA-FINE PARTICLES AND SOURCE IDENTIFICATION BY STABLE ISOTOPE RATIOS

by

Jec-Kong Gone

Submitted to the Department of Nuclear Engineering on May 15, 1998
in Partial Fulfillment of the Requirements for the Degree of Doctor of Philosophy
in Nuclear Engineering

ABSTRACT

Fine (d_a < 2.1 μm) and ultra-fine (d_a < 0.1μm) atmosphere particulate samples collected from two sites in the United States were analyzed for elemental compositions by Instrumental Neutron Activation Analysis (INAA) at Massachusetts Institute of Technology. The eastern site samples were collected at the Great Smoky Mountain National Park from July 15 to August 25, 1995. The western site samples were collected from a rooftop in Pasadena, California over one winter month in January/February, 1996. Elemental concentrations determined by INAA for the eastern site samples were compared with results from samples (d_a <2.4 μm) collected concurrently but analyzed by other techniques. The results showed consistency between different analytical techniques. Factor Analysis (FA) and Absolute Factor Score-Multiple Linear Regression (AFS-MLR) methods were used to identify sources and their contributions to fine particulate samples at the eastern site. The results showed that the crustal contribution to fine aerosol mass was significant around July 24-26, 1995, and the coal combustion contribution peaked around August 14-18, 1995. The average contribution from crustal sources to the fine particulate mass was 7±3 % for the 2.1μm samples and 11±4 % for the 2.4 μm samples. The mass difference may be due to the different maximum size of the particles. The average contribution from combustion sources was 77±4 % for the 2.1μm samples and 90±6 % for the 2.4 μm samples. Elemental patterns were used to identify sources of ultra-fine particles. Motor vehicle emissions might be the cause of the increase in the ultra-fine particle concentration of Al and Fe at the western site.

Variations in stable isotope ratios of $^{130}Ba/^{138}Ba$, $^{121}Sb/^{123}Sb$, $^{84}Sr/^{86}Sr$ and $^{79}Br/^{81}Br$ were investigated using INAA. This technique was applied to fine particulate samples with sources identified by FA. The results showed that the $^{130}Ba/^{138}Ba$ ratio of the dust sample was 0.00151±0.00008, and the ratio was 0.00109±0.00003 for the combustion sample. This suggests that the $^{130}Ba/^{138}Ba$ ratio can be used to separate contributions from soil and combustion sources even if they have similar chemical compositions. Crustal material may have a lower $^{121}Sb/^{123}Sb$ ratio than the combustion source of fine particles. The $^{84}Sr/^{86}Sr$ and $^{79}Br/^{81}Br$ ratios also showed differences between these samples, but the differences were not greater than the statistical uncertainty of the measurements.

Thesis Supervisor: Dr. Ilhan Olmez
Title: Principal Research Scientist of Nuclear Reactor Laboratory and Nuclear Engineering

To Dad and In Memory of Mom

Acknowledgements

This work could not be done without great help from Dr. Ilhan Olmez. His constant support and friendly advice have made the research possible. His wisdom provided me the right direction for the accomplishment, and it was my great honor to work with him for the past five years. I also thank Dr. John Bernard and the MIT research reactor team for their help. Dr. Bernard not only helped me with my research, but his humor also smoothed all the odds that I faced in the past few years. I owe great thanks to the people from the Environmental Research and Radiochemistry group of the Nuclear Reactor Laboratory at Massachusetts Institute of Technology. Mrs. Jianmei Che and Dr. Michael Ames helped me to settle the experiment and running sample analysis. Their constant support made this research an excellent experience. Mr. Francis Pink, Dr. Jack Beal, and Dr. Gulen Gullu helped me with data interpretation. Their knowledge and experience gave me great inspiration for my work. I also thank Miss. Lara Hughes and Professor Glen Cass from the California Institute of Technology to provide me size-segregated CIT/MOUDI samples, and great thanks to Professor Lynn Hildemann from the Stanford University who provided me the 2.1μm MIT/SU samples. Professor Peter McMurry and his group from the University of Minnesota helped me with sample collection at the Great Smoky Mountain National Park, and I also thank him to have provided me the UMn/MOUDI samples. I appreciated Dr. Stefan Musarra, Dr. Pradeep Saxena from the Electric Power Research Institute, and Dr. Thomas Cahill from the University of California at Davis to provide me the NPS/IMPROVE data. I thank Professor Sidney Yip from the Department of Nuclear Engineering for his friendly help. His advice has made my graduate study easier at the Massachusetts Institute of Technology.

Support from friends has made my study a wonderful experience. I thank Mr. Kuo-Shen Chen, Mr. Yu-Hsuan Su, Mr. Tsu-Mu Kao, Mr. Wen-Yih Tseng, Dr. Sinan Keskin and Dr. Xudong Huang for their friendships. Mr. Juane-Long Lin and Dr. Sol-Il Su helped me with my settling. Their generosity was the best support on my first arrival.

Family is always my greatest assets. My beloved mother and uncle passed away during my graduate study, but support from my family helped me face all the odds. My father

was always there when I needed him. His spirit inspired me and his love gave me the courage to face all the challenges. My sister Jane and my brother Jimmy always gave me the best advice and helped me on everything. I could not have gone this far without their support. My *fiancée* Yuh-Mei Chen supported me all the time. Her love keeps my greatest comfort and her spirit inspires me in my life.

TABLE OF CONTENTS

LIST OF FIGURES

LIST OF TABLES

Chapter 1

INTRODUCTION

Aerosols, the suspension of solid or liquid particles in a gas, such as air, are ubiquitous in our environment. Wind-blown dust, volcanic eruptions, vegetation and, of course, human activities all contribute to the generation of aerosols and each of these sources creates aerosols of different sizes and chemical compositions. Aerosols are known to play important roles in human health, light scattering and visibility change, cloud formation and in the energy balance of the atmosphere. Human activities have increased aerosol emissions which may increase toxic metal concentrations in the atmosphere (Galloway, et al., 1982). A recent study also shows that aerosols may be important for ozone depletion in the stratosphere because aerosols can provide significant surface areas for heterogeneous chemical reactions important for halogen chemistry (Solomon, et al., 1996). The U.S. Environmental Protection Agency (EPA) recently proposed new regulations (40 CFR Part 64) covering pollutant-specific emissions monitoring of aerosols (Ellis, 1997). A thorough knowledge of the properties of aerosols is the first step to set regulations on their emissions and to protect our environment.

Aerosol sizes are usually classified in terms of their aerodynamic diameter (d_a). Aerodynamic diameter is the diameter of a unit density sphere (i.e. a water droplet, density $1 g/cm^3$) having the same aerodynamic property as the particle in question. It is convenient to think of aerosols as spherical particles which simplifies the calculations. However, except for the liquid droplets, aerosols may have many shapes. Size classification is usually done based on the particle settling velocity in the atmosphere. Particles with the same settling velocities are considered to be of the same size, regardless of their real sizes, compositions, and morphologies.

Particle size modes can be used to identify the particle's origins and the particle's chemical compositions may be important for health assessments. Whitby (1978) found that the size distribution of particles in urban atmospheric aerosols showed a trimodal distribution

with peaks around 0.015-0.04 μm, 0.15-0.5 μm, and 5-30 μm. Dodd et al. (1991) found additional size distributions depending upon the particles' sources, age, and atmospheric transformations by studying particles with d_a less than 2.5 μm from a rural site close to the Deep Creek Lake, Maryland. Particles with d_a less than 0.1 μm are called Aitken nuclei and are produced mostly from high temperature combustion processes or gas condensation (Fergusson, 1992). In this thesis, they will be referred to as ultra-fine particles.

Fine particles ($d_a < 2.5$ μm) originate mostly from the accumulation of smaller particles; coarse particles ($d_a > 2.5$ μm) are the products of a mechanical process such as erosion (Fergusson, 1992). The sizes of particles usually determine their lifetime in the atmosphere. Fine and ultra-fine particles are transported high into the troposphere and incorporated into raindrops. Wet deposition is therefore important for their removal from the atmosphere. Coarse particles, on the other hand, usually can not reach high altitude and are mainly removed by dry deposition. Gravitational settling can remove coarse particles and these particles' environmental impact is therefore more localized. In contrast, fine and ultra-fine particles may travel hundreds of miles before they are removed from the atmosphere by rain or impaction and their influence can be regional, even global.

Light scattering by particles is strongly dependent on their size and chemical composition. Visibility refers to the degree to which the atmosphere is transparent to visible light. Meteorologists use light extinction coefficients to quantify the visibility change. The light extinction coefficient is defined as the fraction of light that is reduced by scattering and absorption as it travels through a unit length of the atmosphere. It is dependent on the particle size distribution in the atmosphere (Reist, 1984). Fine particles scatter more visible light than coarse particles and have larger light extinction coefficients. The chemical composition of aerosols also affects light extinction (Ouimette et al., 1981). The extinction efficiency of elemental carbon in low humidity conditions is about three times larger than that of sulfates, nitrates, and organic carbon (Mathai, 1995) and it is about 17 times higher than that of coarse particles. Knowledge of the compositions of aerosols, especially fine and ultra-fine aerosols, is important in understanding visibility degradation.

Aerosol sizes have different human health impacts because of the geometry of the lung and the depth of penetration of these particles. Particles with an d_a less than 10 μm are

classified as inhalable particles. Coarse particles (d_a > 2.5 μm) are deposited in the nasopharyngeal region, and smaller particles (d_a < 2.5 μm) will deposit in the tracheobronchial region (Fergusson, 1990). Particles in the range of 0.1-1 μm can penetrate as far as the alveolar region. The heavy metal uptake by human blood can be very efficient for small particles. Fine particles (d_a < 2.5 μm) and sulfate may cause increased mortality in urban areas (Dockery, et al., 1993). Oberdorster et al. (1994) used TiO_2 particles of 20 nm and 250 nm diameters to study the correlation between particle size and lung injury. The result showed that the smaller particles caused a persistently high inflammatory reaction in the lungs of rats compared to the larger-size particles. This suggests that particle surface area may be more important than the total mass in regard to lung injury. Hall et al. (1992) estimated an increased risk of death of 1/10,000 in a year for the residents of the South Coast Air Basin of California and a loss of 1600 lives per year due to elevated inhalable particle mass. Oberdorster (1996) found that crystalline SiO_2 shows a different dose response for lung injury compared to other fine particles. This suggests that chemical composition also may be important for these particles. Sweet et al. (1993) found that toxic elements in d_a < 10 μm samples showed variations independent of particle mass. Chiou and Manuel (1986) found that most of Se, Te and other heavy volatile metals are in the fine aerosols, highlighting the importance of particle compositions. For especially fine and ultra-fine particles, it may be more important to base regulations on the particle's composition than total mass.

Because fine and ultra-fine particles are so important for environmental and human health issues, the first goal of this study is to determine their compositions. Instrumental Neutron Activation Analysis (INAA) is a very sensitive analytical technique that can determine more than 40 elements in a sample (Olmez, 1989; Parry, 1991). Samples are first irradiated with thermal neutrons, and then gamma rays emitted from activated nuclei are detected by High Purity Germanium (HPGe) detectors which have high energy resolutions. Because gamma rays are generated from each activated nucleus, the technique is sensitive to small amounts and can be used to measure elemental compositions down to absolute levels of a few nanograms. This analytical technique is used to determine the elemental concentrations of fine and ultra-fine particles in this study.

Compositions of fine and ultra-fine particles are also important because they can be used to identify their atmospheric sources. Atmospheric emissions from different sources have different elemental "signatures" especially with respect to their trace metal compositions (Olmez et al., 1996). Different models have been developed during the past few decades to assess source impacts in various regions. Traditional models such as dispersion models use input from emission sources and mass balance calculations to estimate impacts from suspended particulate matter and from other air pollutants. However, the physical and chemical processes in the atmosphere may change properties of aerosols. Even if dispersion models were correct, the source emission inventories upon which they rely are frequently not well known, or may change over time because of improved regulations. Receptor models, including chemical mass balances and factor analysis, have been used widely to assess impacts at a receptor site (Olmez et al., 1988, Olmez et al., 1996, Thurston and Spengler, 1985, Okamoto et al., 1990). Chemical Mass Balance models (CMB) assume that the emissions from various sources have different composition patterns and they can be separated by measuring the concentrations of many species in samples collected at a receptor site. However, CMB relies on the fact that all particles are primary and of the same composition as those released from the sources (Gordon, 1988). The CMB models are good for inactive species such as crustal elements, but they can not handle secondary species such as sulfate because sulfate is formed slowly from SO_2 gases in the atmosphere. Factor Analysis (FA), on the other hand, allows the identification and impact assessment of different sources at a receptor site without prior knowledge of the sources' characteristics. It uses statistical multi-variate methods to test for correlations among the measured species or parameters. The factors are extracted so that the first factor accounts for the largest amount of the total variance in the data. The second component accounts for the maximum amount of the remaining variance. When applied to a series of environmental samples, each factor represents a source type or region which influences the concentrations of the measured species. Back-projected wind trajectories can also be used to identify the source's location or region. The use of factor analysis is therefore extremely important in many situations for identifying the sources of a variety of environmental species and apportioning the relative

impact of these sources. FA combined with elemental concentrations determined by INAA was used to determine the source contributions of fine aerosol masses in this study.

There are, however, certain limitations to FA. In order to analyze the statistical variations among the samples, a minimum number of samples is needed (Henry, 1991). Also FA can not separate sources that fluctuate together. If emissions from more than one source are always transported together, FA will not be able to separate them because the signatures from these sources will follow the same variations. For the ultra-fine particle studies in this thesis, because the mass from ultra-fine particles was small compared to fine and coarse particles, samples were collected over periods ranging from several days to a week in order to improve the analytical results. These integrated samples smear sample variations from different sources and FA can not be used to identify their origins.

The use of Enrichment Factors (EF) can also be used to assess the crustal contribution to the observed elemental concentrations. The EF compares the elements in an aerosol to the corresponding compositions in other source materials, such as crustal components. By using a double normalization, elements from earth's crust will have EFs less than 10 due to natural variations. If an EF significantly exceeds a value of 10, it suggests sources other than single crustal material exist in the aerosol (Zoller et al., 1974; Radlein and Heumann, 1995). However, a single crustal composition EF calculation may not be correct due to elemental patterns at different size ranges (Whitby, 1978; Dodd et al., 1991). It is only used to identify sources of the fine, not ultra-fine, particles in this study.

Because FA can not always be used to identify sources of fine and, especially ultra-fine particles, different methodologies must be developed. Stable isotopes have been used to identify source contributions in different fields (Versini et al., 1997; Jackson, et al., 1996; Ingraham, et al., 1994; Steedman, 1988; Sturges and Barrie, 1989a, 1989b; Hackley et al., 1990; Macko and Ostrom, 1994). In stable isotope study, delta value (δ) is usually used to calculate the differences in stable isotope ratios. The delta value is defined as :

$$\delta = \{ (R/R_s)-1\}\times 10^3 \ (‰) \qquad (1.1)$$

where

R = isotope ratio measured in a sample, and

R_s = isotope ratio of a reference sample

Kohl et al. (1971) used the stable isotope ratio of nitrogen to determine the contributions of nitrate from fertilizer and soil in surface waters. Their idea is based on the fact that fertilizer has an $^{15}N/^{14}N$ ratio similar to atmospheric nitrogen ($\delta^{15}N$ = +3.7 ‰), but the soil nitrogen is enriched in ^{15}N ($\delta^{15}N$ = +13 ‰) because of de-nitrification. The difference is significant enough to be detected by a mass spectrometer and can be quantitatively used to estimate the contributions in surface waters. Burnett and Schaeffer (1980) used the $^{13}C/^{12}C$ ratio to identify the organic carbon from sludge disposal and marine sediment in sediment samples of the New York Bight. Their results showed that sludge is more depleted in ^{13}C ($\delta^{13}C$= -25.8 ‰) compared to the marine sediment ($\delta^{13}C$= -22 ‰). Sturges and Barrie (1987) found that the $^{206}Pb/^{207}Pb$ ratio of atmospheric particulate matter in the eastern United States (1.21~1.22) is higher than the isotopic ratio in eastern Canada (1.15). The difference was because the lead additive in gasoline had a higher $^{206}Pb/^{207}Pb$ ratio in the United States than in Canada. Sturges and Barrie applied the same idea to determine the origins of lead in aerosols at a rural site in eastern Canada and the result showed there were different contributors to the atmospheric burden, namely: Canadian automobile emissions, Canadian smelters, and eastern American sources (Sturges and Barrie, 1989a). Nriagu et al. (1991) used the stable isotope ratio of $^{34}S/^{32}S$ to identify sources for Canadian Arctic haze and found that most of the sulfur originated from Europe based on the fact that the sulfur released from the European region had a higher $^{34}S/^{32}S$ ratio than that from the local anthropogenic or biogenic emissions. Christensen et al. (1997) showed that the $^{208}Pb/^{206}Pb$ ratio from Pacific iron-manganese crusts correlates with climate change in the past and the lead isotope ratios can be used to probe climate-driven changes in ocean circulation because $^{208}Pb/^{206}Pb$ ratio and $\delta^{18}O$, which is a measure of temperature change, track each other well. These and many other findings have encouraged us to use stable isotope ratios to identify sources of fine and ultra-fine particles in the atmosphere.

Traditionally, mass spectrometry is used to determine isotopic ratios. For mass spectrometry, samples must either be digested by chemicals or ionized thermally (Cornides, 1988). The chemicals added to samples may cause contamination, and the molecular ions formed by a thermal ionization device may impact the reliability of the quantitative results. The INAA, on the other hand, does not require chemical separation or heating. Isotope concentrations are determined from gamma ray counting at specific energies. Sample handling and processing is minimal, and because gamma rays are generated from each activated nuclei, extremely small amounts of sample, such as ultra-fine particles, can be analyzed by INAA.

However, the measurement of stable isotope ratios by INAA also has certain limitations. The selected isotopes must have a large enough interaction probability (cross section) with thermal neutrons. The half-lives of the activated isotopes must be within a certain range in order to detect a sufficient number of gamma rays in reasonable time (usually within days). Gamma ray interference from other excited nuclei should be small and, if present, properly accounted for. Gamma energies should be in a certain energy region for a higher detector efficiency. Because of these restrictions, only a limited number of elements can be used for this purpose. The establishment of a new technique to identify sources of fine aerosol samples based on INAA and stable isotope ratios will be covered in the last part of this study.

Chapter 1 is a brief introduction to the research goals for the thesis. Chapter 2 covers sample collection, trace element analysis, determination of the minimum detection limits of INAA, experimental results and data comparison for fine and ultra-fine particulate samples. Chapter 3 covers source apportionment of fine and ultra-fine particles. It includes factor analysis, Absolute Factor Score – Multiple Linear Regression (AFS-MLR), enrichment factor calculation, particle size distributions, and elemental patterns. Chapter 4 shows the new technique for source apportionment of atmospheric particles by INAA and stable isotope ratios. It includes element selection, a test of the technique, and results from atmospheric samples. It is a new technique that has not been used before. Chapter 5 is a summary of this research.

Chapter 2

COMPOSITION OF FINE AND ULTRA-FINE PARTICLES

Particles in the ambient atmosphere may contain low concentrations of ionic materials, sea-salt, sulfates, natural organic substances, diluted combustion species, and soil dust. These aerosols can serve as condensation and heterogeneous reaction centers for atmospheric reactions, and over time, transformation of species between gas and particulate phases may change the compositions of the aerosols until thermodynamic equilibrium is reached. These aged fine particulates carry the elemental signatures of their origins as well as their past histories in the atmosphere. Their compositions can be used to assess source contributions at different locations.

Trace elements of fine aerosols are important for both environmental and human health issues. Elements with specific patterns can be used to identify atmospheric emission sources (Gordon, 1988; Olmez and Gordon, 1985). Trace elements such as Cd, Cu, Pb, and Zn were found to increase in the atmosphere due to human activities (Galloway, et al., 1982, Nriagu and Pacyna, 1988) and they may be potentially toxic to humans and other organisms. Knowledge of the compositions is the first step in the study of fine particle properties.

2.1 Sample Collection

Fine ($d_a < 2.5$ μm) and ultra-fine ($d_a < 0.1$ μm) particles were collected by three different aerosol samplers. These samplers use the process of filtration or impaction to segregate the particles. Impaction is the process in which particles in a flowing gas suddenly change direction due to an object placed in the airstream; those particles with sufficient inertia will strike the object and be removed from the airstream. Particles of different sizes will have different inertias and can be selectively removed by a specifically designed air gap between impacting stages and selected airflow rates (Reist, 1984).

Fine and ultra-fine particles were collected from two sites in the United States. The eastern site was located at Look Rock which is on the western edge of the Great Smokey Mountain National Park, Tennessee. Several aerosol samplers operated concurrently at this site as part of the Southeastern Aerosol and Visibility Study (SEAVS) supported by the Electric Power Research Institute (EPRI). Field sampling at this eastern site was conducted from July 15 to August 25, 1995, when several groups collected and analyzed aerosols by a wide variety of methods. The western site samples were collected over one winter month in January/February, 1996 from a rooftop in Pasadena, California as part of the ultrafine particle study at the California Institute of Technology (CIT).

Table 2.1 lists the properties of the different aerosol samplers, and Figures 2.1 to 2.3 are schematics of these samplers. The fine atmospheric particulate material obtained at the eastern site was collected by researchers from Stanford University (SU), the University of Minnesota (UMn), and the National Park Service (NPS). The SU samplers used an AIHL-design cyclone with sizecut at 2.1 μm, and 47 mm Teflon® membrane filters (Musarra and Saxena, 1996). These samples were collected from 07:00 to 19:00 on a daily basis for the duration of site operation. They were used by SU for gravimetric aerosol mass determinations at a relative humidity between 40 and 55%, and were sent to the Massachusetts Institute of Technology (MIT) after these analyses were completed (MIT/SU samples).

The UMn samples were collected using a MicroOrifice Uniform Deposit Impactor (MOUDI) sampler with a 1.8 μm inlet cyclone. The MOUDI sampler collects and separates the aerosols into seven size fractions by impacting them onto 37 mm Teflon® membrane filters (McMurry, 1996). In order to collect sufficient material for analysis from all of the impactor stages, each set of samples covered five 12 hour sampling periods (07:00 to 19:00) run over five consecutive days. The MOUDI samples were sent directly to MIT following their collection (UMn/MOUDI samples).

The aerosol samples collected by NPS used Interagency Monitoring of Protected Visual Environments (IMPROVE) samplers, which have inlet cyclones with a cutpoint of 2.4 μm (Day, et al., 1996). The IMPROVE sampler was designed for the IMPROVE/NPS network and has been operated since 1988. It has four independent modules equipped with different filters for chemical analyses. The primary filter is Teflon® and it is the one used in

this study. These samplers were also operated from 07:00 to 19:00 on a daily basis for the duration of site operation (NPS/IMPROVE samples). These samples were analyzed at the University of California, Davis and were used for data comparisons in this study.

Vapor phase mercury was found to be the major composition of mercury in the atmosphere (Ames, 1995) and it is important for health assessment. These samples were only collected at the eastern site. This was done by using a modified Anderson VOTA sampler unit which can be programmed to take four independent samples per week. The activated carbon sorbant used for vapor phase mercury collection was prepared at MIT from coconut charcoals containing 5% by weight KI_3 ($KI + I_2$). The sorbant tubes are made of acid cleaned Teflon® tubing with glass wool packing. A membrane filter in front of the sorbant is used to exclude particles. The vapor phase mercury sampler with a flow rate at 1 L/min collected four 24 hour samples per week (Ames, 1995).

An automatic dichotomous sampler for the daily collection of fine ($d_a < 2.5$ μm) and coarse ($2.5 < d_a < 10$ μm) aerosols was also installed at the eastern sampling site by MIT and operated by researchers from UMn. However, because of the partial blockage of the sampler's internal inlet nozzle, none of the data obtained from these samples was deemed to be reliable enough to be used in this study.

At the western site, size-segarated aerosol samples were collected by a 10-stage MOUDI sampler (MOUDI, MSP Corp., Model 100) (Marple, 1991) with a Teflon-coated cyclone separator in front of the inlet of each impactor. This was done in order to remove coarse particles ($d_a > 1.8$ μm) that might distort the mass distribution. The fine and ultra-fine particles were collected on stages 5-10 of the impactor over the size range of 0.056-1.8 μm. Teflon filters with a pore size of 1.0 μm (Teflo, Gelman Science) were used as substrates for stages 1-10 and a Teflon after filter with pore size 1.0 μm (Zefluor, Gelman Science) was used to collect particles less than 0.056 μm. The sampler was operated continuously for a 24-hour period and aerosol samples were collected separately at 6-day intervals from January 23 until February 17, 1996. A total of five runs was made during this period (CIT/MOUDI samples).

Table 2.1. Properties of Aerosol Samplers

Sampler	MIT/SU	UMn/MOUDI	CIT/MOUDI	NPS/IMPROVE
Type	Filtration	Impactor	Impactor	Filtration
Inlet Cyclone Sizecut	2.1 μm	1.8 μm	1.8 μm	2.4 μm
Flow Rate	28L/min	30L/min	30L/min	23L/min
Size Range	< 2.1 μm	<0.056-1.8 μm	<0.056-1.8 μm	< 2.4 μm
Humidity Control	No	No	No	No
Operation Time	12 hours daily	12 hours for 5 days	24 hours every 6 days	12 hours daily
Analytical Technique	INAA	INAA	INAA	XRF, PIXE Ion chromatography

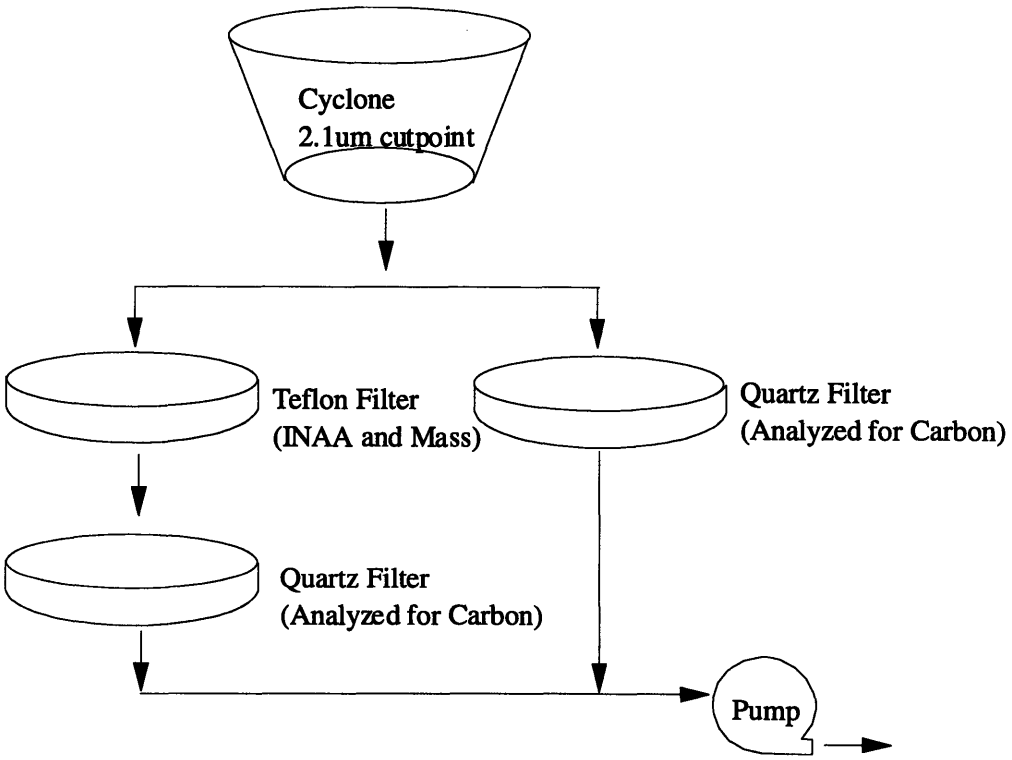

Figure 2.1. Structure of Stanford University AIHL-Designed Sampler (Musarra and Saxena, 1996)

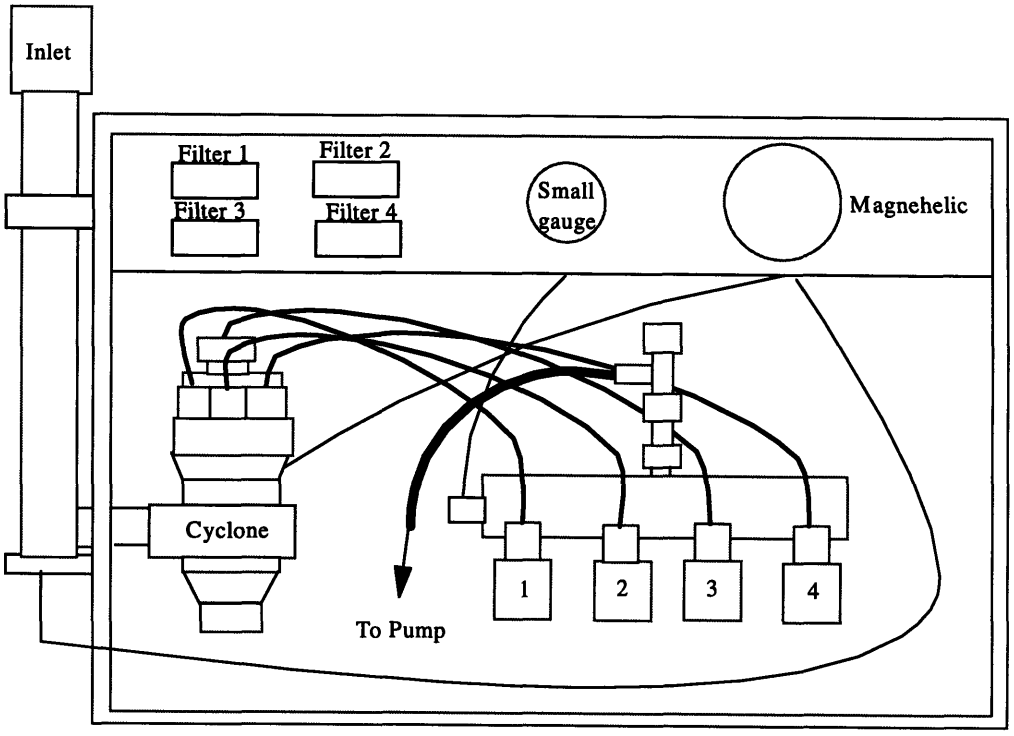

Figure 2.2. Structure of NPS/IMPROVE Sampler (Day, et al., 1996).

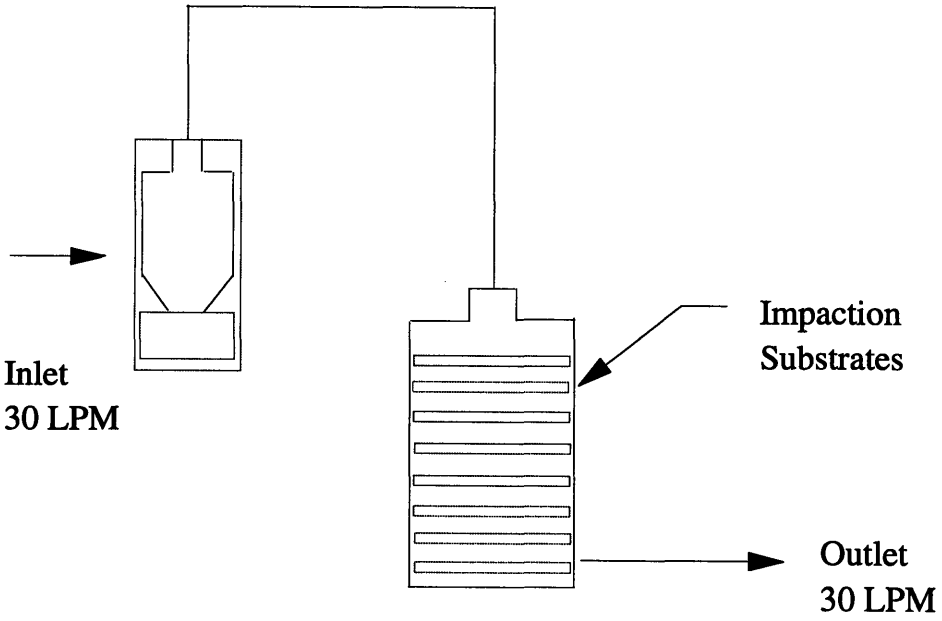

Figure 2.3. Structure of CIT/MOUDI Impactor Sampler (Hughes, et al, 1998).

2.2 Trace Element Analysis

All particulate samples except the NPS/IMPROVE samples were analyzed for elemental concentrations by Instrumental Neutron Activation Analysis (INAA) at MIT. INAA is one of the most simple, sensitive, and selective techniques for elemental analysis. When a sample material is irradiated with thermal neutrons, some of the nuclei within the material absorb neutrons and became unstable radionuclides which may subsequently give off some of their excess energy in the form of one or more gamma rays as they decay to a stable state. The activation equation is given below:

$$A = \sigma N \phi (1-e^{-\lambda t_i}) e^{-\lambda t_c} \xi \Upsilon \qquad (2.1)$$

where

A = The induced radioactivity measured by detector (counts per second),
σ = Activation cross section, in barns (barn = 10^{-24} cm^2),
N = Number of target nuclei present,
ϕ = Thermal neutron flux, neutrons/cm^2 s,
λ = Decay constant,
t_i = Irradiation time,
t_c = Cooling time,
ξ = Absolute detector efficiency, and
Υ = Branching ratio of specific energy gamma ray from activated nucleus.

Because each radionuclide emits gamma rays at characteristic energies, the number of original nuclei can be quantified by measuring the intensity of these gamma rays. The extremely high energy resolution which can be achieved using High Purity Germanium (HPGe) gamma ray detectors, allows up to 45 elements to be quantified in a single sample without the need for chemical separations or extractions. The elemental concentrations can be determined from measurements of the gamma intensities and the parameters of the neutron irradiation. However, more often a standard material of known elemental concentrations is irradiated under identical conditions as the samples, and the unknown concentrations of the sample are then determined by comparing the number of gamma rays emitted by the sample

with those emitted by the standard. This reduces the impact of the uncertainties associated with both the measurement and the irradiation parameters.

The atmospheric particulate material collected by the MIT/SU, UMn/MOUDI and CIT/MOUDI samples were analyzed using the same procedures and with equipment similar to that described by Olmez (1989). Forty-two MIT/SU, 81 UMn/MOUDI, and 39 CIT/MOUDI samples were analyzed. Filters from the same batch (some of which remained in the lab and some which were sent to the field) were also analyzed so that corrections could be made for the elemental content of the filter material itself. Upon receiving the filters at MIT, they were unpacked, examined for damage, and cut from their plastic support rings using a stainless steel scalpel in a class 100 laminar flow clean hood. The filters were then folded with the collection surface on the inside, and placed into small acid-cleaned polyethylene bags. For the CIT/MOUDI samples, only half of the filters were mailed to MIT for elemental analysis.

Irradiations were performed at the MIT Research Reactor (MITR-II) with a thermal neutron flux of 8×10^{12} n/cm^{2}s. Each of the particulate samples was first irradiated for 10 minutes, placed in a clean, un-irradiated polyethylene bag, and then transferred to a separate room for gamma ray counting. The emitted gamma rays were counted first for 7 minutes to observe radioisotopes with very short half-lives (the shortest being 2.2 minutes for Al-28) and then for 30 minutes to observe radioisotopes with somewhat longer half-lives (up to 15 hours for Na-24). The samples were then repackaged in small acid-cleaned polyethylene vials, irradiated again for 12 hours, and allowed to decay for 2-3 days. Their gamma spectra were then counted for 8 to 12 hours to observe radioisotopes with long half-lives (up to 12 years for Eu-152). Table 2.2 lists the half-life, gamma ray energy, and counting group of each element determined by INAA.

The vapor phase mercury samples (which were collected on charcoal sorbants) were irradiated for six hours, allowed to decay for about six days, and then counted for about eight hours each.

Standard reference materials were obtained from the National Institute of Standards and Technology (NIST). The standards used were: Coal Fly Ash (SRM1633), Mercury in Tennessee River Sediments (SRM8408), and Orchard Leaves (SRM1571). These were

irradiated either at the same time as the samples (for the 12 hour irradiations) or on the same day and under identical conditions as the samples (for the short runs). These materials were also used for quality control by performing comparisons both the between different analyses and with the NIST certified concentration values.

All of the gamma ray spectroscopy was performed using four high purity germanium (HPGe) detectors coupled to the Genie software system operating on a VAX 3100 workstation. Elemental concentrations were determined using custom-made, interactive peak fitting and analysis software (all nuclear hardware and software from Canberra Industries, Inc. Meriden, CT).

The NPS/IMPROVE samples were analyzed for elemental concentrations by Proton Induced X-ray Emission (PIXE) and X-Ray Fluorescence (XRF). Sulfate and nitrite concentrations were determined by ion chromatography from samples collected concurrently (Day, et al., 1996). Ammonium ion concentration was measured by colorimetric analysis. Samples were weighed at a controlled relative humidity between 31 and 45% at the University of California, Davis (UCD). Analytical results provided by the NPS were used both independently and in combination with results obtained by MIT in receptor modeling as discussed in the next chapter.

Table 2.2. The half-life, gamma energy and counting group of elements determined by INAA

Element	Half-Life	Gamma Energy (keV)	Counting Group
Na	15.02 h	1368.5	Short 2
Mg	9.46 m	843.8	Short 1
Al	2.24 m	1779	Short 1
Cl	37.24 m	1642	Short 2
K	12.36 h	1524.7	Short 2
Sc	83.83 d	889.3	Long 2
Ti	5.76 m	320.1	Short 1
V	3.75 m	1434.2	Short 1
Cr	27.7 d	320	Long 2
Mn	2.58 h	846.6	Short 2
Fe	44.5 d	1291.6	Long 2
Co	5.27 y	1332.5	Long 2
Zn	243.9 d	1115.5	Long 2
Ga	14.1 h	834	Short 2
As	26.32 h	559.5	Long 1
Se	119.77 d	264.5	Long 2
Br	35.3 h	554.3	Long 1
Rb	18.66 d	1076.6	Long 2
Sr	2.81 h	388.4	Short 2
Zr	64.02 d	756.7	Long 2
Mo	66.02 h	140.5	Long 1
Cd	53.46 h	336	Long 1
In	54.15 m	417	Short 2
Sb	60.2 d	1691	Long 2
Cs	2.06 y	795.8	Long 2
Ba	84.63 m	165.8	Short 2
La	40.27 h	1596	Long 1
Ce	32.5 d	145.4	Long 2
Nd	10.98 d	91	Long 1
Sm	46.7 h	103.2	Long 1
Eu	13.33 y	1407.9	Long 2
Tb	72.3 d	298.6	Long 2
Yb	4.19 d	282.5	Long 1
Lu	6.71 d	208.4	Long 1
Hf	42.39 d	482.2	Long 2
Ta	114.5 d	1221.5	Long 2
Au	2.7 d	411.8	Long 1
Hg	64.1 h	77	Long 1
Th	27 d	311.9	Long 2
U	2.36 d	106.4	Long 1

2.3 Detection Limits of INAA for Different Elements

The minimum detection limits (MDL) for individual elements are calculated by modifying the approach used by Jaklevic and Walter (1977) for X-ray fluorescence. They are determined for typical atmospheric samples and include the effects from other elements present in the samples and filters. A high concentration of a single element may result an elevated background level in the rest of the spectra and thus result in a decreased signal-to-noise ratio. This results in a higher detection limit for that sample for the rest of the elements. The equation used in this calculation is:

$$C = 3.29 \times \frac{(\frac{R_b}{t})^{1/2}}{S} \qquad (2.2)$$

where

C = minimum detection limit (ng),
R_b = counts per second of background under the photopeak used,
t = counting time (seconds) of spectrum used for determine C, and
S = sensitivity (counts per second per ng)

The MDL was then converted from ng to ng/m^3 based on the total air volume represented each sample.

The MDL, average concentrations, and standard deviations of MIT/SU 2.1 μm data are listed in Table 2.3. As shown in this table, the average elemental concentrations of MIT/SU samples are higher than the MDL of INAA. The UMn/MOUDI and CIT/MOUDI samples are not included in Table 2.3 because they have different average concentrations at different size ranges, which will be shown in a later section.

Crustal elements, which in many cases have standard deviations larger than their average values, had much greater variations in their concentration during the sampling period due to a dust event. More detailed statistical information for the measured concentrations are given in the next chapter.

Table 2.3. Minimum Detection Limit (MLD), average elemental concentrations and standard deviations of MIT/SU 2.1 μm samples

Element	MDL (ng/m^3)	Average Concentration and Standard Deviations (ng/m^3)
Na	0.056	65 ± 43
Mg	10	50 ± 34
Al	3.3	139 ± 205
Cl	1.7	21 ± 28
K	2.1	64 ± 69
Sc	0.00051	0.022 ± 0.029
Ti	2.9	16 ± 13
V	0.14	0.48 ± 0.39
Cr	0.18	0.83 ± 0.63
Mn	0.19	1.5 ± 1.7
Fe	8.8	93 ± 100
Zn	0.79	11 ± 11
Ga	0.02	0.30 ± 0.34
As	0.014	0.31 ± 0.19
Se	0.0051	0.88 ± 0.81
Br	0.025	0.82 ± 0.87
Rb	0.37	0.45 ± 0.12
Sr	1.8	2.4 ± 1.5
Mo	0.051	0.13 ± 0.15
Cd	0.037	0.094 ± 0.068
In	0.001	0.0017 ± 0.0011
Sb	0.026	0.33 ± 0.26
Cs	0.004	0.032 ± 0.024
Ba	1.5	4.0 ± 2.2
La	0.006	0.11 ± 0.15
Ce	0.031	0.22 ± 0.33
Nd	0.23	0.32 ± 0.18
Sm	0.00042	0.012 ± 0.02
Eu	0.0035	0.0094 ± 0.0069
Tb	0.002	0.0061 ± 0.0054
Yb	0.0025	0.012 ± 0.007
Lu	0.001	0.0019 ± 0.0011
Ta	0.014	0.054 ± 0.016
Au	0.00051	0.0053 ± 0.0034
Hg	0.005	0.035 ± 0.032
Th	0.0051	0.049 ± 0.037
U	0.0074	0.018 ± 0.018

2.4 Experimental Results

Trace element concentrations in fine and ultra-fine aerosols are important because they can be used to identify specific emission sources, and additionally some of these substances are hazardous air pollutants as defined by the Clean Air Act. Ultra-fine particles may be present in great numbers even if they only contribute to a small portion of the total mass of fine aerosols. Their compositions should therefore be identified in order to assess their potential health impacts (Hughes, et al., 1998).

A summary of the elemental concentrations for the 2.1 μm Stanford samples (MIT/SU) is given in Table 2.4. The full data set for these samples is given in Appendix A beginning on page 126. During the six-week sampling period, different events such as a dust episode, a hurricane influenced period, and a high pollution period were observed at the site which in turn caused broad variation of elemental concentrations. The dust event was observed from July 23 to July 26,1995; and a hurricane influenced the sampling site between August 2 and August 5. A pollution episode was observed from August 14 to August 18 associated with elevated concentration of sulfates. As expected, concentrations of crustal elements such as Al, Sc, Ti, Mn, Fe, and the Rare Earth Elements (REE) were high during the dust episode, and lower during the hurricane period because they were mostly washed out by rain. Elements released mostly from human activities such as As, Se, Br and Sb were higher during the pollution episode and were lower after the hurricane when the air was clean. Figures 2.4 and 2.5 show the time series distribution of selected elements.

Tables 2.5 and 2.6 show the average and standard deviations of size-fractionated UMn/MOUDI and CIT/MOUDI samples. The full data set for these samples is given in Appendix A beginning on page 137. The fraction size listed in the table is the lower limit of the particle diameter which was included in that fraction based on a criterion that 50% of particles at that size be in the next larger fraction. The fact that some of the elements have a standard deviation larger than their average value indicates a wide variation for that element's measured concentrations among the sample set. Data with no standard deviation listed are from a single measurement. The UMn/MOUDI sampler was attached to an inlet cyclone which removed coarse particles (John and Reischl, 1980) and it may have changed the

collecting efficiencies at the larger sizes. Because of limited knowledge of collection efficiencies of particles greater than 1.8 μm, only particles with an d_a less than 1.8 μm are included in Table 2.5. In the CIT/MOUDI samples, Zefluor filters were used to collect particles less than 0.056 μm. However, following the long irradiations, filter materials became brittle and some parts of them were not recovered. These samples are not included in Table 2.6.

Elements formed primarily by high-temperature anthropogenic activities, and as secondary aerosols such as As, Br, Cr, Sb, and Se show a maximum concentration at sub-micron sizes as shown in the UMn/MOUDI samples. Elements primarily formed by natural mechanical processes and from crustal materials such as Al, Fe, La, Mg, Mn, Na, Sc, Sm, and Ti have maximum concentrations at sizes larger than 1μm, and thus only the lower tail of their size distribution is seen in this data. The same trend was also found in CIT/MOUDI samples. Table 2.7 shows the analytical result of NPS/IMPROVE samples. These data are compared with the MIT/SU samples in the next section of this thesis.

Four 24-hour vapor phase Hg samples were collected during each week of the field operation at the eastern site. Atmospheric vapor and particulate phase Hg concentrations measured in this study compared well with values reported in the literature (Table 2.8). Because vapor phase Hg has an atmospheric lifetime of about one year, it is well mixed hemispherically. Therefore, its atmospheric concentrations do not vary as greatly as compared with the particulate phase, which has a lifetime on the order of several days. The average vapor phase concentration for the sampling period was 1.8 ng/m^3 with a standard deviation of 0.6 ng/m^3. As has been found previously (Olmez et al., 1996), there was essentially no correlation between the vapor and particulate phase measurements (r^2 =0.077), and the vapor phase comprises the vast majority (98%) of the total atmospheric burden. The full data set for these samples is given in Appendix A on page 171.

Table 2.4. Summary statistics of MIT/SU 2.1 μm samples (ng/m^3)

Element	N	Mean	Median	Geometric mean	σ	Minimum	Maximum	% Observed
Na	42	65	59	51	43	8.2	210	100
Mg	29	50	41	41	34	12	130	69
Al	38	139	63	65	205	1.1	920	90
Cl	25	21	8.0	8.8	28	0.2	110	60
K	28	64	39	41	69	7.7	320	67
Sc	42	0.022	0.0093	0.012	0.029	0.0027	0.14	100
Ti	32	16	12	12	13	3.7	61	76
V	40	0.49	0.41	0.36	0.39	0.012	1.9	95
Cr	40	0.83	0.73	0.69	0.63	0.27	3.7	95
Mn	42	1.5	1.0	1.0	1.7	0.30	8.5	100
Fe	42	93	55	64	100	8.0	510	100
Co	42	0.15	0.13	0.12	0.10	0.018	0.56	100
Zn	42	11	8.0	6.0	11	0.2	42	100
Ga	6	0.30	0.19	0.20	0.34	0.056	0.98	14
As	42	0.30	0.29	0.25	0.19	0.054	0.77	100
Se	40	0.88	0.62	0.60	0.81	0.068	3.52	95
Br	41	0.82	0.44	0.51	0.87	0.086	3.90	98
Rb	3	0.45	0.44	0.44	0.16	0.33	0.56	7
Sr	11	2.4	2.0	1.9	1.5	0.37	5.6	26
Mo	16	0.13	0.099	0.10	0.15	0.041	0.67	38
Cd	24	0.094	0.075	0.073	0.068	0.011	0.29	57
In	22	0.0017	0.0017	0.0014	0.0011	0.00033	0.0036	52
Sb	38	0.33	0.24	0.25	0.26	0.020	1.37	90
Cs	20	0.032	0.029	0.023	0.024	0.0033	0.082	48
Ba	23	4.0	3.7	3.5	2.2	1.2	8.8	55
La	24	0.11	0.064	0.046	0.15	0.001	0.64	57
Ce	19	0.22	0.090	0.093	0.33	0.011	1.30	45
Nd	15	0.32	0.33	0.28	0.18	0.11	0.68	36
Sm	42	0.012	0.0043	0.0060	0.018	0.0006	0.089	100
Eu	23	0.009	0.0077	0.0070	0.0069	0.0011	0.027	55
Tb	13	0.006	0.0046	0.0047	0.0054	0.0009	0.022	31
Yb	23	0.011	0.011	0.010	0.0073	0.0040	0.031	55
Lu	10	0.0019	0.0021	0.0015	0.0011	0.00033	0.0038	24
Hf	6	0.0090	0.0073	0.0080	0.0051	0.0044	0.019	14
Ta	5	0.054	0.050	0.052	0.016	0.035	0.071	12
Au	10	0.0053	0.0055	0.0038	0.0034	0.00033	0.011	24
Hg	37	0.035	0.025	0.026	0.032	0.0077	0.17	88
Th	2	0.049	0.049	0.042	0.037	0.023	0.076	5
U	8	0.018	0.013	0.013	0.018	0.0058	0.060	19

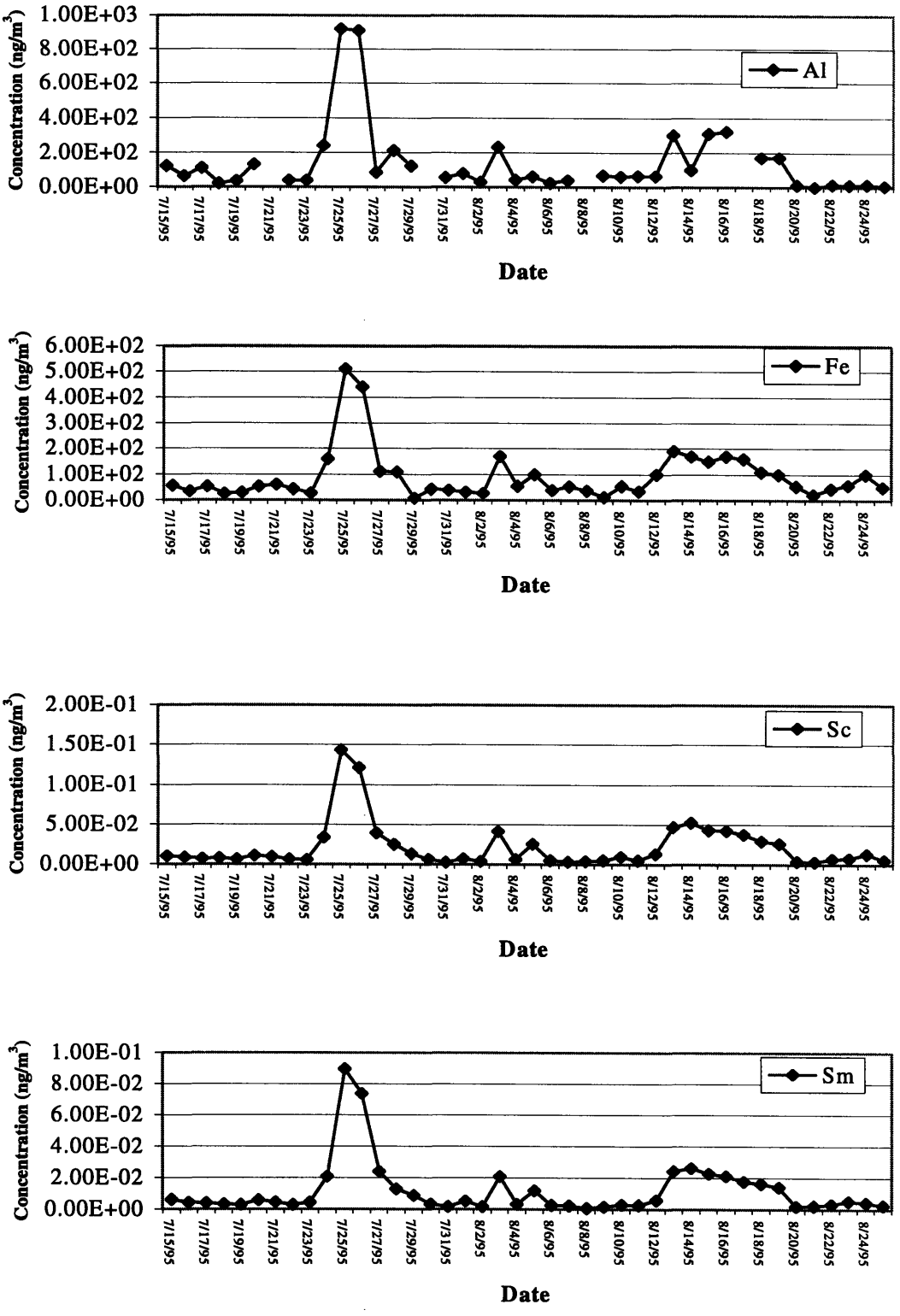

Figure 2.4. MIT/SU 2.1 μm samples time series plots of crustal elements

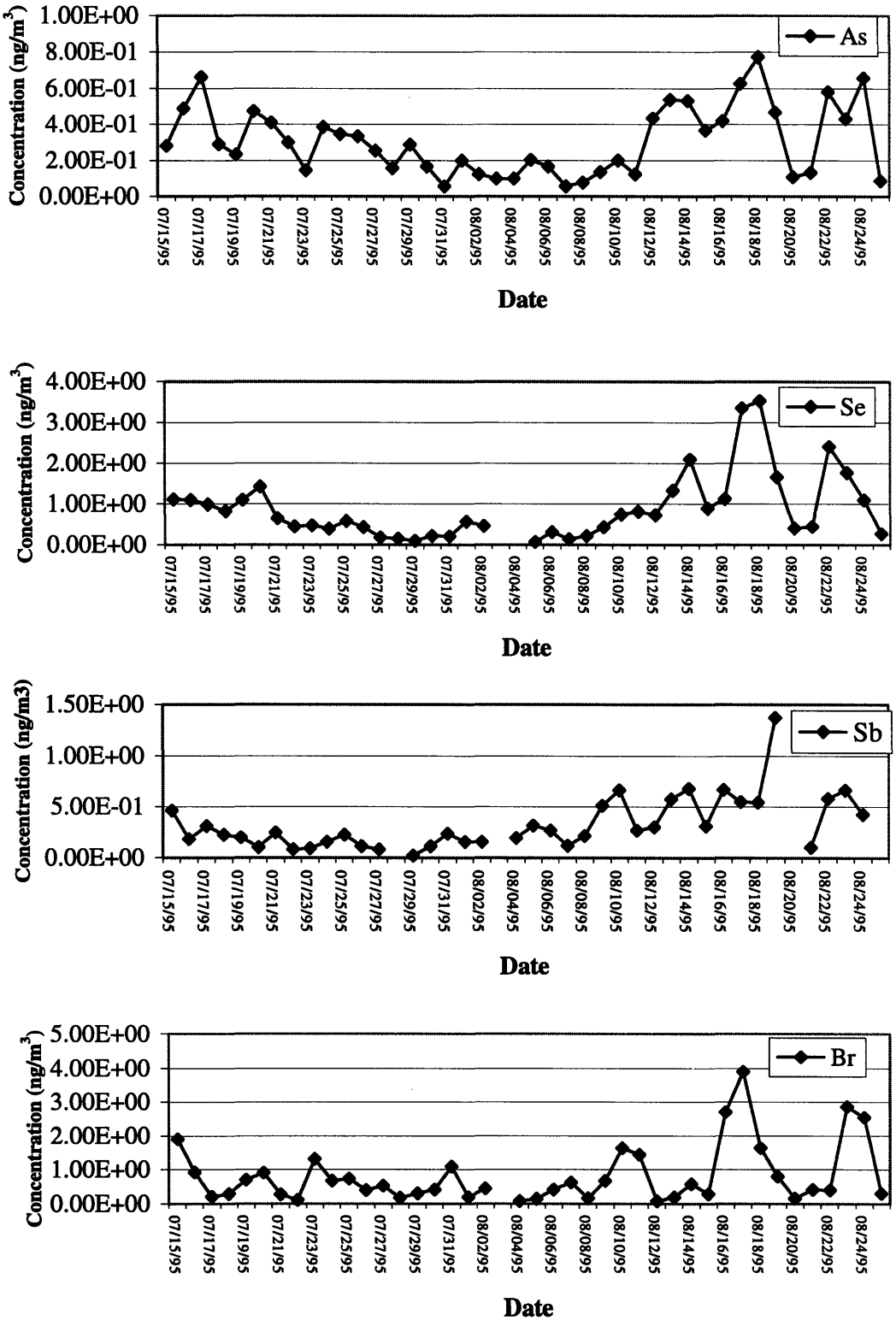

Figure 2.5. MIT/SU 2.1 μm samples time series plots of selected elements.

Table 2.5. Average elemental concentrations (ng/m^3) and standard deviations among the sample sets for each UMn/MOUDI size fraction.

Size (μm)	< 0.056	0.056	0.098	0.175	0.32	0.56	1
Na	0.57 ± 0.53	0.46 ± 0.40	0.54 ± 0.45	2.2 ± 1.0	3.5 ± 1.4	5.7 ± 2.1	22 ± 10
Mg	0.46 ± 0.39	0.70 ± 0.42	0.60 ± 0.54	0.87 ± 0.44	1.8 ± 2.4	3.4 ± 1.8	12 ± 5
Al	0.91 ± 1.01	1.1 ± 0.7	2.8 ± 5.1	13 ± 31	2.2 ± 2.3	19 ± 24	53 ± 46
Cl	0.39 ± 0.34	0.46 ± 0.19	0.49 ± 0.49	0.65 ± 0.68	0.73 ± 0.95	0.44 ± 0.31	1.6 ± 2.6
K	1.0 ± 0.3	1.1 ± 0.6	2.5 ± 0.9	7.2 ± 2.8	11 ± 5	11 ± 5	15 ± 10
Sc			0.00005	0.00008 ± 0.00009	0.0003 ± 0.0004	0.0018 ± 0.0029	0.0089 ± 0.0092
Ti	0.03	0.38	0.19 ± 0.22	0.22 ± 0.15	0.64 ± 0.20	0.82 ± 1.01	3.0 ± 2.9
V	0.032 ± 0.027	0.005	0.021	0.057 ± 0.082	0.12 ± 0.06	0.11 ± 0.06	0.10 ± 0.08
Cr	0.8 ± 1.1	0.30 ± 0.10	0.08 ± 0.10	0.23 ± 0.32	0.23 ± 0.41	0.39 ± 0.52	0.18 ± 0.16
Mn	0.10 ± 0.13	0.021 ± 0.020	0.007 ± 0.008	0.039 ± 0.037	0.11 ± 0.10	0.27 ± 0.16	0.59 ± 0.42
Fe	4.1 ± 5.0	0.92	0.78 ± 0.28	2.8 ± 1.0	2.8 ± 3.5	9.5 ± 10.0	28 ± 26
Zn	0.53 ± 0.55	0.22 ± 0.17	0.09 ± 0.09	0.55 ± 0.35	0.90 ± 0.56	1.7 ± 2.3	0.83 ± 0.47
As	0.0006	0.0012 ± 0.0008	0.0079 ± 0.0053	0.046 ± 0.015	0.089 ± 0.040	0.096 ± 0.064	0.047 ± 0.029
Se	0.0010	0.0062 ± 0.0044	0.0056 ± 0.0046	0.055 ± 0.042	0.18 ± 0.10	0.27 ± 0.22	0.18 ± 0.18
Br		0.0017	0.014 ± 0.012	0.13 ± 0.08	0.37 ± 0.23	0.55 ± 0.46	0.13 ± 0.09
Mo	0.010 ± 0.008	0.0036 ± 0.0021	0.0034 ± 0.0014	0.013 ± 0.008	0.016 ± 0.008	0.015 ± 0.009	0.013 ± 0.006
Cd	0.0004	0.0068 ± 0.0039	0.0028 ± 0.0007	0.005 ± 0.003	0.011 ± 0.013	0.007 ± 0.007	0.008 ± 0.009
In	0.00013 ± 0.00002	0.00012 ± 0.00005	0.00015 ± 0.00006	0.00027 ± 0.00006	0.00034 ± 0.00020	0.00057 ± 0.00048	0.00063 ± 0.00038
Sb	0.05 ± 0.03	0.06 ± 0.05	0.06 ± 0.04	0.09 ± 0.02	0.13 ± 0.07	0.13 ± 0.08	0.11 ± 0.06
Cs	0.0025 ± 0.0008	0.0031 ± 0.0025	0.0031 ± 0.0018	0.0026 ± 0.0009	0.0035 ± 0.0015	0.0047 ± 0.0028	0.0065 ± 0.0035
Ba	0.28 ± 0.30	0.19 ± 0.22	0.13 ± 0.14	0.18 ± 0.12	0.20 ± 0.16	0.24 ± 0.16	0.76 ± 0.44
La	0.00028 ± 0.00014	0.00033 ± 0.00027	0.00045 ± 0.00023	0.00076 ± 0.00077	0.0015 ± 0.0015	0.008 ± 0.012	0.038 ± 0.037
Nd	0.02 ± 0.01	0.02 ± 0.02	0.02 ± 0.01	0.05 ± 0.03	0.10 ± 0.11	0.20 ± 0.25	0.043 ± 0.031
Sm	0.00005 ± 0.00003	0.00004 ± 0.00003	0.00004 ± 0.00003	0.00008 ± 0.00007	0.00019 ± 0.00021	0.0011 ± 0.0018	0.0049 ± 0.0053
Eu	0.0011 ± 0.0008	0.0009 ± 0.0005	0.0008 ± 0.0006	0.0008 ± 0.0002	0.0010 ± 0.0003	0.0011 ± 0.0010	0.0020 ± 0.0011
Au	0.00008 ± 0.00007	0.00029 ± 0.00080	0.00008 ± 0.00010	0.00008 ± 0.00007	0.00008 ± 0.00008	0.00023 ± 0.00050	0.00018 ± 0.00026
Hg	0.0010 ± 0.0003	0.0007 ± 0.0004	0.0013 ± 0.0010	0.0012 ± 0.0005	0.0014 ± 0.0007	0.0012 ± 0.0009	0.0022 ± 0.0009
U	0.00039	0.00025		0.00059 ± 0.00017	0.00091 ± 0.00088	0.00087 ± 0.00007	0.00066 ± 0.00032

Table 2.6. Average elemental concentrations (ng/m^3) and standard deviations among the sample sets for each CIT/MOUDI size fraction.

Size (μm)	0.056	0.097	0.18	0.32	0.56	1
Na	1.1 ± 0.7	3.8 ± 1.6	7.4 ± 3.2	8.9 ± 1.8	15 ± 9	76 ± 68
Al	13 ± 10	3.6 ± 2.9	3.5 ± 3.0	2.9 ± 1.0	11 ± 13	22 ± 17
Cl	0.6 ± 0.3	1.5 ± 0.9	3.2 ± 3.5	9.0 ± 5.1	22 ± 18	11 ± 12
Sc	0.0025 ± 0.0026	0.0006	0.0020 ± 0.0018	0.0007 ± 0.0005	0.0028 ± 0.0014	0.0029 ± 0.0019
V	0.05	0.20 ± 0.17	0.90 ± 0.68	2.0 ± 1.5	1.5 ± 1.6	0.54 ± 0.69
Mn	0.12 ± 0.13	0.37 ± 0.30	0.34 ± 0.24	1.1 ± 0.85	1.0 ± 0.69	0.80 ± 0.19
Fe	51 ± 41	23 ± 21	26 ± 23	33 ± 21	36 ± 23	65 ± 32
Zn	3.0 ± 3.7	1.9 ± 2.5	3.1 ± 3.3	5.8 ± 6.6	5.8 ± 4.4	3.6 ± 1.5
As	0.009 ± 0.005	0.019 ± 0.009	0.035 ± 0.027	0.035 ± 0.018	0.016 ± 0.015	0.014 ± 0.008
Se	0.005	0.10 ± 0.15	0.08 ± 0.14	0.24 ± 0.22	0.27 ± 0.33	0.13 ± 0.12
Br	0.014 ± 0.008	0.21 ± 0.13	0.48 ± 0.38	0.49 ± 0.22	0.48 ± 0.45	0.08 ± 0.08
Cd	0.011 ± 0.005	0.01 ± 0.02	0.04 ± 0.03	0.05 ± 0.05	0.02 ± 0.02	0.05 ± 0.06
Sb	0.043 ± 0.045	0.14 ± 0.06	0.26 ± 0.09	0.36 ± 0.11	0.46 ± 0.14	0.49 ± 0.13
Ba	2.4	1.3 ± 0.3	3.0 ± 0.7	3.6	3.4 ± 1.9	4.9 ± 1.3
La	0.007 ± 0.009	0.0035 ± 0.0025	0.018 ± 0.015	0.042 ± 0.049	0.048 ± 0.024	0.106 ± 0.076
Ce	0.015 ± 0.002		0.04 ± 0.02	0.08 ± 0.08	0.08 ± 0.05	0.07 ± 0.04
Sm	0.0009 ± 0.0011	0.0003 ± 0.0002	0.0008 ± 0.0006	0.0006 ± 0.0002	0.0011 ± 0.0006	0.0035 ± 0.0022
Au*	0.10 ± 0.07	0.21 ± 0.18	0.36 ± 0.23	0.52 ± 0.26	0.51 ± 0.25	0.64 ± 0.36

* pg/m^3

Table 2.7. Summary statistics of NPS/IMPROVE 2.4 μm samples (ng/m^3) (n=41).

Element	N	Average	σ	Median	Geometric mean	Min	Max	% Observed
Al	32	210	220	110	150	40	970	78
Si	39	380	420	220	260	97	1960	95
S	41	3200	2800	1900	2300	380	12400	100
K	41	82	37	76	76	30	210	100
Ca	39	62	46	52	49	10	210	95
Fe	41	80	99	40	47	7.2	460	100
Cu	40	2.1	2.0	1.5	1.6	0.5	10.6	98
Zn	41	6	3.7	5.5	5.1	1.2	20	100
Pb	38	2.9	1.2	2.5	2.6	1.1	5.3	93
Se	36	1.5	1.2	0.99	1.1	0.13	5.8	88
Br	41	2.0	0.8	1.9	1.8	0.5	4.5	100
SO_4	41	9700	9100	5200	6500	1100	43000	100
NH_4	41	1800	1350	1200	1300	61	4980	100

Table 2.8. Average vapor and particulate phase atmospheric mercury concentrations.

Location	Vapor-phase (ng/m^3)	Particulate (pg/m^3)	Reference
North Pacific	1.77	< 2	Fitzgerald et al. 1991
Wisconsin	1.57	22	Fitzgerald et al. 1991
Tennessee	2.15	30	EPRI Report 1994
Nordic	2.5 – 2.8	60	Iverfeldt, 1991
Florida	1.64	1.5 – 8	Landing et al., 1994
New York	2.2 – 2.6	37 – 62	Olmez et al., 1996
Tennessee	1.8	35	This study

2.5. Data Comparison

In order to assess the consistency of the data to be used for further interpretation, a comparison was made of the elemental concentrations as measured by INAA for the UMn/MOUDI and MIT/SU samples and those concentrations measured by XRF and PIXE for the NPS/IMPROVE samples. Some differences were to be expected because of the different inlet cyclones used on these samplers, with the UMn/MOUDI cyclone having a sizecut at 1.8 μm, MIT/SU at 2.1 μm, and NPS/IMPROVE at 2.4 μm. Because the UMn/MOUDI samples covered five days, the MIT/SU and NPS/IMPROVE measurements were averaged over the same period as the UMn/MOUDI samples in order to make the comparison. Also, the measurements for the MOUDI samples needed to be summed over all of the size fractions. Figure 2.6 shows the results of these comparisons for crustal elements, while Figure 2.7 shows elements mostly associated with human activities. Because crustal element concentrations peak at larger sizes, the differences in inlet sizecut may cause greater differences in the final measurements for these elements. As expected, the UMn/MOUDI samples, which have the smallest inlet sizecut, show the smallest average concentrations among them. Samples from NPS with the largest inlet sizecut showed the largest average concentrations.

Potassium concentrations are not consistent between the UMn/MOUDI and MIT/SU results. The detection of K is relatively poor using INAA, and fluctuations from the different measurements may have caused the observed shifts. Figure 2.7 compares other elements from different origins. Selenium from NPS/IMPROVE measurements was the highest of all. In a previous study (Olmez, 1988), the Se concentrations as measured by XRF were found to be higher than those measurements by INAA in a number of samples. Bromine is lower in MIT/SU than in the UMn/MOUDI samples. Because Br is known to be easily lost to volatilization and because the MIT/SU samples were stored for more than a year before analysis, Br may have been lost during the storage before it was analyzed by INAA. Figures 2.8 and 2.9 show the time series plots of selected elements from the MIT/SU and NPS/IMPROVE samples. Agreement between the two data sets is very good for the crustal elements and for many other elements which have relatively

high concentrations. However, for some elements which are present at levels of a few ng/m^3 and below, significant differences can be found between the two data sets.

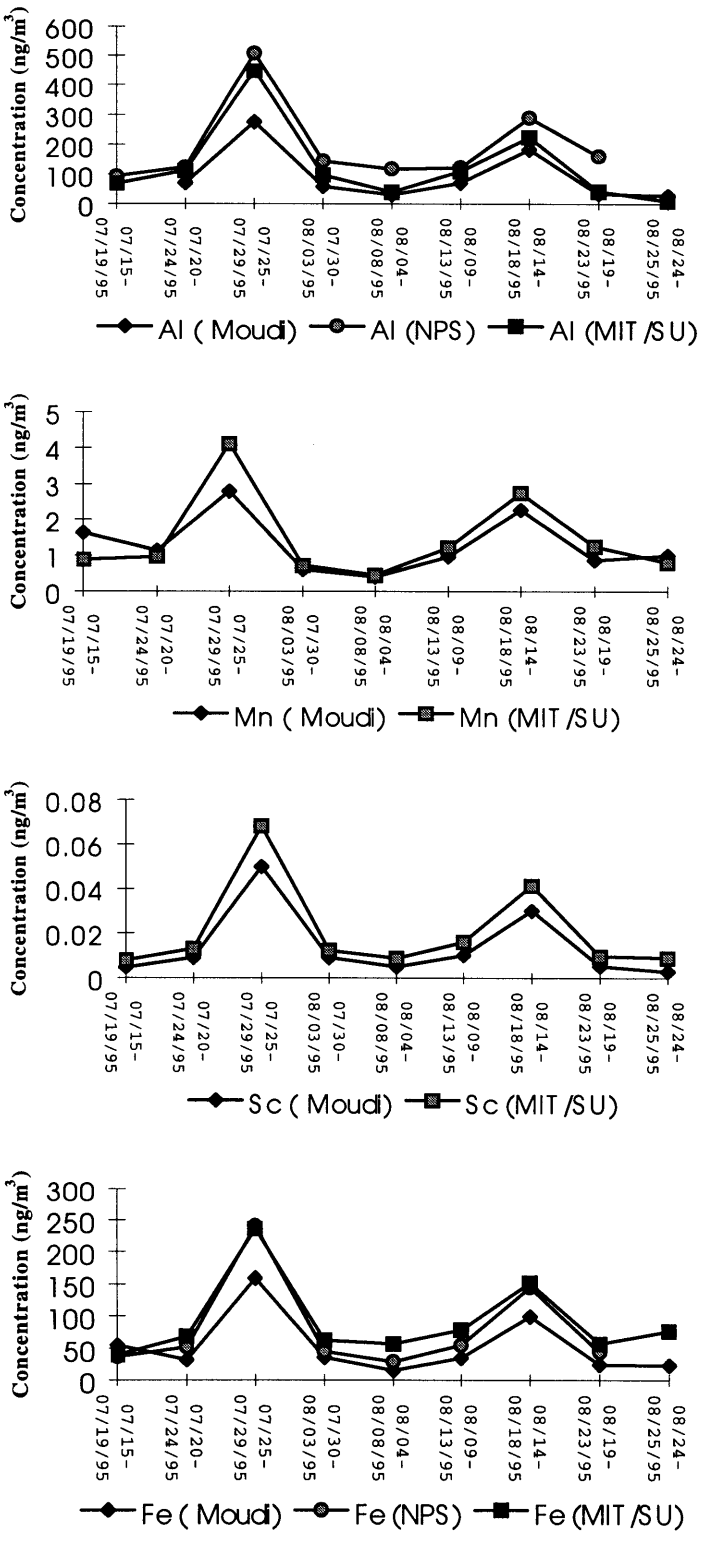

Figure 2.6. Comparison of elemental concentrations for MIT/SU with MOUDI and NPS (if available) samples.

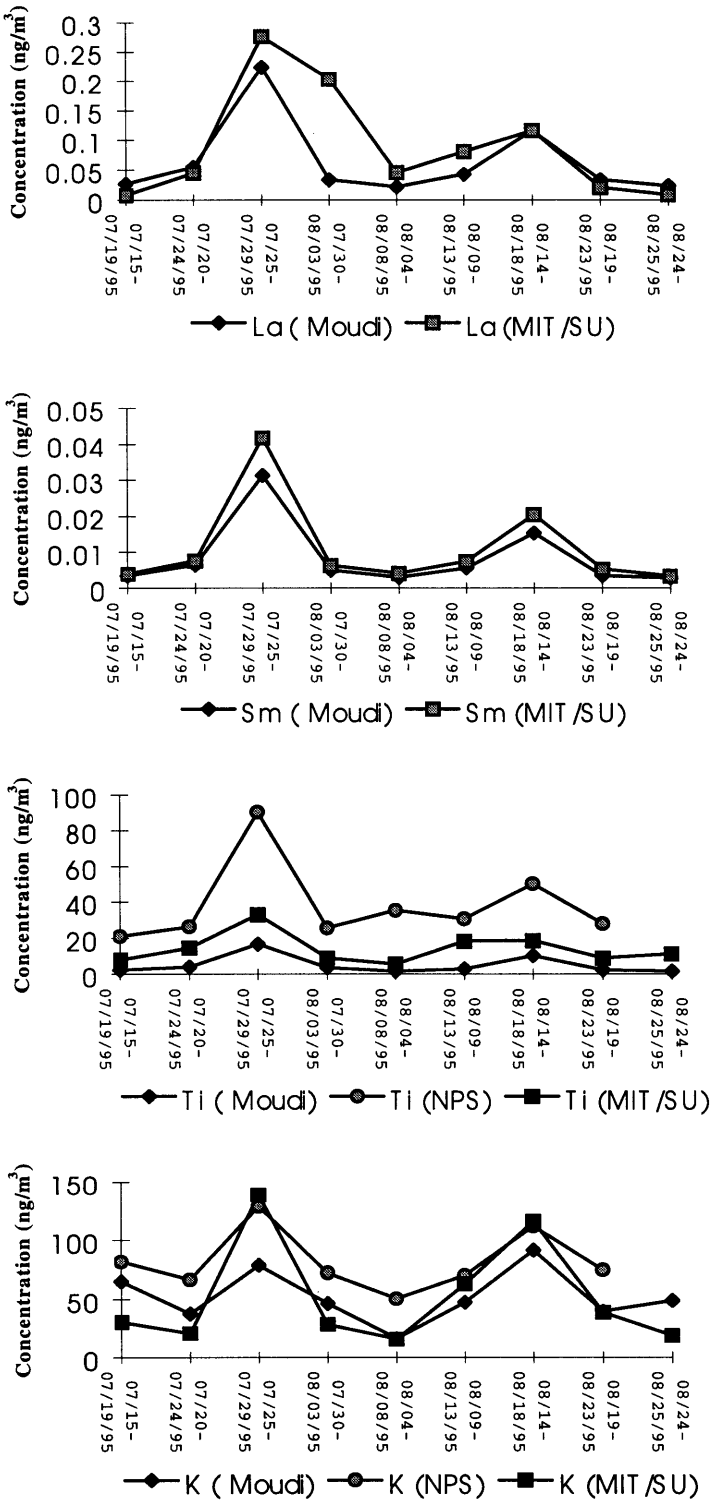

Figure 2.6. Comparison of elemental concentrations for MIT/SU with MOUDI and NPS (if available) samples (Continued).

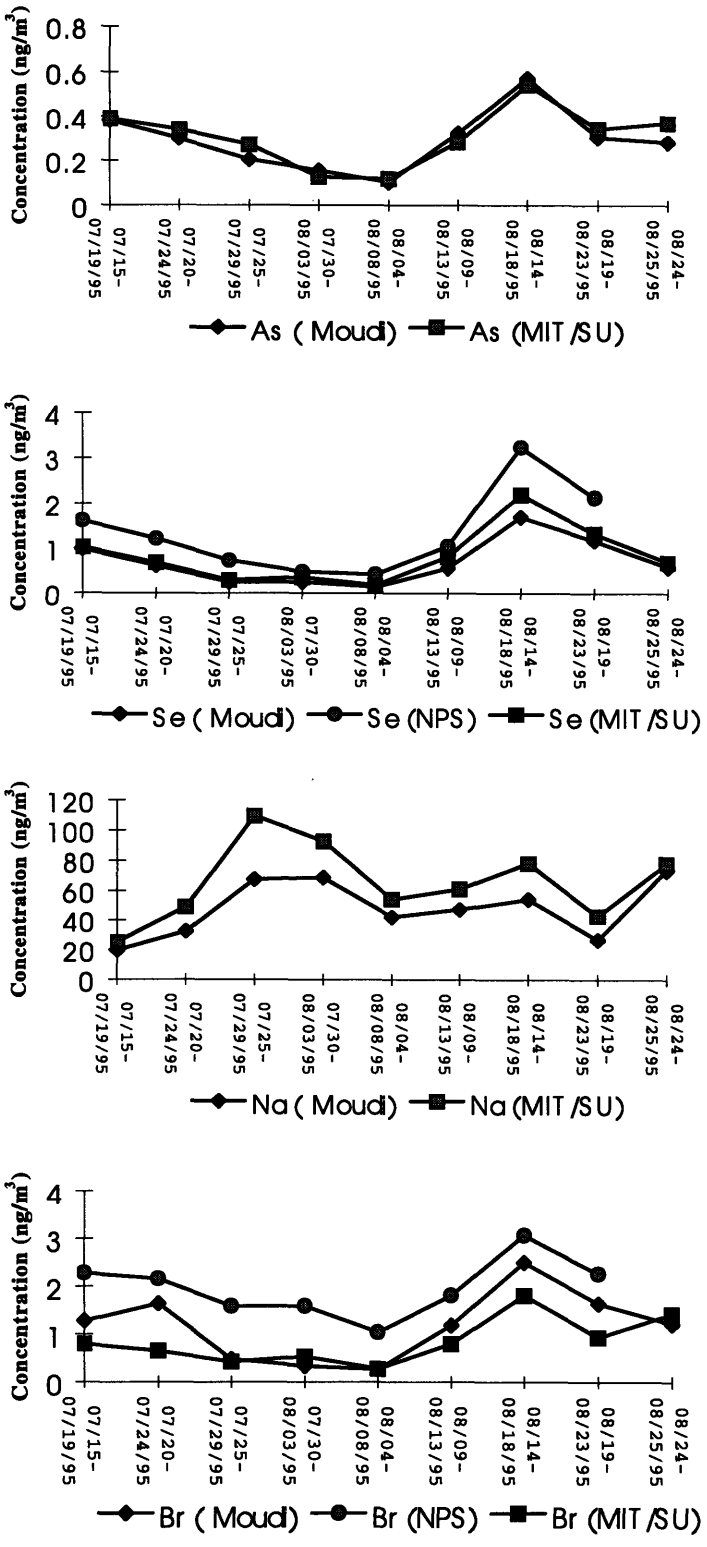

Figure 2.7. Comparison of elemental concentrations for MIT/SU with MOUDI and NPS (if available) samples.

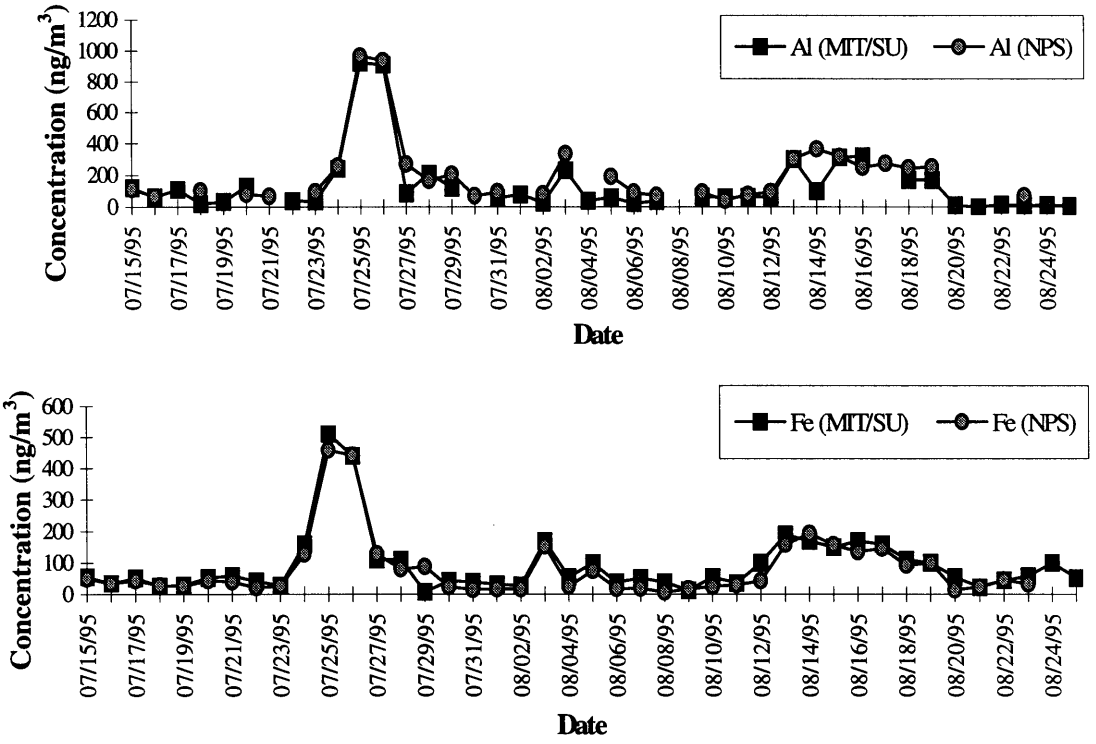

Figure 2.8. Time series plots of selected crustal elements (from MIT/SU & NPS).

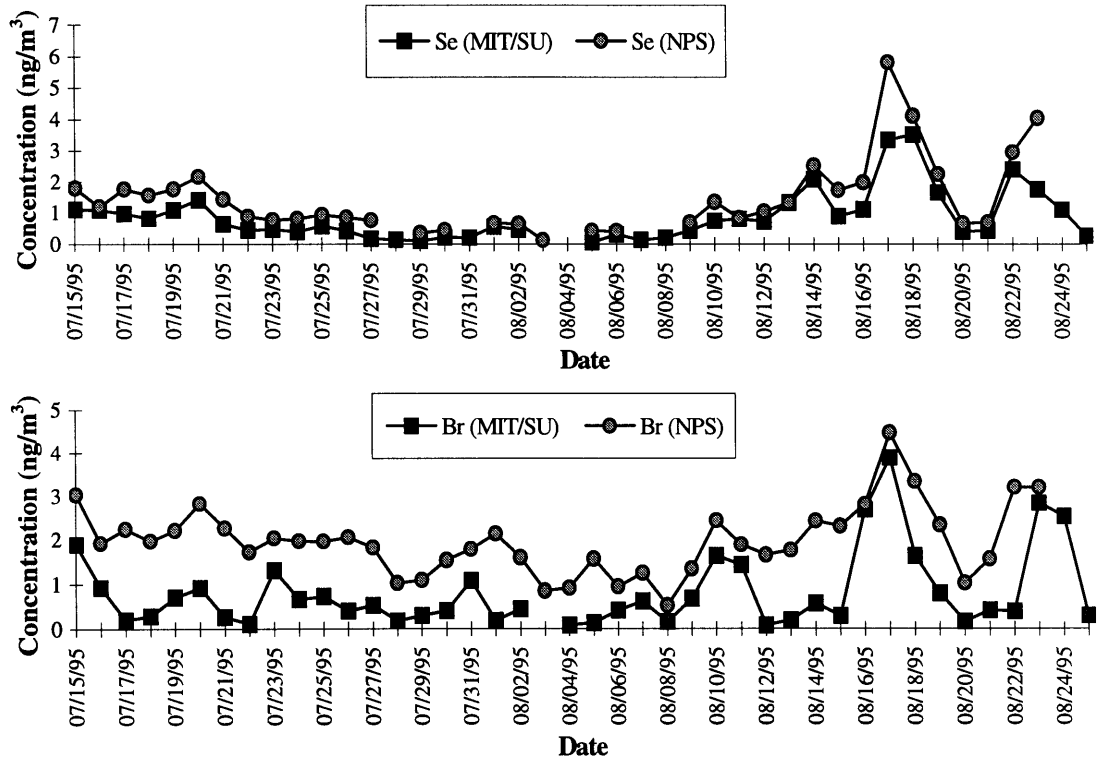

Figure 2.9. Time series plots of selected anthropogenic elements (from MIT/SU & NPS).

Chapter 3

SOURCE APPORTIONMENT OF FINE AND ULTRA-FINE PARTICLES

Particles released into the atmosphere bear specific chemical compositions that can be used to identify their origins. Wind-blown fine dust particles have a similar elemental composition to the earth's crust. Fresh sea-salt aerosol has the same composition as bulk seawater because it is generated by the bursting of bubbles from the surface water layer (Blanchard and Woodcock, 1980). Traditional approaches such as dispersion models use emission inventories from different sources as inputs in combination with mass balance calculations to identify source impacts on specific sites. However, because of physical and chemical transformations in the atmosphere, such as the conversion of SO_2 to sulfate in fine aerosol, chemical compositions of particles after release may change as they travel. Even if the dispersion model correctly accounts for these changes, the source emissions which it is based upon may have changed because of improved technologies, or they may subject to progressive changes over time. Also, fugitive emissions such as wind-blown dust and gases are difficult to include in dispersion models because they are not easily inventoried.

To understand the sources and transport of environmental species at the receptor site, factor analysis, a receptor model, is used in this study. Factor analysis uses statistical multi-variate methods to test for correlations among the measured species or parameters. This allows the identification and impact assessment of different sources on a receptor site without prior knowledge of the sources' characteristics (Hopke, 1991; Henry et al., 1984). Unlike chemical mass balance models, which require detailed knowledge of the sources of the particles and/or their possible transport pathways and chemical transformations, factor analysis is capable of evaluating uncharacterized area sources such as fugitive emissions or wind-blown crustal material. The use of factor analysis is

therefore extremely useful in many situations for identifying the sources of environmental species. The Absolute Factor Score (AFS) generated from factor analysis represents the normalized impact of the identified factor (i.e. source) on an individual sample. Multiple Linear Regression (MLR) can then be used to convert the AFS into mass contributions for each source and sample. Figure 3.1 shows the procedure for using factor analysis and multiple linear regression for source apportionment of fine aerosols. The theory of this methodology will be included in next section.

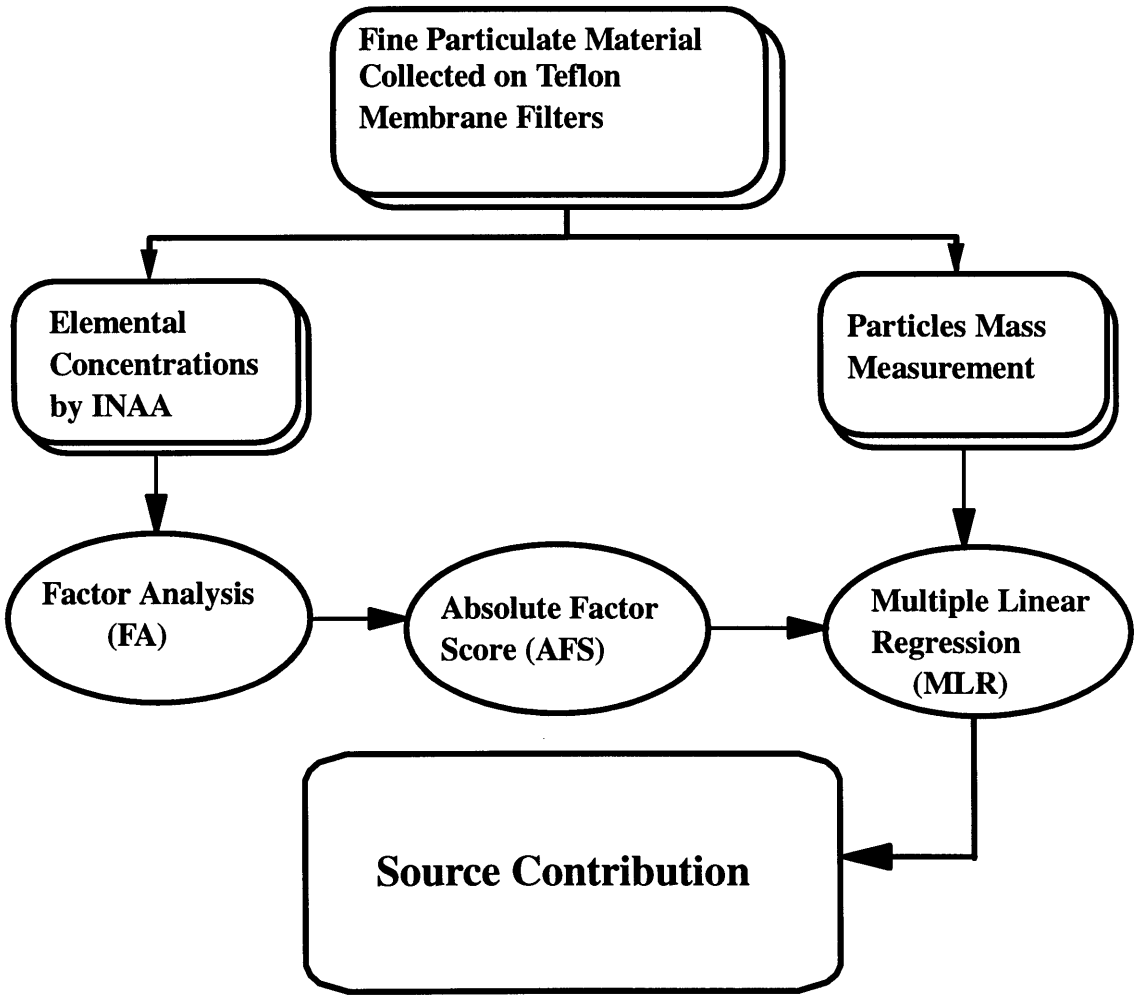

Figure 3.1. Source apportionment of fine aerosol by factor analysis and multiple linear regression.

3.1 Factor Analysis and Multiple Linear Regression

The goal of receptor modeling is to understand the sources and transport of environmental species by examining its properties at a receptor site. The method of receptor modeling employed in this study is Factor Analysis (FA). One of the most common uses of FA is to determine quantitatively source contributions to fine aerosol mass. Factor analysis has two main advantages over previously applied techniques. First, the only prior knowledge of the sources required for the model is one or more measurable marker species or ratios for each source type. Detailed information about the composition or strength of the source emissions is not needed. Second, it is not essential that all of the components of the aerosols are measured. For example, the contribution of coal combustion aerosols can be determined without any information about the major constituent of these aerosols, sulfate. Likewise, the contributions of water and organic matter to the mass of a particular type of aerosol is included in the regression even if these species are not measured.

Mathematically, the purpose of FA is to reduce the dimensionality of a data set by combining interrelated variables so that a minimum number of components or factors can explain the maximum variance of the original data. When applied to a series of environmental samples, each factor often represents a source type or region which influences the concentrations of the measured species. The factors are extracted so that the first factor accounts for the largest amount of the total variance in the data, and the second component accounts for the maximum amount of the remaining variance. The application of this method is based on the hypothesis that the original data matrix can be separated into the products of two matrices: the factor loading matrix and the factor score matrix (Equation 3.1)

$$\mathbf{C = LF + U} \tag{3.1}$$

C : data matrix
L : factor loading matrix
F : factor score matrix
U : unexplained source matrix

This model is mathematically similar to the mass balance equation used to separate the original data matrix into the product of a source composition matrix and a source contribution matrix (Equation 3.2).

$$\mathbf{C = AS + E} \tag{3.2}$$

C : data matrix
A : source composition matrix
S : source contribution matrix
E : random observation error matrix

The factor loading matrix can be used to describe qualitatively the source composition matrix. Specific source types or even regions can then be identified by observing different marker species or ratios in the factor loading matrix. Table 3.1 shows elemental markers used to identify different sources.

Because of the broad range of different elemental concentrations in fine aerosols, the first step in FA is to normalize the elemental data concentrations to a dimensionless standard form (Equation 3.3).

$$\mathbf{Z_{ik} = (C_{ik} - \overline{C_i})/\sigma_i} \tag{3.3}$$

where i=1,2,...n is the number of elements characterized in the analysis, k=1,2,...m is the number of observations or samples. Z_{ik} is the standardized concentration value of element i for observation k, and C_{ik} is the observed concentration value. $\overline{C_i}$ is the mean concentration for the ith element over all observations, and σ_i is the standard deviation of the concentration distribution of the element i.

Table 3.1. Sources of atmospheric particulates and their elemental markers (compiled from the findings of various studies including Olmez and Gordon, 1985; Olmez et al., 1988; Rahn and Lowenthal, 1984; Small et al., 1981; Huang et al., 1994, Olmez et al.., 1996).

Source	Marker Elements
Crustal Material	Sc, Al, REE*
Marine Aerosols	Na, Cl
Coal Combustion	As, Se, Hg
Oil Combustion	V, La, La/Sm
Refineries	La, La/Sm
U.S. Regional	Se, Sb, As
Canadian Regional	V, Na, Cd, Cl
Motor Vehicles	Br, Zn, Sb
Wood Burning	K
Incinerators	Na, K, Cl, In, Hg
Industrial Urban Areas	V, Zn, Se, Mo, Sb
Iron/Steel Works	Fe, Zn, Se, Mo, Sb
Ni, Cu Smelters	Hg, As, As/Se
Zn, Cd, Pb Smelters	In, As, As/Se, Co, Cd, Cr
Aluminum Plant	Al, Mg, Hg
Paint	Ba, Ti
Precious Metals	Au, Cr, Mo

* Rare Earth Elements

We can then use the FA method to separate Z_{ik} into the product of two matrices (Equation 3.4):

$$\mathbf{Z_{ik}} = \sum_{j=1}^{p} W_{ij} P_{jk} \tag{3.4}$$

where j represents the number of sources, W_{ij} is the factor loading matrix, and P_{jk} is the factor score matrix. The factor scores are correlated with the respective sources that are impacting the sampling site. A higher factor score implies a higher impact by source j during observation k. Because the scores are calculated from a normalized data matrix Z_{ik}, they too are normalized. Each component value within P_{jk} represents the number of standard deviations of the factor from its mean, which has a value of zero because of the normalization. If these factor scores are used to perform a regression onto a measured

variable such as the aerosol mass, the linear coefficient relating the two is zero because of the normalization. In order to keep the information about each element in absolute terms (i.e., distance from zero), Thurston and Spengler (1985) developed a method called absolute factor score analysis where they artificially added an extra sample to the data set with all the measured values set equal to zero. After the FA calculation, this artificial 'zero' sample generates a factor score, $P_{0,}$ for each of the j components. The Absolute Factor Scores (AFS) for each component on each day can then be calculated by subtracting this P_0 value from the original factor score P_{jk} (Equation 3.5).

$$\mathbf{[AFS]_{jk} = [P]_{jk} - [P_0]_{jk}} \tag{3.5}$$

The AFS gives the same score that would have been achieved had the original scoring been executed using un-normalized data.

Because the factor scores are now absolutely correlated with the impact of their associated sources, a multiple regression of these AFS's onto the measured masses produces the coefficients that convert the AFS into the source's mass contribution to each sample day (Equation 3.6)

$$\mathbf{M_k} = \zeta_0 + \sum_{j=1}^{p} \zeta_j [AFS]_{\mathbf{jk}} \tag{3.6}$$

where M_k is the measured fine particle mass during observation k; $[AFS]_{jk}$ is the rotated absolute factor score for component j on observation k; $\zeta_j[AFS]_{jk}$ is the particle mass contribution on observation k by the pollution source identified with component j; and ζ_0 is the particle mass contribution made by sources not covered in the FA. The terms M_k, $\zeta_{0,}$ and $\zeta_j[AFS]_{jk}$ are all in units of concentration (e.g. ng/m^3). The same multiple regression method can also be used to estimate contributions from the identified source to the measured elemental concentrations (Equation 3.7).

$$\mathbf{C_{ik}} = \boldsymbol{a_0} + \sum_{j=1}^{p} a_{ij} [AFS]_{jk} \tag{3.7}$$

where C_{ik} is the concentration of an element i during observation k; $[AFS]_{jk}$ is the rotated absolute factor score for component j on observation k; a_{ij} is the mean mass fraction of source j's particles represented by element i; a_0 is the contribution made by sources not

covered in the FA; and a_{ij} $[AFS]_{jk}$ is the estimate of the contribution by the jth source to the ambient concentrations of element i during observation k.

3.2. Source Apportionment of Fine Aerosol

The source contributions of the fine aerosols were determined by applying FA to two independent sets of concentration measurements at the eastern site: the MIT/SU data set which was determined by INAA, and the NPS/IMPROVE data set which was determined by PIXE, XRF, ion chromatography, and colorimetry. The intrinsic differences between the analytical techniques used to produce these data sets resulted in their having only five elements in common. Species which were observed in fewer than 80% of the samples, and those of limited use in source identification were excluded from the modeling. The aerosol masses used for the Multiple Linear Regression (MLR) were measured at the University of California, Davis, using the NPS/IMPROVE samples. The FA and MLR analyses were performed using PC software, Statgraphics Plus 6.0.

Elemental concentrations below detection limits were replaced by the most frequently occurring values for each element before running the FA (Gullu, 1996; Olmez et al., 1996). The most frequently occurring values are different from natural background because of the increased elemental emissions from accumulated human activities and natural fluctuations at different receptor sites. For environmental samples, elemental concentration usually follows a log normal distribution (Ott, 1990) and this value can be determined from a log normal fit of the species' frequency distribution as shown in Figure 3.2. Table 3.2 shows the most frequently occurring values for each element used for the MIT/SU and NPS/IMPROVE samples. Samples were collected by two samplers with different inlet sizecuts and they were analyzed by different instruments, which may have caused the differences in the most frequently occurring values.

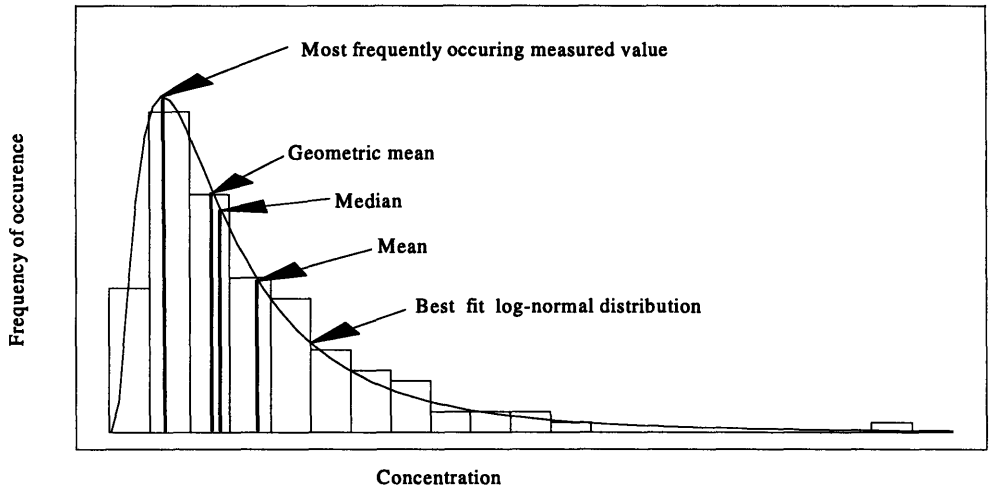

Figure 3.2. Histogram for calculation of most frequently occurring measured value.

Table 3.2. Most frequently observed values for elements in the MIT/SU and NPS IMPROVE data sets (ng/m^3). (Elements not measured are left as blanks)

Element	MIT/SU	NPS/IMPROVE
Na	29	
Al	34	79
Si		130
S		1200
K		60
Ca		34
Sc	0.0058	
V	0.23	
Mn	0.52	
Fe	38	24
Co	0.066	
Cu		0.85
Zn	2.9	3.2
As	0.13	
Se	0.36	0.7
Br	0.27	1.5
Sb	0.16	
Sm	0.0029	
Hg	0.014	
Pb		2.1
NH_4(NPS)		700
SO_4(NPS)		3200

3.2.1 Source Identification

The results of the FA for the MIT/SU and NPS/IMPROVE data sets are shown in Table 3.3 and Table 3.4 respectively, with three factors derived from each data set. The selection of factors is based on their eigenvalues being greater than unity. The eigenvalues in FA may be thought of as signal-to-noise ratios for each factor. Three factors showed eigenvalues greater than one and were used in the factor analysis. In the MIT/SU data, 73% of the total sample variance was explained by three factors, while in the NPS/IMPROVE data, 91% of the sample variance was explained by three factors.

The crustal factor is identified in both of the analyses by the presence of Al and Fe in the factor loadings, with Sc and Sm acting as additional markers in the MIT/SU analysis, and Si, K, and Ca in the NPS/IMPROVE analysis. Coal combustion emissions are identified by the high loadings of Se and Sb in MIT/SU data and by the high loadings of S, SO_4, and Se in NPS/IMPROVE data. The As/Se ratio is included in the MIT/SU FA data to assess the possible influence of metal smelters on the As and Se concentrations. Both As and Se are present in coal combustion and smelting emissions, but the ratio of As to Se is elevated in emissions from metal smelters (Small, et at. 1981). Because the high loading for As/Se did not appear in the same factor as the Se, and because the ratio was not found to be elevated significantly for any of the samples, the As and Se levels are not related to smelter emissions. The factor scores for each sample were then converted to Absolute Factor Scores (AFS's) based on equation 3.5. Figures 3.3 and 3.4 are the time series plots of the AFS for the identified factors. The same patterns of AFS prove that they were from the same origins.

There is an unidentified factor for each of the two data sets. The factor derived from the NPS/IMPROVE data set with high loading of Cu and the factor with high loadings of Zn, As and Hg using MIT/SU data set have no known sources. Nriagu and Pacyna (1988) reported that non-ferrous metal industry accounts for the largest fraction of As, Cu and Zn emissions to the atmosphere worldwide. If the unidentified factors in both data sets are due to the same facility, the AFS should follow the same pattern for both the MIT/SU and NPS/IMPROVE samples. Figure 3.5 is the time series plot of AFS for this

unidentified factor. The few high episodes shown on NPS/IMPROVE samples do not match with the MIT/SU data. The cause of the August 9, 1995 episode in NPS/IMPROVE data set is not clear. Also, the origin of the August 24, 1995 episode in MIT/SU data needs to be identified.

Table 3.3. Varimax rotated factor loading matrix for the MIT/SU data set.

(Loadings greater than 0.25 are in boldface)

Element	Crustal	Combustion	Unidentified
Na	**0.81**	-0.07	-0.21
Al	**0.95**	-0.08	0.06
Sc	**0.98**	0.06	0.03
V	**0.93**	0.03	0.07
Cr	**0.38**	**0.63**	0.23
Mn	**0.96**	0.19	0.08
Fe	**0.98**	0.09	0.04
Co	0.20	**0.47**	**0.45**
Zn	-0.23	0.29	**0.71**
As	0.21	**0.62**	**0.56**
Se	0.02	**0.85**	0.20
Br	0.003	**0.84**	-0.09
Sb	0.04	**0.68**	0.01
Sm	**0.98**	0.02	0.02
Hg	0.04	-0.18	**0.84**
As/Se	0.17	-0.47	0.02
Cum. Perc. Variance	41.8	64.1	73.2

Table 3.4. Varimax rotated factor loading matrix of NPS/IMPROVE data set.

(Loadings greater than 0.25 are in boldface)

Element	Combustion	Crustal	Unidentified
Al	-0.04	**0.99**	-0.02
Si	0.05	**0.99**	-0.0005
S	**0.93**	0.08	0.20
K	0.22	**0.93**	0.03
Ca	0.15	**0.93**	0.11
Fe	0.03	**0.99**	-0.01
Cu	**0.31**	0.05	**0.93**
Zn	**0.91**	0.08	0.04
Pb	**0.93**	0.07	0.13
Se	**0.94**	0.05	0.05
Br	**0.92**	0.13	-0.02
SO4	**0.91**	0.09	0.19
NH4	**0.92**	0.04	0.21
Cum. Perc. Variance	52.1	85.2	91.5

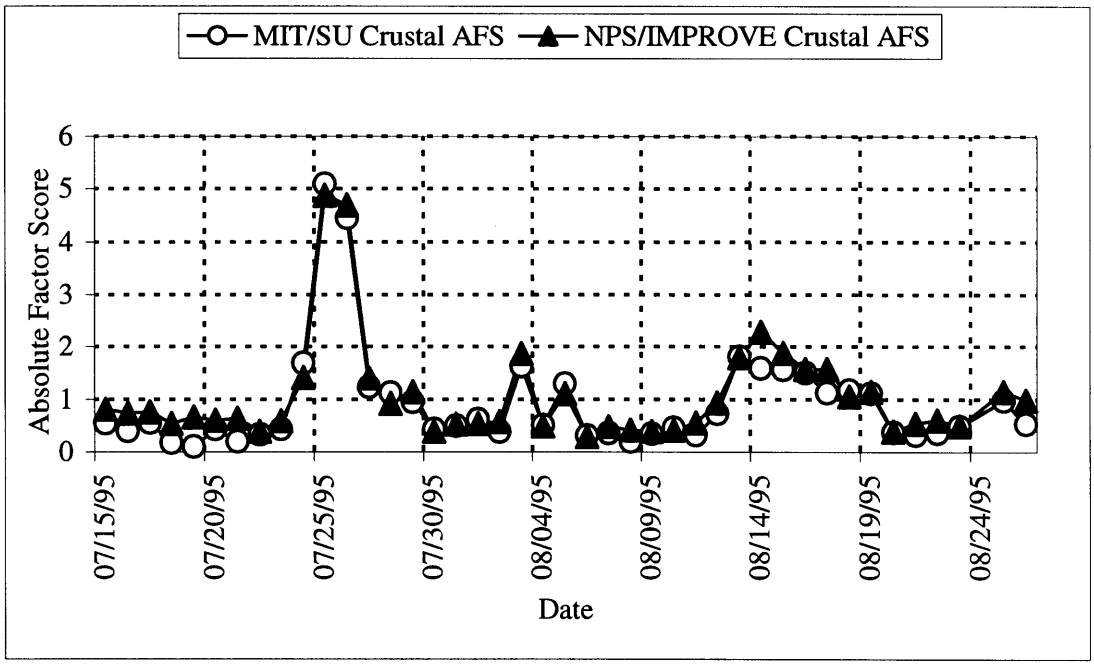

Figure 3.3. Time series plot of Absolute Factor Scores of crustal factor using the MIT/SU and NPS/IMPROVE data sets.

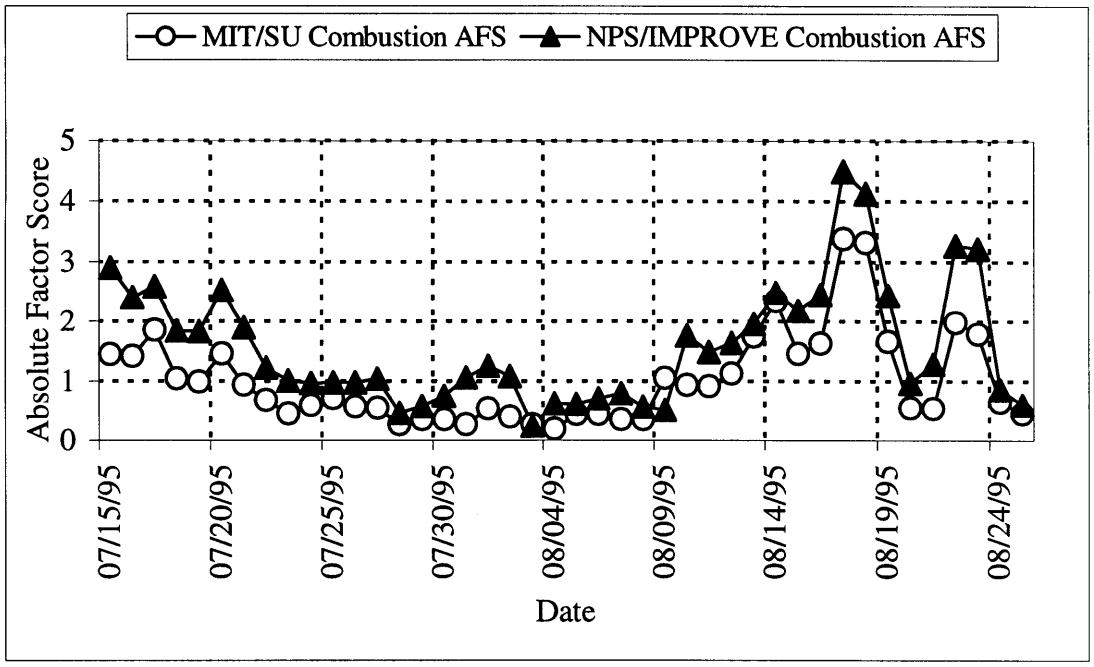

Figure 3.4. Time series plot of Absolute Factor Scores of combustion factor using the MIT/SU and NPS/IMPROVE data sets.

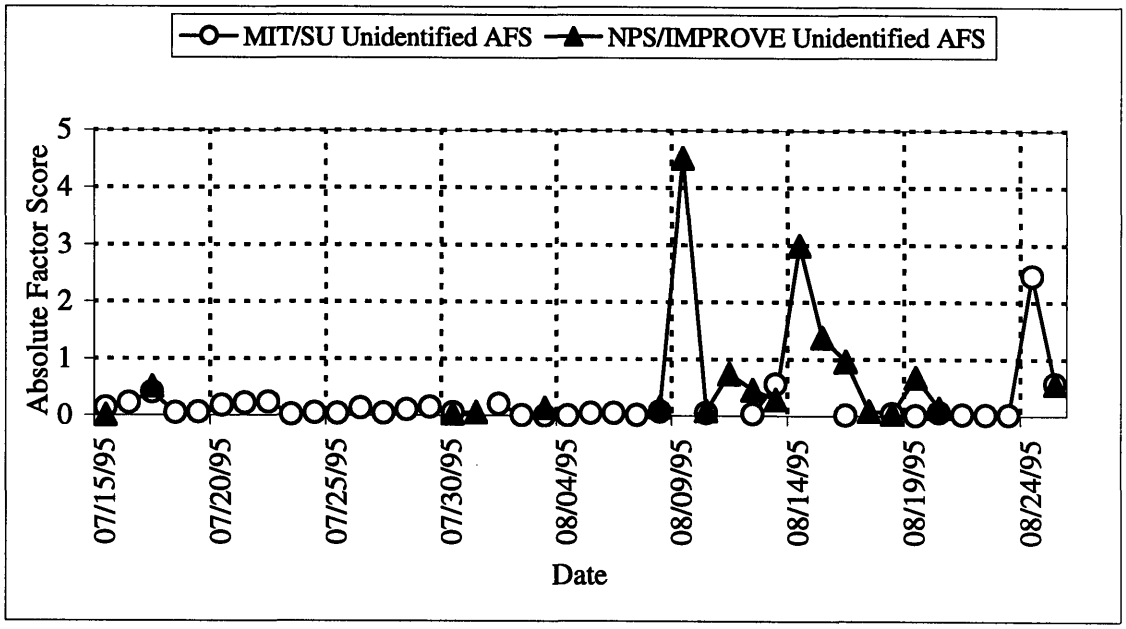

Figure 3.5. Time series plot of Absolute Factor Scores of unidentified factor using the MIT/SU and NPS/IMPROVE data sets.

3.2.2 Mass Regression and Crustal Contribution

To determine source contributions to fine aerosol mass, the AFS were used as independent variables in a multiple linear regression (Equation 3.6), with the measured aerosol mass as the dependent variable. The regression coefficients were then used to convert the daily AFS's into daily mass contributions (= ζ_j $[AFS]_{jk}$, Equation 3.6) from each source type and each sample. The results of these calculations for the MIT/SU and the NPS/IMPROVE data sets are shown with the NPS/IMPROVE measured mass in Figures 3.6 and 3.7, (and given in table form in Appendix B). The mass measurements for the MIT/SU samples were subject to great uncertainties and the mass data from these samples were not used for regression.

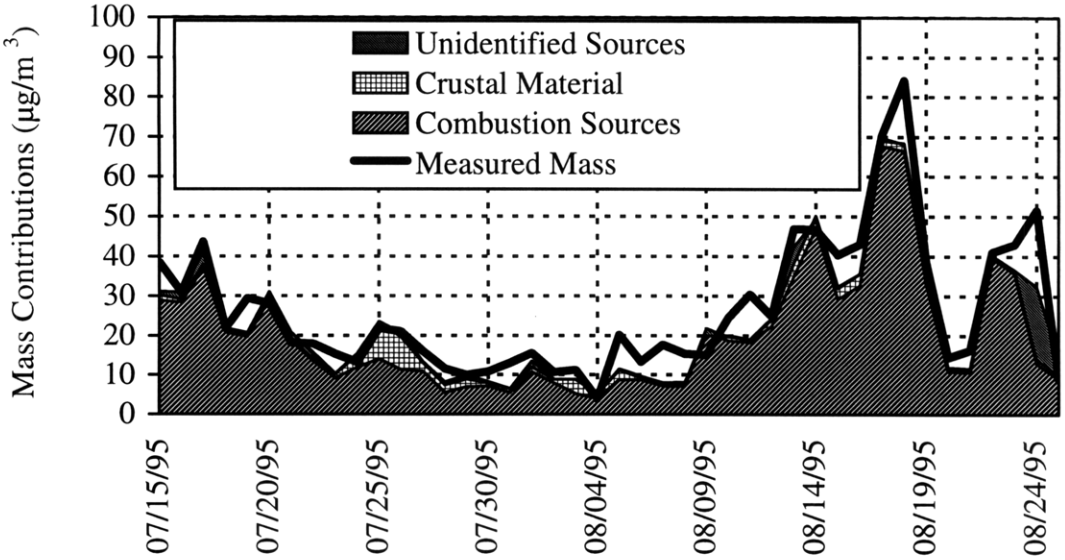

Figure 3.6. Source contributions to fine aerosol mass as calculated by receptor modeling using the MIT/SU data set.

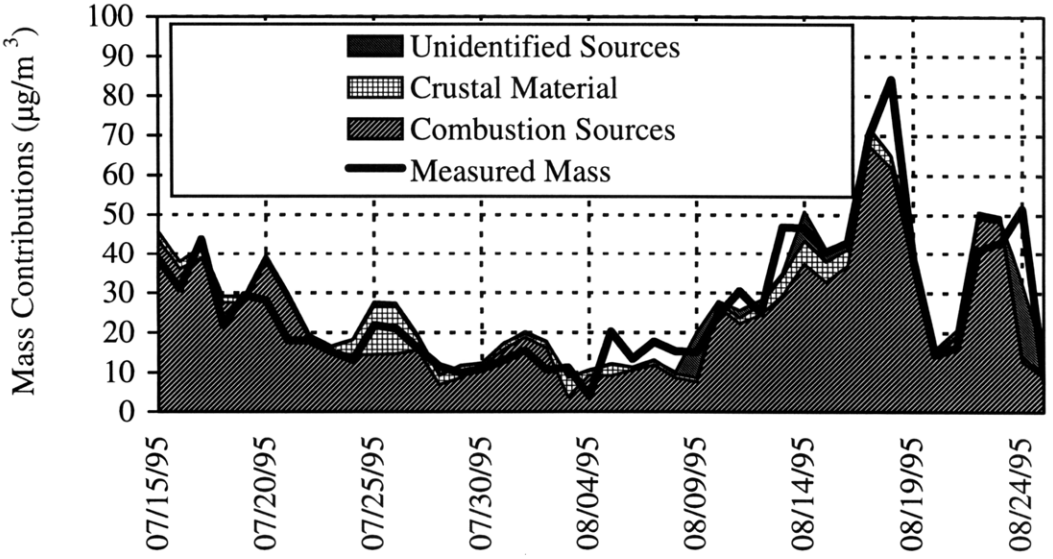

Figure 3.7. Source contributions to fine aerosol mass as calculated by receptor modeling using the NPS/IMPROVE data set.

Two identified major sources and one minor unidentified source had contributions to fine aerosol masses at this site. The first identified source was the crustal source. Crustal particles are one of the major components of the atmospheric aerosol and have a major size mode greater than 1 μm (Whitby, 1978). They are generated from wind-blown dust, or are re-suspended from the earth's surface due to human activities. Crustal particles contribute a considerable amount of mass to atmospheric aerosols and their concentrations are subject to great fluctuations at different locations (Cahill et al., 1981; Fergusson, 1992). The concentrations of elements such as Ca and Si have been found to be dependent on their source locations and they may be used to identify soils of different origin (Suzuki et al., 1993). Single soil source profiles may not be applicable in determining contributions to the fine aerosol mass because the source composition may change at different locations.

The crustal contribution to fine aerosol mass was compared between the AFS-MLR technique and a method of oxide summation, which converts the measured masses of major crustal elements to the masses of their most common crustal oxides (i.e. Al_2O_3, SiO_2, K_2O, CaO, MnO_2, Fe_2O_3) and then summing these values. The oxide method may underestimate the crustal mass contribution because all of the constituents of the crustal material may not have been measured, or because some of these constituents may have been measured but not attributed to crustal contributions. This estimate of the crustal contribution was used as a lower limit when compared with the model results.

Calculated daily crustal contributions based on these two data sets are compared in Figure 3.8, along with the daily crustal contribution as estimated by the sum of the major measured crustal elements from both of the data sets. In the oxide calculation, elemental concentrations of Al, Mn and Fe were taken from the MIT/SU data set, and the Si, K and Ca data were from the NPS/IMPROVE data set. The oxide method showed lower contributions from crustal sources than the AFS-MLR results. Differences among the crustal contribution calculations can be attributed to differences in the sample collection parameters, in the species which were analyzed, and in the nature of the calculations.

Some of the difference between the two AFS-MLR results in the MIT/SU and NPS/IMPROVE data sets may be due to the different inlet cyclones used for these samplers (the NPS/IMPROVE sizecut was 2.4 μm, and the MIT/SU was 2.1 μm). Size-segregated elemental concentrations measured form the UMn/MOUDI samples, show that the crustal elements (mainly Al and Fe) have distributions peaked toward larger diameters (Table 2.5). The difference between the two calculated crustal contributions may therefore be due to material between 2.1 μm and 2.4 μm particle diameter. The crustal estimates based on AFS-MLR modeling calculations account for components of the aerosol which may not have been measured, or which were not attributed to crustal sources. These estimates are higher than those derived from the summation of the measured crustal oxide masses. Water, organic, or inorganic species other than the oxides mentioned above will be included with the crustal matter if they co-vary with the major crustal species. In this way the modeling may give a better estimate of the total mass of the crustal material than the sum of the oxides. However, species which co-vary with the crustal material, but which are not of crustal origin will also be included by the model, thus overestimating the crustal mass. Vanadium and Na are good marker elements for oil combustion emissions and marine related aerosols respectively. The presence of V and Na in the crustal factors shown in Table 3.3 are due to the atmospheric mixing of emissions from these sources with crustal aerosols during the period of July 24-26, 1995. This is supported by the air mass trajectory analysis presented later. The agreement between the values for crustal contributions to the total aerosol mass as determined from the two independent data sets indicates the validity of the method and results.

Figure 3.9 shows the percentage of the measured mass composed of crustal material as calculated by these three crustal contribution estimates. Table 3.5 contains the mean contributions (in $\mu g/m^3$, and as a % of total measured mass) from each of the identified source groups based on the FA of the two data sets, and the mean crustal contribution based on the sum of the measured major crustal elements from both of the data sets. The ± values in Table 3.5 are based on the standard error of the MLR.

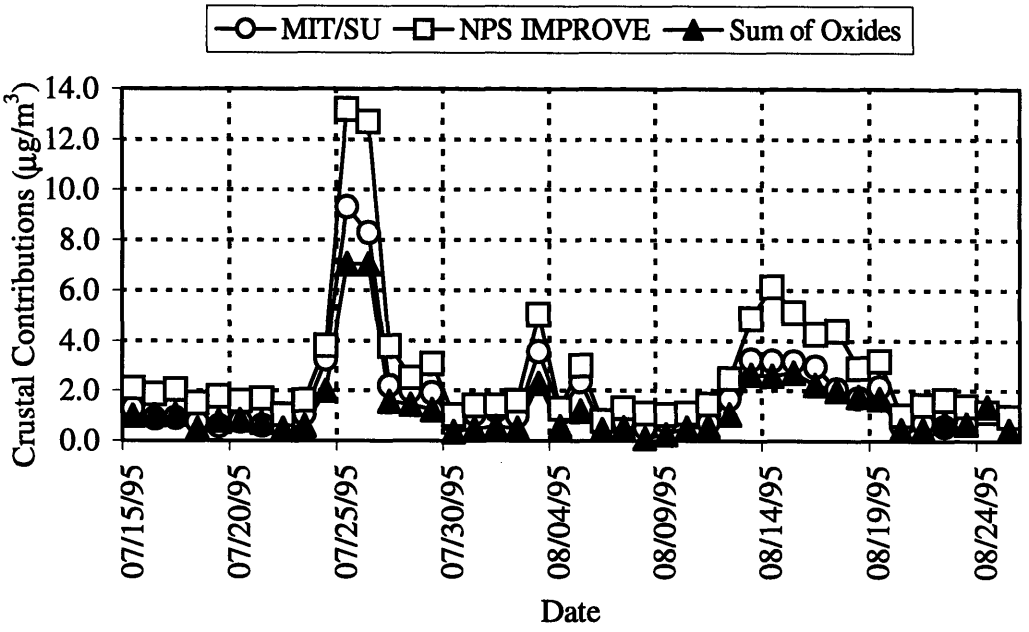

Figure 3.8. Crustal material contributions to fine aerosol mass as calculated by receptor modeling using the MIT/SU and NPS/IMPROVE data sets, and by the summation of the masses of the oxides of the major measured crustal elements.

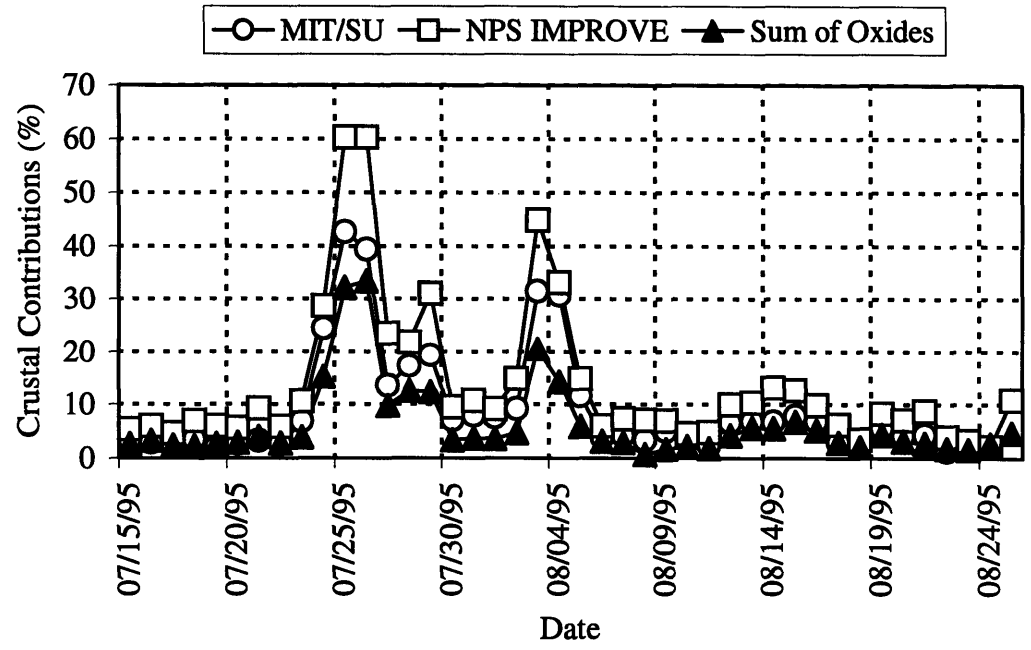

Figure 3.9. The percentage of the fine aerosol mass composed of crustal material as calculated by receptor modeling using the MIT/SU and NPS/IMPROVE data sets, and by the summation of the masses of the oxides of the major measured crustal elements.

Table 3.5. Absolute ($\mu g/m^3$) and percent mean aerosol mass contributions from identified sources as calculated by receptor modeling using MIT/SU and NPS/IMPROVE data sets, and by the summation of the masses of the oxides of the measured major crustal elements.

Data	Combustion Sources	Crustal Sources	Unidentified Sources	Calculated Sum / Measured
MIT/SU	20.2 ± 1.6 ($77 \pm 4\%$)	1.8 ± 0.7 ($7 \pm 3\%$)	1.0 ± 0.3 ($4 \pm 1\%$)	0.88
NPS IMPROVE	23.8 ± 1.5 ($90 \pm 6\%$)	2.8 ± 1.0 ($11 \pm 4\%$)	1.1 ± 0.3 ($4 \pm 1\%$)	1.05
Sum of oxides		1.4 (6%)		

For most of the sampling days, the crustal contribution to the total fine mass is small, less than 2 $\mu m/m^3$ or 10% of the total. However, during three periods, the crustal contributions were more significant. The most obvious was around July 24-26, 1995 which is referred to as the "dust event" due to the large amount of crustal material and the relatively low amount of combustion-related aerosols such as sulfates. The high percentage contributions around August 3, 1995 coincide with uncharacteristically low total aerosol masses. During this "clean period" the influence of Hurricane Erin produced exceptionally clear air for several days. From August 14 through August 18, the crustal contribution rises somewhat, although the total mass during this time is dominated by combustion-related sources.

Meteorological conditions of the dust episodes observed between July 24-26 and August 14-18 suggested that dust particles that caused the two episodes may have originated from different locations. Figures 3.10 and 3.11 are the general wind trajectories for these two events. During July 24-25, wind passed over the Atlantic Ocean, the Gulf of Mexico, and coast of Texas and Louisiana to the sampling site. Between August 14 and 18, the wind mostly blew from the U.S. inland (Sherman, et al., 1997). The wind

trajectories of the sampling site suggest that dust particles may have originated from the Sahara desert for the first event, and dust particles originating from north Africa such as the Sahara desert have been found to travel across the Atlantic Ocean and reach the southern United States. This is especially likely to occur during the summer months when wind patterns favor such transportation (Gatz and Prospero, 1996). Gatz and Prospero (1996) used Si/Al and Ca/Al ratios to identify particles that originated from the Sahara desert and found the values are around 2.0 and 0.3. The Si/Al and Ca/Al ratios of the July 24-26 event are 2.02±0.08 and 0.24±0.06, and the ratios for the August 14-18 episode are 2.28±0.2 and 0.38±0.06. These ratios suggest that particles collected during these two episodes might originate from different sources, but the statistical uncertainties were too large to separate them. Stronger evidence based on stable isotope ratios of $^{130}Ba/^{138}Ba$ will be shown in the next chapter to identify sources. Dust from the second episode originated from inland continental U.S. also included species from combustion processes such as Se and sulfate.

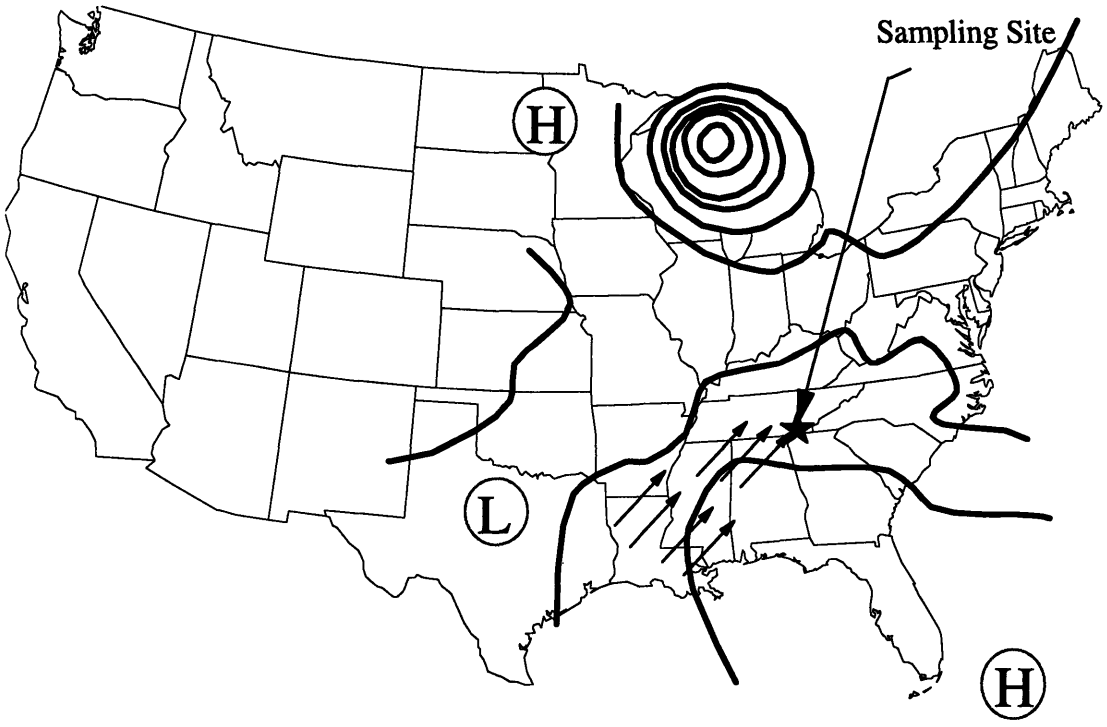

Figure 3.10. Synoptic plot of general wind pattern between 07/24 and 07/26/95

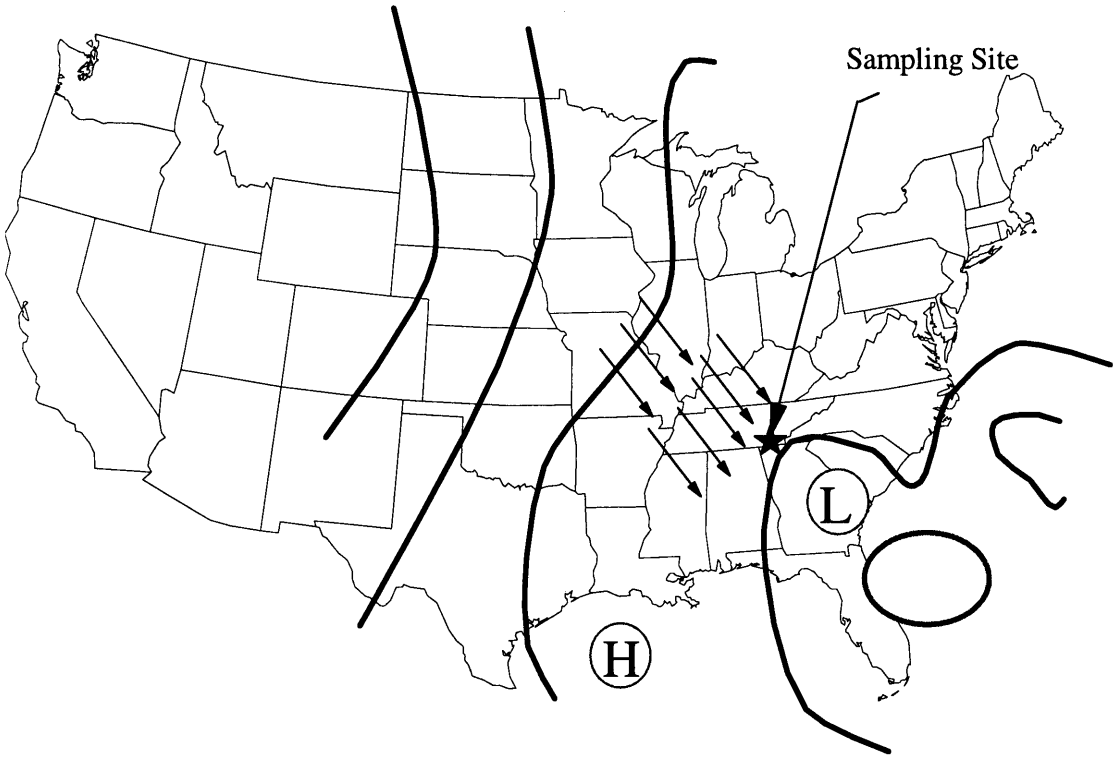

Figure 3.11. Synoptic plot of general wind pattern between 08/14 and 08/18/95

3.2.3 Mass Contribution from Combustion Source and Origin of Sulfate

Combustion-related species, such as sulfate, nitrate, and organic plus elemental carbon contribute most of the mass to fine aerosols (Seinfeld, 1986) and have been recognized to have regional origins. These species exhibit higher concentrations in fine particles compared to crustal and sea-salt elements which are found to be predominantly associated with coarse particles (2.5 μm < d_a < 10 μm) (Maenhaut et al., 1996). Figures 3.12 and 3.13 show the concentration (μg/m^3) of the measured mass related to combustion material as determined by AFS-MLR results and the percentage mass contribution of sulfate to the identified combustion material. The average contribution from combustion sources to the fine particulate mass is 77±4 % for the MIT/SU samples and 90±6% for the NPS/IMPROVE samples (Table 3.5). In order to estimate the sulfate

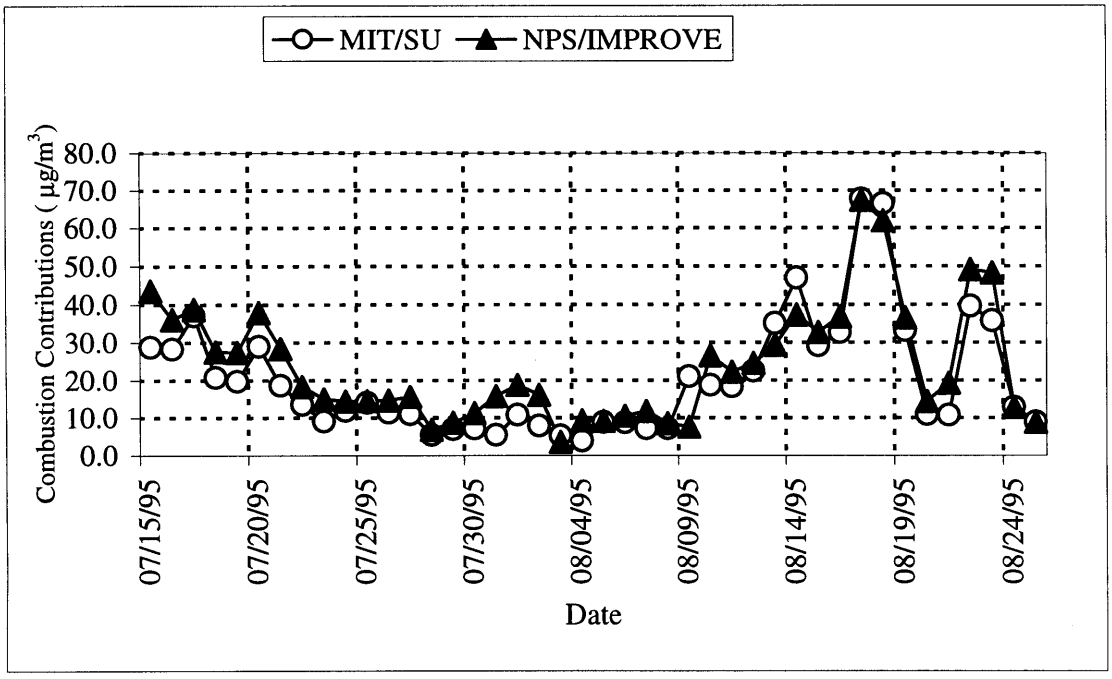

Figure 3.12. The concentration of fine aerosol mass composed of combustion material as calculated by receptor modeling using the MIT/SU and NPS/IMPROVE data.

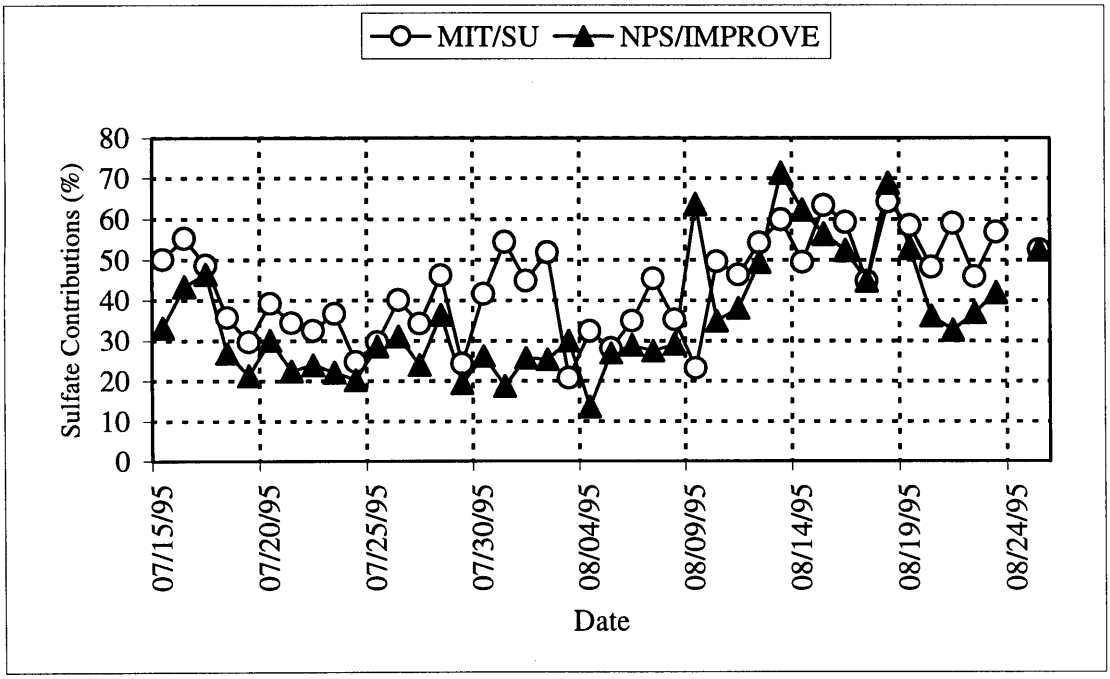

Figure 3.13. The percentage contributions of sulfate to the combustion material as calculated by receptor modeling using the MIT/SU and NPS/IMPROVE data.

contribution to combustion material for the MIT/SU samples, sulfate measured by ion chromatography from the Harvard-EPA Annular Denuder System operated concurrently with the same 2.1 μm cyclone sizecut was used. The average sulfate contribution to combustion material is 43.6% for the MIT/SU samples and 36% for the NPS/IMPROVE samples. There are no sulfate data available on August 24 from the NPS/IMPROVE samples and the data are not included in Figure 3.13.

Because sulfate is related to combustion emissions and is the major contributor to fine aerosol mass (Figure 3.13), it is important to know its origin. Sulfate (SO_4) aerosols are formed as secondary aerosols from the oxidation of sulfur dioxide (SO_2) during transport. The burning of coal is the major source of SO_2 in the atmosphere of the eastern United States. Sulfates may also be released as primary aerosols from oil-fired power plants (Olmez et al., 1988). Selenium has been found to have the same regional pattern as sulfate (Tuncel, et al. 1985; Eldred, 1997), and therefore Se may be used as a surrogate for sulfate. Selenium's high EF values, which will be included in the next section, show that most Se comes from anthropogenic emissions, primarily from coal combustion (Mosher and Duce, 1987). The contributions of Se from natural sources such as soil and the marine biosphere are much smaller and more localized compared with the contributions from anthropogenic sources (Eldred, 1997).

Figure 3.14 shows the correlation of sulfate with Se. Selenium was measured by INAA on Teflon filters collected by Stanford University (MIT/SU samples), and sulfate was measured by ion chromatography using samples from the Harvard-EPA Annular Denuder System (HEADS). The HEADS equipment had the same cyclone inlet sizecut, 2.1 μm, and was operated concurrently with the Stanford University sampler. The strong correlation between sulfate and Se (r^2=0.87) indicates that they either came from the same regional sources, or there is a strong local source emitting both sulfate and Se.

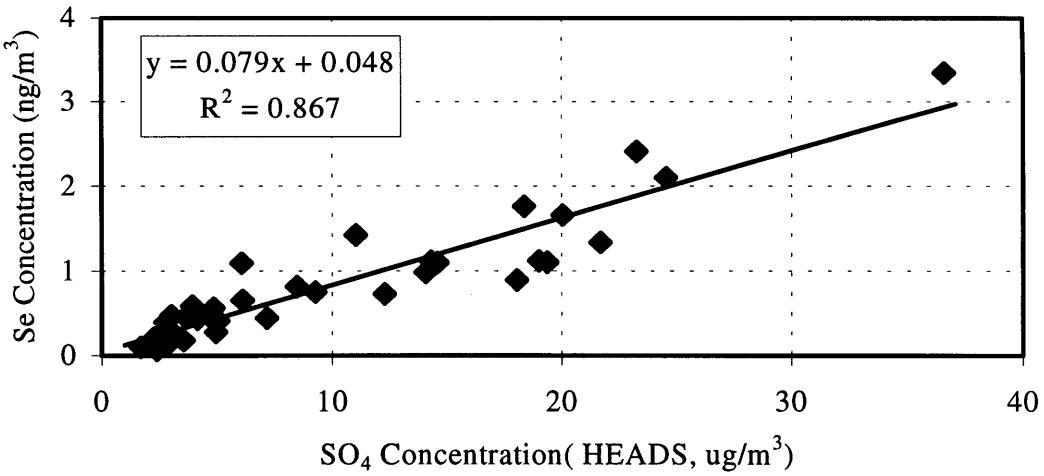

Figure 3.14. Correlation of MIT/SU selenium with HEADS sulfate concentrations.

When S and Se are emitted from coal-fired power plants, they are primarily in the vapor phase (Tuncel et al., 1985). Because the Se vapor condenses rapidly on fine particulate and the SO_2 converts to sulfate slowly, the S to Se concentration ratio for fine particulates increases as the plume ages and eventually reaches an asymptotic value (Tuncel et al., 1985; Ondov et al., 1989). At urban sites, with high coal combustion impacts, the S/Se ratio has been measured as 1000±500, and in the Shenandoah valley as 3400±1400 (Tuncel et al., 1985). Eldred (1997) reported a median value of the S/Se ratio of 2300 in rural sites of the eastern U.S. during summer with one-half of the measurements between 1900 and 2700. Tuncel's Se concentrations were measured by INAA and Eldred's concentrations were measured by XRF. If we assume that measured Se concentrations are higher when measured by XRF than by INAA in a ratio of 1.47±0.18 (Olmez et al., 1988), and adjust the XRF Se measurements, then the median value of the S/Se ratio from Eldred's calculation is also 3400. Figure 3.15 shows the resulting S/Se ratio for the 2.1 μm samples. Sulfur values were converted from sulfate measurements from the HEADS sampler and Se values were from the MIT/SU samples. The gray area corresponds to ratios of 3400±1400. During the sampling period, the median S/Se ratio is 4000±1400, and most of the ratios fell within this range. This indicates that the major source of the sulfate is aged aerosols generated by coal combustion.

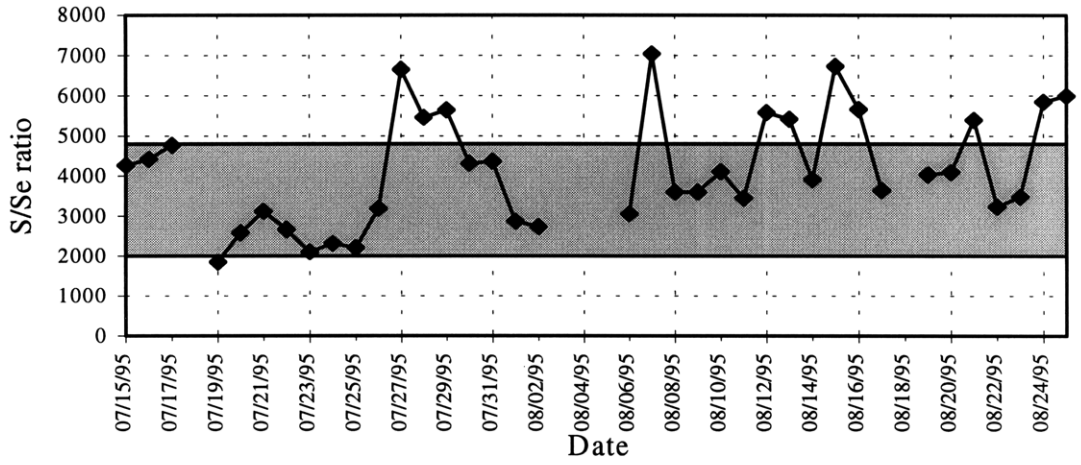

Figure 3.15. Time series plot of sulfate to selenium ratio in fine aerosols.

There are some days with higher S/Se ratios than the expected range indicating that there might be other sources emitting either higher concentrations of sulfate or lower concentrations of Se. Olmez et al. (1988) found that primary sulfate emitted from oil-fired power plants has a S/Se ratio higher than that for coal-fired power plants, but the influence is more localized. If the elevated S/Se ratio is due to a local oil-fired power plant, V, which is also a marker element for oil combustion, should be higher on those days. However, the correlation between the S/Se ratio and total V was poor (r^2=0.021), indicating that oil combustion is probably not the reason for the high S/Se ratios. Because the S/Se ratios higher than 5000 were for samples with Se concentrations less than 0.2 ng/m^3, the high S/Se values appear to be due to low Se levels.

3.2.4 Enrichment Factor (EF)

Enrichment Factor (EF) analysis was used to assess the general trends in the data set and to identify elements originating mainly from non-crustal sources. The EF technique employs a simple double normalization of the data (Equation 3.8).

$$EF(X)_{sample} = \frac{R_{sample}}{R_{crustal\ average}} = \frac{(X/Y)_{sample}}{(X/Y)_{crustal\ average}} \qquad (3.8)$$

The first step is to calculate the sample ratio, R_{sample}, of an element X to a normalizing element Y from the same sample, where the normalizing element Y originates exclusively from crustal material. The next step is to divide the sample ratio R_{sample} by the global, average crustal ratio of the same two elements to obtain $R_{crustal\ average}$. The resultant EF (X) is the enrichment factor of element X relative to the natural crustal abundance pattern. It should be equal to one if X solely originates from soil; a high EF indicates that there are other source(s) of element X in that sample.

Aluminum or Sc are usually chosen as normalization elements because, in atmospheric particulates, their source is primarily natural crustal dust, and their concentrations do not vary greatly around the world. However, it has been found that, in some locations, there are anthropogenic sources that may contribute significantly to the aluminum concentrations of fine particulates (Olmez et al., 1996). Scandium was chosen as the normalizing element for this work. Taylor's crustal composition (Taylor, 1964) was used as the natural crustal average composition.

Because average crustal concentration ratios were used to calculate EF values and because elemental concentration distributions may vary among various particle sizes, EF analysis was only performed for integrated fine particulate samples. Figure 3.16 shows the median values and ranges of calculated EF values for elements measured by INAA (MIT/SU samples). Elements are arranged based on increasing median enrichment values and hence increasing contribution from anthropogenic sources. Although the EF's should be unity for elements of crustal origin, the values may vary somewhat because of variations in crustal compositions, analytical uncertainties, additional sources, size fractionations, etc..

Elements may be roughly divided into three different groups based on their median EF values. Elements with EF's less than 10 are referred to as non-enriched elements, moderately enriched elements have an EF between 10 and 100, and highly enriched elements have an EF over 100. Although elements of mostly crustal origin have

EF values in the non-enriched range, some elements with other known sources such as Na (from marine aerosols) and V (from oil combustion) also fall into this range. This may be due to the limited contributions of these additional sources at the receptor site during the sampling period.

Moderately enriched elements (10<EF<100) such as Cr, Ba and In may come from both crustal and non-crustal sources (e.g. Cr from smelters, In from incinerators and Ba from the paint industry). Due to the small number of samples and statistical limits in the factor analysis, separate factors for contributions from these sources could not be derived.

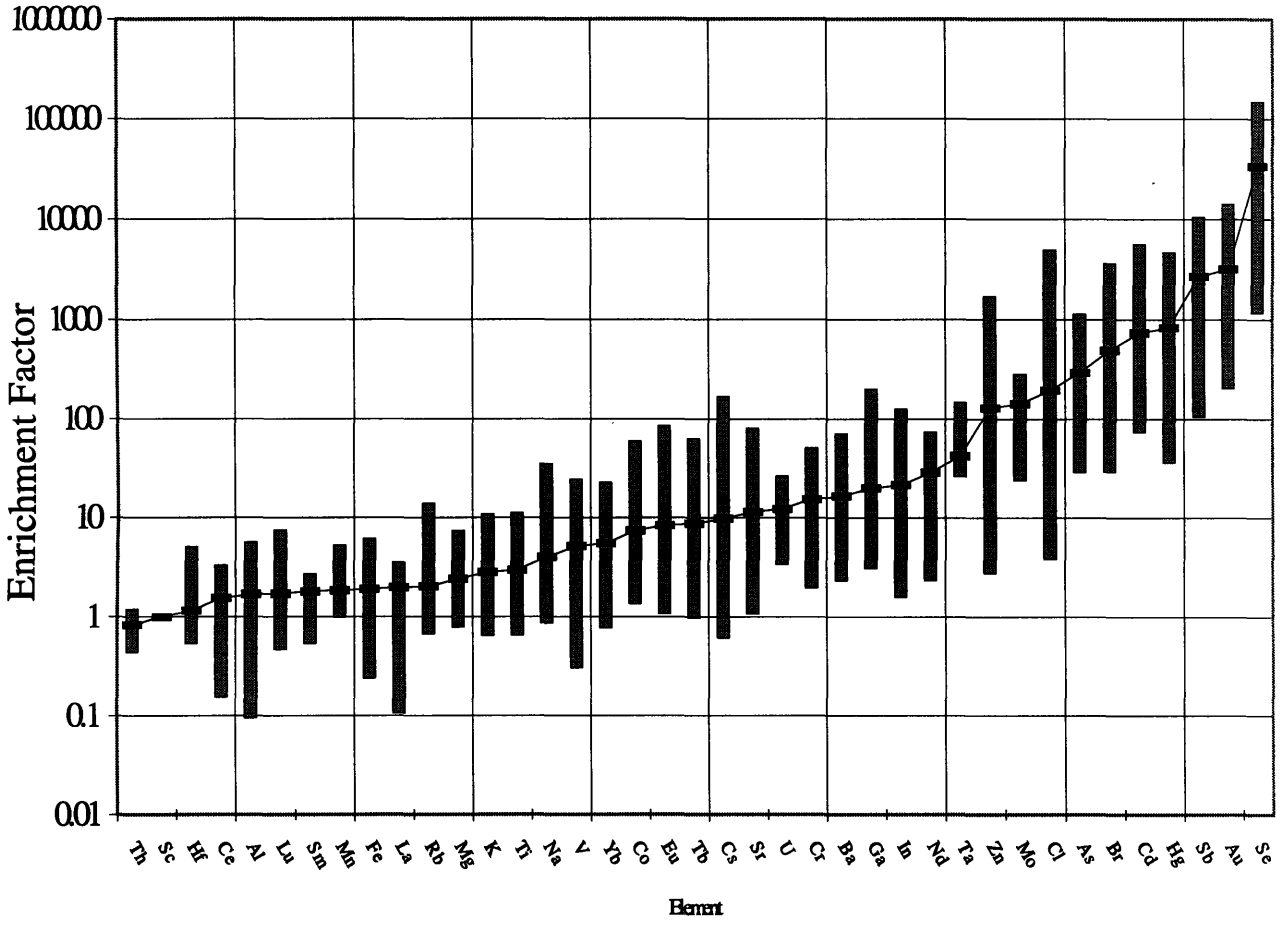

Figure 3.16. Median, minimum, and maximum enrichment factors for elements measured in the MIT/SU samples by INAA.

Elements that are highly enriched (Zn, Mo, Cl, As, Br, Cd, Hg, Sb, Au and Se) are primarily of anthropogenic origins and may have been released to the atmosphere as fine particles or as gases. Selenium has the highest EF and is commonly found to have high EF's even at remote areas such as the South Pole (Maenhaut et al., 1979). Known sources for Se include volcanoes, fossil fuel burning, and industrial activities. However, in the eastern U.S., Se originates primarily from coal combustion (Tuncel et al., 1985). The result of factor analysis shows a strong correlation of Se with sulfate and other volatile elements such as Zn and Br (Tables 3.3 and 3.4). Antimony and Br may have local sources such as motor vehicle emissions (Huang et al., 1994), or antimony roasting or smelting (Dzubay et al., 1988). Bromine is also used in organic synthesis and is a constituent in oxidizing and bleaching agents and in various solvents. We cannot identify the sources of these elements, but the high EF values indicate that they originate from other than crustal material.

3.2.5 Elemental Source Contributions

The elemental contributions to the measured aerosol concentrations from each of the sources identified by receptor modeling are displayed in Tables 3.6 and 3.7. These were calculated by applying an MLR of the source's AFS's onto the measured elemental concentrations (Equation 3.7) from both the MIT/SU and the NPS/IMPROVE data sets. The major crustal elements (e.g., Al, Fe, Si, Ca, Mn and Sm) are well explained by the crustal factor, and sulfate is mainly explained by the combustion factor. Although there are some species for which the estimates are too low (e.g. Na, Br, Sb, K) or too high (e.g. Mn, Sm, Si, SO_4), the overall agreement is acceptable considering the limited number of samples. If the total of the contributions overestimates the average measured concentration, the ratio of sum of the calculations to the measured concentration may be greater than one.

Table 3.6. Mean calculated elemental source contributions (in ng/m^3) to the measured fine aerosol concentrations based on the MIT/SU data.

(a) Element	Combustion Sources	Crustal Material	Unidentified Sources	Sum of Calculations/ Measured Concentration
Na		32		0.49
Al		170	15.6	1.43
Sc	0.0015	0.026	0.0011	1.30
V	0.011	0.32	0.034	0.78
Cr	0.35	0.22	0.19	0.94
Mn	0.28	1.5	0.17	1.29
Fe	8.3	90	4.9	1.11
Co	0.041	0.018	0.06	0.79
Zn	2.8		10	1.19
As	0.10	0.037	0.14	0.89
Se	0.60	0.015	0.22	0.97
Br	0.64	0.003		0.79
Sb	0.15	0.008	0.0032	0.52
Sm	0.00025	0.016	0.00043	1.39
Hg		0.0012	0.034	1.10

Table 3.7. Mean calculated elemental or inorganic species source contributions (in ng/m^3) to the measured fine aerosol concentrations based on the NPS/IMPROVE data.

Element or Species	Combustion Sources	Crustal Material	Unidentified Sources	Sum of Calculations/ Measured Concentration
Al		210		1.17
Si	35	440		1.25
S	4050	240	160	1.39
K	13	37	0.3	0.61
Ca	10.7	45	1.5	0.92
Fe	4.0	106		1.36
Cu	0.95	0.11	0.53	0.80
Zn	5.2	0.31	0.041	0.91
Pb	1.7	0.9	0.04	0.94
Se	1.7	0.058	0.016	1.27
Br	1.1	0.11		0.61
SO_4	13000	870	500	1.45
NH_4	1900	61	80	1.07

3.3 Source Apportionment of Size-Segregated Impactor Samples

3.3.1 Source Identification of Impactor Samples

Two size-segregated impactor samplers (MOUDI samplers) were used in this study to collect particles in the same size ranges. Samples were collected from two sites in the United States, an eastern, rural site located in the Great Smoky Mountain National Park, Tennessee, and a western, urban site located in Pasadena, California. Samples were collected at different times of the year (the eastern samples were collected during the summer, and the western samples were collected during the winter).

Elements released from the same source should have the same concentration vs. size distribution and these unique patterns may be used to identify the sources. Because the particulate samples used in this study were collected from two sites influenced by

very different sources, the comparison of elemental patterns of these fine particles may establish source profiles that can be used for further studies. Figures 3.17 and 3.18 show the average concentrations of selected crustal and rare earth elements collected from these two sites. Particles with an d_a greater than 1.8 μm were not included in these figures. The UMn/MOUDI samples were collected from an eastern rural site and crustal elements peaked at larger sizes as expected (Seinfeld, 1986; Whitby, 1978). However, crustal elements show very different patterns for the CIT/MOUDI samples which were collected from an urban site. Aluminum and iron show higher average concentrations at ultra-fine size ranges on this urban site. The concentrations of the light rare earth elements such as La and Ce were also higher than samples collected from the rural site. Motor vehicle and oil refinery sources release relatively high levels of the light rare earth elements (Olmez and Gordon, 1985) and the higher concentrations observed at the urban site suggest the influence of these sources. However, because the urban samples were collected from five separate runs, the average concentrations do not reveal the exact time of the impact. It is important to check the elemental patterns of each run in order to resolve the time frame of source impacts. This will be shown later in this section.

Figure 3.19 shows the average concentration of selected elements that have higher contributions from anthropogenic origins. Elements related to combustion processes such as As and Se are comparable at these two sites, although other elements such as Zn and Sb are much higher at the urban site. Huang et al. (1994) found that Zn, Sb and Br are potential marker elements for motor vehicle emissions and all of these elements have higher fine-to-coarse particle ratios. The higher concentrations of these elements observed at the urban site indicate that motor vehicles are an important source at the urban location. The size distribution of these elements (except Sb) at the urban site show higher concentrations at smaller size ranges which is quite different from the crustal and rare earth elements. The elevated concentrations of these elements at smaller sizes suggest that they may have potential influence on human health and need to be further evaluated. Vanadium is also higher at the urban site and it is a good marker element for oil combustion emissions.

The elemental patterns of the size segregated samples (UMn/MOUDI samples) are first examined to find potential source patterns based on the source identifications of specific episodes described in the previous section. A dust event was found between July 24 and 26, and the contribution from combustion emissions increased between August 14 to 18 at this eastern site. The UMn/MOUDI sampler collected samples every five days at this site and the dust event was not covered by a single sample set. However, samples collected between July 25 and 29 covered most of the event and the elemental pattern from those samples is representative of the dust episode. Samples collected between August 14 and 18 by the UMn/MOUDI sampler overlapped with the pollution episode and their elemental patterns were used to represent combustion emissions.

Figures 3.20 and 3.21 show the elemental patterns of crustal and rare earth elements corresponding to these two episodes. The crustal and rare earth elements show higher concentrations at larger size and their patterns did not change during these two events. Figure 3.22 shows the elements related to anthropogenic emissions. The concentrations of combustion-related elements such as As, Se, and Zn increased during the pollution episode especially in the particle diameter range of 0.56 to 1 μm. In contrast, vanadium concentrations did not increase during the pollution episode. This indicates that the source of the V is not the same as the source of the As, Se, and Zn. These elemental patterns, are used to identify potential source contributions to the fine particle samples collected from the urban site.

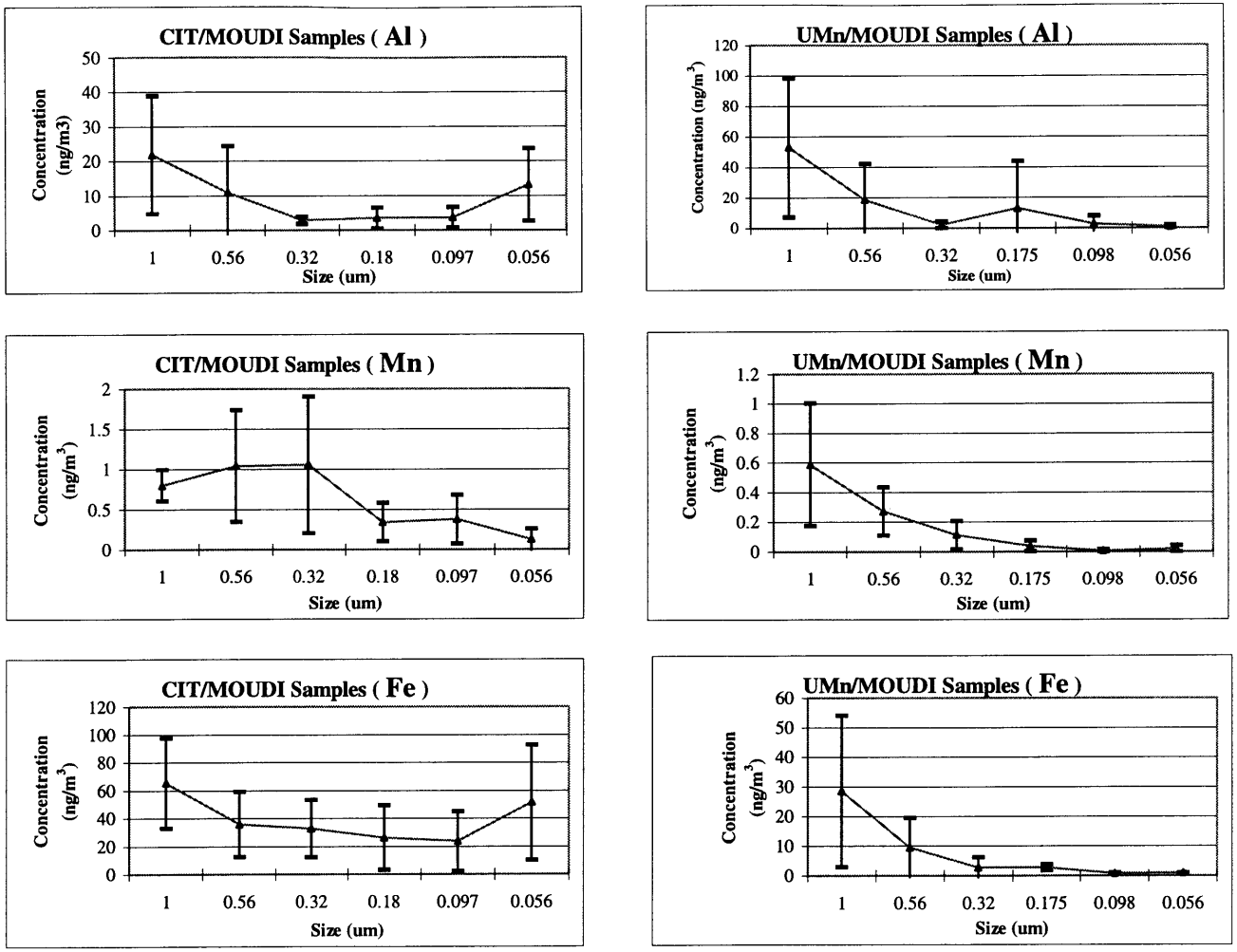

Figure 3.17. The average concentrations of crustal elements in UMn/MOUDI and CIT/MOUDI Samples.

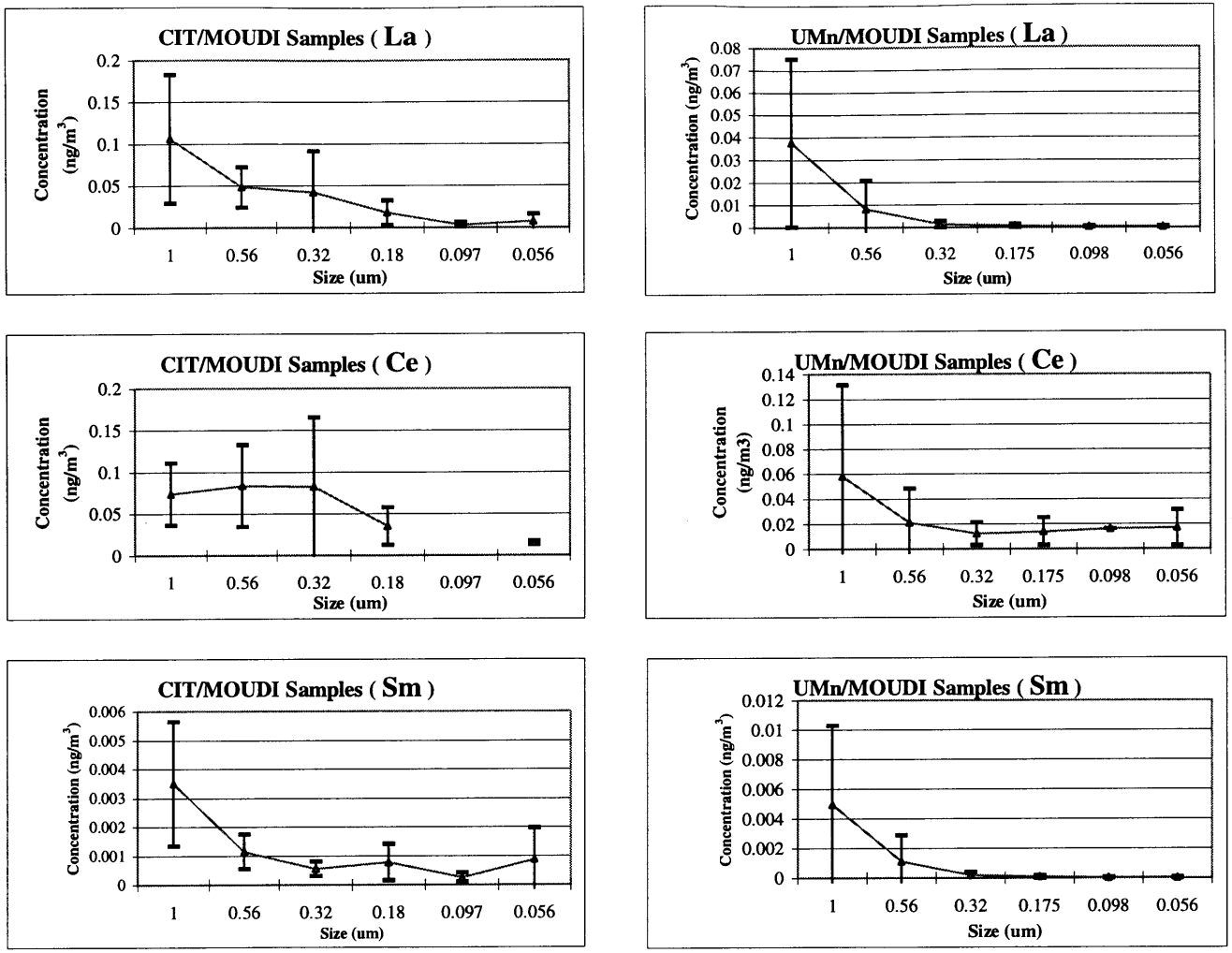

Figure 3.18. The average concentrations of rare earth elements in UMn/MOUDI and CIT/MOUDI samples.

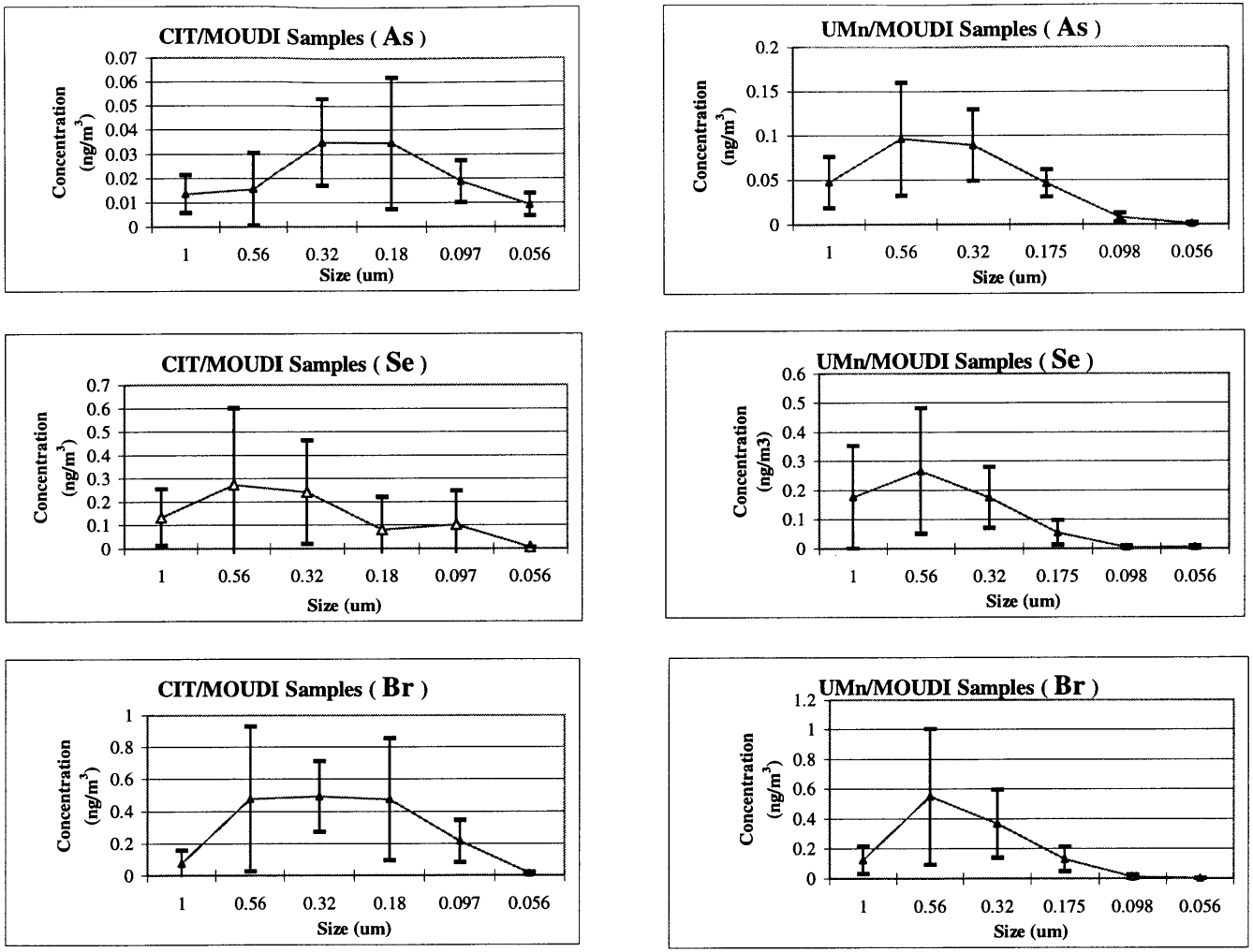

Figure 3.19. The average concentrations of elements with greater contribution from anthropogenic emissions in UMn/MOUDI and CIT/MOUDI samples.

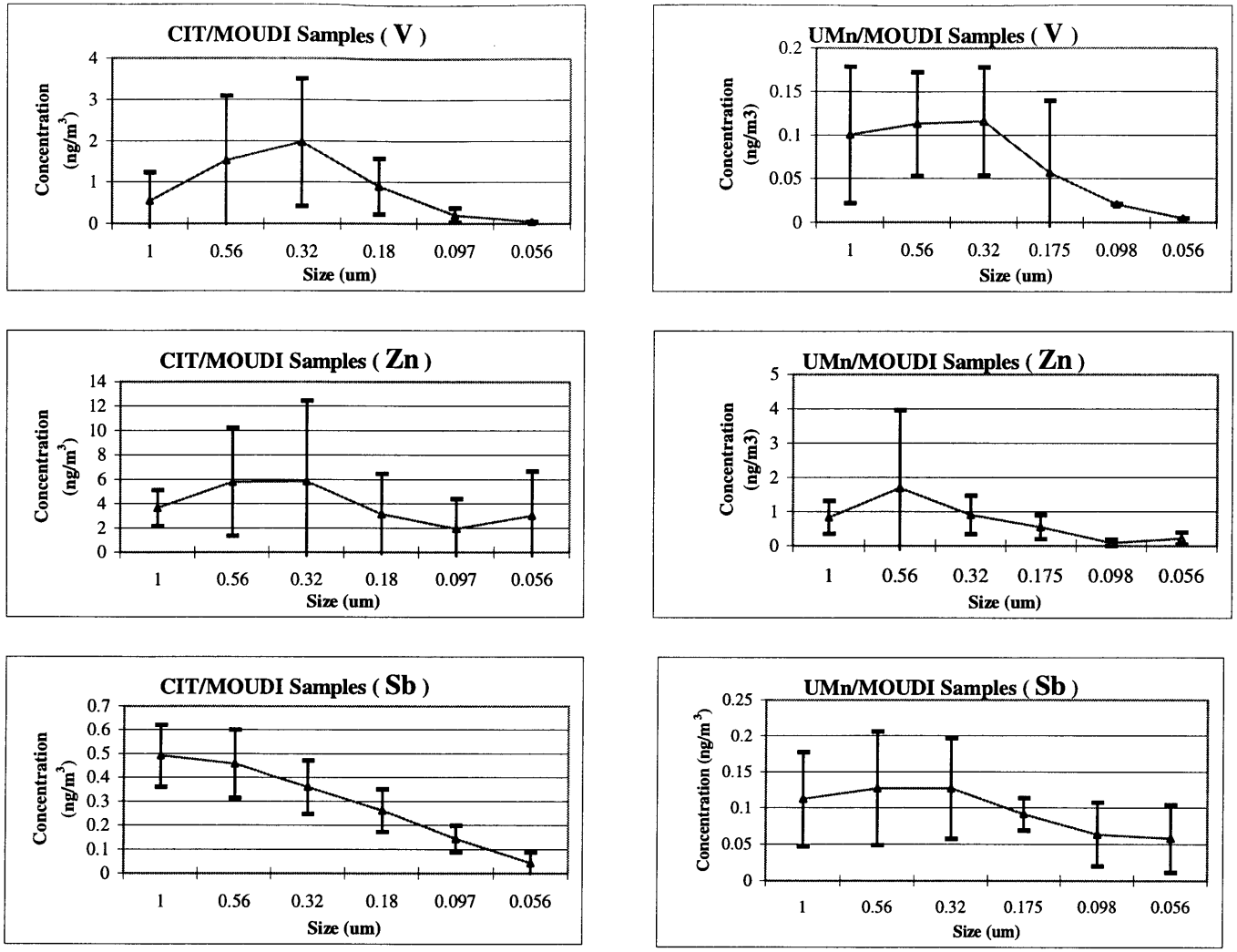

Figure 3.19. (Continued) The average concentration of elements with greater contribution from anthropogenic emissions in UMn/MOUDI and CIT/MOUDI samples

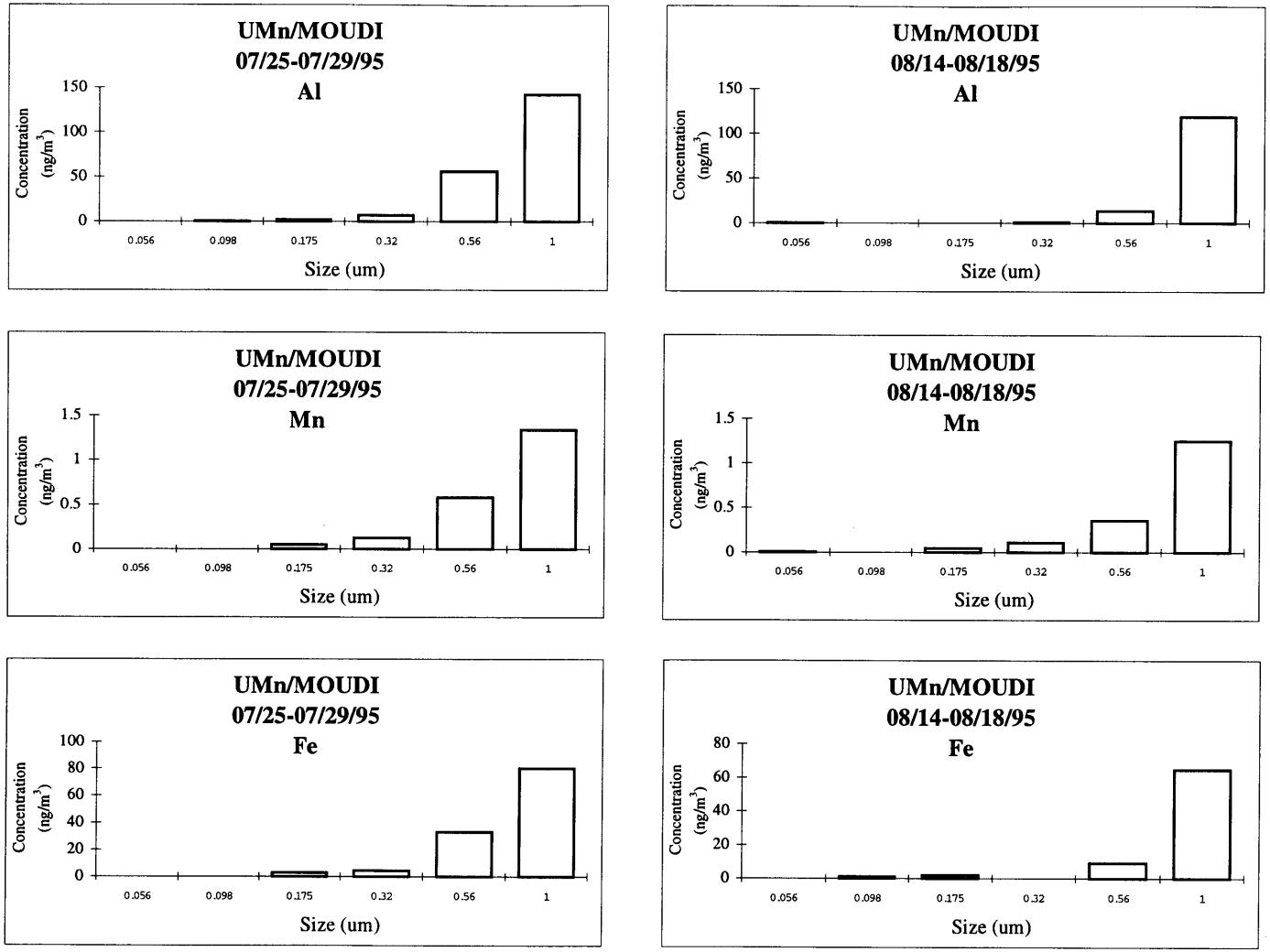

Figure 3.20. Concentration of crustal elements in UMn/MOUDI samples during dust (07/25-07/29/95) and pollution (08/14-08/18/95) episodes.

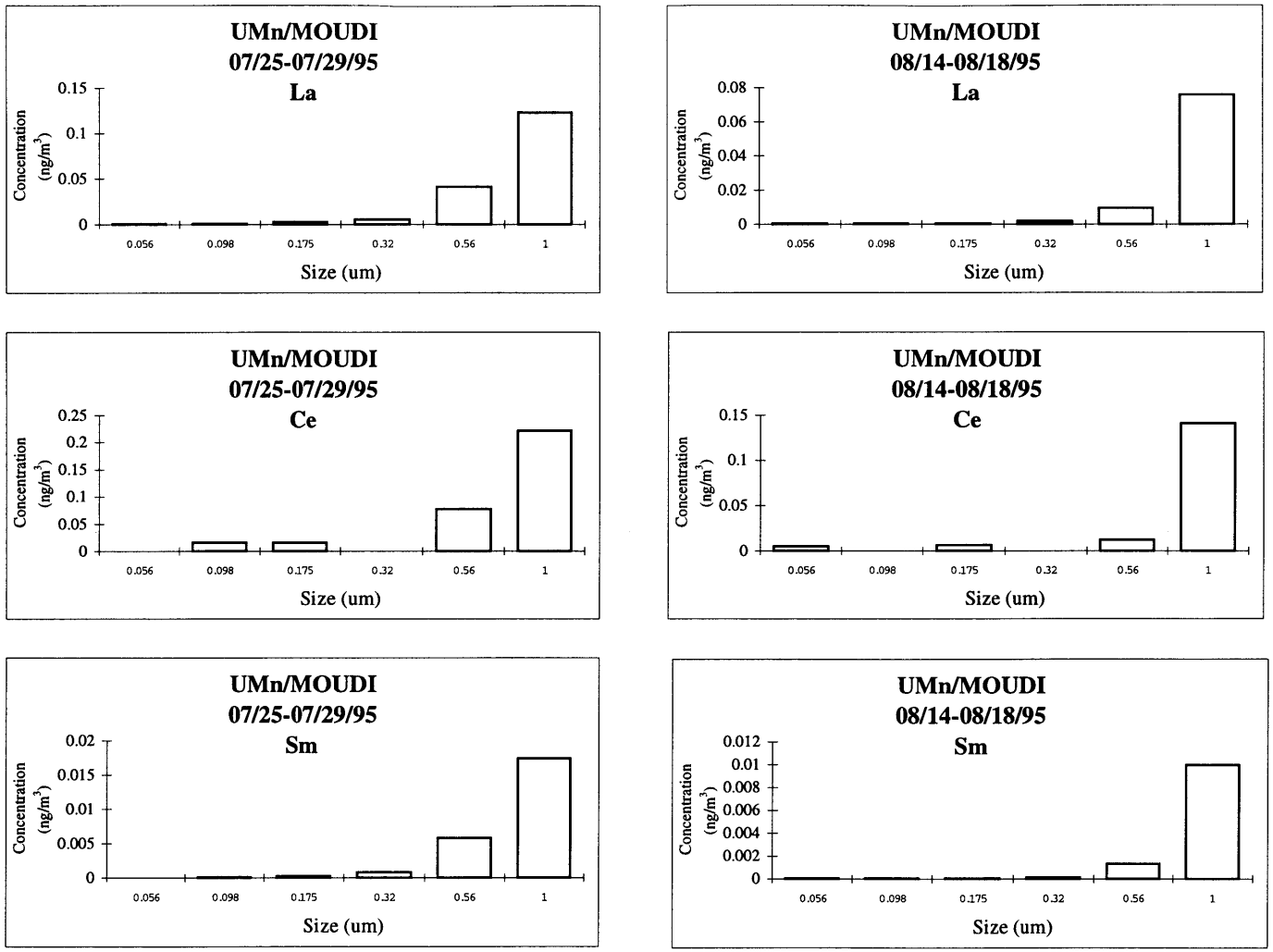

Figure 3.21. Concentration of rare earth elements in UMn/MOUDI samples during dust (07/25-07/29/95) and pollution (08/14-08/18/95) episodes.

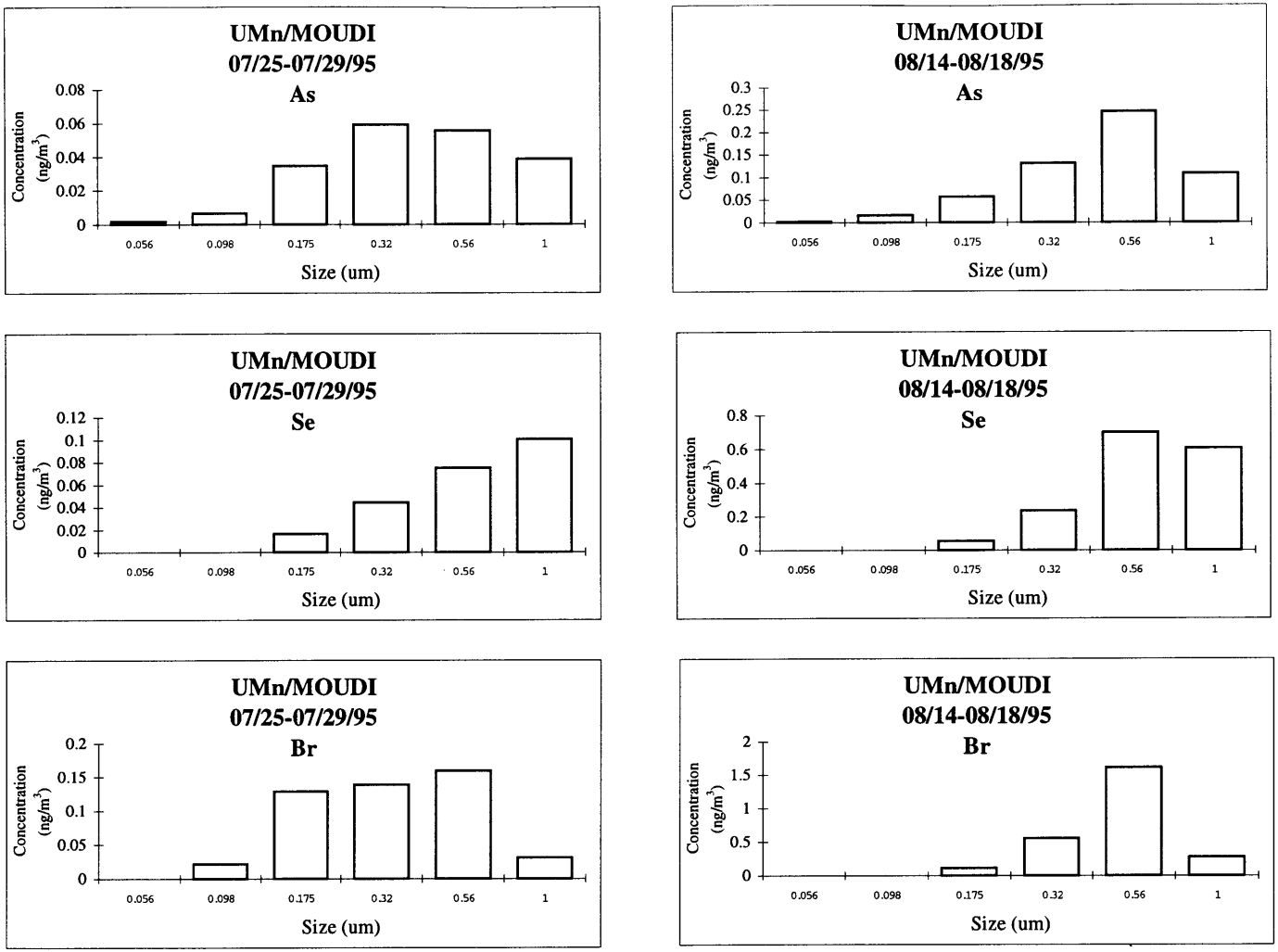

Figure 3.22. Concentration of elements with greater contribution from anthropogenic emissions in UMn/MOUDI samples during dust (07/25-07/29/95) and pollution (08/14-08/18/95) episodes

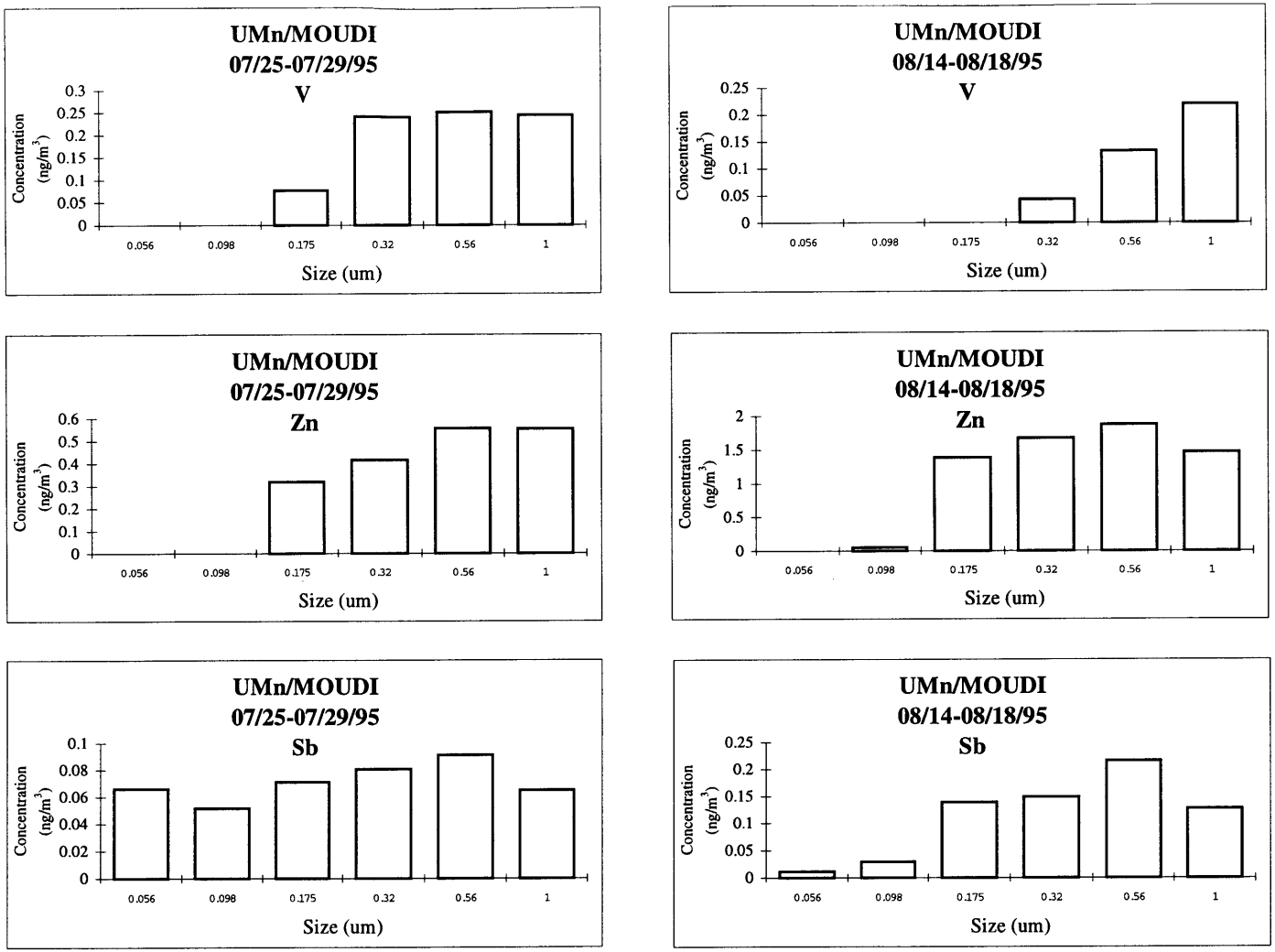

Figure 3.22. (Continued) Concentration of elements with greater contribution from anthropogenic emissions in UMn/MOUDI samples during dust (07/25-07/29/95) and pollution (08/14-08/18/95) episodes

Elemental patterns of fine particulate samples collected from the urban site are quite different from those obtained from the rural site as shown in Figures 3.17 and 3.18. Crustal and rare earth elements have the same pattern and peak at larger sizes for the rural site. This pattern holds for both dust and combustion periods as shown in Figure 3.20. However, elements such as Al and Fe showed higher concentrations on ultra fine stage (0.056-0.097 μm) at the urban site and this pattern is very unique. The light rare-earth elements La and Ce but not Sm were also higher at the urban site. This suggests that there was a source other than crustal material that had an influence on the urban site and caused the observed shift of elemental distributions.

In order to determine the source of the Al and Fe on the ultra fine stage of the urban site, the elemental pattern was examined for each sample set. Figure 3.23 shows the concentration distributions of Al, Fe, Sm and Sc for the last two runs. Samarium and Sc are mostly generated from soil dust in the form of fine particles with no known anthropogenic sources. Their concentration distributions may be used to represent the impact from dust particles. The increased concentration of these elements on the ultra fine stage on February 10, which matched the increased Fe and Al concentrations on the same stage, indicated that very fine dust particles may have caused the increase of the ultra fine Fe loading on February 10. However, the increased concentration shown on the ultra fine stage of Al and Fe did not match the pattern of Sm and Sc on February 17. Aluminum concentration was especially increased on the ultra fine stage on that day, and an additional source other than crustal origin may be important for its increased concentration.

The Los Angeles basin is well known for its high level of motor vehicle traffic and motor vehicles are known to be an important source of fine particles. Huang et al. (1994) has shown that motor vehicles emit considerable amount of rare earth elements such as La and Ce because of their use in catalytic converters. Figure 3.24 shows the concentrations of La, Ce and V for the last two runs of the urban site. Lanthanum and Ce may also have come from a crustal source, and the first four runs showed their distribution to be quite like a crustal element such as Sm. However, during the last run La

and Ce patterns changed drastically and they did not match Sm. This indicates that they may have come from another source.

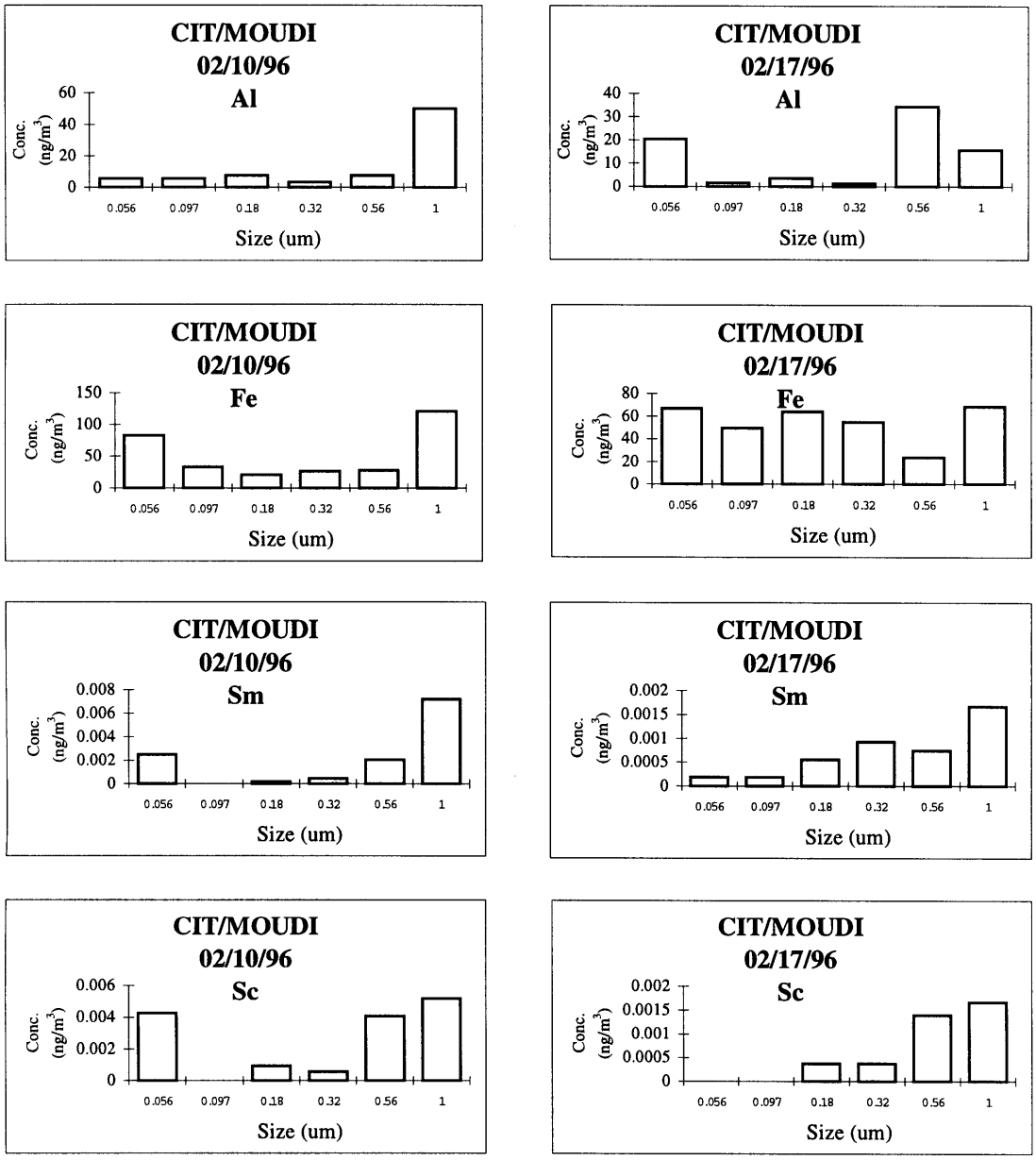

Figure 3.23. Concentration distributions of Al, Fe, Sm and Sc on CIT/MOUDI samples collected for the last two runs

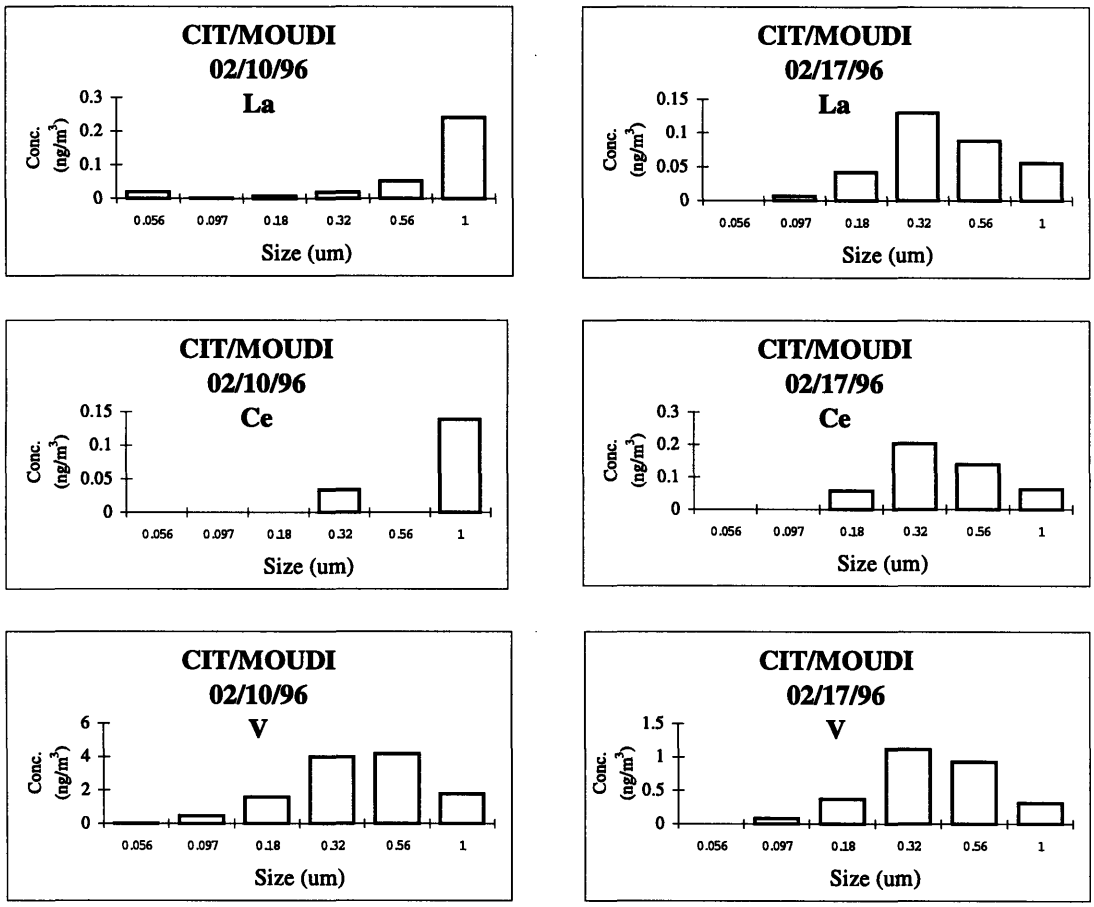

Figure 3.24. Concentration distributions of La, Ce, and V on CIT/MOUDI samples collected for the last two runs

Lanthanum and Cerium may also be emitted from oil fired power plants due to the use of Zeolite cracking catalysts during fuel oil refining processes (Olmez, 1985). However, if they were released from oil combustion, V, which is a good marker element for oil combustion, should have also changed during this period. The La and Ce concentrations on the last run were increased significantly in 0.32-1.0 μm range, but the V pattern did not change during the entire period and its concentration was higher on January 29 among 0.32-1.0 μm range than during the last run. This indicates that the increased concentrations of La and Ce in the last run may due to an increased concentration of emissions from motor vehicles which also have caused the increase in Al and Fe concentrations in the ultra-fine range (0.056-0.097 μm).

3.3.2 Depletion of Chlorine on Fine Aerosols

Sodium and chlorine in fine aerosol originate mostly from sea salt which is generated by the bursting of bubbles from the surface water layer (Blanchard and Woodcock, 1980). Fresh sea-salt aerosol has the same composition as bulk seawater with Cl/Na mass ratio of 1.8, identical to bulk sea water. The sea-salt aerosol over the tropical Pacific was found to be centered at 0.1 μm size (Hoppel and Frick, 1990) and 0.09 μm in the remote tropical Atlantic (Hoppel et al., 1985). As the sea-salt aerosol grows, different atmospheric reactions may affect the Cl/Na ratio. Legrand and Delmas (1988) found that over the Antarctic the reaction of excess sulfate with sea-salt particles results in the release of HCl gas into the atmosphere and the retention of Na_2SO_4 in the aerosol. The process causes a considerable amount of Cl loss. Raemdonck and Maenhaut (1986) showed as much as 40% Cl had been lost in submicrometer particles. In urban areas, an excess amount of NO_2 may dissolve into fine water droplets and generate HNO_3. The nitric acid may interact with NaCl and generate HCl gas and $NaNO_3$ (Hood, 1971). This chemical reaction may also cause loss of Cl from the sea-salt aerosol. Figure 3.25 shows

the average concentration of Na and Cl on UMn/MOUDI and CIT/MOUDI samples. Sodium has the highest concentration at 1.0-1.8 μm range, but Cl shows a higher concentration in the range of 0.56-1.0 μm at the urban site and in the range of 1.0-1.8 μm range at the rural site.

Table 3.8 shows the Cl/Na mass ratio of fine particulates from UMn/MOUDI and CIT/MOUDI samples for the entire sampling period. Sodium may also be found in crustal material, but the contribution from that source is much lower than that from marine emissions. The small Cl/Na mass ratios indicate that these fine particles are highly aged sea-salt aerosols which have lost Cl during transport. The only Cl/Na ratio that is larger than the ratio of Cl to Na in sea water on the UMn/MOUDI samples occurred between August 14 and 18, 1995 when combustion emissions contributed a considerable amount to the total fine aerosol mass. The increased ratio of Cl/Na in the 0.32-1.0 μm range on February 17, 1996 of the CIT/MOUDI samples matched the increased La and Ce concentrations on that day. Huang, et al (1994) reported that the Cl emission from motor vehicles may be up to 16000 ng/m^3 with a median value of 770 ng/m^3 for fine ($d_a < 2.5$ μ m) aerosol. Motor vehicle emissions on February 17, 1996 at the urban site as indicated earlier may also have increased the Cl emission and hence increased the Cl/Na ratio on that day.

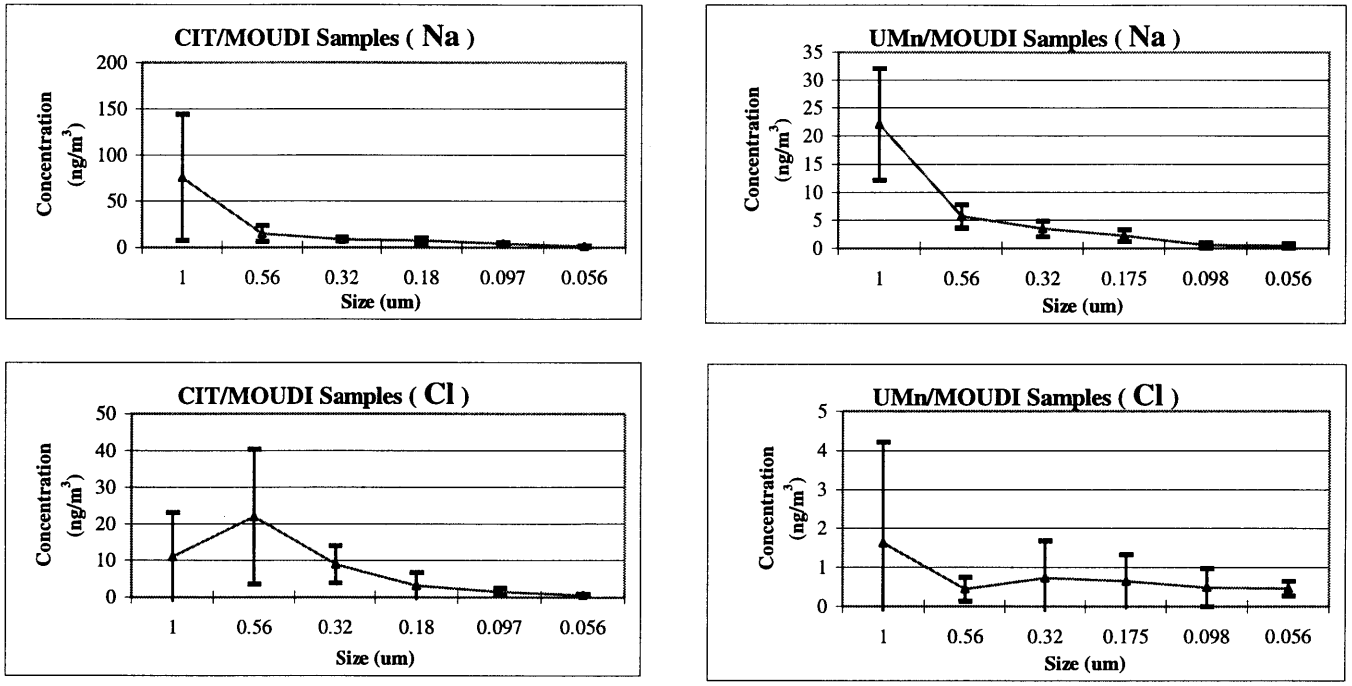

Figure 3.25. The average concentration of Na and Cl on UMn/MOUDI and CIT/MOUDI samples

Table 3.8. Cl/Na mass ratio of UMn/MOUDI and CIT/MOUDI samples at different stages

CIT/MOUDI

Size/Period	1/23/96	1/29/96	2/4/96	2/10/96	2/17/96
0.056-0.097 um		0.66	0.50	1.19	0.23
0.097-0.18 um	0.39	0.68	0.06	0.48	0.34
0.18-0.32 um	0.75	0.14	0.38	0.37	0.19
0.32-0.56 um	1.71	0.64	0.49	0.50	2.16
0.56-1.0 um	0.61	1.16	0.55	1.18	3.74
1.0-1.8 um	0.06	0.07	0.04	0.15	0.33

UMn/MOUDI

Size/Period	07/15/1995 - 07/19/95	07/20/1995 - 07/24/95	07/25/1995 - 07/29/95	07/30/1995 - 08/03/95	08/04/1995 - 08/08/95	08/09/1995 - 08/13/95	08/14/1995 - 08/18/95	08/19/1995 - 08/23/95	08/24/1995 - 08/25/95
0.056-0.098 um	1.54			1.02	1.22	1.13	2.39	1.80	0.61
0.098-0.175 um	1.16	0.73	0.07	0.01					1.61
0.175-0.32 um	0.72	0.14	0.08	0.27					0.01
0.32-0.56 um	0.63	0.22	0.07	0.12		0.25	0.03	0.04	
0.56-1.0 um	0.38	0.14	0.04	0.05		0.04	0.04	0.05	0.04
1.0-1.8 um	0.13	0.01	0.02	0.10		0.01	0.01	0.03	0.21

Chapter 4

SOURCE IDENTIFICATION BY STABLE ISOTOPE RATIOS

Different isotopes of a given element have unequal masses due to a different number of neutrons in their nuclei. The chemical properties of isotopes are similar because they have identical number of electrons, but the binding energies of chemical compounds they form may be different because of the mass differences as explained by statistical mechanics (Bigeleisen and Mayer, 1947; Kaye, 1992; Galimov, 1985; Hoefs, 1997). The bonds formed by a lighter isotope are weaker than the bonds formed by a heavier one and thus molecules bearing the lighter isotope will, in general, react slightly faster than molecules bearing the heavier isotope. This may cause an 'isotopic fractionation' in chemical reactions that slightly enriches the relative concentration of the lighter isotope in the product.

A second factor that can cause isotope fractionation has been found to be independent of mass (Thiemens and Heidenreich, 1983; Thiemens, 1992, Cliff and Thiemens, 1997). This unusual isotope fractionation occurs when ozone is produced from an electrical discharge in pure O_2. An equal enrichment of ^{17}O and ^{18}O was observed in the reaction product, rather than $\delta^{17}O = 0.5\ \delta^{18}O$ as expected from a mass-dependent process. The reason for the mass-independent effect might be related to the symmetry of the molecule due to the chemical reaction rate change that occurs when the nuclear symmetry of the system is reduced by isotope substitution (Gellene, 1996). A decrease in symmetry may enhance the stabilization step for ozone formation and change the enrichment of different oxygen isotopes.

The stable isotope ratio is defined as the relative abundance of two different isotopes of a given element. In this thesis, the isotope ratio is defined as the ratio of the lighter isotope to the heavier one. Changes in isotope ratio may change the equilibrium constant and the result of a chemical reaction. Because isotope ratios are affected by the

equilibrium state of a chemical reaction, the isotopic ratio of the reaction products might be used to identify the type of reaction which produced the species being studied.

4.1 Element Selection

Stable isotope ratios were determined by applying the INAA technique. Although this method is very sensitive for many elements and is inherently an isotopic analysis, there are several limitations in its application. The first requirement for INAA is that the interaction probability of a nucleus with thermal neutrons, which is called the thermal neutron cross section, is large for the selected isotope. This is necessary in order to produce enough activated nuclei in a reasonable irradiation time. Another limitation for INAA is that the half-life of activated nuclei should be roughly within a range of minutes to years. A half-life longer than about one minute provides enough time to transfer the sample from the reactor to the detector without significant loss of the activated isotope. The half-life shorter than a few years ensures that the gamma detectors can detect enough decays within a few days. The percentage of gamma rays emitted at a specific energy, which is called the branching ratio, should be high enough so that sufficient gamma rays are emitted for an accurate activity determination.

INAA has a minor problem of gamma ray interference which may reduce the reliability of the result. Primary interference occurs when the isotope used to determine a specific element is also produced from another element present in the sample. For example, ^{28}Al, which is used to determine the aluminum concentration in a sample may be generated from both the ^{27}Al (n, γ) and the ^{28}Si (n, p) reactions. The only way to correct for such interference is to irradiate a known amount of Si with the sample and then use the activity from Si as a correction. Secondary interference occurs when the gamma rays emitted from different isotopes are of such similar energies that they can't be resolved by the gamma ray detector. This problem can be reduced either by allowing a sample to decay for several days before counting so as to eliminate gamma rays from short half-life elements, or by using a higher resolution detector. In this study, interference was minimized by the appropriate choice of elements and by the use of a

High Purity Germanium detector with an energy resolution of about 1.7 keV at the 1332 keV ^{60}Co peak.

The stable isotopes that satisfy most of these requirements and are measured routinely by INAA in atmosphere particulate samples are listed in Table 4.1. These elements exhibit a variety of chemical properties which might make them useful for source identification.

Table 4.1. Potential elements and isotopes used for stable isotope ratio study *

Element	Isotope	Cross Section (b)	Isotope Abundance	Half Life	Gamma Ray Energy (keV)	Branching Ratio (%)	Interference
Zn	64	0.76	0.486	243.9 d	1115.55	50.75	Sc-46, Eu 152, Tb-160, Ta-182
	68	0.07	0.188	13.76 h	438.6	94.8	Ce-137
Se	74	51.8	0.009	119.77 d	264.65	58.6	Ta-182, Cd-115, Bi-210
	80	0.08	0.4982	57.25 m	103	10.5	Sm-153, Sm-155, Eu-159, Ir-196m
Br	79	11.1	0.5069	17.68 m	617	7.2	Os-190, Pd-111
	81	2.6	0.4931	35.3 h	776.5	83.4	Mo-99, Pd-111
Sr	84	0.81	0.0056	64.84 d	514	99.3	
	86	0.769	0.0986	2.81 h	388.4	83	Zn-71m, Os-193, Kr-79
Sb	121	6.255	0.573	2.7 d	564.1	70	As-76, Cs-134, Eu-152, Ir-194m
	123	4.048	0.427	60.2 d	1690.98	49	
Ba	130	11	0.00106	11.8 d	496.3	43.8	Ru-103, Sm-145
	138	0.4	0.717	84.63 m	165.8	22	

* All values in this table is based on Neutron Activation Analysis Tables by Michael D. Glascock of University of Missouri Research Reactor Facility, 1985.

4.2 Stable Isotope Ratios for Selected Standards

Well-homogenized standard reference materials of different origins were used to determine whether stable isotope ratio differences could be observed by INAA. The standard reference materials that were used in this study were the National Institute of Standards and Technology's (NIST) Coal Fly Ash (SRM1633), Orchard Leaves (SRM1571), Bovine Liver (SRM 1577), and Coal (SRM 1635). Also used was an U.S.

Geological Survey (USGS) standard AGV-1 Andesite. In Table 4.2, concentrations and standard deviations of certified elemental concentrations are given.

Table 4.2. Elemental concentrations of selected elements in standards

Element	Standard (unit : ppm)				
	SRM 1571 (OL)	SRM 1577 (BL)	SRM 1633 (FA)	SRM 1635 (Coal)	AGV-1 (AN)
Zn	25±3	130±6	210±20	4.7±0.5	88±2
Se	0.08±0.01	1.1±0.1	9.7±0.7	0.9±0.3	
Br	9.7±1.1	9.2±1.1	8.6±2.3		0.34±0.17
Sr	37±1	0.14	1410±120		662±9
Sb	2.9±0.3	0.009±0.005	6.8±0.6	0.14	4.4±0.6
Ba	42±9	1.6±1.4	2700±200		1221±16

Standard samples weighting 30-50 mg were irradiated twice in the MITR-II reactor at a thermal neutron flux of 8×10^{12} n/cm^{2}s for two different time intervals and measured for gamma spectra over four different combinations of decay times and counting durations to get the best results for each isotope. Samples were first irradiated for 50 seconds and counted as soon as was possible for 30 minutes to observe gamma rays from ^{79}Br. They were then counted for one hour right after the 30 minute counting to observe gamma rays from ^{80}Se, ^{86}Sr and ^{138}Ba. After being allowed to decay for several days, samples were irradiated again for six hours and cooled for four days before counting. They were then counted for nine hours to observe gamma rays from ^{81}Br, ^{121}Sb, and ^{130}Ba. Following a second cooling period of two weeks, they were re-counted for 10 hours to observe the activities of ^{64}Zn, ^{74}Se, ^{84}Sr, and ^{123}Sb. Figure 4.1 shows the schematic of the counting geometry on HPGe detectors. The Cu/Al layer was used to reduce the *bremsstrahlung* induced in the lead shielding. The standards were packed in 1 ml vials and positioned identically for each counting. Background activities for all of the detectors were carefully determined at different energies and, if necessary, the background activities were subtracted before calculating the specific activity and isotopic ratios.

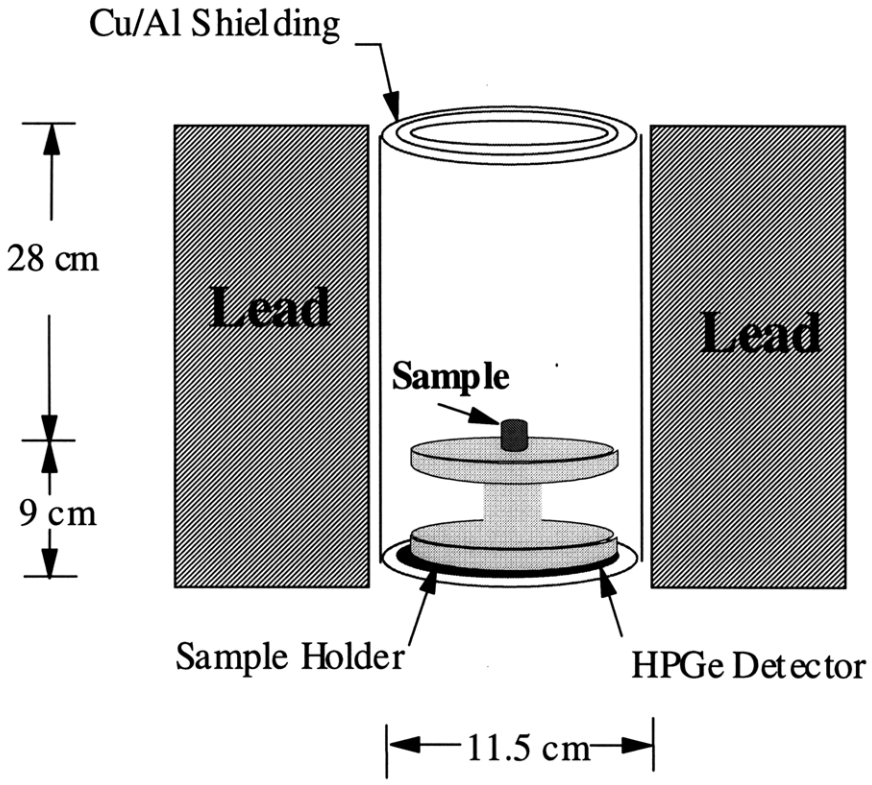

Figure 4.1 Schematics for sample counting on HPGe detectors

In order to check the stability of the neutron flux during short irradiation, gold flux monitors were irradiated at the beginning and end of the experiment and were counted for 20 minutes after being allowed to decay for five days. Table 4.3 lists the activities and calculated thermal neutron fluxes at two different times. The flux variation was found to be less than 1%. Absolute detector efficiencies were determined for each detector by using a mixed-radionuclide point-source standard (NIST SRM 4275C) with gamma rays covering the energy range of 86.5 to 1596 keV. The point standard was counted in the same geometry as the standard samples. The efficiency curve of each detector is given in Figure 4.2.

Table 4.3. Thermal neutron flux calculated using gold flux monitors

Gold Flux Monitor	Mass(g)	Half-Life (day)	Cross Section (barn)	Activity (counts/s)	Thermal Neutron Flux (n/cm^2 s)
Beginning	0.000101	2.7	98.65	297	8.43E+12
End	0.000101	2.7	98.65	301	8.54E+12

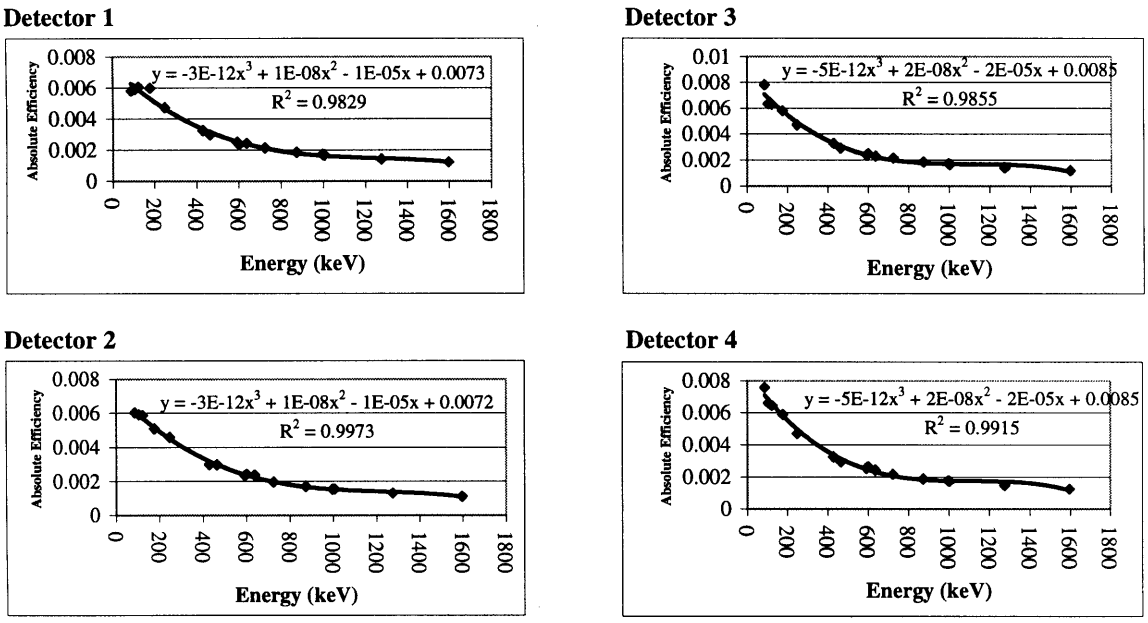

Figure 4.2. Absolute efficiencies of the HPGe detectors at different energies

Summary Tables 4.4 and 4.5 show the average specific activity and isotopic ratios of the selected elements (based on the criteria of Section 4.1) for the five standards. The full data are included in Appendix C. Eight samples of each standard were irradiated and if the net number of counts for each isotope was greater than 500 after background corrections, the results were included in further calculations. The "$\pm$" column represents the range of the measurements. The datum with no "$\pm$" shown is from a single measurement. Zinc and selenium are not included in this table because of the poor detection limits. The isotope Zn-68 has the smallest thermal neutron cross section among all of the candidate isotopes and its activity was too low to be detected. The detection of

selenium isotope ^{74}Se is complicated by a secondary interference from ^{210}Bi. This was difficult to correct for in the samples because ^{210}Bi is also a daughter product from ^{238}U decay. Therefore, Zn and Se were not used for further isotopic ratio analyses.

In Table 4.5, Ba shows the most significant differences in isotopic ratios among the different reference materials. Antimony also shows differences in isotopic ratios among the samples, but because of the long half-life of ^{123}Sb, only a small number of counts were recorded from this isotope, and this increased the statistical error and uncertainty of these ratios. Strontium also showed different $^{84}Sr/^{86}Sr$ ratios between the fly ash and AGV-1 Andesite samples, but the results contained large standard deviations. The isotopic ratio of $^{79}Br/^{81}Br$ was subject to great uncertainty in the two biological standards (Orchard Leaves and Bovine Liver) because of the small number of counts recorded. Additionally, the sodium activities in these biological samples were high after irradiation, and the Compton scattering from Na increased the background of the gamma ray spectra. The natural abundance of ^{130}Ba is only 0.106%. However, the large thermal neutron cross section of ^{130}Ba (11 barns) makes it easily detected by neutron activation analysis. Barium concentrations in fly ash and AGV-1 Andesite are high (2700 and 1221 ppm) and the isotope ratio difference is clear. Each fly ash and AGV-1 Andesite sample was checked for the $^{130}Ba/^{138}Ba$ ratio and these results are shown in Table 4.6. To compare the Ba isotope ratios determined in this study with those reported previously, isotopic ratios of $^{130}Ba/^{138}Ba$ were converted to delta values based on Equation 1.1. In the calculation of delta values listed in Table 4.6, the average ratio of $^{130}Ba/^{138}Ba$ in fly ash was used as a reference (R_s). The result showed that all the AGV-1 Andesite samples have higher $^{130}Ba/^{138}Ba$ ratios (positive δ values) than the coal fly ash.

To obtain the results shown in Table 4.6, reference materials were counted on four HPGe detectors to save counting time. Two samples of each reference materials were counted on the same detector (first two samples of each group such as FA001, FA002, AGV1001 and AGV1002 were counted on detector 1. The two samples next to them in the sequence FA003, FA004, AGV1003 and AGV1004 were counted on detector 2, etc.). Corrections to the number of counts based on the absolute detector efficiencies shown in Figure 4.2 were made to produce the isotope ratios. Additional uncertainties from curve

fittings performed to determine absolute detector efficiencies may also have affected the final results. To eliminate this uncertainty and to confirm the findings for $^{130}Ba/^{138}Ba$ ratios, six new fly ash and AGV-1 Andesite samples were irradiated following the same procedure described above. These were then all counted on the same detector. The experimental results and delta values from these analyses are listed in Table 4.7. The seal of one sample in the fly ash group (FA002) was broken after irradiation and it was not included in Table 4.7. The positive delta values on all AGV-1 samples substantiate the finding of different $^{130}Ba/^{138}Ba$ ratios in the fly ash and Andesite.

Table 4.4. Specific isotopic activities (counts/s g) determined by INAA

	Half Life	Energy (keV)	FA	OL	AGV1	COAL	BL
Br-79	17.68m	616.2		13.81 ± 4.49			11.21 ± 0.62
Br-81	35.3 h	776.8		116 ± 5			111 ± 6
Sr-84	64.84 d	514	1.62 ± 0.38		0.71 ± 0.10		
Sr-86	2.81 h	388.4	45 ± 2	2.48	21 ± 4	4.37 ± 0.40	
Sb-121	2.7 d	564.1	87 ± 6	37 ± 4	58 ± 6	2.48 ± 0.72	3.35 ± 0.41
Sb-123	60.2 d	1690.98	0.60 ± 0.07	0.24 ± 0.02	0.44 ± 0.05		
Ba-130	11.8 d	496.3	13 ± 1	0.29	6.37 ± 0.63	0.59 ± 0.34	
Ba-138	84.63 m	165.8	201 ± 5		89 ± 6	6.68 ± 3.27	

Table 4.5. Isotopic ratios determined by INAA

	FA	OL	AGV1	COAL	BL	Ref.*
Br-79/81		0.87 ± 0.30			0.85 ± 0.19	1.03
Sr-84/86	0.047 ± 0.013		0.045 ± 0.008			0.057
Sb-121/123	1.01 ± 0.06	1.09 ± 0.07	0.99 ± 0.06			1.34
Ba-130/Ba138	0.00108 ± 0.00006		0.00120 ± 0.00006	0.00163 ± 0.00001		0.0015

* Reference calculation is based on the isotope abundance listed in Table 4.1

FA = Coal Fly Ash, OL = Orchard Leaves, AGV1 = AGV-1 Andesite, BL = Bovine Liver

Table 4.6. Specific activity, isotopic ratio, and delta value of $^{130}Ba/^{138}Ba$ in each of the fly ash and AGV-1 Andesite samples

Sample ID	Specific Activity Ba-130 (c/s/g)	Specific Activity Ba-138 (c/s/g)	Ba-130/Ba138 Isotope Ratio	Delta Value (FA Reference)
FA001	13.7	206	0.00112	
FA002	13.5	197	0.00115	
FA003	12.2	204	0.00097	
FA004	12.6	192	0.00107	
FA005	12.5	206	0.00103	
FA006	13.4	201	0.00113	
FA007	13.5	208	0.00110	
FA008	12.3	198	0.00105	
AGV1001	6.9	92	0.00124	148
AGV1002	7.0	93	0.00125	162
AGV1003	6.9	89	0.00126	172
AGV1004	6.2	89	0.00114	55
AGV1005	6.7	100	0.00116	72
AGV1006	6.1	84	0.00123	140
AGV1007	6.1	88	0.00118	93
AGV1008	6.6	102	0.00110	22

Table 4.7. Experimental result of $^{130}Ba/^{138}Ba$ ratio on fly ash and AGV-1 samples counted on the same HPGe detector.

Sample ID	Specific Activity Ba-130 (c/s/g)	Specific Activity Ba-138 (c/s/g)	Ba-130/Ba138 Isotope Ratio	Delta Value (FA Standard)
FA001	13.0	235	0.00112	
FA002				
FA003	12.5	233	0.00108	
FA004	12.4	241	0.00104	
FA005	14.3	255	0.00114	
FA006	12.0	219	0.00111	
AGV1001	7.0	104	0.00135	236
AGV1002	6.1	109	0.00112	24
AGV1003	6.3	106	0.00120	99
AGV1004	7.1	124	0.00116	57
AGV1005	6.4	109	0.00119	85
AGV1006	6.2	106	0.00117	69

4.3 Source Identification of Fine Particles by Stable Isotope Ratios

One major reason for using stable isotope ratios in this study was to attempt to identify particles of different origins in the atmosphere by their different stable isotope ratios. In the previous section, it was demonstrated that INAA can be used to detect differences in the stable isotope ratio between some reference materials with high concentrations of the elements of interest. The same procedure was used to test isotope ratios of fine atmospheric particles with known origins.

Fine particulate samples collected previously and analyzed for their elemental compositions (MIT/SU samples described in Section 3.2) were used for the isotope ratio study. The sources of these particles (i.e. crustal and combustion emissions) were identified and their contributions to fine aerosol masses determined (Section 3.2). The

distinct contributions from these two sources during two sampling periods provided an opportunity to study the isotope ratios of the four selected elements, Br, Sr, Sb and Ba.

To increase the total number of counts measured for each isotope and reduce statistical errors, groups of fine particulate samples known to be from the same source were wrapped together in a 37 mm Teflon® filter. Teflon® filters used to wrap the integrated samples were analyzed for their elemental concentrations by INAA and the results are listed in Table 4.8. Of the elements used in the isotope ratio study, Br and Sb are found in significant levels in the Teflon® filter material. However, the integrated fine particulate samples have much higher Br and Sb concentrations (17.9 and 90.7 ng for Br, 5 and 27.5 ng for Sb) and the blank corrections for the Teflon® filter were negligible.

Table 4.8. Element concentrations in 37mm Teflon filter (ng/filter).

Element	Concentration (ng/Filter)
Na	42±9
Al	65±13
Cl	34±14
Sc	0.026±0.002
Ti	28± 20
V	2±0.1
Cr	8±2.5
Mn	4.3±1.8
Fe	220±30
Co	2.8±0.3
Zn	23±7
As	0.1± 0.06
Se	1.2±0.1
Br	0.68±0.05
Cd	0.36±0.28
Sb	0.25±0.2

The 2.1 μm fine particulate samples which originated primarily from crustal emissions and which were collected between 07/24/95 and 07/26/95 were grouped together, and samples which primarily contain combustion emissions obtained between

08/14/95 and 08/18/95 were also grouped together. Table 4.9 shows the enrichment factor (EF) for the four selected elements during these two periods. The EF values between 07/24/95 and 07/26/95 were closer to unity for all elements compared to the EF values between 08/14/95 and 08/18/95. This indicated that natural soil had a greater contribution to these elements between 07/24/95 and 07/26/95.

Table 4.9. Average enrichment factors of Br, Sr, Sb and Ba during crustal dust and combustion episodes.

Element	Dust Episode (07/24/95-07/26/95)	Combustion Episode (08/14/95 – 08/18/95)
Br	82±78	420±350
Sr*	2.28	4.17
Sb	260±220	1500±460
Ba	3.41±1.21	6.25±5.08

* Only one measurement above detection limits during the sampling period

The two integrated samples were irradiated for 40 minutes and they were then transferred to un-irradiated 1 ml polyethylene vials for counting. Samples were counted twice on the same HPGe detector for 30 minutes to measure activities from ^{79}Br and ^{138}Ba. Their average values were then used to improve the statistical results. Isotopes with less than 500 counts were not included in the isotope ratio calculation. The integrated combustion sample was also counted for 2 hours after the two 30 minute counts to measure the activity of ^{138}Ba. Two-hour counting was not done on the integrated crustal sample because of low activity after a one-hour decay of that sample. Differences in the thermal neutron flux were less than 1% as monitored by the gold flux monitors described earlier.

Integrated samples were allowed to decay for several days and then irradiated again for 24 hours. They were allowed to decay for five days, then transferred to un-irradiated 1 ml polyethylene vials and counted twice on the same HPGe detector as before

for 12 hours to measure activities from ^{81}Br and ^{121}Sb. Samples were again counted on the same detector for seven days after the two 12 hour counts to measure activities from ^{130}Ba and ^{123}Sb. Figure 4.3 shows the irradiation and counting scheme for the integrated samples. The absolute detector efficiency was determined again by using the same mixed-source standard (SRM 4275C) and the result is shown in Figure 4.4. The distance from sample to detector was reduced from 9 cm to 6 cm to increase the absolute detector efficiency for these samples.

The results obtained from these integrated particulate samples are listed in Table 4.10 and the complete data are included in Appendix C. The "$\pm$' column shown in Table 4.10 represents the range of the calculations from the two counts on the same integrated sample. Samples were counted twice on the same HPGe detector to get the average value. An exception was the 7 days counts to determine ^{130}Ba and ^{123}Sb. These were done only once. The background value was subtracted from the sample activities before calculating the isotope ratio.

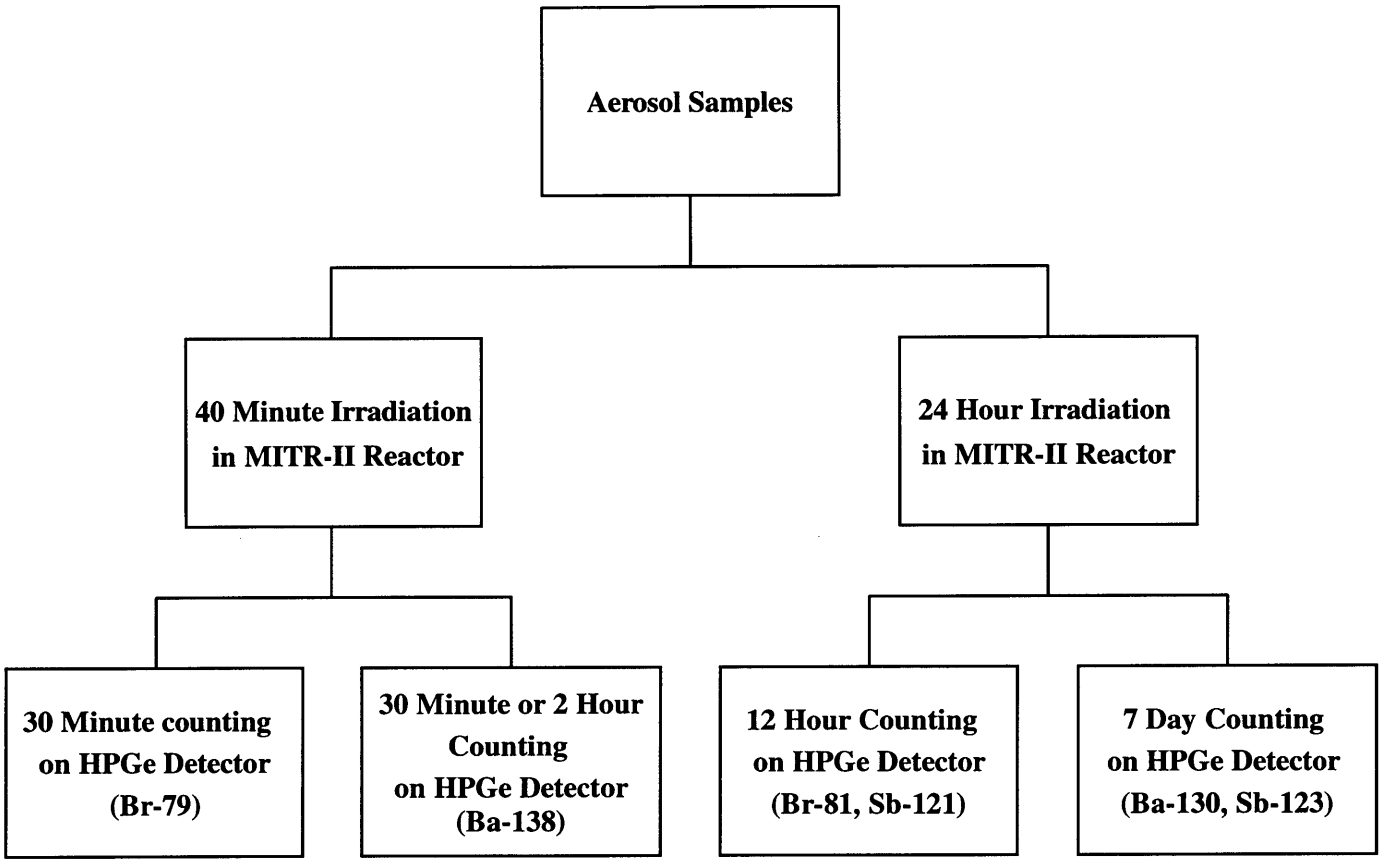

Figure 4.3. Thermal neutron irradiation and counting diagram for integrated fine aerosol samples in stable isotope study.

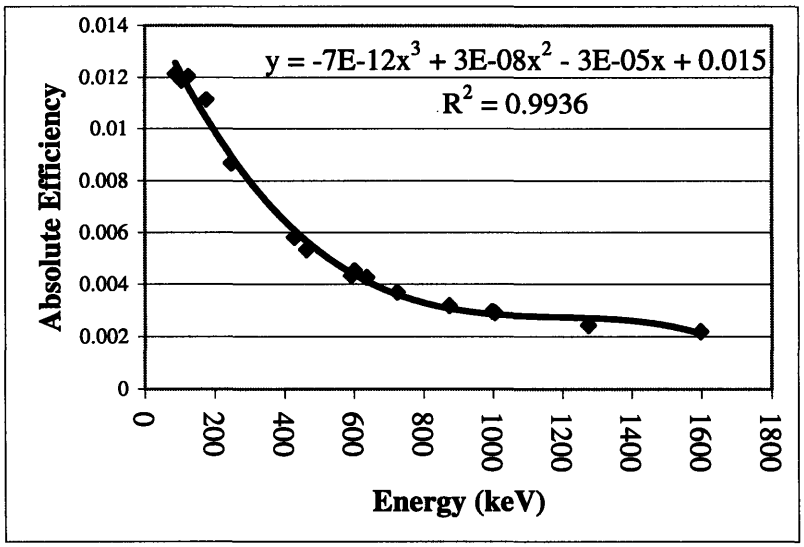

Figure 4.4. Absolute detector efficiency of HPGe detector used in determining fine aerosol isotope ratios.

Table 4.10. Stable isotope ratios from integrated crustal and combustion samples

	Dust	Combustion
Br-79/81	0.253 ± 0.003	0.150 ± 0.001
Sr-84/86		
Sb-121/123	1.75 ± 0.13	2.24 ± 0.21
Ba-130/138	0.00151 ± 0.00008	0.00109 ± 0.00003

Table 4.10 does not include the stable isotope ratio of Sr because of the low number of counts detected by the HPGe detector. Strontium concentrations were high in the SRM standards (1410 ppm in fly ash and 662 ppm in AGV-1 Andesite), but they were low in these fine particulate samples (only 5.6 ng/m^3 on 07/25/95 and 2.1 ng/m^3 on 08/18/95). The small thermal neutron cross sections of the Sr isotopes combined with low natural abundance made them undetectable by INAA at such low concentrations. The stable isotope ratios of $^{121}Sb/^{123}Sb$ in both integrated fine particulate samples were significantly higher than the ratio in the SRM samples, which ranged from 0.99 to 1.09, and the combustion sample had the highest $^{121}Sb/^{123}Sb$ ratio. The $^{79}Br/^{81}Br$ ratios in these

integrated samples were very different between the two episodes, and were much lower than in the standards in which they could be measured (i.e. Orchard Leaves and Bovine Liver). The $^{130}Ba/^{138}Ba$ ratios also differed significantly between the two episodes, although the values were in the same range as the ratios for the standards (fly ash, Andesite, coal, Table 4.5).

It has thus been demonstrated that INAA can be used to measure stable isotope ratios in both laboratory standard materials and, more importantly, in samples of atmospheric particulate material. The fact that significant differences in the isotope ratios of these elements were observed between aerosol samples dominated by two different source types indicates that these isotope ratios can be an extremely useful measurement for identifying the sources of atmospheric particulates. If a sufficient library of isotope ratios is tabulated for the sources of atmospheric particulates, this technique may make it possible to identify the sources contributing to single aerosol samples. Additionally, the technique may be applied to other types of environmental samples such as ground water and sediments. It is likely that it will be possible to measure the isotope ratios of elements other than those determined in this study of aerosols only.

CHAPTER 5

SUMMARY

5.1 Thesis Summary

Pollution source identification has always been a challenging topic for scientists. Knowledge of pollution sources is essential in controlling their emissions so as to protect the environment. Studies of fine particles in the atmosphere show that the amount of these particles has increased due to human activities, and the toxic metals attached to them may have a significant impact on human health. Ultra-fine particles may be especially hazardous because of their ability to penetrate deeply into the lungs. However, their compositions are still rarely studied because of sampling and analytical constraints.

There are several major contributions to the field of environmental sciences from this study. The first achievement is to determine the elemental compositions of fine and ultra-fine particles in the atmosphere. The thesis focused on particles with an aerodynamic diameter less than 2.4 μm because they are more important for human health and visibility. After determining the composition of these particles, the next objective is to identify the source of these fine particles. Several techniques, such as Factor Analysis (FA) combined with Absolute Factor Score-Multiple-Linear Regression (AFS-MLR), Enrichment Factor (EF) calculation, and elemental patterns were used for this purpose. The problems in identifying pollution sources mostly result from the complexity of the atmosphere. Changes in the properties of pollutants during atmospheric transport make traditional dispersion models of only limited use. Factor analysis is a statistical technique that reduces the dimensionality of a data set by combining interrelated variables so that a minimum number of components or factors can explain the maximum variance of the original data. When applied to a series of environmental samples, each factor often represents a source type or region which influences the concentrations of the measured

species. This technique combined with multiple linear regression is used widely by environmental scientists to identify sources of fine particles in the atmosphere. Factor analysis does not require *a priori* knowledge of the sources impacting a certain area, but it can not separate sources that fluctuate together such as pollutants carried by winds from the same direction. Enrichment factor analysis using a double normalization and average crustal concentration ratios can only be applied to fine particles due to changes in average crustal composition among different size fractions.

Because existing source identification techniques have certain limitations, the last contribution of this thesis is to develop an additional technique to identify atmospheric pollution sources. Stable isotope ratios primarily measured by mass spectrometry have previously been used for this purpose. However, the isotope ratio may change during the ionization process, and complex sample preparation is often required. Because Instrumental Neutron Activation Analysis (INAA) is very sensitive for determining the concentrations of isotopes with large thermal neutron cross sections, it has the potential to be used for measuring stable isotope ratios in fine particles.

Particulate samples used in this study were collected from two sites in the United States. Fine and ultra-fine particles were collected at the eastern site in the Great Smokey Mountain National Park from July 15 to August 25, 1995. Two sets of fine particle samples were examined: MIT/SU samples with a maximum size of 2.1 μm, and NPS/IMPROVE samples with a maximum size of 2.4 μm. Size-segregated particles were collected at the western site from a rooftop in Pasadena, California over one winter month in January/February, 1996. The MIT/SU and western samples were analyzed for elemental concentrations at MIT by using instrumental neutron activation analysis, and the NPS/IMPROVE samples were analyzed by X-Ray Fluorescence (XRF) and other analytical techniques. Data from all of these analyses were included in the source apportionment.

The elemental concentrations determined by INAA for the eastern site particle samples were compared with results from samples collected concurrently but analyzed by other techniques, and the results showed consistency between different analytical techniques. Factor Analysis was applied to the INAA results for the eastern site fine

particles to determine the sources of these particles. The factor analysis results showed at least three sources impacting the site. The crustal source contribution was most significant around July 24-26, 1995 which is referred to as the "dust event" due to the large amount of crustal material and the relatively low levels of combustion-related aerosols such as sulfates. The combustion source had significant contributions around August 14-18, 1995 when most of the fine particle mass was due to sulfate; the concentrations of the combustion marker element Se was also high in these samples. From August 14 through August 18 the crustal contribution rose somewhat, although the total mass during this time was dominated by combustion-related sources. The synoptic wind patterns, and the Si/Al and Ca/Al ratios for these samples suggest two distinct source regions for the crustal material in these two periods. The stable isotope ratio of Ba developed in this study gives additional evidence to separate these crustal materials. The third source has not been identified, but its contribution to fine aerosol mass is not as significant as the other two sources.

Most of the fine particulate mass at the eastern site originates from combustion sources and sulfate is the major component. The average contribution from combustion sources to the fine particulate mass is 77$\pm$4 % for the MIT/SU 2.1μm samples and 90$\pm$6% for the NPS/IMPROVE 2.4 μm samples. The average sulfate component of the combustion related particles is 44% in the MIT/SU 2.1μm samples and 36% in the NPS/IMPROVE 2.4 μm samples. The average contribution from crustal sources to the fine particulate mass is 7$\pm$3 % for the MIT/SU 2.1μm samples and is 11$\pm$4% for the NPS/IMPROVE 2.4 μm samples. The difference in the crustal contributions between the MIT/SU and NPS/IMPROVE samples are not statistically significant, but it might be due to differences in the cyclone inlet sizecut of the two aerosol samplers, as the crustal material is primarily found at sizes larger than 2 μm. This difference can be seen in the concentrations of a typical crustal element such as aluminum. The AFS-MLR method for determining the crustal contribution to fine aerosol mass was compared with the oxide summation method, which is based on converting the mass of the major crustal elements to the mass of their corresponding oxide form for each sample. Because the oxide summation method does not account for crustal material other than the oxides of

measured species, it was expected to provide a lower bound for the AFS-MLR analysis. Taking this and the differences in the maximum sampled sizes into account, the calculated crustal contribution results agree rather well.

Enrichment factors were used to assess the crustal contributions of each element in the fine particulate samples collected at the eastern site. The EF compares the elements in an aerosol to the corresponding compositions in other source materials, in this case the global average abundance of crustal components. Elements with EF's less than 10 are referred to as non-enriched elements, and most of these originate from crustal material. Some elements with other known origins such Na (from marine aerosols) and V (from oil combustion) also fall into this range. This may be due to the fact that additional sources for these elements had only a limited impact on the receptor site and thus the elements' natural abundances were not greatly perturbed. Moderately enriched elements ($10<EF<100$) such as Cr, Ba and In may come from both crustal and non-crustal sources (e.g. Cr from smelters, In from incinerators and Ba from the paint industry). Because of the small number of samples and statistical limits, FA could not derive separate factors for the contributions from these sources. Elements that are highly enriched (Zn, Mo, Cl, As, Br, Cd, Hg, Sb, Au and Se) are primarily of anthropogenic origin and may be released to the atmosphere as fine particles or as gases. Selenium has the highest EF, and a strong correlation of Se with sulfate indicates that Se may come from coal combustion.

Elemental patterns for different particle sizes are used to identify sources of ultra-fine particles. Elemental patterns of selected representative elements for sources identified by factor analysis at the eastern site were first determined, and the patterns were then compared with elemental patterns at the western site. The western site is located in the Los Angeles basin, and impacts from urban related sources were significant at this site. Aluminum and iron concentrations were found to be high in the ultra-fine particle range (0.056-0.097μm) at the western site compared to those found at the eastern site. Comparison of the elemental patterns of La, Ce and Sm showed that the increased loading of Al and Fe at the ultra-fine stage of the western site may be related to motor vehicle emissions.

A new technique of using stable isotope ratios determined by instrumental neutron activation analysis to identify sources of fine particulate samples was developed in this research. Four elements Br, Sr, Sb and Ba with more than one stable isotope and large thermal neutron absorption cross sections were used for this purpose. Four standard reference materials from the National Institute of Standards and Technology (NIST) including Coal Fly Ash (SRM1633), Orchard Leaves (SRM1571), Bovine Liver (SRM 1577), Coal (SRM 1635) and a U.S. geological survey standard AGV-1 Andesite were examined first. The results showed that the average $^{130}Ba/^{138}Ba$ ratio was lower in coal fly ash (0.00108 ± 0.00006) than in AGV-1 Andesite (0.00120 ± 0.00006) or coal (0.00163 ± 0.00001). Antimony also showed different isotopic ratios, but the small number of counts from ^{123}Sb recorded by the HPGe detector due to antimony's long half-life increased statistical errors and uncertainties. The $^{84}Sr/^{86}Sr$ ratios in fly ash (0.047 ± 0.013) and AGV-1 Andesite (0.045 ± 0.008) are not statistically different, and it was also subject to large standard deviations due to the low number of counts. Isotopic ratios of $^{79}Br/^{81}Br$ were also subject to greater uncertainties in the two biological standards (Orchard Leaves and Bovine Liver) because of the small number of counts recorded by the detectors. The sodium activities in these biological samples were high after irradiation, and the Compton scattering from Na also increased the background of the gamma spectra.

The use of differences in the $^{130}Ba/^{138}Ba$ ratio between the reference materials was then examined for the purposes of source identifications in fine aerosol samples. The first step to achieve this goal is to build a library of stable isotope ratios from different sources. Fine particulate samples collected from the eastern site with known source impacts were used for this purpose, and the $^{130}Ba/^{138}Ba$ ratio was examined first in these samples. Several particulate samples with the same major source impact were wrapped together in 37 mm Teflon® filters to increase the total number of counts on a HPGe detector and to reduce statistical errors. The contributions from the Teflon® filters to the integrated samples were negligible because of their low elemental concentrations, and did not affect the stable isotope ratios. The crustal aerosol sample was collected between July 24-26, 1995 when natural dust was the major source of fine aerosol mass. The combustion samples were collected from August 14 to August 18, 1995 when the sulfate

and other combustion-related material contributions to fine aerosol mass were high. Gold standards were used to monitor the thermal neutron flux during irradiation, and flux differences were less than 1%.

The results showed that the $^{130}Ba/^{138}Ba$ ratio of the dust sample was 0.00151 ± 0.00008, and the ratio was 0.00109 ± 0.00003 for the combustion sample. The enrichment factor of Ba in these two integrated samples showed that the major source of Ba seemed to be crustal material. Since both natural soil and coal fly ash have elemental patterns similar to crustal material, their contributions may not be separated by statistical methods such as factor analysis. Indirect information such as wind trajectories and SO_2 measurements are necessary to determine the origins of these crustal materials, but there are always uncertainties in the measurements because of the complications of meteorological analyses. The stable isotope ratio of $^{130}Ba/^{138}Ba$ in the combustion sample is close to the ratio for coal fly ash (0.00108 ± 0.00006) and it is very different from the ratio for the dust sample. Coal fly ash may travel with other substances generated from the combustion process and contribute most of the Ba mass. The result indicates that the stable isotope ratio of Ba can be used to separate the contributions from soil and fly ash, and it may be applied to separate sources of different origins of fine particulate samples.

The $^{121}Sb/^{123}Sb$ ratio in fly ash (1.01 ± 0.06) is smaller than in the particulate samples, but the ratio is close to the value in AGV-1 Andesite (0.99 ± 0.06) which is also a crustal substance. The large enrichment factors for the integrated samples indicate that Sb was mostly not of crustal origin. The $^{121}Sb/^{123}Sb$ ratio of the airborne dust sample' studied (1.75 ± 0.13) was between the ratios for fly ash and the combustion sample (2.24 ± 0.07), but it was higher than the ratio in crustal material. There was a large mass contribution from crustal material to the dust sample, which can be seen from the lower enrichment factor and the AFS-MLR result, and the low $^{121}Sb/^{123}Sb$ ratio in crustal material might have reduced the isotope ratio of Sb on this sample. The experimental result suggests that crustal material may have a lower $^{121}Sb/^{123}Sb$ ratio than other sources of fine particles, and its contribution can be separated from other sources by measuring the $^{121}Sb/^{123}Sb$ ratio.

The isotope ratios of $^{79}Br/^{81}Br$ in particulate samples are smaller than the ratios in biological standards, but the small net area from ^{79}Br increases the statistical uncertainty and error. The dust sample has a higher $^{79}Br/^{81}Br$ ratio than the combustion sample. This result suggests that the stable isotope of bromine may also be used for source identification, but it should be treated carefully because of its larger uncertainty.

5.2 Recommendations for Future Work

The use of stable isotope ratios and INAA greatly improves the technique for source identification of fine particles in the atmosphere. The use of the $^{130}Ba/^{138}Ba$ ratio enabled the separation of contributions from soil and coal fly ash which have similar compositions. However, a major problem for this technique is the lack of measured isotope ratios from different source types. To obtain quantitative estimates of source contributions in a sample, isotope ratios must first be determined from different sources. Then, simple mass balance calculations can be done on different samples. A source library is not available now, and it must be built before quantitative assessment is possible.

The size-segregated fine and ultra-fine particulate samples must be collected long enough to get sufficient mass to improve the detection limits. However, sources that contribute to these particles may have changed during collection because of changes in meteorological conditions. An aerosol sampler with a larger flow rate is necessary for future research to collect enough particulate mass in a shorter time period. Integrated fine particulate samples ($d_a < 2.5$ μm) collected concurrently with ultra-fine particles are necessary in order to identify major sources at the receptor site. Local impacts on isotope ratios should also be considered by measuring the isotope ratios of coarse particles, and these should be included in the source library.

The greatest difficulty in determining stable isotope ratios by INAA is probably the long counting time required for each sample. In order to get better statistical results, integrated samples were counted for 7 days for ^{130}Ba and ^{123}Sb. The long counting time makes it impossible to process a large number of samples, and it would be impractical for

this method to become a routine analysis. Irradiation of samples with a higher thermal neutron flux, collection of more particulate mass, or a larger detector with a higher absolute detection efficiency might reduce the counting time. The spiking of samples with a known amount of an enriched isotope may improve the results and reduce the counting time.

REFERENCES

Ames, M. R., "Development and application of a methodology for measuring atmospheric mercury by instrumental neutron activation analysis", Doctoral dissertation. Dept. of Nuclear Engineering, School of Engineering, Massachusetts Institute of Technology , 1995.

Bigeleisen, J., and Mayer, M. G., "Calculation of equilibrium constants for isotopic exchange reactions", *Journal of Chem. Phys.* 15, 261-267, 1947.

Blanchard, D. C., A. H. Woodcock , "The production, concentration and vertical distribution of sea-salt aerosol", *Ann. N.Y. Acad. Sci.*, 338, 330-347, 1980.

Burnett, W. C., and O. A. Schaeffer, "Effect of ocean dumping on $^{13}C/^{12}C$ ratios in marine sediments from the New York Bight", *Estuarine and Coastal Marine Science*, II, 605-611, 1980.

Cahill, T., A., L. L. Ashbaugh, R. A. Eldred, P. J. Feeney, B. H. Kusko, and R. G. Flocchini, In "Atmospheric Aerosol"; Macias, E., S.; and Hopke, P., K., Ed.; *ACS Symposium Series 167*; American Chemical Society: Washington, DC, 269-285, 1981.

Chiou, K. Y., O. K. Manuel, "Tellurium and Selenium in aerosols", *Environ. Sci. Technol.*, 20, 987-991, 1986.

Christensen, J. N., A. N. Halliday, L. V. Godfrey, J. R. Hein, and D. K. Rea, "Climate and ocean dynamics and the lead isotopic records in Pacific ferromanganese crusts", *Science*, 277, 913-918, 1997.

Cliff, S. S., M. H. Thiemens, "The $^{18}O/^{16}O$ and $^{17}O/^{16}O$ ratios in atmospheric nitrous oxide: a mass-independent anomaly", *Science*, 278, 1174-1175, 1997.

Cornides, I.; "Mass spectrometric analysis of inorganic solids-the historical background", in *Inorganic Mass Spectrometry*, John Wiley & Sons Company, New York, 1-15, 1988.

Day, D. E., W. C. Malm, and S. M. Kreidenweis, "Preliminary report submitted to EPRI for SEAVS study", 1996.

Dockery, D. W., C. A. Pope III, X. Xu, J. D. Spengler, J. H. Ware, M. E. Fay, B. G. Ferris, and F. E. Speizer, "An association between air pollution and mortality in six U.S. cities", *The New England Journal of Medicine*, 329, 1753-1759, 1993.

Dodd J. A., J. M. Ondov, G. Tuncel, T. G. Dzubay, R. K. Stevens, "Multimodal size spectra of submicrometer particles bearing various elements in rural air", *Environ. Sci. Technol.*, 25, 890-903, 1991.

Dzubay, T. G., R. K. Stevens, G. E. Gordon, I. Olmez, A. E. Sheffield, and W. Courtney, "A composite receptor method applied to Philadelphia aerosols", *Environ. Sci. Technol.*, 22, 46-52, 1988

Eldred, R. A., "Comparison of selenium and sulfur at remote sites through the United States", *Journal of the Air and Waste Management Association*, 47, 204-211, 1997.

Ellis, H.; "The compliance assurance monitoring rule: a summary", *Environmental Manager*, November, 1997.

Electric Power Research Institute, "Electric utility trace substances synthesis report", EPRI TR-104214, R. H. Osa Ed., 1994.

Fergusson, J. E.; "The heavy elements: chemistry, environmental impact and health effects", *Pergamon Press*, Oxford, 1990.

Fergusson, J. E.; "Dust in the environment: elemental composition and sources", *ACS Symposium Series 483*; American Chemical Society: Washington, DC, 117-133, 1992.

Fitzgerald, W. F., G. V. Vandal, and R. P. Mason, "Atmospheric cycling and air-water exchange of mercury over mid-continental lacustrine regions", *Water, Air, and Soil Pollution*, 56, 1991.

Galimov, E. M.; "The biological fractionation of isotopes", *Academic Press Inc., Harcourt Brace Jovanovich Publisher*, 1985.

Galloway, J. N., J. D. Thornton, S. A. Norton, H. L. Volchok, and R. A. N. McLean, "Trace metals in atmospheric deposition: a review and assessment", *Atmos. Environ.*, 16, 1677-1700, 1982.

Gatz, D. F., and J. M. Prospero, "A large silicon-Aluminum aerosol plume in central Illinois: North African desert dust", *Atmos. Environ.*, 30, 3789-3799, 1996.

Gellene, G. I.; "An explanation for symmetry-induced isotopic fractionation in ozone", *Science*, 274, 1344-1346, 1996.

Gordon, G., E.; "Receptor models", *Environ. Sci. Technol.*, 22, 1132-1142, 1988.

Gullu, G., "Long range transport of aerosols", Doctoral dissertation. Dept. of Environmental Engineering, School of Engineering, Middle East Technical University, 1996.

Hackley, K. C., D. H. Buchanan, K. Coombs, C. Chaven, and C. W. Kruse, "Solvent extraction of elemental sulfur from coal and a determination of its source using stable sulfur isotopes", *Fuel Processing Technology*, 24, 431-436, 1990.

Hall, J. V., A. M. Winer, M. T. Kleinman, F. W. Lurmann, V. Brajer, and S. D. Colome, "Valuing the health benefits of clean air", *Science*, 255, 812-817, 1992.

Henry, R., C., C. W. Lewis, P. K. Hopke, and H. J. Williamson, "Review of receptor model fundamentals", *Atmos. Environ.*, 18, 1507-1515, 1984.

Henry, R. C.; "Multivariate receptor models, in Receptor modeling for air quality management", *Elsevier Scientific Publisher*, New York, 117-147, 1991.

Hoefs, J.; "Stable isotope geochemistry, 4th Completely reversion", *Springer-Verlag Publisher,* Berlin, Heidelberg, New York, 1997.

Hood, D. W., "Impingment of man on the ocean", *Wiley-Interscience, New York,* in *Atmospheric precipitation and weathering*, 12-13, 1971.

Hopke, P.; "Receptor Modeling for Air Quality Management", *Elsevier Scientific Publisher*, New York, 1-10, 1991.

Hoppel, W. A., J.W. Fitzgerald, R. E. Larson, "Aerosol size distributions in air masses advecting off the east coast of the United States", *J. of Geophys. Res.,* 90, 2365-2379, 1985.

Hoppel, W. A., G. M. Frick, "Submicron aerosol size distributions measured over the tropical and south Pacific", *Atmos. Environ.*, 24A, 645-659, 1990.

Huang, X., I. Olmez, and N. Aras, "Emissions of trace elements from motor vehicles: Potential marker elements and source composition profile", *Atmos. Environ.*, 28, 1385-1391 ,1994.

Hughes, L. R., G. R. Cass, J. Gone, M. Ames, and I. Olmez, "Physical and chemical characterization of atmospheric ultrafine particles in the Los Angeles area", *Submitted to Environ. Sci. Technol.*, 1998.

Ingraham, N. L., R. J. Johnson, and R. Broadbent, "Facility-altered stable isotopic ratios of power generation cooling wastewater: opportunity for tracking leakages", *Environ. Sci. Technol.*, 28, 1983-1986, 1994.

Iverfeldt, A., "Occurrence and turnover of atmospheric mercury over the Nordic countries", *Water Air, and Soil Pollution*, 56, 251-266, 1991.

Jackson, A. W., J. H. Pardue, and R. Araujo, "Monitoring crude oil mineralization in salt marshes: use of stable carbon isotope ratios", *Environ. Sci. Technol.*, 30, 1139-1144, 1996.

Jaklevic, J. M, and R. L. Walter, "X-ray Fluorescence Analysis of Environmental Samples", T. G. Dzubay Ed., *Ann Arbor Science Publishing Inc.*, 1977.

John, W, and G. Reischl, "A cyclone for size-selective sampling of ambient air", *Journal of the Air Pollution Control Association*, 30, 872-876, 1980.

Kaye, J. A.; "Isotope effects in gas-phase chemical reactions and photodissociation processes", *ACS Symposium Series 502*, American Chemical Society: Washington, DC, 1-14, 1992.

Kohl, D. H., G. B. Shearer, and B. Commoner, "Fertilizer nitrogen: contribution to nitrate in surface water in a corn belt watershed", *Science*, 174, 1331-1334, 1971.

Landing, W. M., J. L. Guentzel, G. A. Gill, and C. D. Pollman, "Relationship between the atmospheric deposition of mercury, trace elements and major ions in Florida: The FAMS Project (1992-1993)". Paper presented at the third International Conference of Mercury as a global pollutant, Whistler, BC, July 10-14, 1994.

Legrand, M., R. J. Delmas, "Formation of HCl in the Antarctic atmosphere", *J. of Geophys. Res.*, 93, 7153-7168, 1988.

Macko, S. A., N. E. Ostrom, "Pollution studies using stable isotopes", in *Stable Isotopes in Ecology and Environmental Science*, Blackwell Scientific Publications, 45-62, 1994.

Maenhaut, W., W. H. Zoller, R. A. Duce, and G. L. Goffman, "Concentration and size distribution of particulate trace elements in the south polar atmosphere", *J. of Geophys. Res.*, 84, 2421-2431, 1979.

Maenhaut, W., F. Francois, J. Cafmeyer, and O. Okunade, "Size-fractionated aerosol composition at Gent, Belgium, results from a one-year study", *Nuclear Instruments and Methods in Physical Research* B, 109/110, 476-481, 1996.

Marple, V. A., K.L. Rubow, S.M. Behm, "A Microorifice Uniform Deposit Impactor (MOUDI), description, calibration, and use", *Aerosol Science and Technology*, 14, 434-446, 1991.

Mathai, C. V., "The Grand Canyon visibility transport commission and visibility protection in class I areas", *Environmental Manager*, December, 1995.

McMurry, P. H., personal communication, 1996.

Mosher, B. W., and R. A. Duce, "A global atmospheric selenium budget", *J. of Geophys. Res.*, 92, 289, 1987.

Musarra, S., and P. Saxena, "SEAVS first topic report: Characterization of concentration and composition of atmospheric aerosols collected at Look Rock, Tennessee"; EPRI draft report for SEAVS study team, 1996.

Nriagu, J. O., and J. M. Pacyna, "Quantitative assessment of worldwide contamination of air, water and soil by trace metals", *Nature*, 333, 134-139, 1988.

Nriagu, J. O., R. D. Coker, and L. A. Barrie, "Origin of sulphur in Canadian Arctic haze from isotope measurements", *Nature*, 349, 142-145, 1991.

Oberdorster, G., J. Ferin, and B. E. Lehnert, "Correlation between particle size, in vivo particle persistence, and lung injury", *Environmental Health Perspectives*, 102 (Suppl. 5), 173-179, 1994.

Oberdorster, G., "Significance of particle parameters in the evaluation of exposure-dose-response relationships of inhaled particles", *Particulate Science and Technology*, 14, 135-151, 1996.

Okamoto, S., M. Hayashi, M. Nakajima, Y. Kainuma, and K. Shiozawa, " A factor analysis-multiple regression model for source apportionment of suspended particulate matter", *Atmos. Environ.*, 24A, 2089-2097, 1990.

Olmez, I., and G. E. Gordon, "Rare earths: atmospheric signatures for oil-fired power plants and refineries", *Science*, 229, 966-968, 1985.

Olmez, I., G. E. Gordon, J. E. Houck, L. C. Pritchett, J. A. Cooper, T. G. Dzubay, and R. L. Bennett, "Compositions of particles from selected sources in Philadelphia for receptor modeling applications", *JAPCA*, 38, 1392-1402, 1988.

Olmez, I.; "Instrumental neutron activation analysis of atmospheric particulate matter", in *Methods of Air Sampling and Analysis, 3rd edition*, Lewis Publisher, Inc., 143-150, 1989.

Olmez, I., G. Gullu, M. Ames, X. Huang, S. Keskin, J. Che, A. Wakefield, J. Gone, and J. Beal, "Upstate New York Trace Metals Program Vol. II- Trace Metals", MIT Report No. MITNRL-064 , 1996.

Ondov, J. M., C. E. Choquette, W. H. Zoller, G. E. Gordon, A. H. Biermann, and R. E. Heft, "Atmospheric behavior of trace elements on particles emitted from a coal-fire power plant", *Atmos. Environ.*, 23, 2193, 1989.

Ott, W. R., "A physical explanation of the lognormality of pollutant concentrations", *J. Air Waste Manage. Assoc.*, 40, 1378-1383, 1990.

Ouimette, J. R., R. C. Flagan, and A. R. Kelso, "Chemical species contributions to light scattering by aerosols at a remote arid site", in *ACS Symposium Series 167*, American Chemical Society: Washington, DC, 125-156, 1981.

Parry, S. J.; "Activation spectrometry in chemical analysis", *John Willey & Sons Company*, New York, 1991.

Radlein, N., and K. G. Heumann, "Size fractionated impactor sampling of aerosol particles over the Atlantic Ocean from Europe to Antarctica as a methodology for source identification of Cd, Pb, Tl, Ni, Cr , and Fe"; *Fresenlus's Journal of Analytical Chemistry*, 352, 748-755, 1995.

Raemdonck, H., and W. Maenhaut, "Chemistry of marine aerosol over the tropical and equatorial pacific", *J. of Geophys. Res.*, 91, 8623-8636, 1986.

Rahn, K. A., and D. H. Lowenthal, "Elemental tracers of distance regional pollution aerosols", *Science*, 223, 132-138, 1984.

Reist, P. C., "Introduction to aerosol science", *Macmillan Publishing Company*, New York, 1984.

Seinfeld, J. H.; "Atmospheric chemistry and physics of air pollution", *John Wiley & Sons, Inc.*, New York, 1986.

Sherman, D. E., S. Kreidenweis, and T. McKee, "The influence of synoptic and local meteorological conditions on ambient particle concentrations during the southeastern aerosol and visibility study, volume I and II", Colorado State University, ISSN No. 0737-5352-34, February, 1997.

Small, M., M. S. Germani, A. M. Small, W. H. Zoller, and J. L. Moyers, "Airborne plume study of emissions from the processing of copper ores in southeastern Arizona", *Environ. Sci. Technol.*, 15, 293-299, 1981.

Solomon, S., R. W. Portmann, R. R. Garcia, L. W. Thomason, L. R. Poole, and M. P. McCormick, "The role of aerosol variations in anthropogenic ozone depletion at northern midlatitudes", *J. of Geophys. Res.*, 101, D3, 6713-6727, 1996.

Steedman, W., "Stable isotope ratio analysis in fossil fuel co-processing", *Trends in analytical chemistry*, 7, 121-122, 1988.

Sturges, W. T., and L. A. Barrie, "Lead 206/207 isotope ratios in the atmosphere of north America as tracers of US and Canadian emissions", *Nature*, 329, 144-146, 1987.

Sturges, W. T., and L. A. Barrie, "The use of stable lead 206/207 isotope ratios and elemental composition to discriminate the origins of lead in aerosols at a rural site in eastern Canada", *Atmos. Environ.*, 23, 1645-1657, 1989a.

Sturges, W. T., and L. A. Barrie, "Stable lead isotope ratios in Arctic aerosols: evidence for the origin of Arctic air pollution"; *Atmos. Environ.*, 23, 2513-2519, 1989b.

Suzuki, K., K. Maeda, Y. Sasa, A. Okada, K. Sakamato, and T. Ozawa, "Application of PIXE to source identification of Kosa aerosol: analysis of desert soils in China", *Nuclear Instruments and Methods in Physical Research*, B25, 317-320, 1993.

Sweet, C. W., S. J. Vermette, and S. Landsberger, "Sources of toxic trace elements in urban air in Illinois", *Environ. Sci. Technol.*, 27, 2502-2510, 1993.

Taylor, S. R.; "Abundance of chemical elements in the continental crust: a new table", *Geochimica et Cosmochimica Acta*, 28,1273 , 1964.

Thiemens, M. H., and J. E. Heidenreich, "The mass independent fractionation of oxygen- a novel isotope effect and its cosmochemical implications", *Science*, 219, 1073-1075, 1983.

Thiemens, M. H., "Mass-independent isotope fractionations and their applications", *ACS Symposium Series 502*, American Chemical Society: Washington, DC, 138-154, 1992.

Thurston, G. D., and J. D. Spengler, "A quantitative assessment of source contributions to inhalable particulate matter pollution in metropolitan Boston", *Atmos. Environ.*, 19, 9-25 , 1985.

Tuncel, S. G., I. Olmez, J. R. Parrington, G. E. Gordon, and R. K. Stevens, 'Composition of fine particle regional sulfate component in Shenandoah Valley", *Environ. Sci. Technol.*, 19, 529-537 , 1985.

Versini, G., A. Monetti, and F. Reniero, "Monitoring authenticity and regional origin of wines by natural stable isotope ratio analysis", *ACS Symposium Series 661*, American Chemical Society: Washington, DC, 113-130, 1997.

Whitby, K. T.; "The physical characterisitics of sulfur aerosols", *Atmos. Environ.*, 12, 135-159, 1978.

Zoller, W. H., E. S. Gladney, G. E. Gordon, and J. J. Bors, "Trace substances in environmental health-VIII", A symposium, University of Missouri, Columbia, 167, 1974.

APPENDIX A ELEMENTAL CONCENTRATION DATA

Concentrations for which no analytical error is shown are below the detection limit for that element and sample. The detection limit for each element differs from sample to sample due to the varying concentrations of other elements in the sample and due to variations in analytical parameters.

* The UMn/MOUDI sampler operated with an inlet cyclone having a 1.8 μm cutpoint, therefore measurements for the first (3.2 μm) and second (1.8 μm) stages do not represent a complete sample of that size fraction.

Elemental Concentrations (ng/m^3) of MIT/SU 2.1 μm Aerosol Samples

Date	7/15/95		7/16/95		7/17/95		7/18/95	
Element	conc.	+/-	conc.	+/-	conc.	+/-	conc.	+/-
Na	42	4	26	2	35	3	14	2
Mg	27	24	16	11	23	23	19	
Al	120	10	63	6	110	10	20	11
Cl	24	7	11	4	47	10	15	4
K	30	30	49	36	8.8	8.8	58	30
Sc	0.0098	0.0026	0.0090	0.0021	0.0072	0.0018	0.0077	0.0022
Ti	6.3	4.6	11	5	7.4	4.1	14	
V	0.41	0.06	0.32	0.06	0.47	0.06	0.14	
Cr	1.5	0.2	0.80	0.19	1.1	0.1	1.2	0.3
Mn	1.2	0.1	0.74	0.12	1.2	0.1	0.75	0.12
Fe	56	16	34	13	52	11	26	14
Co	0.18	0.04	0.17	0.04	0.28	0.04	0.14	0.04
Zn	28	3	15	2	34	4	41	5
Ga	0.49		0.26		0.02		0.66	
As	0.28	0.03	0.49	0.04	0.66	0.08	0.29	0.03
Se	1.1	0.3	1.1	0.3	0.98	0.16	0.82	0.21
Br	1.9	0.6	0.92	0.24	0.20	0.07	0.29	0.09
Rb	0.56	0.56	1.1		0.44		0.78	
Sr	3.9	2.1	3.3		2.1	1.2	1.9	1.0
Zr	2.1		2.1		2.1		2.1	
Mo	0.14	0.07	0.18		0.22		0.12	0.06
Cd	0.13	0.10	0.059	0.058	0.044	0.044	0.011	0.011
In	0.00068	0.00068	0.00100		0.0010		0.00067	0.00066
Sb	0.47	0.10	0.18	0.08	0.31	0.07	0.23	0.10
Cs	0.0040		0.017	0.016	0.0040		0.038	0.037
Ba	3.9	1.5	1.9	1.7	4.5		4.1	
La	0.016	0.007	0.0060		0.0060		0.0011	0.0011
Ce	0.034	0.033	0.078	0.077	0.011	0.011	0.12	
Nd	0.68	0.41	0.23		0.11	0.11	0.22	0.22
Sm	0.0059	0.0007	0.0041	0.0006	0.0036	0.0009	0.0032	0.0005
Eu	0.011	0.011	0.0022		0.0035		0.0022	0.0022
Tb	0.0035	0.0030	0.010	0.010	0.0067	0.0065	0.0046	0.0045
Yb	0.0074	0.0053	0.0078	0.0053	0.0015		0.010	
Lu	0.0027		0.0032		0.0020		0.00067	0.00066
Hf	0.022		0.022		0.022		0.011	
Ta	0.035	0.019	0.093		0.071		0.079	
Au	0.00051		0.00033	0.00033	0.00051		0.00051	
Hg	0.056	0.011	0.060	0.010	0.12	0.01	0.022	0.006
Th	0.0051		0.0051		0.0051		0.0051	
U	0.0051		0.0047		0.055		0.031	

Elemental Concentrations (ng/m^3) of MIT/SU 2.1 μm Aerosol Samples

Date	7/19/95		7/20/95		7/21/95		7/22/95	
Element	conc.	+/-	conc.	+/-	conc.	+/-	conc.	+/-
Na	10	1	18	2	20	2	23	2
Mg	18		8.9		4.0		28	22
Al	34	6	130	10	3		39	8
Cl	1.7		83	17	22	6	1.7	
K	7.7	7.7	5.5		34		22	
Sc	0.0063	0.0021	0.0107	0.0017	0.0096	0.0026	0.0061	0.0019
Ti	7.0	5.2	15		17	4	12	9
V	0.12	0.02	0.24	0.06	0.05	0.01	0.22	0.06
Cr	0.43	0.15	1.1	0.2	0.48	0.14	0.53	0.17
Mn	0.52	0.12	1.0	0.1	0.85	0.12	0.41	0.12
Fe	29	12	53	14	60	18	42	12
Co	0.12	0.04	0.11	0.04	0.20	0.04	0.18	0.04
Zn	25	3	22	3	42	4	11	2
Ga	0.27		0.23	0.23	0.02		0.23	
As	0.23	0.02	0.48	0.06	0.41	0.04	0.30	0.03
Se	1.1	0.3	1.4	0.3	0.65	0.21	0.45	0.21
Br	0.71	0.19	0.92	0.25	0.27	0.08	0.11	0.03
Rb	1.1		0.77		0.37		0.66	
Sr	4.1		3.9		2.9		3.9	
Zr	2.1		2.1		2.1		2.1	
Mo	0.036		0.20		0.065	0.056	0.072	0.054
Cd	0.034	0.034	0.066	0.066	0.031	0.030	0.037	
In	0.0017	0.0016	0.0018	0.0017	0.00100		0.00044	0.00044
Sb	0.20	0.09	0.10	0.06	0.25	0.08	0.081	0.060
Cs	0.0040		0.0040		0.0040		0.0040	
Ba	2.2	1.8	8.1	2.7	4.2	2.0	0.7	
La	0.0060		0.0077	0.0055	0.0066	0.0055	0.0060	
Ce	0.033	0.033	0.031		0.011	0.011	0.031	
Nd	0.23		0.23		0.23		0.22	0.22
Sm	0.0030	0.0005	0.0056	0.0009	0.0043	0.0007	0.0030	0.0005
Eu	0.0035		0.0035		0.0089	0.0088	0.0033	0.0033
Tb	0.017		0.0020		0.0020		0.022	
Yb	0.0062		0.013		0.0059		0.0098	0.0046
Lu	0.0024		0.00011		0.0018		0.00011	
Hf	0.0044	0.0044	0.022		0.013		0.010	
Ta	0.083		0.083		0.044	0.019	0.082	
Au	0.0050	0.0049	0.010	0.010	0.0017	0.0016	0.00051	
Hg	0.027	0.010	0.056	0.013	0.064	0.011	0.063	0.009
Th	0.0051		0.0051		0.0051		0.0051	
U	0.035		0.046		0.015	0.013	0.034	

Elemental Concentrations (ng/m^3) of MIT/SU 2.1 μm Aerosol Samples

Date	7/23/95		7/24/95		7/25/95		7/26/95	
Element	conc.	+/-	conc.	+/-	conc.	+/-	conc.	+/-
Na	65	5	120	10	210	10	140	11
Mg	18	14	51	30	120	30	130	40
Al	37	7	240	10	920	50	910	50
Cl	19	6	5.7	3.7	5.8	3.7	5.8	3.7
K	21	21	61		320	70	160	70
Sc	0.0058	0.0017	0.034	0.004	0.143	0.011	0.12	0.01
Ti	12	6	18	7	52	13	61	12
V	0.29	0.06	0.85	0.08	1.8	0.1	1.9	0.1
Cr	0.31	0.13	0.85	0.17	2.2	0.2	1.1	0.1
Mn	0.52	0.12	2.1	0.1	8.5	0.1	7.6	0.1
Fe	28	10	160	20	510	20	440	20
Co	0.13	0.04	0.12	0.04	0.22	0.04	0.19	0.04
Zn	4.3	1.3	2.2	1.2	8.0	1.4	5.0	1.4
Ga	0.49		0.19	0.18	1.4		1.3	
As	0.14	0.03	0.39	0.06	0.34	0.04	0.33	0.03
Se	0.48	0.19	0.40	0.20	0.59	0.19	0.43	0.17
Br	1.3	0.3	0.66	0.19	0.73	0.20	0.40	0.11
Rb	0.67		1.3		1.0		0.33	0.33
Sr	4.1		4.5		5.6	3.1	5.7	
Zr	2.1		2.1		2.1		2.1	
Mo	0.21		0.087	0.060	0.29		0.21	
Cd	0.0011		0.14	0.13	0.29	0.27	0.18	0.18
In	0.0010		0.0010		0.0020	0.0020	0.00089	0.00088
Sb	0.092	0.069	0.16	0.07	0.23	0.08	0.11	0.07
Cs	0.0040		0.0040		0.032	0.032	0.0040	
Ba	5.2	2.1	3.1	1.0	6.4	2.0	7.4	2.9
La	0.028	0.007	0.14	0.01	0.64	0.04	0.49	0.03
Ce	0.031		0.19	0.12	1.3	0.1	0.88	0.13
Nd	0.33	0.33	0.23		0.23		0.23	
Sm	0.0042	0.0008	0.020	0.002	0.089	0.008	0.074	0.007
Eu	0.027	0.011	0.0035		0.021	0.013	0.014	0.010
Tb	0.0020		0.0034	0.0034	0.0057	0.0056	0.0057	0.0056
Yb	0.0060	0.0032	0.021	0.007	0.031	0.011	0.017	0.012
Lu	0.0010		0.0010		0.0031	0.0021	0.0038	0.0020
Hf	0.0089		0.0077	0.0077	0.019	0.019	0.0089	0.0088
Ta	0.080		0.11		0.10		0.084	
Au	0.00051		0.00051		0.00051		0.00051	
Hg	0.013	0.007	0.014	0.010	0.019	0.017	0.042	0.014
Th	0.0051		0.0051		0.076	0.031	0.023	0.023
U	0.019	0.014	0.014	0.009	0.060	0.022	0.046	

Elemental Concentrations (ng/m^3) of MIT/SU 2.1 μm Aerosol Samples

Date	7/27/95		7/28/95		7/29/95		7/30/95	
Element	conc.	+/-	conc.	+/-	conc.	+/-	conc.	+/-
Na	37	3	61	5	99	7	79	6
Mg	34	12	22	22	47	17	6	
Al	85	46	210	12	120	10	3.3	
Cl	1.7		1.3	1.3	3.6	2.7	2.4	2.4
K	48		20	19	54	38	41	
Sc	0.039	0.004	0.025	0.003	0.013	0.003	0.0065	0.0019
Ti	27	9	14	7	11	4	4.5	1.7
V	0.69	0.24	0.54	0.06	0.40	0.06	0.01	0.01
Cr	0.72	0.17	0.32	0.18	0.42	0.12	0.39	0.11
Mn	1.8	0.1	1.5	0.1	1.1	0.1	0.30	0.12
Fe	110	20	110	20	8	20	43	13
Co	0.07	0.04	0.06	0.04	0.03	0.03	0.03	0.03
Zn	5.0	1.5	0.2	0.2	3.0	1.2	0.77	0.77
Ga	0.19	0.18	0.53		0.65		0.54	
As	0.25	0.02	0.16	0.02	0.29	0.04	0.17	0.02
Se	0.18	0.17	0.14	0.14	0.10	0.10	0.22	0.14
Br	0.53	0.14	0.18	0.06	0.30	0.09	0.41	0.11
Rb	1.1		1.0		0.37		0.55	
Sr	0.73	0.73	2.0	0.8	3.9		2.3	
Zr	2.1		2.1		2.1		2.1	
Mo	0.13		0.041	0.029	0.16		0.14	
Cd	0.027	0.026	0.17	0.15	0.10	0.10	0.021	
In	0.0010		0.0010		0.0010		0.0010	
Sb	0.081	0.069	0.092		0.020	0.020	0.11	0.07
Cs	0.0033	0.0033	0.0040		0.0040		0.0040	
Ba	4.5	2.0	1.8	1.3	1.1		4.1	
La	0.14	0.01	0.082	0.012	0.036	0.007	0.0060	
Ce	0.27	0.12	0.033	0.033	0.055	0.055	0.031	
Nd	0.23		0.23		0.23		0.33	0.33
Sm	0.024	0.002	0.013	0.001	0.0085	0.0010	0.0031	0.0005
Eu	0.0035		0.0055	0.0055	0.0035		0.0035	
Tb	0.013		0.00033		0.0057	0.0056	0.0020	
Yb	0.0042	0.0035	0.0030		0.011	0.006	0.013	0.004
Lu	0.0022	0.0013	0.00033	0.00033	0.0013		0.0020	
Hf	0.012		0.0044		0.022		0.022	
Ta	0.094		0.11		0.016		0.088	
Au	0.00051		0.00051		0.00051		0.00051	
Hg	0.013	0.007	0.031	0.008	0.042	0.008	0.021	0.008
Th	0.0051		0.0051		0.0051		0.0051	
U	0.030		0.032		0.0080		0.032	

Elemental Concentrations (ng/m^3) of MIT/SU 2.1 μm Aerosol Samples

Date	7/31/95		8/1/05		8/2/95		8/3/95	
Element	conc.	+/-	conc.	+/-	conc.	+/-	conc.	+/-
Na	100	10	94	7	60	5	130	10
Mg	50		18	8	12		65	38
Al	56	8	78	8	28	6	230	10
Cl	1.7		1.7		110	20	72	11
K	2.1		19	19	39	34	28	28
Sc	0.0027	0.0017	0.0072	0.0019	0.0038	0.0016	0.042	0.004
Ti	7.7	4.4	14		4.3	4.2	20	8
V	0.23	0.07	0.25	0.06	0.34	0.06	0.66	0.07
Cr	0.43	0.11	0.50	0.11	0.27	0.13	0.74	0.17
Mn	0.30	0.12	0.63	0.12	0.30	0.12	2.1	0.1
Fe	40	14	31	10	28	10	170	10
Co	0.02	0.02	0.07	0.04	0.07	0.04	0.10	0.04
Zn	2.9	1.2	0.44	0.44	3.3	1.2	4.5	1.3
Ga	0.65		0.76		0.02		0.65	
As	0.055	0.014	0.20	0.03	0.12	0.02	0.10	0.02
Se	0.21	0.16	0.56	0.20	0.47	0.21	0.005	
Br	1.1	0.3	0.19	0.07	0.44	0.12	0.03	
Rb	0.55		0.66		0.33		0.66	
Sr	3.6	1.3	3.9		3.9		4.1	
Zr	2.1		2.1		2.1		2.1	
Mo	0.18		0.13		0.10		0.12	
Cd	0.14	0.14	0.066	0.066	0.037		0.013	
In	0.00088	0.00088	0.00088	0.00088	0.00089		0.0028	0.0020
Sb	0.24	0.08	0.16	0.06	0.16	0.10	0.081	
Cs	0.0040		0.0040		0.0040		0.0040	
Ba	1.2	0.9	0.41		2.1	1.3	4.5	1.7
La	0.0060		0.0060		0.0060		0.20	0.02
Ce	0.031		0.031		0.033		0.21	0.12
Nd	0.23		0.23		0.23		0.23	
Sm	0.0017	0.0005	0.0050	0.0007	0.0014	0.0006	0.020	0.002
Eu	0.0022	0.0022	0.0035		0.0035		0.0077	0.0077
Tb	0.010		0.0020		0.0011		0.0020	
Yb	0.015		0.0095		0.010		0.013	0.007
Lu	0.0028		0.0012		0.0016		0.00044	0.00042
Hf	0.022		0.022		0.022		0.0066	0.0066
Ta	0.098		0.10		0.060		0.067	
Au	0.00051		0.00051		0.00051		0.00051	
Hg	0.013	0.012	0.065	0.009	0.011	0.007	0.0086	
Th	0.0051		0.0051		0.0051		0.0051	
U	0.038		0.012	0.008	0.0064	0.0050	0.024	

Elemental Concentrations (ng/m^3) of MIT/SU 2.1 μm Aerosol Samples

Date	8/4/95		8/5/95		8/6/95		8/7/95	
Element	conc.	+/-	conc.	+/-	conc.	+/-	conc.	+/-
Na	91	7	120	10	23	4	29	2
Mg	37	24	66	27	28		12	11
Al	41	6	60	26	24	8	37	6
Cl	35	6	1.7		1.7		1.7	
K	28		16	15	2.1		2.1	
Sc	0.0065	0.0020	0.026	0.003	0.0051	0.0027	0.0033	0.0016
Ti	7.1	4.2	5.9	5.0	14		10	
V	0.14	0.05	0.59	0.11	0.22	0.04	0.28	0.04
Cr	0.52	0.17	0.83	0.19	0.15		0.45	0.15
Mn	0.30	0.12	1.1	0.1	0.30	0.18	0.30	0.12
Fe	55	19	99	17	38	23	52	15
Co	0.04	0.04	0.08	0.04	0.12	0.06	0.16	0.04
Zn	1.7	1.1	2.0	1.2	0.70	0.69	0.79	0.78
Ga	0.43		0.78		0.07		0.02	
As	0.10	0.02	0.20	0.02	0.17	0.06	0.054	0.010
Se	0.005		0.068	0.067	0.31	0.28	0.14	0.13
Br	0.086	0.039	0.14	0.05	0.42	0.14	0.62	0.17
Rb	0.89		1.1		0.52		0.11	
Sr	3.3		2.5		4.9		1.8	0.9
Zr	2.1		2.1		2.1		2.1	
Mo	0.12		0.19		0.014		0.063	0.036
Cd	0.057		0.029	0.029	0.033		0.014	
In	0.0045		0.00090	0.00090	0.0010		0.0010	
Sb	0.19	0.08	0.32	0.09	0.27	0.12	0.12	0.07
Cs	0.0040		0.061	0.048	0.0040		0.0040	
Ba	0.8		4.7		3.8	1.7	3.5	
La	0.0060		0.046	0.009	0.0060		0.0060	
Ce	0.031		0.090	0.090	0.070		0.031	
Nd	0.23		0.56	0.48	0.23		0.23	
Sm	0.0032	0.0007	0.012	0.001	0.0024	0.0011	0.0023	0.0005
Eu	0.0035		0.0035		0.0035		0.0011	0.0011
Tb	0.0023		0.0035		0.0037		0.0020	
Yb	0.0023		0.021	0.014	0.021		0.0055	0.0042
Lu	0.0019		0.0033		0.0030		0.0025	
Hf	0.016		0.016		0.014		0.022	
Ta	0.072		0.0037		0.10		0.052	
Au	0.00051		0.00051		0.00051		0.0085	0.0084
Hg	0.0077	0.0065	0.020	0.009	0.011		0.010	0.005
Th	0.0051		0.0051		0.0051		0.0051	
U	0.0092	0.0071	0.053		0.044		0.018	

Elemental Concentrations (ng/m^3) of MIT/SU 2.1 μm Aerosol Samples

Date	8/8/95		8/9/95		8/10/95		8/11/95	
Element	conc.	+/-	conc.	+/-	conc.	+/-	conc.	+/-
Na	8.2	1.4	33	4	57	5	50	5
Mg	9		28	24	19	13	41	29
Al	3		65	8	61	7	63	6
Cl	1.7		1.7		0.22	0.22	1.7	
K	5.6		38	34	2.1		55	40
Sc	0.0038	0.0019	0.0053	0.0020	0.0096	0.0017	0.0053	0.0022
Ti	4.3	2.4	17		21	7	10	6
V	0.14		0.32	0.06	0.39	0.06	0.22	0.05
Cr	0.29	0.17	0.49	0.19	1.1	0.2	0.16	
Mn	0.30	0.12	0.64	0.12	0.74	0.12	1.0	0.1
Fe	38	14	12	9	55	13	36	19
Co	0.11	0.04	0.07	0.04	0.03	0.03	0.10	0.04
Zn	8.0	1.4	1.8	1.1	21	2	17	2
Ga	0.12		0.24		0.38		0.55	
As	0.077	0.010	0.14	0.02	0.20	0.02	0.12	0.03
Se	0.21	0.20	0.44	0.20	0.75	0.21	0.82	0.30
Br	0.16	0.05	0.68	0.18	1.6	0.4	1.4	0.3
Rb	1.0		0.45		0.37		0.37	
Sr	0.2		3.4		1.9	1.5	4.8	
Zr	2.1		2.1		2.1		2.1	
Mo	0.10		0.11		0.13		0.31	
Cd	0.081	0.081	0.041	0.040	0.11	0.11	0.86	
In	0.0010		0.00045		0.0010		0.0030	0.0030
Sb	0.21	0.09	0.51	0.10	0.67	0.12	0.27	0.10
Cs	0.0044	0.0044	0.050	0.048	0.0040		0.0067	0.0060
Ba	3.0		0.78		4.3		7.3	3.0
La	0.0060		0.0060		0.0060		0.0060	
Ce	0.089		0.031		0.031		0.22	
Nd	0.23		0.23		0.23		0.22	0.22
Sm	0.00056	0.00040	0.0016	0.0005	0.0029	0.0007	0.0025	0.0009
Eu	0.0067	0.0066	0.0056	0.0056	0.0044	0.0044	0.0035	
Tb	0.0034	0.0034	0.0020		0.0034	0.0034	0.00090	0.00089
Yb	0.0047	0.0040	0.014	0.010	0.017		0.016	
Lu	0.0029		0.0024		0.0035		0.0010	
Hf	0.019		0.011		0.012		0.023	
Ta	0.079		0.067		0.067		0.070	0.035
Au	0.0061	0.0061	0.00051		0.00051		0.00051	
Hg	0.026	0.010	0.015	0.006	0.030	0.008	0.025	0.016
Th	0.0051		0.0051		0.0051		0.0051	
U	0.018		0.0058	0.0058	0.024		0.038	

Elemental Concentrations (ng/m^3) of MIT/SU 2.1 μm Aerosol Samples

Date	8/12/95		8/13/95		8/14/95		8/15/95	
Element	conc.	+/-	conc.	+/-	conc.	+/-	conc.	+/-
Na	56	5	110	10	92	7	86	7
Mg	46	33	92	31	110	30	71	40
Al	63	6	300	10	99	45	310	10
Cl	1.7		1.7		1.7		1.7	
K	2.1		95	51	83	51	200	50
Sc	0.013	0.003	0.047	0.004	0.053	0.005	0.043	0.004
Ti	26	9	18	10	17	11	30	11
V	0.43	0.05	0.79	0.10	0.83	0.23	0.64	0.09
Cr	0.44	0.18	0.92	0.29	0.93	0.21	0.39	0.16
Mn	1.1	0.1	2.7	0.1	2.7	0.1	2.4	0.1
Fe	100	20	190	20	170	20	150	20
Co	0.06	0.04	0.19	0.04	0.23	0.04	0.19	0.04
Zn	5.1	1.4	9.2	1.4	10	1	4.0	1.4
Ga	0.50		0.77		0.88		0.68	
As	0.43	0.07	0.54	0.06	0.53	0.06	0.37	0.05
Se	0.73	0.23	1.3	0.4	2.1	0.4	0.89	0.23
Br	0.086	0.044	0.19	0.06	0.58	0.16	0.29	0.08
Rb	0.89		0.37		0.44	0.44	0.37	
Sr	4.2		5.5		3.4		6.1	
Zr	2.1		2.2		2.1		2.1	
Mo	0.37		0.13	0.11	0.22		0.28	
Cd	0.40		1.1		0.20	0.20	0.13	
In	0.0027	0.0026	0.0010		0.0019	0.0018	0.0034	0.0034
Sb	0.30	0.08	0.58	0.11	0.68	0.13	0.31	0.09
Cs	0.071	0.047	0.018	0.017	0.038	0.037	0.025	0.025
Ba	5.2		2.2	1.9	3.4	1.9	1.1	
La	0.012	0.008	0.15	0.01	0.16	0.01	0.12	0.01
Ce	0.17		0.25	0.18	0.21	0.16	0.30	0.17
Nd	0.23		0.56	0.56	0.23		0.23	
Sm	0.0058	0.0012	0.024	0.002	0.026	0.002	0.022	0.002
Eu	0.0100	0.0110	0.0035		0.012	0.012	0.022	0.013
Tb	0.0020		0.0020		0.0034	0.0034	0.0020	
Yb	0.011	0.006	0.027	0.020	0.014	0.007	0.013	0.010
Lu	0.0037		0.0056		0.0016	0.0017	0.0021	0.0017
Hf	0.022		0.031		0.012		0.0069	0.0068
Ta	0.050	0.026	0.011		0.017		0.084	
Au	0.00051		0.00051		0.00051		0.0029	0.0028
Hg	0.010		0.17	0.01	0.030	0.010	0.0089	
Th	0.0051		0.0051		0.0051		0.0051	
U	0.048		0.033		0.033		0.033	

Elemental Concentrations (ng/m^3) of MIT/SU 2.1 μm Aerosol Samples

Date	8/16/95		8/17/95		8/18/95		8/19/95	
Element	conc.	+/-	conc.	+/-	conc.	+/-	conc.	+/-
Na	86	7	71	6	55	5	100	10
Mg	110	50	37	26	85	51	42	18
Al	320	10	3		170	10	170	10
Cl	2.5	2.5	1.7		4.6	3.7	8.0	4.7
K	130	50	84	42	83	41	95	51
Sc	0.043	0.004	0.038	0.004	0.029	0.003	0.026	0.003
Ti	25	10	6.4	3.2	15	11	14	9
V	0.59	0.07	0.13	0.01	0.80	0.10	0.57	0.08
Cr	0.81	0.24	3.7	0.2	0.78	0.24	0.49	0.17
Mn	2.7	0.1	3.0	0.1	2.9	0.1	2.0	0.1
Fe	170	20	160	20	110	20	100	20
Co	0.20	0.04	0.22	0.04	0.19	0.04	0.17	0.04
Zn	13	2	16	2	11	2	8.0	1.4
Ga	0.67		0.02		0.54		0.056	0.055
As	0.42	0.05	0.63	0.07	0.77	0.08	0.47	0.04
Se	1.1	0.3	3.3	0.5	3.5	0.5	1.7	0.4
Br	2.7	0.7	3.9	1.0	1.6	0.4	0.80	0.22
Rb	0.91		0.78		1.2		0.78	
Sr	5.3		3.9		2.1	1.8	5.7	
Zr	2.1		2.1		2.1		2.1	
Mo	0.11	0.08	0.67	0.19	0.10	0.08	0.16	0.10
Cd	0.51		1.4		0.50		0.76	
In	0.00045		0.0036	0.0004	0.0030	0.0029	0.0010	
Sb	0.67	0.11	0.55	0.11	0.54	0.11	1.4	0.2
Cs	0.061	0.048	0.0067	0.0067	0.049	0.048	0.012	0.012
Ba	2.7	1.9	8.8	2.1	6.3		6.2	
La	0.12	0.01	0.094	0.012	0.093	0.012	0.021	0.007
Ce	0.10	0.10	0.067	0.067	0.031		0.011	0.011
Nd	0.23		0.11	0.11	0.23		0.23	
Sm	0.021	0.002	0.017	0.002	0.016	0.002	0.014	0.001
Eu	0.0057	0.0056	0.0022	0.0022	0.014	0.013	0.0089	0.0080
Tb	0.0020		0.0020		0.0020		0.0020	
Yb	0.018		0.019		0.0082	0.0063	0.019	
Lu	0.0042		0.0041		0.00066		0.0024	0.0020
Hf	0.019		0.018		0.028		0.016	
Ta	0.078		0.076		0.071	0.045	0.072	
Au	0.00051		0.0095	0.0095	0.00051		0.00051	
Hg	0.028	0.012	0.018	0.009	0.014	0.011	0.020	0.011
Th	0.0051		0.0051		0.0051		0.0051	
U	0.032		0.038		0.029		0.0068	

Elemental Concentrations (ng/m^3) of MIT/SU 2.1 μm Aerosol Samples

Date	8/20/95		8/21/95		8/22/95		8/23/95	
Element	conc.	+/-	conc.	+/-	conc.	+/-	conc.	+/-
Na	19	2	26	2	32	3	37	3
Mg	11		10		13		45	32
Al	11	9	1.1	1.1	15	11	11	10
Cl	17	4	3.5	2.7	1.7		1.3	1.3
K	8.9	8.9	2.1		21	21	31	30
Sc	0.0036	0.0024	0.0031	0.0017	0.0071	0.0019	0.0075	0.0020
Ti	11		3.7	2.3	11		14	
V	0.43	0.17	0.47	0.17	0.32	0.07	0.41	0.13
Cr	0.82	0.23	0.32	0.11	0.66	0.16	0.88	0.19
Mn	0.74	0.12	0.52	0.12	1.3	0.1	1.7	0.1
Fe	55	21	22	11	45	16	59	21
Co	0.18	0.04	0.08	0.04	0.05	0.04	0.27	0.04
Zn	14	2	6.2	1.5	14	2	11	2
Ga	0.14	0.14	0.42		0.98	0.62	0.65	
As	0.11	0.01	0.13	0.01	0.58	0.05	0.43	0.04
Se	0.41	0.19	0.44	0.17	2.4	0.4	1.8	0.4
Br	0.17	0.06	0.42	0.12	0.40	0.11	2.9	0.8
Rb	1.4		0.37		0.37		0.37	
Sr	2.2		0.4	0.4	2.2		2.8	
Zr	2.2		2.1		2.1		2.1	
Mo	0.052	0.051	0.058	0.037	0.12	0.04	0.20	
Cd	0.037	0.036	0.070	0.069	0.080	0.080	0.12	0.12
In	0.00055	0.00055	0.00055	0.00055	0.0026	0.0026	0.00033	0.00031
Sb	0.19		0.10	0.08	0.58	0.10	0.67	0.12
Cs	0.082	0.055	0.0040		0.025	0.025	0.035	0.035
Ba	3.7	1.4	2.4	1.0	4.6		5.2	
La	0.0060		0.0060		0.012	0.005	0.030	0.006
Ce	0.19		0.011		0.031		0.18	
Nd	0.33	0.33	0.23		0.11	0.11	0.33	0.33
Sm	0.0018	0.0004	0.0023	0.0005	0.0033	0.0006	0.0051	0.0007
Eu	0.0100		0.0035		0.0033	0.0032	0.015	0.013
Tb	0.031		0.0020		0.0019		0.0020	
Yb	0.011	0.008	0.011		0.0041	0.0038	0.017	
Lu	0.0021		0.0019		0.0021		0.0036	
Hf	0.023		0.022		0.012		0.0077	
Ta	0.11		0.081		0.088		0.098	
Au	0.00051		0.00051		0.0060	0.0060	0.0028	0.0027
Hg	0.027	0.006	0.013	0.006	0.010	0.005	0.0028	
Th	0.0051		0.0051		0.0051		0.0051	
U	0.0039		0.029		0.038		0.029	

Elemental Concentrations (ng/m^3) of MIT/SU 2.1 μm Aerosol Samples

Date	8/24/95		8/25/95	
Element	conc.	+/-	conc.	+/-
Na	71	6	85	7
Mg	17		21	16
Al	13	9	7	7
Cl	19	4	4	3
K	23	23	14	13
Sc	0.013	0.003	0.0054	0.0019
Ti	12		11	3
V	0.93	0.33	0.19	0.07
Cr	2.0	0.3	0.87	0.18
Mn	1.3	0.1	0.31	0.12
Fe	100	20	52	15
Co	0.56	0.05	0.37	0.05
Zn	18	2	2.7	1.5
Ga	0.88		0.56	
As	0.66	0.07	0.09	0.01
Se	1.1	0.3	0.27	0.20
Br	2.5	0.7	0.30	0.09
Rb	1.1		1.3	
Sr	2.6		0.6	
Zr	2.1		2.1	
Mo	0.10	0.07	0.030	
Cd	0.093		0.053	
In	0.0010		0.0024	0.0020
Sb	0.43	0.13	0.11	
Cs	0.0089	0.0089	0.0040	
Ba	4.6		1.7	1.6
La	0.0089	0.0065	0.0060	
Ce	0.031		0.057	
Nd	0.45	0.44	0.23	0.22
Sm	0.0041	0.0006	0.0024	0.0005
Eu	0.0033		0.0046	
Tb	0.022	0.015	0.024	
Yb	0.0040	0.0035	0.017	
Lu	0.0022	0.0017	0.0032	
Hf	0.022		0.014	
Ta	0.094		0.11	
Au	0.00051		0.00051	
Hg	0.023	0.007	0.038	0.010
Th	0.0051		0.0051	
U	0.044		0.041	

Elemental concentrations (ng/m^3) of UMn/MOUDI Aerosol Samples

Date	07/15 - 07/19/95		07/15 - 07/19/95		07/15 - 07/19/95		07/15 - 07/19/95	
Upper cutsize	3.2 μm		1.8 μm		1.0 μm		0.56 μm	
Element	conc.	+/-	conc.	+/-	conc.	+/-	conc.	+/-
Na	0.29	0.06	3.43	0.30	6.12	0.43	2.85	0.21
Mg	0.7	0.5	4.7	1.1	7.8	1.8	4.3	2.3
Al	2.5	0.2	12.5	1.0	42.4	2.2	63.0	3.1
Cl	0.16		0.64	0.15	0.82	0.22	1.09	0.21
K	1.5		4.8	1.9	10.8	2.2	15.4	2.1
Sc	0.00001	0.00001	0.00136	0.00010	0.00284	0.00022	0.00043	0.00011
Ti	0.19		0.49	0.21	1.31	0.43	0.46	
V	0.017		0.012	0.003	0.041	0.005	0.038	0.005
Cr	0.11	0.01	0.26	0.01	0.48	0.02	1.05	0.10
Mn	0.037	0.002	0.190	0.010	0.406	0.011	0.274	0.010
Fe	1.9	0.9	7.1	1.1	13.8	2.2	8.0	2.1
Co	0.026		0.024		0.019		0.025	
Zn	0.02	0.02	0.20	0.05	1.48	0.22	1.10	0.10
Ga	0.021		0.021	0.010	0.051		0.024	0.015
As	0.0036	0.0005	0.0091	0.0010	0.0582	0.0054	0.1222	0.0103
Se	0.008	0.008	0.017	0.009	0.181	0.022	0.296	0.041
Br	0.0047		0.0010	0.0010	0.1327	0.0323	0.4139	0.1129
Rb	0.043	0.034	0.058		0.079	0.047	0.133	
Sr	0.061		0.101		0.162		0.099	0.042
Zr	0.80	0.75	1.12		1.51	1.29	2.87	
Mo	0.005	0.002	0.009	0.003	0.014	0.003	0.020	0.005
Cd	0.0028		0.0023		0.0008	0.0008	0.0010	0.0010
In	0.00011	0.00009	0.00017	0.00014	0.00033	0.00024	0.00051	0.00029
Sb	0.190	0.030	0.018	0.007	0.116	0.022	0.050	0.009
Cs	0.0026	0.0008	0.0048	0.0010	0.0048	0.0012	0.0020	0.0009
Ba	0.09	0.04	0.27	0.06	0.48	0.09	0.20	0.07
La	0.00152	0.00010	0.00752	0.00051	0.01401	0.00108	0.00226	0.00031
Ce	0.0102	0.0102	0.0234	0.0112	0.0162	0.0086	0.0144	0.0092
Nd	0.020	0.005	0.008	0.004	0.010	0.003	0.076	0.011
Sm	0.00021	0.00002	0.00096	0.00009	0.00183	0.00022	0.00027	0.00003
Eu	0.0008	0.0001	0.0013	0.0004	0.0009	0.0003	0.0007	0.0003
Tb	0.0005	0.0004	0.0008	0.0006	0.0007	0.0007	0.0006	0.0006
Yb	0.00035		0.00050	0.00015	0.00059	0.00040	0.00033	0.00018
Lu	0.00011		0.00007	0.00004	0.00011	0.00005	0.00007	0.00006
Ta	0.0006		0.0043		0.0046		0.0044	
Au	0.00193	0.00051	0.00009	0.00002	0.00079	0.00022	0.00015	0.00004
Hg	0.0007	0.0003	0.0015	0.0003	0.0014	0.0005	0.0010	0.0004
Th	0.0016		0.0023	0.0006	0.0027	0.0010	0.0016	0.0010
U	0.00041		0.00038	0.00019	0.00088	0.00025	0.00092	0.00027

Elemental concentrations (ng/m^3) of UMn/MOUDI Aerosol Samples

Date	07/15 - 07/19/95		07/15 - 07/19/95		07/15 - 07/19/95		07/15 - 07/19/95	
Upper cutsize	0.32 µm		0.175 µm		0.098 µm		0.056 µm	
Element	conc.	+/-	conc.	+/-	conc.	+/-	conc.	+/-
Na	4.47	0.31	2.22	0.20	0.39	0.06	0.13	0.05
Mg	5.4	2.9	1.0	0.9	1.2	0.7	0.5	0.3
Al	437.8	20.4	82.8	4.1	10.5	1.0	2.1	0.2
Cl	2.81	0.51	1.59	0.31	0.45	0.12	0.20	0.08
K	22.4	2.0	9.6	1.5	1.9	0.6	1.0	0.6
Sc	0.00028	0.00010	0.00013		0.00014		0.00013	
Ti	0.48	0.48	0.12		0.11		0.27	
V	0.143	0.010	0.001	0.001	0.008		0.006	
Cr	1.14	0.10	0.18	0.01	0.01	0.01	0.33	0.02
Mn	0.354	0.010	0.058	0.010	0.001	0.001	0.052	0.002
Fe	10.0	3.1	2.0		0.8	0.8	0.9	0.9
Co	0.010	0.002	0.016		0.015		0.013	
Zn	1.80	0.20	0.66	0.09	0.01	0.01	0.47	0.07
Ga	0.036	0.018	0.010		0.019		0.023	
As	0.1417	0.0102	0.0499	0.0051	0.0025	0.0005	0.0002	0.0002
Se	0.345	0.041	0.130	0.020	0.011	0.009	0.011	0.011
Br	0.5845	0.1530	0.1458	0.0407	0.0155	0.0061	0.0020	
Rb	0.367		0.015		0.046		0.142	
Sr	0.056	0.056	0.096		0.066		0.068	
Zr	7.24		0.94	0.89	1.02		2.75	
Mo	0.022	0.006	0.003	0.002	0.002	0.002	0.007	0.002
Cd	0.0017	0.0017	0.0027		0.0016		0.0012	
In	0.00083	0.00038	0.00030	0.00019	0.00013	0.00008	0.00010	0.00010
Sb	0.150	0.020	0.096	0.014	0.072	0.011	0.140	0.020
Cs	0.0042	0.0011	0.0041	0.0010	0.0019	0.0007	0.0036	0.0010
Ba	0.19	0.06	0.13	0.05	0.07	0.03	0.11	0.04
La	0.00173	0.00031	0.00013	0.00013	0.00056	0.00008	0.00018	0.00006
Ce	0.0245		0.0244		0.0193		0.0048	
Nd	0.011	0.011	0.030	0.006	0.020	0.005	0.009	0.005
Sm	0.00015	0.00002	0.00007	0.00002	0.00008	0.00001	0.00001	0.00001
Eu	0.0012	0.0004	0.0009	0.0003	0.0005	0.0002	0.0005	0.0003
Tb	0.0012		0.0010	0.0006	0.0011	0.0006	0.0016	0.0007
Yb	0.00095		0.00025	0.00015	0.00025	0.00013	0.00039	
Lu	0.00032		0.00007	0.00005	0.00009		0.00013	
Ta	0.0045		0.0042		0.0037		0.0046	
Au	0.00025	0.00007	0.00021	0.00006	0.00003	0.00001	0.00007	0.00002
Hg	0.0011	0.0006	0.0013	0.0004	0.0007	0.0003	0.0006	0.0003
Th	0.0153	0.0031	0.0012		0.0010		0.0008	
U	0.00029	0.00029	0.00071	0.00025	0.00044		0.00007	

Elemental concentrations (ng/m^3) of UMn/MOUDI Aerosol Samples

Date	07/15 - 07/19/95		07/20 - 07/24/95		07/20 - 07/24/95		07/20 - 07/24/95	
Upper cutsize	After Filter		3.2 µm		1.8 µm		1.0 µm	
Element	conc.	+/-	conc.	+/-	conc.	+/-	conc.	+/-
Na	0.11	0.05	0.65	0.10	6.94	0.48	13.74	1.01
Mg	0.8		0.6	0.4	2.3	0.6	7.8	1.8
Al	2.9	0.2	1.8	0.1	19.4	1.0	35.8	2.0
Cl	0.60	0.18	0.17		0.30		0.16	0.08
K	2.4		1.3		2.9		9.7	2.0
Sc	0.00013		0.00022	0.00008	0.00223	0.00019	0.00601	0.00040
Ti	0.03	0.03	0.19		0.97	0.19	2.45	0.40
V	0.008	0.003	0.005		0.004	0.003	0.060	0.006
Cr	2.76	0.10	0.02	0.01	0.06		0.21	0.03
Mn	0.291	0.010	0.006	0.001	0.121	0.010	0.513	0.010
Fe	13.0	1.0	1.2	0.6	6.8	1.6	16.0	6.1
Co	0.023	0.003	0.005		0.009		0.023	
Zn	0.42	0.07	0.11		0.05	0.03	0.78	0.10
Ga	0.037		0.004	0.004	0.036		0.057	
As	0.0006	0.0003	0.0011	0.0006	0.0172	0.0019	0.0324	0.0030
Se	0.008		0.010		0.006	0.006	0.099	0.020
Br	0.0009		0.0013	0.0013	0.0018	0.0018	0.0862	0.0202
Rb	0.075		0.003		0.050	0.035	0.557	
Sr	0.054	0.028	0.030	0.024	0.095		0.074	
Zr	0.98		0.60		1.62		7.99	
Mo	0.028	0.007	0.004		0.001		0.010	0.006
Cd	0.0025		0.0002	0.0002	0.0024	0.0024	0.0048	0.0048
In	0.00014	0.00013	0.00011	0.00010	0.00031	0.00025	0.00057	0.00034
Sb	0.057	0.010	0.007	0.004	0.022	0.006	0.230	0.030
Cs	0.0007		0.0005		0.0017	0.0008	0.0425	
Ba	0.10	0.05	0.06	0.04	0.16	0.06	0.62	0.10
La	0.00018	0.00007	0.00219	0.00019	0.01431	0.00095	0.03339	0.00202
Ce	0.0193		0.0051	0.0051	0.0277	0.0076	0.0063	0.0017
Nd	0.019	0.006	0.006		0.006		0.023	0.018
Sm	0.00004	0.00001	0.00022	0.00003	0.00172	0.00019	0.00374	0.00030
Eu	0.0011	0.0004	0.0009	0.0004	0.0014	0.0004	0.0018	0.0004
Tb	0.0005	0.0005	0.0017		0.0011	0.0005	0.0008	0.0005
Yb	0.00035		0.00030		0.00105	0.00029	0.00064	0.00063
Lu	0.00009		0.00008		0.00024	0.00008	0.00023	0.00018
Ta	0.0043		0.0012	0.0010	0.0033		0.0035	
Au	0.00011	0.00002	0.00001	0.000003	0.00001		0.00001	
Hg	0.0011	0.0005	0.0006	0.0003	0.0007	0.0003	0.0012	0.0007
Th	0.0006		0.0008		0.0033	0.0009	0.0111	0.0030
U	0.00039	0.00016	0.00023	0.00022	0.00069	0.00031	0.00044	0.00042

Elemental concentrations (ng/m^3) of UMn/MOUDI Aerosol Samples

Date	07/20 - 07/24/95		07/20 - 07/24/95		07/20 - 07/24/95		07/20 - 07/24/95	
Upper cutsize	0.56 μm		0.32 μm		0.175 μm		0.098 μm	
Element	conc.	+/-	conc.	+/-	conc.	+/-	conc.	+/-
Na	5.28	0.39	2.66	0.19	2.66	0.19	1.51	0.10
Mg	2.4	1.5	0.5		0.4		0.4	
Al	12.9	1.0	2.3	0.2	1.3	0.2	0.2	0.1
Cl	0.73	0.19	0.59	0.14	0.36	0.11	1.11	0.19
K	6.6	1.5	10.5	1.0	7.0	1.1	4.4	1.0
Sc	0.00091	0.00010	0.00007	0.00007	0.00023		0.00021	
Ti	0.48	0.24	0.21		0.37	0.21	0.04	0.04
V	0.106	0.010	0.105	0.010	0.046	0.005	0.021	0.003
Cr	0.07	0.02	0.12	0.01	0.88	0.03	0.15	0.02
Mn	0.209	0.010	0.102	0.010	0.121	0.010	0.012	0.001
Fe	1.8		2.0	1.2	3.9	1.0	0.5	0.5
Co	0.026		0.020		0.019	0.003	0.011	0.002
Zn	7.49	0.77	0.83	0.10	0.54	0.08	0.13	0.04
Ga	0.039		0.033		0.013	0.011	0.024	
As	0.0839	0.0087	0.1044	0.0096	0.0545	0.0057	0.0096	0.0010
Se	0.201	0.029	0.228	0.029	0.084	0.010	0.003	0.003
Br	0.5333	0.1446	0.7021	0.1915	0.2898	0.0765	0.0336	0.0105
Rb	0.183		0.105		0.047	0.024	0.239	
Sr	0.066		0.030		0.074	0.039	0.073	
Zr	2.80		1.72		0.18		3.53	
Mo	0.013	0.004	0.017	0.005	0.020	0.005	0.006	0.003
Cd	0.0031	0.0031	0.0026	0.0026	0.0071	0.0071	0.0032	0.0032
In	0.00041	0.00024	0.00039	0.00019	0.00032	0.00021	0.00024	0.00015
Sb	0.133	0.019	0.132	0.019	0.103	0.019	0.025	0.007
Cs	0.0004		0.0029	0.0010	0.0011	0.0007	0.0018	
Ba	0.22	0.06	0.09	0.05	0.45	0.07	0.15	0.05
La	0.00550	0.00048	0.00105	0.00019	0.00041	0.00013	0.00033	
Ce	0.0086	0.0072	0.0105	0.0067	0.0191		0.0172	
Nd	0.125	0.019	0.105	0.019	0.049	0.009	0.026	0.010
Sm	0.00064	0.00006	0.00019	0.00004	0.00011	0.00002	0.00003	0.00001
Eu	0.0007	0.0002	0.0007		0.0006	0.0003	0.0004	0.0002
Tb	0.0003		0.0011		0.0011		0.0011	
Yb	0.00183		0.00049	0.00027	0.00047		0.00029	0.00023
Lu	0.00013	0.00010	0.00006		0.00012		0.00023	
Ta	0.0029		0.0034		0.0036		0.0033	
Au	0.00154	0.00019	0.00003	0.00001	0.00007	0.00001	0.00011	0.00001
Hg	0.0006	0.0004	0.0006	0.0003	0.0008	0.0003	0.0004	0.0004
Th	0.0042	0.0013	0.0021		0.0014		0.0050	0.0017
U	0.00082	0.00032	0.00153	0.00038	0.00047	0.00032	0.00075	

Elemental concentrations (ng/m^3) of UMn/MOUDI Aerosol Samples

Date	07/20 - 07/24/95		07/20 - 07/24/95		07/25 - 07/29/95		07/25 - 07/29/95	
Upper cutsize	0.056 µm		After Filter		3.2 µm		1.8 µm	
Element	conc.	+/-	conc.	+/-	conc.	+/-	conc.	+/-
Na	0.31		0.26		2.58	0.19	22.72	1.93
Mg	0.3		0.4		1.7	0.6	10.6	1.9
Al	0.4		0.3	0.1	8.5	0.4	65.8	2.9
Cl	0.30	0.10	0.30		0.22	0.07	0.73	0.10
K	1.2		1.7		3.7	1.1	14.5	2.9
Sc	0.00011		0.00010		0.00119	0.00010	0.01131	0.00096
Ti	0.17		0.19		0.23	0.16	3.97	0.48
V	0.003		0.010		0.005	0.002	0.125	0.010
Cr	0.38	0.02	0.60	0.02	0.05		0.10	0.01
Mn	0.029	0.001	0.064	0.010	0.084	0.010	0.700	0.010
Fe	2.1		1.9	0.7	2.6	0.9	40.3	2.9
Co	0.008		0.018		0.013		0.039	0.004
Zn	0.13		0.15		0.17		0.11	0.04
Ga	0.019		0.014	0.010	0.005	0.005	0.047	
As	0.0011	0.0006	0.0006		0.0013	0.0004	0.0116	0.0019
Se	0.009		0.001	0.001	0.007		0.029	0.008
Br	0.0054		0.0021		0.0046		0.0039	
Rb	0.033		0.043		0.106		0.260	
Sr	0.054	0.034	0.083		0.016		0.106	0.067
Zr	0.26	0.25	0.42		0.88		1.45	1.16
Mo	0.003	0.002	0.009	0.002	0.0002		0.003	0.003
Cd	0.0060	0.0060	0.0026		0.0016		0.0013	
In	0.00011	0.00009	0.00010		0.00013	0.00011	0.00043	
Sb	0.033	0.007	0.0071	0.0034	0.045	0.009	0.028	0.006
Cs	0.0014	0.0009	0.0031	0.0008	0.0027	0.0010	0.0067	0.0015
Ba	0.07		0.06	0.04	0.25	0.05	0.66	0.09
La	0.00020		0.00012	0.00005	0.00588	0.00039	0.05299	0.00385
Ce	0.0162		0.0068	0.0042	0.0073		0.0877	0.0087
Nd	0.008		0.017	0.004	0.011	0.004	0.049	0.011
Sm	0.00004	0.00001	0.00002	0.00001	0.00085	0.00008	0.00732	0.00067
Eu	0.0005		0.0008	0.0002	0.0006	0.0003	0.0026	0.0004
Tb	0.0004	0.0003	0.0003	0.0003	0.0006	0.0005	0.0013	0.0004
Yb	0.00032		0.00018		0.00036	0.00013	0.00299	0.00058
Lu	0.00009		0.00005		0.00003	0.00002	0.00036	0.00011
Ta	0.0032		0.0032		0.0010	0.0010	0.0012	0.0012
Au	0.00001	0.000003	0.00003	0.000004	0.00005	0.00001	0.00004	0.00001
Hg	0.0004	0.0003	0.0010	0.0002	0.0005	0.0002	0.0005	0.0005
Th	0.0010		0.0009		0.0022	0.0006	0.0116	0.0010
U	0.00025	0.00022	0.00052		0.00047		0.00116	

Elemental concentrations (ng/m^3) of UMn/MOUDI Aerosol Samples

Date	07/25 - 07/29/95		07/25 - 07/29/95		07/25 - 07/29/95		07/25 - 07/29/95	
Upper cutsize	1.0 μm		0.56 μm		0.32 μm		0.175 μm	
Element	conc.	+/-	conc.	+/-	conc.	+/-	conc.	+/-
Na	31.25	2.04	7.87	0.58	3.27	0.29	1.33	0.10
Mg	18.4	4.1	4.6	1.2	0.9	0.8	0.3	
Al	142.4	10.2	55.8	2.9	7.3	0.4	2.1	0.2
Cl	0.78	0.10	0.33	0.09	0.24	0.08	0.11	0.06
K	28.6	4.1	12.7	2.9	12.6	1.9	4.9	1.0
Sc	0.02835	0.00204	0.00939	0.00068	0.00101	0.00010	0.00014	0.00009
Ti	9.12	0.92	2.84	0.49	0.89	0.39	0.07	0.07
V	0.245	0.020	0.253	0.019	0.242	0.019	0.077	0.010
Cr	0.19	0.02	0.07	0.01	0.01	0.01	0.08	0.02
Mn	1.336	0.020	0.581	0.010	0.123	0.010	0.047	0.002
Fe	80.5	6.1	32.9	2.9	4.4	1.0	2.8	2.0
Co	0.059	0.005	0.015	0.003	0.022		0.015	0.003
Zn	0.55	0.08	0.56	0.08	0.42	0.07	0.32	0.06
Ga	0.036	0.025	0.039		0.023		0.017	
As	0.0388	0.0041	0.0555	0.0058	0.0590	0.0058	0.0348	0.0039
Se	0.100	0.010	0.075	0.012	0.044	0.009	0.016	0.007
Br	0.0309	0.0102	0.1589	0.0390	0.1385	0.0387	0.1286	0.0386
Rb	0.715		0.282		0.008		0.309	
Sr	0.491	0.133	0.061	0.061	0.046	0.042	0.078	
Zr	5.93		2.43		0.80		2.80	
Mo	0.011	0.004	0.002	0.002	0.003	0.002	0.013	0.003
Cd	0.0086	0.0061	0.0021	0.0021	0.0024	0.0024	0.0014	0.0014
In	0.00048	0.00043	0.00026	0.00022	0.00023	0.00018	0.00019	0.00014
Sb	0.065	0.012	0.091	0.015	0.081	0.014	0.071	0.013
Cs	0.0102	0.0020	0.0063	0.0014	0.0048	0.0012	0.0025	0.0010
Ba	1.33	0.10	0.61	0.09	0.31	0.07	0.18	0.05
La	0.12265	0.01022	0.04090	0.00292	0.00542	0.00039	0.00241	0.00029
Ce	0.2351	0.0204	0.0779	0.0117	0.0222		0.0154	0.0077
Nd	0.077	0.021	0.070	0.013	0.039	0.009	0.081	0.015
Sm	0.01737	0.00102	0.00575	0.00049	0.00074	0.00007	0.00024	0.00003
Eu	0.0047	0.0006	0.0013	0.0004	0.0014	0.0004	0.0008	0.0003
Tb	0.0013	0.0009	0.0011	0.0005	0.0003		0.0006	0.0003
Yb	0.00583	0.00112	0.00156	0.00039	0.00037	0.00019	0.00067	
Lu	0.00093	0.00025	0.00017	0.00007	0.00006	0.00003	0.00014	
Ta	0.0052	0.0022	0.0043		0.0040		0.0037	
Au	0.00005	0.00001	0.00005	0.00001	0.00015	0.00003	0.00012	0.00002
Hg	0.0003		0.0008	0.0004	0.0009	0.0003	0.0008	0.0003
Th	0.0378	0.0051	0.0107	0.0010	0.0024	0.0007	0.0071	0.0014
U	0.00184		0.00097	0.00029	0.00030	0.00024	0.00067	0.00029

Elemental concentrations (ng/m^3) of UMn/MOUDI Aerosol Samples

Date	07/25 - 07/29/95		07/25 - 07/29/95		07/25 - 07/29/95		07/30 - 08/03/95	
Upper cutsize	0.098 µm		0.056 µm		After Filter		3.2 µm	
Element	conc.	+/-	conc.	+/-	conc.	+/-	conc.	+/-
Na	0.28	0.05	0.40		0.27		2.69	0.19
Mg	0.3	0.3	0.1		0.4		1.3	1.2
Al	0.4	0.1	0.5		0.4		2.2	0.1
Cl	0.02	0.02	0.23		0.01	0.01	1.22	0.19
K	2.6	0.5	1.3		1.0	0.7	1.7	0.6
Sc	0.00005	0.00005	0.00014		0.00011		0.00026	0.00010
Ti	0.18		0.16		0.24		0.22	0.16
V	0.009		0.008		0.002		0.014	0.003
Cr	0.04		0.043		0.07	0.01	0.052	
Mn	0.041		0.001	0.001	0.033		0.013	0.001
Fe	2.0		1.2		2.0		2.0	
Co	0.008		0.006		0.008		0.010	0.002
Zn	0.21		0.14		1.71	0.19	0.66	0.09
Ga	0.004		0.011		0.013		0.024	0.023
As	0.0067	0.0008	0.0017	0.0004	0.0009		0.0007	
Se	0.008		0.003		0.009		0.010	
Br	0.0214	0.0077	0.0041		0.0004		0.0056	
Rb	0.145	0.068	0.045	0.024	0.065		0.058	
Sr	0.055		0.054		0.070		0.085	
Zr	1.16	0.96	0.39		0.93		0.69	
Mo	0.001		0.001	0.001	0.002	0.002	0.002	
Cd	0.0017		0.0019		0.0029		0.0139	0.0097
In	0.00010	0.00010	0.00005	0.00005	0.00011	0.00008	0.00007	
Sb	0.052	0.009	0.066	0.011	0.042	0.010	0.024	0.007
Cs	0.0041	0.0017	0.0041	0.0011	0.0036	0.0012	0.0023	0.0009
Ba	0.06	0.03	0.11	0.04	0.07		0.10	0.05
La	0.00078	0.00012	0.00030	0.00008	0.00029	0.00007	0.00184	0.00019
Ce	0.0164	0.0087	0.0203		0.0260		0.0092	
Nd	0.034	0.009	0.018	0.004	0.019	0.007	0.015	
Sm	0.00010	0.00001	0.00002	0.00001	0.00003		0.00024	0.00004
Eu	0.0012	0.0004	0.0008	0.0003	0.0008	0.0003	0.0005	0.0003
Tb	0.0008		0.0007		0.0008	0.0004	0.0007	0.0004
Yb	0.00042		0.00062		0.00030		0.00034	
Lu	0.00010		0.00005	0.00002	0.00010		0.00010	
Ta	0.0037		0.0034		0.0028		0.0044	
Au	0.00009	0.00002	0.000020	0.000005	0.000020	0.000005	0.00015	0.00004
Hg	0.0002	0.0002	0.0005	0.0002	0.0009	0.0002	0.0003	
Th	0.0038	0.0011	0.0008		0.0015		0.0004	
U	0.00049		0.00041		0.00067		0.00085	

Elemental concentrations (ng/m^3) of UMn/MOUDI Aerosol Samples

Date	07/30 - 08/03/95		07/30 - 08/03/95		07/30 - 08/03/95		07/30 - 08/03/95	
Upper cutsize	1.8 μm		1.0 μm		0.56 μm		0.32 μm	
Element	conc.	+/-	conc.	+/-	conc.	+/-	conc.	+/-
Na	20.86	0.97	30.33	2.05	6.53	0.49	4.54	0.29
Mg	10.6	1.9	16.4	4.1	4.8	1.6	0.5	
Al	11.9	1.0	31.1	1.0	10.1	1.0	2.6	0.2
Cl	6.24	0.87	3.14	0.51	0.31	0.09	0.52	0.12
K	7.2	2.1	9.1	2.1	6.8	1.4	7.6	1.6
Sc	0.00168	0.00019	0.00619	0.00041	0.00111	0.00010	0.00008	0.00008
Ti	0.41	0.27	1.66	0.41	0.32	0.32	0.70	0.29
V	0.012	0.003	0.052	0.006	0.077	0.006	0.165	0.010
Cr	0.025		0.06	0.01	0.04		0.03	0.02
Mn	0.084	0.010	0.253	0.010	0.085	0.010	0.094	0.010
Fe	4.5	1.2	22.4	5.1	3.9	1.2	0.9	0.9
Co	0.016		0.006	0.002	0.012		0.035	0.004
Zn	0.14	0.04	0.24	0.05	0.53	0.08	0.28	0.06
Ga	0.042	0.027	0.097		0.054		0.048	
As	0.0022	0.0008	0.0164	0.0021	0.0508	0.0049	0.0495	0.0049
Se	0.011		0.033	0.012	0.075	0.013	0.115	0.019
Br	0.0034		0.0115	0.0051	0.1301	0.0391	0.1390	0.0388
Rb	0.164		0.236	0.164	0.029		0.456	
Sr	0.090	0.054	0.185		0.042		0.116	
Zr	1.45		0.94		1.07	0.88	4.46	
Mo	0.005		0.006	0.004	0.003	0.002	0.012	0.004
Cd	0.0371	0.0222	0.0017		0.0053	0.0053	0.0159	0.0146
In	0.00018		0.00030	0.00030	0.00041	0.00026	0.00028	0.00026
Sb	0.025	0.008	0.015	0.009	0.063	0.014	0.289	0.049
Cs	0.0027	0.0009	0.0042	0.0014	0.0027	0.0009	0.0033	0.0010
Ba	0.17	0.06	0.38	0.08	0.11	0.05	0.04	
La	0.00744	0.00058	0.01846	0.00103	0.00488	0.00039	0.00074	0.00019
Ce	0.0135	0.0135	0.0369	0.0123	0.0313		0.0349	
Nd	0.011	0.009	0.053		0.052	0.011	0.076	0.022
Sm	0.00106	0.00010	0.00277	0.00021	0.00068	0.00007	0.00011	0.00002
Eu	0.0012	0.0003	0.0017	0.0004	0.0008	0.0002	0.0010	0.0004
Tb	0.0006	0.0004	0.0011	0.0006	0.0008	0.0004	0.0008	0.0004
Yb	0.00065	0.00051	0.00123	0.00051	0.00048		0.00095	
Lu	0.00007	0.00005	0.00029		0.00007	0.00004	0.00025	
Ta	0.0047		0.0072		0.0041		0.0049	
Au	0.00004	0.00001	0.00005	0.00001	0.00006	0.00001	0.00011	0.00002
Hg	0.0002		0.0008		0.0008	0.0005	0.0016	0.0005
Th	0.0022	0.0007	0.0070	0.0024	0.0029	0.0008	0.0146	0.0029
U	0.00084		0.00070	0.00068	0.00095		0.00081	0.00036

Elemental concentrations (ng/m^3) of UMn/MOUDI Aerosol Samples

Date	07/30 - 08/03/95		07/30 - 08/03/95		07/30 - 08/03/95		07/30 - 08/03/95	
Upper cutsize	0.175 µm		0.098 µm		0.056 µm		After Filter	
Element	conc.	+/-	conc.	+/-	conc.	+/-	conc.	+/-
Na	4.15	0.29	0.85	0.10	0.49	0.07	0.23	
Mg	1.5	1.2	0.4		1.2	0.3	0.3	
Al	2.5	0.2	0.1	0.1	0.3	0.1	0.43	
Cl	1.12	0.19	0.01	0.01	0.50	0.12	0.17	
K	10.7	1.9	1.8	0.5	1.8	0.8	1.3	
Sc	0.00002	0.00002	0.00014		0.00019		0.00012	
Ti	0.23	0.18	0.21		0.38	0.29	0.20	
V	0.232	0.010	0.017		0.005	0.002	0.008	
Cr	0.16	0.01	0.063		0.06		0.53	0.02
Mn	0.033	0.002	0.028		0.018	0.001	0.039	0.002
Fe	3.6	1.1	1.9		1.5		2.1	0.7
Co	0.225	0.010	0.017		0.018		0.019	
Zn	0.46	0.07	0.21		0.14	0.04	0.21	
Ga	0.044		0.029		0.032		0.019	
As	0.0310	0.0029	0.0064	0.0008	0.0015	0.0003	0.0005	
Se	0.026	0.010	0.012		0.003	0.003	0.005	
Br	0.0496	0.0145	0.0008	0.0008	0.0015		0.0009	
Rb	0.136		0.072		0.232		0.043	
Sr	0.107		0.057	0.027	0.071		0.031	0.031
Zr	1.36		1.45	0.97	2.32		0.64	
Mo	0.029	0.007	0.003	0.002	0.004	0.002	0.008	0.002
Cd	0.0061	0.0061	0.0019	0.0019	0.0110	0.0097	0.0020	
In	0.00030	0.00019	0.00010	0.00010	0.00015	0.00014	0.00006	
Sb	0.066	0.015	0.025	0.008	0.123	0.019	0.0101	0.0039
Cs	0.0032	0.0012	0.0032	0.0010	0.0030	0.0010	0.0024	0.0009
Ba	0.23	0.06	0.12	0.04	0.15	0.04	0.07	
La	0.00136	0.00019	0.00037	0.00010	0.00019	0.00010	0.00009	0.00002
Ce	0.0320	0.0155	0.0300		0.0165	0.0126	0.0043	
Nd	0.046	0.013	0.037	0.009	0.053	0.016	0.012	0.004
Sm	0.00012	0.00002	0.00003	0.00002	0.00003	0.00001	0.00002	0.00001
Eu	0.0006	0.0003	0.0006	0.0002	0.0009	0.0004	0.0006	0.0003
Tb	0.0014	0.0005	0.0010		0.0011	0.0011	0.0003	0.0002
Yb	0.00024	0.00021	0.00032		0.00030	0.00021	0.00007	0.00007
Lu	0.00223	0.00048	0.00004	0.00004	0.00018		0.00007	
Ta	0.0028	0.0014	0.0043		0.0027	0.0015	0.0019	0.0012
Au	0.00007	0.00002	0.00009	0.00002	0.00242	0.00048	0.00003	0.00001
Hg	0.0010	0.0006	0.0009	0.0004	0.0005	0.0003	0.0010	0.0003
Th	0.0018	0.0011	0.0013		0.0035	0.0015	0.0004	0.0003
U	0.00126	0.00039	0.00064		0.00054	0.00030	0.00069	

Elemental concentrations (ng/m^3) of UMn/MOUDI Aerosol Samples

Date	08/04 - 08/08/95		08/04 - 08/08/95		08/04 - 08/08/95		08/04 - 08/08/95	
Upper cutsize	3.2 µm		1.8 µm		1.0 µm		0.56 µm	
Element	conc.	+/-	conc.	+/-	conc.	+/-	conc.	+/-
Na	5.63	0.37	11.65	0.93	20.22	0.98	3.73	0.28
Mg	2.1	0.9	2.6	1.0	8.8	1.7	1.0	0.7
Al	1.6	0.1	6.3	0.3	19.0	1.0	4.3	0.3
Cl	0.20	0.06	2.28	0.46	0.33		0.23	
K	1.7	0.6	2.7		6.3	1.8	3.8	0.9
Sc	0.00013	0.00007	0.00124	0.00009	0.00338	0.00029	0.00057	0.00009
Ti	0.17		0.48	0.25	1.00	0.29	0.33	0.22
V	0.002		0.017		0.028	0.004	0.075	0.009
Cr	0.07		0.10	0.01	0.08		0.16	0.01
Mn	0.053	0.009	0.062	0.009	0.184	0.010	0.091	0.009
Fe	0.8		1.9	1.6	10.6	2.0	2.3	1.1
Co	0.012		0.017		0.017		0.025	
Zn	0.17		0.20		0.14	0.04	0.17	0.05
Ga	0.036		0.047		0.059		0.023	0.017
As	0.0001	0.0001	0.0015	0.0006	0.0108	0.0020	0.0365	0.0037
Se	0.008		0.011	0.007	0.037	0.012	0.052	0.009
Br	0.0022		0.0046		0.0218	0.0079	0.1808	0.0468
Rb	0.111		0.194		0.157		0.064	0.043
Sr	0.080		0.102		0.138		0.080	
Zr	1.20		2.13		1.08	0.79	1.31	
Mo	0.002	0.001	0.006		0.006	0.003	0.008	0.002
Cd	0.0012		0.0011	0.0011	0.0013		0.0028	
In	0.00026	0.00018	0.00015	0.00013	0.00024		0.00031	0.00018
Sb	0.192	0.028	0.027	0.006	0.049	0.009	0.048	0.008
Cs	0.0010	0.0003	0.0029	0.0007	0.0022	0.0007	0.0022	0.0008
Ba	0.14	0.05	0.08	0.04	0.28	0.06	0.12	0.04
La	0.00056	0.00011	0.00528	0.00046	0.01375	0.00098	0.00290	0.00028
Ce	0.0074	0.0052	0.0222	0.0074	0.0147	0.0079	0.0042	
Nd	0.006	0.004	0.014		0.014	0.006	0.037	0.007
Sm	0.00010	0.00001	0.00070	0.00006	0.00177	0.00020	0.00039	0.00004
Eu	0.0007		0.0008	0.0003	0.0010	0.0004	0.0007	0.0002
Tb	0.0002		0.0015	0.0005	0.0009	0.0004	0.0009	0.0005
Yb	0.00082		0.00040	0.00024	0.00070	0.00045	0.00042	
Lu	0.00009		0.00011		0.00021	0.00008	0.00003	
Ta	0.0014	0.0014	0.0036		0.0039		0.0031	
Au	0.000023	0.000005	0.00002	0.00001	0.00004	0.00001	0.00003	0.00001
Hg	0.0048	0.0003	0.0034	0.0006	0.0023	0.0007	0.0008	0.0004
Th	0.0006	0.0006	0.0021		0.0036	0.0010	0.0004	
U	0.00069		0.00019		0.00079		0.00094	

Elemental concentrations (ng/m^3) of UMn/MOUDI Aerosol Samples

Date	08/04 - 08/08/95		08/04 - 08/08/95		08/04 - 08/08/95		08/04 - 08/08/95	
Upper cutsize	0.32 µm		0.175 µm		0.098 µm		0.056 µm	
Element	conc.	+/-	conc.	+/-	conc.	+/-	conc.	+/-
Na	1.00	0.09	0.54	0.09	0.34		0.50	0.06
Mg	0.7	0.4	0.6	0.2	0.5		0.2	0.2
Al	0.27	0.07	0.53		0.27		0.2	
Cl	0.24		0.20		0.19		0.61	0.09
K	2.4	0.7	2.0	0.6	0.9		0.6	0.3
Sc	0.00010		0.00012		0.00006		0.00009	
Ti	0.23		0.19		0.06		0.08	
V	0.084	0.009	0.006	0.002	0.002		0.002	
Cr	0.21	0.02	0.032		0.013		0.017	
Mn	0.020	0.001	0.001	0.001	0.039		0.027	
Fe	0.4	0.4	1.9		1.6		1.4	
Co	0.011		0.014		0.007		0.007	
Zn	0.44	0.07	0.25	0.05	0.18		0.18	0.05
Ga	0.009	0.008	0.007	0.004	0.011	0.005	0.019	
As	0.0251	0.0028	0.0223	0.0019	0.0073	0.0008	0.0011	0.0003
Se	0.040	0.008	0.012	0.006	0.001	0.001	0.010	
Br	0.0467	0.0139	0.0215	0.0074	0.0037		0.0015	
Rb	0.205		0.241		0.023	0.021	0.070	
Sr	0.066		0.051		0.045		0.025	0.016
Zr	0.83		2.60		0.90		0.54	0.40
Mo	0.009	0.003	0.005		0.003		0.003	
Cd	0.0033		0.0008	0.0008	0.0022		0.0014	
In	0.00015	0.00013	0.00006		0.00006		0.00018	0.00012
Sb	0.045	0.008	0.071	0.011	0.083	0.013	0.041	0.007
Cs	0.0016	0.0008	0.0023	0.0009	0.0021	0.0011	0.0028	0.0006
Ba	0.06	0.04	0.17	0.04	0.07	0.03	0.07	
La	0.00051	0.00011	0.00005		0.00011		0.00015	
Ce	0.0051	0.0048	0.0121		0.0130		0.0139	
Nd	0.018	0.007	0.011	0.009	0.013	0.004	0.019	0.005
Sm	0.00006	0.00001	0.00001	0.00001	0.00001	0.00001	0.00001	0.00001
Eu	0.0006	0.0004	0.0006	0.0003	0.0005	0.0003	0.0003	
Tb	0.0011		0.0003	0.0003	0.0004	0.0004	0.0008	0.0005
Yb	0.00018	0.00015	0.00083	0.00047	0.00012	0.00009	0.00029	0.00016
Lu	0.00017		0.00019		0.00006	0.00004	0.00002	0.00002
Ta	0.0031		0.0027		0.0011	0.0007	0.0019	0.0019
Au	0.000020	0.000005	0.000015	0.000004	0.000016	0.000003	0.000009	0.000003
Hg	0.0009	0.0005	0.0017	0.0005	0.0009	0.0002	0.0008	0.0003
Th	0.0043	0.0013	0.0057	0.0015	0.0002		0.0001	
U	0.00055	0.00027	0.00008		0.00057		0.00057	

Elemental concentrations (ng/m^3) of UMn/MOUDI Aerosol Samples

Date	08/04 - 08/08/95		08/09 - 08/13/95		08/09 - 08/13/95		08/09 - 08/13/95	
Upper cutsize	After Filter		3.2 µm		1.8 µm		1.0 µm	
Element	conc.	+/-	conc.	+/-	conc.	+/-	conc.	+/-
Na	0.09		1.28	0.09	13.50	0.93	24.15	1.96
Mg	0.2	0.2	0.3	0.2	3.4	0.6	8.8	2.0
Al	0.29		1.6	0.1	17.9	0.9	46.5	2.0
Cl	0.16		0.20		0.09	0.08	0.13	0.11
K	0.8		3.2	0.6	8.5	1.9	7.8	1.6
Sc	0.00007		0.00016	0.00006	0.00291	0.00019	0.00711	0.00049
Ti	0.13		0.26		1.04	0.28	1.98	0.39
V	0.002		0.004		0.012	0.003	0.098	0.010
Cr	0.021		0.017		0.052		0.001	0.001
Mn	0.018		0.002	0.001	0.182	0.009	0.528	0.010
Fe	1.3		0.6	0.6	8.1	2.8	20.4	2.9
Co	0.005		0.005		0.011		0.019	
Zn	0.11	0.04	0.13		0.08	0.04	0.85	0.10
Ga	0.017		0.024		0.050		0.069	
As	0.0004		0.0009	0.0003	0.0068	0.0010	0.0472	0.0049
Se	0.008		0.008		0.018	0.006	0.155	0.020
Br	0.0021		0.0026		0.0057	0.0037	0.1800	0.0491
Rb	0.034	0.016	0.077		0.269		0.011	
Sr	0.055		0.064		0.139		0.097	0.060
Zr	0.36		0.73		2.13		1.96	
Mo	0.003		0.003		0.004	0.003	0.012	0.004
Cd	0.0032		0.0016		0.0009	0.0009	0.0016	
In	0.00005		0.00016	0.00012	0.00019	0.00012	0.00052	0.00034
Sb	0.038	0.006	0.005	0.002	0.060	0.010	0.165	0.029
Cs	0.0010	0.0006	0.0015		0.0021	0.0009	0.0047	0.0011
Ba	0.01		0.09	0.03	0.31	0.06	0.54	0.09
La	0.00013		0.00157	0.00019	0.01204	0.00093	0.02750	0.00196
Ce	0.0039	0.0028	0.0081		0.0204	0.0046	0.0403	0.0098
Nd	0.010	0.003	0.002		0.010	0.007	0.016	0.009
Sm	0.00002		0.00022	0.00002	0.00148	0.00009	0.00354	0.00029
Eu	0.0004		0.0006	0.0002	0.0011	0.0003	0.0020	0.0004
Tb	0.0002	0.0002	0.0008		0.0004	0.0004	0.0009	
Yb	0.00008	0.00008	0.00011	0.00008	0.00034	0.00031	0.00138	0.00039
Lu	0.00006		0.00006		0.00021	0.00009	0.00011	0.00009
Ta	0.0028		0.0025		0.0032		0.0017	0.0013
Au	0.00003	0.00001	0.000001	0.0000002	0.000022	0.000009	0.00021	0.000039
Hg	0.0004		0.0006	0.0002	0.0009	0.0005	0.0015	
Th	0.0010		0.0011		0.0032	0.0012	0.0054	0.0015
U	0.00025	0.00022	0.00064		0.00093	0.00065	0.00314	0.00079

Elemental concentrations (ng/m^3) of UMn/MOUDI Aerosol Samples

Date	08/09 - 08/13/95		08/09 - 08/13/95		08/09 - 08/13/95		08/09 - 08/13/95	
Upper cutsize	0.56 μm		0.32 μm		0.175 μm		0.098 μm	
Element	conc.	+/-	conc.	+/-	conc.	+/-	conc.	+/-
Na	4.47	0.28	2.86	0.19	2.02	0.19	0.20	0.05
Mg	1.3	0.7	0.4	0.3	0.2		0.2	0.2
Al	4.7	0.3	0.8	0.1	1.8	0.2	0.31	
Cl	0.20	0.08	0.71	0.19	0.32		0.11	
K	9.4	1.9	10.2	1.9	6.0	1.0	1.8	0.6
Sc	0.00052	0.00008	0.00021		0.00012		0.00012	
Ti	0.27		0.14		0.05		0.19	
V	0.103	0.009	0.050	0.005	0.002	0.002	0.002	
Cr	0.052		0.014	0.011	0.015	0.015	0.027	
Mn	0.184	0.009	0.090	0.009	0.023	0.001	0.022	
Fe	5.3	2.5	0.9	0.9	6.5		1.3	
Co	0.007		0.009		0.010		0.002	
Zn	0.71	0.09	0.52	0.07	0.39	0.06	0.02	0.02
Ga	0.045		0.042		0.029		0.005	
As	0.0693	0.0066	0.1199	0.0093	0.0677	0.0065	0.0167	0.0019
Se	0.204	0.028	0.147	0.019	0.044	0.008	0.009	
Br	0.6394	0.1685	0.2912	0.0744	0.0818	0.0232	0.0017	0.0017
Rb	0.300		0.167		0.061		0.148	
Sr	0.140		0.112		0.084		0.057	
Zr	3.00		1.67		3.62		1.39	
Mo	0.017	0.005	0.016	0.005	0.004	0.003	0.002	0.002
Cd	0.0069	0.0056	0.0020		0.0046	0.0044	0.0031	
In	0.00039	0.00021	0.00024	0.00020	0.00024	0.00015	0.00014	0.00010
Sb	0.166	0.019	0.119	0.019	0.100	0.019	0.033	0.006
Cs	0.0024	0.0008	0.0017	0.0007	0.0016	0.0007	0.0006	0.0004
Ba	0.21	0.07	0.11	0.04	0.08	0.04	0.06	
La	0.00290	0.00028	0.00041	0.00008	0.00017	0.00013	0.00018	
Ce	0.0050	0.0030	0.0078	0.0036	0.0034	0.0022	0.0070	
Nd	0.215	0.028	0.077	0.012	0.032	0.013	0.006	0.004
Sm	0.00045	0.00005	0.00007	0.00002	0.00004	0.00002	0.00001	0.00001
Eu	0.0003	0.0002	0.0006	0.0003	0.0007	0.0003	0.0006	0.0002
Tb	0.0003	0.0002	0.0005	0.0003	0.0004	0.0003	0.0006	
Yb	0.00038	0.00029	0.00043	0.00040	0.00086		0.00037	
Lu	0.00006		0.00015		0.00026		0.00006	0.00004
Ta	0.0027		0.0027		0.0027		0.0022	
Au	0.000002	0.0000005	0.000011	0.000001	0.000001	0.0000004	0.000001	0.0000002
Hg	0.0011	0.0005	0.0021	0.0004	0.0006	0.0006	0.0021	0.0003
Th	0.0094	0.0019	0.0027	0.0008	0.0269	0.0028	0.0036	0.0009
U	0.00187	0.00056	0.00112	0.00046	0.00055	0.00055	0.00011	

Elemental concentrations (ng/m^3) of UMn/MOUDI Aerosol Samples

Date	08/09 - 08/13/95		08/09 - 08/13/95		08/14 - 08/18/95		08/14 - 08/18/95	
Upper cutsize	0.056 µm		After Filter		3.2 µm		1.8 µm	
Element	conc.	+/-	conc.	+/-	conc.	+/-	conc.	+/-
Na	0.28	0.06	0.12	0.05	1.30	0.09	15.57	0.94
Mg	0.2		0.4		0.5		8.5	1.6
Al	0.4		0.8	0.1	5.0	0.3	50.1	1.9
Cl	0.32	0.10	0.27	0.12	0.26		0.21	0.11
K	1.5		0.8	0.5	2.6	0.8	14.1	2.8
Sc	0.00006		0.00024		0.00063	0.00008	0.00746	0.00047
Ti	0.26		0.25		0.25		3.12	0.38
V	0.002		0.062	0.005	0.011		0.063	0.007
Cr	0.025		0.03	0.01	0.006	0.006	0.048	
Mn	0.032		0.028		0.053	0.002	0.532	0.009
Fe	1.5		1.9		1.2	0.9	24.2	3.8
Co	0.006		0.057	0.005	0.007		0.017	
Zn	0.10		0.06	0.03	0.68	0.08	1.10	0.09
Ga	0.020		0.005	0.005	0.024		0.054	
As	0.0003	0.0002	0.0007		0.0024	0.0006	0.0188	0.0019
Se	0.003		0.009		0.010	0.006	0.139	0.019
Br	0.0050		0.0021		0.0008	0.0008	0.0039	0.0028
Rb	0.065		0.055		0.083	0.038	0.329	
Sr	0.075		0.064		0.028	0.020	0.169	0.085
Zr	0.65		0.53		0.81		2.54	
Mo	0.002	0.001	0.010	0.003	0.002	0.001	0.007	0.004
Cd	0.0024		0.0022		0.0012		0.0079	
In	0.00018	0.00014	0.00014	0.00010	0.00005		0.00013	
Sb	0.049	0.008	0.083	0.012	0.075	0.011	0.068	0.011
Cs	0.0002	0.0006	0.0021	0.0007	0.0030	0.0008	0.0038	0.0010
Ba	0.03	0.03	0.08	0.03	0.09	0.04	0.67	0.08
La	0.00014		0.00043	0.00008	0.00357	0.00028	0.02911	0.00188
Ce	0.0086		0.0111		0.0113		0.0526	0.0075
Nd	0.009	0.004	0.016	0.006	0.011	0.006	0.011	0.010
Sm	0.00002		0.00004	0.00001	0.00046	0.00004	0.00394	0.00038
Eu	0.0003	0.0002	0.0005	0.0002	0.0009	0.0004	0.0011	0.0004
Tb	0.0011		0.0015		0.0015		0.0004	0.0003
Yb	0.00010	0.00008	0.00040	0.00039	0.00028	0.00013	0.00122	0.00075
Lu	0.00006		0.00009		0.00004	0.00004	0.00022	0.00009
Ta	0.0028		0.0034		0.0038		0.0037	
Au	0.0000010	0.0000002	0.00024	0.00003	0.00002	0.000004	0.000011	0.000005
Hg	0.0005	0.0002	0.0007		0.0015	0.0002	0.0014	
Th	0.0004	0.0002	0.0015		0.0015		0.0084	0.0017
U	0.00013		0.00042	0.00028	0.00039	0.00025	0.00188	0.00066

Elemental concentrations (ng/m^3) of UMn/MOUDI Aerosol Samples

Date	08/14 - 08/18/95		08/14 - 08/18/95		08/14 - 08/18/95		08/14 - 08/18/95	
Upper cutsize	1.0 µm		0.56 µm		0.32 µm		0.175 µm	
Element	conc.	+/-	conc.	+/-	conc.	+/-	conc.	+/-
Na	25.48	1.99	6.91	0.47	3.66	0.28	2.24	0.19
Mg	19.9	4.0	3.3	1.6	0.3		0.3	
Al	118.9	10.0	13.6	0.9	1.3	0.1	0.2	0.1
Cl	0.21	0.12	0.30	0.11	0.11	0.08	0.31	
K	35.9	5.0	18.0	2.8	11.3	0.9	9.4	0.9
Sc	0.02066	0.00100	0.00232	0.00019	0.00010	0.00008	0.00012	
Ti	6.40	0.80	0.78	0.28	0.48	0.24	0.08	
V	0.219	0.010	0.133	0.009	0.043	0.004	0.010	
Cr	0.199	0.020	0.104	0.038	0.06	0.03	0.06	0.01
Mn	1.252	0.020	0.358	0.009	0.110	0.009	0.044	0.002
Fe	64.6	4.0	9.3	3.8	6.6		2.0	1.6
Co	0.004	0.002	0.017		0.004	0.002	0.007	
Zn	1.46	0.20	1.87	0.19	1.67	0.19	1.38	0.19
Ga	0.084	0.035	0.033	0.029	0.041		0.016	0.010
As	0.1086	0.0100	0.2458	0.0285	0.1310	0.0094	0.0574	0.0056
Se	0.606	0.070	0.700	0.076	0.234	0.028	0.054	0.008
Br	0.2721	0.0697	1.6071	0.4746	0.5498	0.1508	0.1065	0.0282
Rb	0.279		0.456		0.453		0.047	0.047
Sr	0.498	0.159	0.161		0.113		0.083	
Zr	2.29		3.61		3.39		0.35	0.35
Mo	0.024	0.006	0.031	0.008	0.018	0.006	0.013	0.004
Cd	0.0074	0.0060	0.0232	0.0076	0.0343	0.0094	0.0079	0.0028
In	0.00149	0.00080	0.00058	0.00029	0.00037	0.00018	0.00033	0.00015
Sb	0.127	0.020	0.216	0.028	0.148	0.019	0.139	0.019
Cs	0.0093	0.0020	0.0058	0.0010	0.0025	0.0009	0.0027	0.0010
Ba	1.59	0.20	0.28	0.07	0.15	0.07	0.09	0.05
La	0.07571	0.00498	0.00949	0.00095	0.00160	0.00028	0.00039	0.00013
Ce	0.1494	0.0100	0.0123	0.0047	0.0123		0.0064	0.0046
Nd	0.088	0.016	0.826	0.095	0.358	0.047	0.048	0.009
Sm	0.00996	0.00100	0.00133	0.00009	0.00013	0.00002	0.00005	0.00001
Eu	0.0024	0.0005	0.0011	0.0004	0.0009	0.0003	0.0010	0.0004
Tb	0.0005	0.0003	0.0005		0.0005		0.0006	
Yb	0.00289	0.00110	0.00114	0.00047	0.00113		0.00122	
Lu	0.00063	0.00016	0.00007		0.00038		0.00013	
Ta	0.0044		0.0016	0.0014	0.0043		0.0020	0.0014
Au	0.00004	0.00001	0.00004	0.00001	0.00005	0.00001	0.00017	0.00002
Hg	0.0026	0.0007	0.0012	0.0007	0.0013	0.0008	0.0012	0.0004
Th	0.0189	0.0020	0.0133	0.0028	0.0141	0.0028	0.0011	0.0008
U	0.00319	0.00100	0.00294	0.00095	0.00217		0.00059	0.00039

Elemental concentrations (ng/m^3) of UMn/MOUDI Aerosol Samples

Date	08/14 - 08/18/95		08/14 - 08/18/95		08/14 - 08/18/95		08/19 - 08/23/95	
Upper cutsize	0.098 μm		0.056 μm		After Filter		3.2 μm	
Element	conc.	+/-	conc.	+/-	conc.	+/-	conc.	+/-
Na	0.44	0.07	0.17	0.05	0.33		4.73	0.32
Mg	0.3		0.9	0.7	0.7	0.6	4.2	1.7
Al	0.5		0.8	0.1	0.6	0.1	7.8	0.5
Cl	0.27		0.40	0.12	0.07	0.07	0.01	0.01
K	2.4	0.6	1.4		1.1		2.7	
Sc	0.00011		0.00009		0.00018		0.00141	0.00011
Ti	0.24		0.19		0.15		0.16	0.16
V	0.010		0.003		0.027	0.003	0.016	0.003
Cr	0.06		0.19	0.01	0.07		0.03	
Mn	0.024		0.006	0.001	0.024		0.092	0.011
Fe	1.0	1.0	1.4		0.5	0.4	9.3	
Co	0.019		0.013		0.033	0.003	0.009	
Zn	0.05	0.03	0.16		0.51	0.08	0.17	0.05
Ga	0.016	0.008	0.020		0.013		0.040	
As	0.0160	0.0019	0.0025	0.0004	0.0008		0.0061	0.0008
Se	0.009		0.006		0.006		0.031	0.009
Br	0.0032		0.0017	0.0017	0.0009		0.0038	
Rb	0.254		0.021	0.020	0.035	0.024	0.686	
Sr	0.053		0.062		0.012		0.066	0.036
Zr	1.88		0.55		0.83	0.45	6.22	
Mo	0.005	0.002	0.003	0.001	0.010	0.004	0.004	0.003
Cd	0.0001		0.0034		0.0004	0.0004	0.0038	0.0038
In	0.00013	0.00008	0.00004		0.00012	0.00012	0.00005	
Sb	0.030	0.005	0.012	0.004	0.020	0.006	0.029	0.006
Cs	0.0031	0.0011	0.0008	0.0006	0.0026	0.0008	0.0034	0.0014
Ba	0.06		0.07		0.07		0.12	0.04
La	0.00030	0.00009	0.00027	0.00006	0.00048	0.00011	0.00844	0.00063
Ce	0.0113		0.0048	0.0035	0.0113	0.0066	0.0104	0.0081
Nd	0.014	0.011	0.017	0.005	0.033	0.008	0.060	
Sm	0.00003	0.00001	0.00004	0.00001	0.00006	0.00002	0.00089	0.00008
Eu	0.0004	0.0002	0.0011	0.0004	0.0009	0.0002	0.0008	0.0003
Tb	0.0001		0.0010		0.0005	0.0003	0.0007	0.0004
Yb	0.00092	0.00053	0.00022		0.00103		0.00285	
Lu	0.00019		0.00007		0.00011		0.00006	
Ta	0.0040		0.0035		0.0022		0.0007	
Au	0.00032	0.00004	0.00003	0.000005	0.00005	0.00001	0.00002	
Hg	0.0024	0.0004	0.0009	0.0001	0.0009		0.0020	0.0007
Th	0.0073	0.0014	0.0009	0.0005	0.0015		0.0066	0.0024
U	0.00113	0.00038	0.00047		0.00036	0.00034	0.00072	

Elemental concentrations (ng/m^3) of UMn/MOUDI Aerosol Samples

Date	08/19 - 08/23/95		08/19 - 08/23/95		08/19 - 08/23/95		08/19 - 08/23/95	
Upper cutsize	1.8 μm		1.0 μm		0.56 μm		0.32 μm	
Element	conc.	+/-	conc.	+/-	conc.	+/-	conc.	+/-
Na	0.61	0.11	11.84	1.12	4.35	0.32	2.94	0.21
Mg	1.0	0.6	14.5	4.5	2.1	2.1	0.9	
Al	2.3	0.1	22.8	1.1	2.5	0.2	0.5	0.1
Cl	0.26		0.31	0.13	0.21	0.12	0.11	0.10
K	1.7	0.5	10.3	3.0	10.7	2.1	10.0	1.3
Sc	0.00012	0.00009	0.00351	0.00022	0.00038	0.00009	0.00025	
Ti	0.06		2.04	0.45	0.18	0.18	0.21	
V	0.016		0.068	0.007	0.117	0.011	0.127	0.011
Cr	0.05		0.07		0.03	0.01	0.05	
Mn	0.040		0.478	0.011	0.231	0.011	0.092	0.011
Fe	0.7	0.7	15.4	2.2	3.0	1.5	0.6	0.6
Co	0.023		0.021		0.020		0.025	
Zn	0.02	0.02	1.09	0.11	1.99	0.21	1.24	0.11
Ga	0.019		0.043	0.021	0.007		0.040	
As	0.0004	0.0004	0.0604	0.0067	0.0757	0.0075	0.1048	0.0106
Se	0.006	0.006	0.266	0.034	0.499	0.053	0.284	0.032
Br	0.0046		0.2162	0.0560	0.7818	0.2133	0.4482	0.1165
Rb	0.077		0.257		0.245		0.222	
Sr	0.077		0.213		0.104		0.085	
Zr	1.03		2.80		2.45		1.06	0.85
Mo	0.007		0.011	0.005	0.020	0.005	0.018	0.004
Cd	0.0031	0.0031	0.0262	0.0123	0.0122	0.0064	0.0100	0.0053
In	0.00007		0.00082	0.00048	0.00041	0.00021	0.00030	0.00016
Sb	0.079	0.014	0.101	0.018	0.104	0.011	0.095	0.012
Cs	0.0018	0.0012	0.0044	0.0015	0.0062	0.0013	0.0044	0.0013
Ba	0.08		0.66	0.10	0.10	0.05	0.10	
La	0.00137	0.00021	0.02014	0.00112	0.00309	0.00032	0.00127	0.00021
Ce	0.0264		0.0213	0.0090	0.0098	0.0085	0.0212	
Nd	0.036	0.008	0.057	0.013	0.245	0.032	0.169	0.021
Sm	0.00013	0.00002	0.00201	0.00022	0.00034	0.00003	0.00010	0.00002
Eu	0.0003	0.0003	0.0012	0.0003	0.0007	0.0002	0.0011	0.0003
Tb	0.0004	0.0003	0.0008		0.0010		0.0007	0.0005
Yb	0.00042		0.00084	0.00057	0.00076		0.00061	
Lu	0.00013		0.00019	0.00009	0.00020		0.00017	
Ta	0.0028		0.0009	0.0007	0.0014	0.0012	0.0019	0.0014
Au	0.00006	0.00001	0.00004	0.00001	0.00004	0.00001	0.00003	0.00001
Hg	0.0016	0.0004	0.0038	0.0006	0.0013		0.0014	0.0005
Th	0.0018		0.0019	0.0012	0.0021	0.0012	0.0041	0.0013
U	0.00099		0.00157		0.00060		0.00029	0.00018

Elemental concentrations (ng/m^3) of UMn/MOUDI Aerosol Samples

Date	08/19 - 08/23/95		08/19 - 08/23/95		08/19 - 08/23/95		08/19 - 08/23/95	
Upper cutsize	0.175 μm		0.098 μm		0.056 μm		After Filter	
Element	conc.	+/-	conc.	+/-	conc.	+/-	conc.	+/-
Na	1.78	0.11	0.11	0.04	0.32	0.06	1.03	0.11
Mg	2.0		1.4		0.1		0.2	
Al	0.4		0.3		0.4		0.8	0.1
Cl	0.22		0.32		0.57	0.18	0.51	0.18
K	7.8	1.1	1.4		1.4		1.9	
Sc	0.00015		0.00007		0.00010		0.00014	
Ti	0.05		0.25		0.13		0.27	
V	0.034	0.004	0.013		0.012		0.017	
Cr	0.05		0.03		0.05		0.08	
Mn	0.003	0.001	0.022		0.021		0.012	0.001
Fe	1.6	1.6	0.6		1.0		3.2	1.7
Co	0.026		0.019		0.018		0.022	
Zn	0.70	0.10	0.22	0.06	0.08	0.04	0.40	0.06
Ga	0.019	0.010	0.021		0.021		0.011	0.006
As	0.0603	0.0063	0.0037	0.0010	0.0010		0.0007	
Se	0.104	0.021	0.007	0.007	0.003		0.006	
Br	0.2042	0.0529	0.0139	0.0053	0.0009		0.0025	
Rb	0.275		0.073		0.064	0.054	0.127	
Sr	0.026	0.018	0.048		0.054		0.076	
Zr	2.54		0.78		1.80		1.01	
Mo	0.013	0.004	0.003	0.002	0.005	0.002	0.004	0.002
Cd	0.0089	0.0053	0.0033	0.0030	0.0034	0.0033	0.0037	
In	0.00020	0.00011	0.00010	0.00010	0.00007	0.00006	0.00012	0.00009
Sb	0.091	0.013	0.101	0.014	0.002	0.002	0.083	0.014
Cs	0.0029	0.0013	0.0026	0.0011	0.0031	0.0008	0.0026	0.0007
Ba	0.04	0.03	0.03	0.02	0.07		0.38	0.05
La	0.00058	0.00016	0.00014	0.00005	0.00016	0.00007	0.00024	0.00009
Ce	0.0222		0.0211		0.0099	0.0068	0.0094	
Nd	0.106	0.021	0.024	0.007	0.024		0.005	0.005
Sm	0.00003	0.00001	0.00004	0.00001	0.00002	0.00001	0.00006	0.00001
Eu	0.0009	0.0003	0.0004	0.0003	0.0007	0.0003	0.0005	
Tb	0.0003	0.0003	0.0006	0.0003	0.0008	0.0003	0.0007	
Yb	0.00169		0.00027	0.00015	0.00074	0.00042	0.00006	
Lu	0.00019		0.00011		0.00014		0.00013	
Ta	0.0041		0.0029	0.0016	0.0030		0.0034	
Au	0.00001	0.00001	0.00006	0.00001	0.00005	0.00001	0.00011	0.00002
Hg	0.0012		0.0008		0.0007		0.0007	0.0003
Th	0.0043	0.0014	0.0016		0.0027		0.0005	0.0005
U	0.00049		0.00036		0.00032		0.00028	0.00028

Elemental concentrations (ng/m^3) of UMn/MOUDI Aerosol Samples

Date	08/24 - 08/25/95		08/24 - 08/25/95		08/24 - 08/25/95		08/24 - 08/25/95	
Upper cutsize	3.2 μm		1.8 μm		1.0 μm		0.56 μm	
Element	conc.	+/-	conc.	+/-	conc.	+/-	conc.	+/-
Na	1.57	0.23	17.08	1.16	35.81	2.46	9.31	0.70
Mg	1.3	1.1	2.8	0.9	8.6	2.7	6.6	5.1
Al	0.5	0.1	6.4	0.5	17.1	0.7	1.8	0.2
Cl	0.12	0.12	2.69	0.69	7.51	1.72	0.35	0.23
K	3.5		1.4		15.5	5.2	16.4	3.7
Sc	0.00021		0.00100	0.00019	0.00182	0.00025	0.00023	0.00019
Ti	0.16		0.58	0.30	0.71	0.61	0.28	
V	0.008		0.030		0.088	0.010	0.112	0.009
Cr	0.02	0.02	0.13		0.10	0.02	1.24	0.02
Mn	0.083	0.005	0.102	0.005	0.361	0.025	0.438	0.023
Fe	5.1		5.1		12.5	3.9	11.5	2.6
Co	0.025		0.021		0.059		0.037	
Zn	0.35		0.32	0.09	0.88	0.15	0.82	0.14
Ga	0.051		0.046	0.035	0.024		0.063	
As	0.0012		0.0044	0.0014	0.0516	0.0049	0.1240	0.0117
Se	0.019		0.020		0.118	0.022	0.300	0.047
Br	0.0039		0.0148		0.1749	0.0516	0.4989	0.1404
Rb	0.222		0.394		0.368		0.020	
Sr	0.018		0.255		0.393		0.304	
Zr	2.78		3.01		2.95		0.56	
Mo	0.005	0.004	0.007	0.005	0.020	0.007	0.020	0.008
Cd	0.0074		0.0019		0.0010	0.0010	0.0037	0.0037
In	0.00023	0.00016	0.00028	0.00028	0.00054	0.00044	0.00183	0.00096
Sb	0.411	0.069	0.226	0.046	0.141	0.025	0.275	0.047
Cs	0.0037	0.0014	0.0030	0.0014	0.0120	0.0034	0.0098	0.0030
Ba	0.16	0.06	0.32	0.12	0.93	0.17	0.33	0.12
La	0.00076	0.00028	0.00532	0.00069	0.01351	0.00123	0.00164	0.00037
Ce	0.0394		0.0255		0.0368	0.0147	0.0608	
Nd	0.035	0.014	0.032		0.061	0.017	0.115	0.023
Sm	0.00009	0.00002	0.00060	0.00007	0.00147	0.00015	0.00021	0.00005
Eu	0.0012	0.0006	0.0014		0.0022	0.0007	0.0037	0.0009
Tb	0.0007	0.0005	0.0035		0.0017		0.0022	0.0009
Yb	0.00079	0.00060	0.00049	0.00049	0.00069	0.00044	0.00126	
Lu	0.00021	0.00012	0.00009	0.00009	0.00027		0.00033	
Ta	0.0083		0.0065	0.0035	0.0093		0.0063	
Au	0.00006	0.00001	0.00023	0.00004	0.00023	0.00003	0.00017	0.00003
Hg	0.0016	0.0006	0.0020		0.0018	0.0008	0.0033	0.0012
Th	0.0039		0.0051		0.0016	0.0016	0.0047	
U	0.00227		0.00278		0.00319		0.00257	

Elemental concentrations (ng/m^3) of UMn/MOUDI Aerosol Samples

Date	08/24 - 08/25/95		08/24 - 08/25/95		08/24 - 08/25/95		08/24 - 08/25/95	
Upper cutsize	0.32 µm		0.175 µm		0.098 µm		0.056 µm	
Element	conc.	+/-	conc.	+/-	conc.	+/-	conc.	+/-
Na	5.76	0.46	3.20	0.23	0.53	0.12	1.30	0.16
Mg	1.2		0.5	0.4	0.4		0.7	
Al	2.9	0.2	0.2	0.2	1.3		1.0	0.2
Cl	0.72		0.05	0.05	0.86	0.32	0.79	0.30
K	14.2	2.1	6.0		2.8	1.9	3.0	
Sc	0.00030		0.00042		0.00023		0.00037	
Ti	0.05		0.60		0.35	0.28	0.65	
V	0.081	0.009	0.044		0.019		0.013	
Cr	0.11		0.06		0.06		0.06	
Mn	0.030	0.002	0.019	0.002	0.097		0.053	
Fe	3.0		3.2		3.0		5.1	
Co	0.002	0.002	0.026		0.017		0.022	
Zn	0.88	0.14	0.28	0.09	0.37		0.53	
Ga	0.067		0.053		0.039		0.022	0.013
As	0.0674	0.0070	0.0394	0.0046	0.0026	0.0026	0.0011	
Se	0.146	0.028	0.028	0.014	0.016		0.005	0.005
Br	0.4025	0.1162	0.1489	0.0441	0.0060		0.0022	
Rb	0.232		0.139		0.107		0.278	
Sr	0.186		0.195		0.181		0.072	0.046
Zr	3.02		1.25		0.97		3.24	
Mo	0.033	0.009	0.013	0.005	0.008		0.012	
Cd	0.0009		0.0074		0.0037		0.0058	
In	0.00026	0.00023	0.00016		0.00023	0.00023	0.00025	
Sb	0.085	0.014	0.085	0.019	0.154	0.023	0.054	0.014
Cs	0.0058	0.0019	0.0026	0.0016	0.0067	0.0019	0.0088	0.0025
Ba	0.51	0.12	0.26	0.09	0.44	0.09	0.58	0.12
La	0.00074	0.00030	0.00065	0.00028	0.00058	0.00016	0.00088	0.00030
Ce	0.0256	0.0139	0.0130	0.0100	0.0081		0.0371	0.0255
Nd	0.086	0.014	0.039	0.009	0.039	0.009	0.046	0.016
Sm	0.00016	0.00005	0.00009	0.00005	0.00005	0.00002	0.00012	0.00002
Eu	0.0015	0.0007	0.0013	0.0005	0.0023	0.0007	0.0020	0.0006
Tb	0.0007		0.0019	0.0009	0.0012		0.0022	0.0009
Yb	0.00109		0.00255	0.00139	0.00067	0.00026	0.00086	
Lu	0.00007		0.00021		0.00007	0.00005	0.00028	
Ta	0.0060	0.0035	0.0090		0.0070		0.0065	
Au	0.00008	0.00002	0.00007	0.00002	0.00005	0.00001	0.00004	0.00001
Hg	0.0028	0.0009	0.0023	0.0009	0.0028	0.0007	0.0016	0.0008
Th	0.0009		0.0030		0.0023		0.0044	
U	0.00088		0.00232		0.00197		0.00167	

Elemental concentrations (ng/m^3) of UMn/MOUDI Aerosol Samples

Date	08/24 - 08/25/95	
Upper cutsize	After Filter	
Element	conc.	+/-
Na	1.02	0.14
Mg	0.7	
Al	0.1	0.1
Cl	0.90	0.32
K	1.3	1.3
Sc	0.00035	
Ti	0.23	
V	0.011	
Cr	0.06	
Mn	0.049	
Fe	2.3	
Co	0.030	
Zn	0.51	0.12
Ga	0.049	
As	0.0018	
Se	0.017	
Br	0.0028	
Rb	0.111	
Sr	0.069	0.019
Zr	1.50	
Mo	0.005	0.003
Cd	0.0058	
In	0.00012	
Sb	0.071	0.014
Cs	0.0006	
Ba	0.76	0.12
La	0.00039	0.00019
Ce	0.0347	
Nd	0.037	0.009
Sm	0.00009	0.00002
Eu	0.0028	0.0005
Tb	0.0008	0.0008
Yb	0.00056	0.00044
Lu	0.00019	
Ta	0.0069	
Au	0.00007	0.00002
Hg	0.0015	0.0005
Th	0.0022	
U	0.00194	

Elemental Concentrations (ng/m^3) and Filter Blanks (ng/filter) of CIT/MOUDI Aerosol Samples

Date	01/23/1996		01/23/1996		01/23/1996		01/23/1996	
Lower cutsize	1.8 µm		1.0 µm		0.56 µm		0.32 µm	
Element	conc.	+/-	conc.	+/-	conc.	+/-	conc.	+/-
Na	13	1	24	2	10	1	9	1
Mg	24		38		8		8	
Al	7.6	1.9	4.8	1.9	7.6	1.9	4.0	2.5
Cl	1.6	0.5	1.5	0.4	5.8	1.1	15	3
K	27		67	11	54		44	20
Sc	0.0016	0.0012	0.0043	0.0011	0.0012	0.0012	0.0006	0.0007
Ti	4.0	0.9	5.6	0.9	8.3	0.9	8.3	6.5
V	0.058	0.013	0.077	0.026	0.41	0.05	1.0	0.1
Cr	0.18		0.18		0.18		0.18	
Mn	0.12	0.01	0.72	0.02	2.3	0.1	2.5	0.1
Fe	20	6	45	10	76	13	54	8
Zn	1.7	0.6	4.4	1.0	13	2	17	2
As	0.014		0.0096	0.0055	0.0031	0.0041	0.059	0.011
Se	0.012	0.074	0.06	0.13	0.07	0.14	0.13	0.10
Br	0.0010	0.0062	0.039	0.016	0.13	0.04	0.87	0.23
Mo	0.045	0.018	0.021	0.018	0.092	0.026	0.23	0.06
Cd	0.056	0.028	0.016	0.024	0.057	0.029	0.12	0.05
In	0.0011	0.0009	0.0045	0.0025	0.0037	0.0035	0.0019	
Sb	0.11	0.01	0.38	0.03	0.41	0.03	0.50	0.04
Cs	0.047	0.018	0.051	0.020	0.013	0.013	0.018	0.013
Ba	2.3		4.6	1.1	5.1	1.2	3.6	1.3
La	0.02	0.002	0.075	0.006	0.033	0.003	0.027	0.003
Ce	0.019	0.010	0.046	0.027	0.070	0.025	0.069	0.023
Sm	0.0006	0.0001	0.0029	0.0003	0.0007	0.0001	0.0003	0.0002
Eu	0.012		0.010	0.008	0.020		0.007	0.003
Yb	0.0010	0.0009	0.0035	0.0032	0.0020	0.0012	0.0006	
Lu	0.00065		0.00093		0.00093		0.00093	
Au*	0.16	0.03	0.92	0.09	0.64	0.06	0.80	0.08
Hg	0.0042	0.0019	0.0043	0.0028	0.010	0.003	0.019	0.004
Th	0.010		0.009	0.007	0.018		0.014	
U	0.0069		0.0093		0.0037	0.0025	0.013	

* pg/m^3

Elemental Concentrations (ng/m^3) and Filter Blanks (ng/filter) of CIT/MOUDI Aerosol Samples

Date	01/23/1996		01/23/1996		01/23/1996		01/23/1996	
Lower cutsize	0.18 μm		0.097μm		0.056 μm		< 0.056 μm	
Element	conc.	+/-	conc.	+/-	conc.	+/-	conc.	+/-
Na	12	1	6	1	0.07	0.22	35	5
Mg	37		27		17		31	13
Al	0.3	1.6	3.3		3.3		27	
Cl	9.4	1.9	2.3	0.6	1.0	0.1	21	
K	81	15	22	19	24		44	
Sc	0.0039	0.0008	0.0005		0.0005		0.0054	0.0012
Ti	6.9	0.9	5.6	0.9	3.9	0.9	6.3	
V	0.63	0.06	0.16	0.02	0.035		0.025	0.018
Cr	0.18		0.18		0.18		2.8	
Mn	0.71	0.02	0.23	0.01	0.09	0.01	0.009	0.016
Fe	29	7	8.4	6.7	4.7	3.3	6.5	8.2
Zn	8.8	0.9	5.6	0.7	5.6	0.7	1.0	0.7
As	0.074	0.010	0.029	0.006	0.0059	0.0030	0.026	
Se	0.01	0.06	0.04	0.09	0.01	0.05	0.07	
Br	1.10	0.28	0.41	0.11	0.021	0.017	0.0097	0.0087
Mo	0.15	0.04	0.069	0.025	0.032	0.019	0.039	0.022
Cd	0.083	0.037	0.016	0.015	0.037		0.031	
In	0.0044	0.0030	0.0011		0.0013	0.0013	0.0041	0.0028
Sb	0.39	0.03	0.19	0.02	0.12	0.01	0.37	
Cs	0.031		0.020	0.012	0.022		0.037	0.012
Ba	3.2	0.9	1.4	0.8	0.2		0.8	0.7
La	0.019	0.002	0.002	0.001	0.002	0.001	0.52	0.04
Ce	0.035	0.016	0.010		0.013	0.013	0.87	0.05
Sm	0.0019	0.0002	0.0001	0.0001	0.0004		0.073	0.006
Eu	0.006	0.003	0.006	0.004	0.004	0.002	0.028	0.007
Yb	0.0035		0.0032		0.0028		0.0036	0.0031
Lu	0.00074		0.00074		0.00046	0.00028	0.00028	0.00019
Au*	0.64	0.06	0.49	0.06	0.19	0.03	0.36	0.05
Hg	0.014	0.003	0.014	0.003	0.011	0.003	0.0066	0.0038
Th	0.005	0.004	0.004	0.004	0.008		0.019	0.005
U	0.0053	0.0033	0.0031	0.0027	0.010		0.015	

* pg/m^3

Elemental Concentrations (ng/m^3) and Filter Blanks (ng/filter) of CIT/MOUDI Aerosol Samples

Date	1/29/96		1/29/96		1/29/96		1/29/96	
Lower cutsize	1.8 μm		1.0 μm		0.56 μm		0.32 μm	
Element	conc.	+/-	conc.	+/-	conc.	+/-	conc.	+/-
Na	43	3	82	6	15	1	11	1
Mg	20		9		35		37	
Al	5.7	1.9	16	3	4.8	1.9	2.2	1.4
Cl	0.6	0.1	5.5	0.9	18	3	7.4	1.2
K	29		9		23	17	44	
Sc	0.0029	0.0006	0.0026	0.0009	0.0043	0.0025	0.0015	0.0017
Ti	8	6	9.3	0.9	7.4	4.3	9.3	0.9
V	0.068		0.4	0.1	1.7	0.1	3.2	0.2
Cr	0.18		0.18		0.18		0.18	
Mn	0.093	0.019	0.71	0.03	0.95	0.09	0.64	0.02
Fe	6.6	3.3	48	12	18	8	20	1.7
Zn	0.04	0.29	4.9	0.8	5.6	1.0	5.9	1.2
As	0.014		0.0096	0.0030	0.0050	0.0041	0.022	0.005
Se	0.01		0.01		0.13	0.10	0.26	0.16
Br	0.014	0.003	0.017	0.012	0.19	0.06	0.39	0.10
Mo	0.019	0.011	0.10	0.03	0.086	0.024	0.087	0.025
Cd	0.037		0.004	0.024	0.023	0.016	0.042	0.021
In	0.0016	0.0010	0.0024	0.0024	0.0023		0.0059	0.0036
Sb	0.10	0.01	0.42	0.04	0.40	0.03	0.36	0.03
Cs	0.024		0.042		0.061		0.066	
Ba	2.8		6.5	1.6	3.2		3.1	
La	0.039	0.003	0.093	0.009	0.031	0.003	0.012	0.002
Ce	0.033	0.012	0.066	0.021	0.023	0.020	0.019	
Sm	0.0021	0.0003	0.0031	0.0004	0.0007	0.0001	0.0005	0.0001
Eu	0.009		0.018		0.022		0.024	
Yb	0.0006	0.0006	0.0025	0.0023	0.0011	0.0011	0.0016	0.0009
Lu	0.00009	0.00009	0.00037	0.00028	0.00083		0.00083	
Au*	0.10	0.02	0.39	0.04	0.45	0.04	0.55	0.05
Hg	0.0044	0.0020	0.0045	0.0027	0.0085	0.0019	0.011	0.003
Th	0.002	0.001	0.004	0.003	0.004	0.003	0.016	
U	0.0031	0.0015	0.0067		0.0044		0.0044	

* pg/m^3

Elemental Concentrations (ng/m^3) and Filter Blanks (ng/filter) of CIT/MOUDI Aerosol Samples

Date	1/29/96		1/29/96		1/29/96		1/29/96	
Lower cutsize	0.18 µm		0.097 µm		0.056 µm		< 0.056 µm	
Element	conc.	+/-	conc.	+/-	conc.	+/-	conc.	+/-
Na	8.0	0.8	3.2	0.6	1.1	0.3	32	
Mg	24		13		8	8	29	9
Al	3.3		3.3		3.3		27.0	
Cl	1.1	0.3	2.2	0.5	0.7	0.3	21	
K	56	10	34		25		30	
Sc	0.0007	0.0005	0.0006	0.0004	0.0006	0.0005	0.0038	
Ti	5.0	3.9	2.9		3.6	0.9	6.3	
V	1.7	0.1	0.29	0.03	0.040		0.070	0.019
Cr	0.18		0.18		0.18		2.8	
Mn	0.19	0.02	0.07	0.01	0.19		0.39	
Fe	2.0	4.1	8.8		8.8		39	
Zn	3.1	0.6	1.0	0.3	0.4	0.4	3.9	
As	0.011	0.005	0.014		0.014		0.026	
Se	0.02	0.05	0.01	0.05	0.01		0.07	
Br	0.21	0.06	0.071	0.023	0.0075	0.0062	0.031	
Mo	0.038	0.015	0.033	0.015	0.005		0.020	
Cd	0.014	0.014	0.001	0.011	0.037		0.031	
In	0.0018	0.0013	0.0028	0.0017	0.0009		0.0038	0.0023
Sb	0.25	0.02	0.11	0.01	0.037	0.005	0.37	
Cs	0.025		0.009	0.006	0.017	0.008	0.023	
Ba	3.5	1.6	2.6		0.9		0.3	
La	0.006	0.001	0.001	0.001	0.002	0.001	0.010	0.001
Ce	0.013	0.012	0.003		0.016	0.010	0.015	0.007
Sm	0.0006	0.0001	0.0003	0.0001	0.0005	0.0001	0.0006	0.0001
Eu	0.009		0.007		0.013	0.003	0.008	
Yb	0.0016	0.0016	0.0013	0.0007	0.0017	0.0007	0.0006	0.0005
Lu	0.00046		0.00046		0.00046		0.00037	
Au*	0.25	0.03	0.10	0.02	0.05	0.01	0.09	0.01
Hg	0.012	0.002	0.019	0.002	0.0033	0.0010	0.0041	0.0014
Th	0.007		0.002	0.001	0.007		0.004	0.002
U	0.0039		0.0018	0.0013	0.0009	0.0008	0.0006	

* pg/m^3

Elemental Concentrations (ng/m^3) and Filter Blanks (ng/filter) of CIT/MOUDI Aerosol Samples

Date	2/4/96		2/4/96		2/4/96		2/4/96	
Lower cutsize	1.8 μm		1.0 μm		0.56 μm		0.32 μm	
Element	conc.	+/-	conc.	+/-	conc.	+/-	conc.	+/-
Na	13	1	24	2	9	1	8	1
Mg	24		39		39		34	
Al	6.6	1.9	22	3	0.4	1.3	3.4	1.5
Cl	2.1	0.6	1.0	0.4	4.7	1.1	4.1	1.0
K	37		40		69	18	56	16
Sc	0.0012	0.0014	0.0006	0.0005	0.0029	0.0010	0.0005	
Ti	5.7	0.9	0.8	2.7	7.3	0.9	6.9	0.9
V	0.041	0.014	0.15	0.03	0.48	0.05	0.48	0.06
Cr	0.47	0.10	0.05	0.05	0.03	0.07	0.09	0.06
Mn	0.16	0.01	0.66	0.02	0.79	0.03	0.38	0.02
Fe	16	10	45	7	33	9	9	9
Zn	0.8		1.3	0.4	2.3	0.6	1.0	0.3
As	0.014		0.014		0.010	0.004	0.036	0.010
Se	0.02	0.03	0.01		0.01		0.003	0.053
Br	0.026	0.011	0.012	0.010	0.22	0.06	0.50	0.14
Mo	0.016	0.008	0.025	0.010	0.046	0.014	0.017	0.012
Cd	0.037		0.037		0.002	0.009	0.001	0.013
In	0.0019		0.0044	0.0031	0.0033	0.0031	0.0047	0.0029
Sb	0.13	0.01	0.40	0.03	0.42	0.03	0.29	0.03
Cs	0.046	0.024	0.046	0.013	0.040	0.020	0.034	0.019
Ba	3.2	1.2	3.3	0.9	3.7	1.3	0.9	
La	0.022	0.002	0.067	0.005	0.037	0.003	0.023	0.002
Ce	0.016		0.054	0.017	0.10	0.03	0.024	0.016
Sm	0.0010	0.0001	0.0026	0.0003	0.0015	0.0002	0.0006	0.0002
Eu	0.015	0.008	0.009	0.004	0.021		0.017	0.006
Yb	0.0037		0.0031		0.0006		0.0037	
Lu	0.00046	0.00037	0.00028	0.00019	0.00037	0.00028	0.00056	0.00037
Au*	0.10	0.03	0.28	0.03	0.21	0.03	0.31	0.05
Hg	0.0010		0.0044	0.0019	0.0069	0.0026	0.012	0.004
Th	0.005		0.010		0.009	0.006	0.012	
U	0.0054		0.0060		0.0054		0.0079	

* pg/m^3

Elemental Concentrations (ng/m^3) and Filter Blanks (ng/filter) of CIT/MOUDI Aerosol Samples

Date	2/4/96		2/4/96		2/4/96		2/10/96	
Lower cutsize	0.18 µm		0.097 µm		0.056 µm		1.8 µm	
Element	conc.	+/-	conc.	+/-	conc.	+/-	conc.	+/-
Na	8	1	3	1	0.75	0.39	148	10
Mg	4		25		12		26	8
Al	2.5	1.8	3.3		3.3		73	6
Cl	2.9	0.8	0.2	0.3	0.4	0.3	4.0	1.5
K	41	18	36	12	24		58	
Sc	0.0042	0.0019	0.0005		0.0005		0.0027	0.0007
Ti	5.6	0.9	3.9	2.3	4.1	0.9	12	1
V	0.24	0.03	0.031	0.013	0.023		0.33	0.06
Cr	0.15	0.06	1.5	0.1	0.18		8.5	0.2
Mn	0.15	0.01	0.28	0.02	0.01	0.01	0.79	0.03
Fe	16	7	4	3	9		83	9
Zn	0.8	0.4	0.8		0.8		2.3	0.5
As	0.032	0.005	0.020	0.007	0.014		0.025	0.003
Se	0.004	0.076	0.005		0.01		0.01	0.06
Br	0.51	0.14	0.19	0.06	0.025		0.051	0.023
Mo	0.012	0.007	0.022	0.009	0.010	0.006	0.069	0.035
Cd	0.006	0.011	0.001	0.009	0.007	0.010	0.021	0.005
In	0.0037	0.0037	0.0023		0.0018		0.0032	
Sb	0.23	0.02	0.09	0.01	0.002	0.002	0.20	0.02
Cs	0.046		0.051	0.013	0.019	0.008	0.039	0.012
Ba	2.2	0.8	1.5	0.9	2.1		3.1	1.5
La	0.014	0.002	0.006	0.001	0.006	0.001	0.089	0.006
Ce	0.055		0.035		0.017	0.010	0.055	0.021
Sm	0.0007	0.0001	0.0005	0.0001	0.0004	0.0001	0.0042	0.0005
Eu	0.007	0.005	0.018	0.004	0.009		0.022	0.006
Yb	0.0032		0.0012	0.0009	0.0023		0.010	0.004
Lu	0.00083		0.00056		0.00019	0.00019	0.00065	0.00037
Au*	0.23	0.03	0.09	0.02	0.03	0.01	0.22	0.03
Hg	0.011	0.002	0.0057	0.0019	0.0019	0.0011	0.0060	0.0059
Th	0.001		0.008		0.009		0.003	
U	0.0011		0.0063		0.0045		0.015	

* pg/m^3

Elemental Concentrations (ng/m^3) and Filter Blanks (ng/filter) of CIT/MOUDI Aerosol Samples

Date	2/10/96		2/10/96		2/10/96		2/10/96	
Lower cutsize	1.0 μm		0.56 μm		0.32 μm		0.18 μm	
Element	conc.	+/-	conc.	+/-	conc.	+/-	conc.	+/-
Na	190	10	30	2	10	1	4.3	0.6
Mg	50	15	12		58		4	
Al	50	5	7.6	1.9	3.4	1.5	7.6	1.9
Cl	28	8	35	10	4.8	1.6	1.6	0.8
K	69		54		42		33	
Sc	0.0052	0.0013	0.0041	0.0020	0.0006	0.0010	0.0009	0.0002
Ti	4	6	13	1	13	1	8	1
V	1.8	0.1	4.2	0.3	4.0	0.3	1.6	0.1
Cr	5.0	0.2	1.0	0.1	2.5	0.1	0.75	0.10
Mn	1.1	0.1	0.68	0.03	0.86	0.09	0.19	0.01
Fe	120	19	28	14	26	9	20	9
Zn	3.0	0.7	4.1	1.0	1.6	0.5	1.1	0.4
As	0.010	0.007	0.021	0.005	0.013	0.005	0.014	
Se	0.07	0.08	0.12	0.16	0.21	0.13	0.01	
Br	0.12	0.04	0.66	0.18	0.38	0.10	0.14	0.04
Mo	0.068	0.036	0.10	0.04	0.083	0.029	0.062	0.024
Cd	0.12	0.10	0.024	0.005	0.092	0.074	0.055	0.068
In	0.0065	0.0060	0.012	0.007	0.0050	0.0050	0.0019	
Sb	0.64	0.05	0.71	0.06	0.43	0.04	0.29	0.03
Cs	0.021	0.020	0.11		0.030	0.019	0.053	0.020
Ba	4.1	1.9	4.0		3.3		3.0	
La	0.24	0.02	0.052	0.005	0.018	0.002	0.007	0.001
Ce	0.14	0.04	0.026		0.033	0.027	0.093	
Sm	0.0072	0.0007	0.0020	0.0003	0.0005	0.0002	0.0002	0.0001
Eu	0.024	0.010	0.044		0.009	0.006	0.019	
Yb	0.0058		0.0067		0.0006		0.0039	
Lu	0.0014		0.0013	0.0006	0.0012		0.0011	
Au*	0.49	0.04	0.37	0.03	0.22	0.02	0.12	0.02
Hg	0.0032		0.0059	0.0034	0.0052	0.0022	0.0064	0.0026
Th	0.020		0.031		0.019		0.018	
U	0.013		0.010		0.0080		0.0072	

* pg/m^3

Elemental Concentrations (ng/m^3) and Filter Blanks (ng/filter) of CIT/MOUDI Aerosol Samples

Date	2/10/96		2/10/96		2/10/96		2/17/96	
Lower cutsize	0.097 μm		0.056 μm		< 0.056 μm		1.8 μm	
Element	conc.	+/-	conc.	+/-	conc.	+/-	conc.	+/-
Na	2.1	0.4	0.5	0.1	32		44	3
Mg	39		0.04		35	19	40	
Al	5.7	1.9	5.7	1.0	27	7	27	4
Cl	1.0	0.7	0.6	0.1	21		1.9	0.8
K	30		19		44		41	
Sc	0.0005		0.0043	0.0007	0.0038		0.0016	0.0005
Ti	7	1	1	2	6	2	0.3	0.9
V	0.44	0.04	0.047	0.014	0.10	0.03	0.19	0.07
Cr	5.7	0.1	0.84	0.10	3.4	0.2	7.7	0.2
Mn	0.44	0.02	0.07	0.01	0.51	0.07	1.0	0.1
Fe	33	6	83	9	39		62	6
Zn	0.2	0.3	0.8		1.3	0.7	0.9	0.3
As	0.008	0.005	0.014		0.026		0.009	0.003
Se	0.04	0.06	0.01		0.07		0.01	
Br	0.13	0.04	0.0057	0.0062	0.031		0.025	
Mo	0.047	0.024	0.012		0.21	0.06	0.063	0.022
Cd	0.001	0.005	0.014	0.005	0.11	0.07	0.001	0.019
In	0.0020		0.0011		0.0016		0.0060	0.0040
Sb	0.21	0.02	0.035	0.005	0.37		0.18	0.02
Cs	0.019	0.009	0.019	0.010	0.041	0.014	0.024	0.008
Ba	3.1		2.4	1.6	3.0		1.6	1.0
La	0.001	0.001	0.020	0.002	0.007	0.002	0.011	0.002
Ce	0.082		0.069		0.068	0.034	0.011	
Sm	0.0005		0.0025	0.0003	0.0007		0.0006	0.0002
Eu	0.011	0.006	0.009	0.004	0.019	0.006	0.009	0.004
Yb	0.0037		0.0042	0.0024	0.0045		0.0008	0.0008
Lu	0.00065	0.00037	0.00083		0.0013		0.00028	0.00019
Au*	0.06	0.01	0.09	0.01	2.1	0.1	0.51	0.06
Hg	0.0071	0.0027	0.0045	0.0030	0.0058	0.0044	0.014	0.003
Th	0.014		0.013	0.005	0.005	0.005	0.008	
U	0.0090		0.0067		0.0019		0.010	

* pg/m^3

Elemental Concentrations (ng/m^3) and Filter Blanks (ng/filter) of CIT/MOUDI Aerosol Samples

Date	2/17/96		2/17/96		2/17/96		2/17/96	
Lower cutsize	1.0 μm		0.56 μm		0.32 μm		0.18 μm	
Element	conc.	+/-	conc.	+/-	conc.	+/-	conc.	+/-
Na	59	4	12	1	6.5	0.8	4.9	0.6
Mg	6		41		9		26	
Al	16	2	34	11	1.4	1.9	3.6	1.1
Cl	20	4	46	9	14	3	0.9	0.5
K	29	10	50		51		34	
Sc	0.0017	0.0011	0.0014	0.0009	0.0004	0.0009	0.0004	0.0007
Ti	7	3	13	1	0.4	0.9	2.7	0.9
V	0.31	0.05	0.93	0.09	1.1	0.1	0.37	0.05
Cr	3.7	0.1	1.1	0.1	7.9	0.2	3.2	0.1
Mn	0.76	0.03	0.53	0.02	0.86	0.09	0.45	0.02
Fe	69	15	23	7	55	9	64	7
Zn	4.6	0.9	3.6	0.7	3.6	0.7	2.0	0.5
As	0.025	0.007	0.039	0.009	0.045	0.007	0.023	0.008
Se	0.27	0.10	0.76	0.13	0.60	0.11	0.29	0.08
Br	0.20	0.06	1.2	0.3	0.33	0.09	0.41	0.11
Mo	0.091	0.030	0.065	0.026	0.088	0.027	0.067	
Cd	0.037		0.014	0.028	0.014	0.016	0.024	0.024
In	0.0029		0.0063	0.0048	0.0066	0.0047	0.0027	0.0026
Sb	0.63	0.05	0.36	0.03	0.21	0.02	0.15	0.01
Cs	0.036	0.022	0.031	0.019	0.023	0.013	0.052	0.015
Ba	5.9	1.3	1.4	0.8	2.9		2.4	
La	0.056	0.005	0.088	0.006	0.13	0.01	0.042	0.004
Ce	0.063	0.027	0.14	0.03	0.20	0.04	0.057	0.020
Sm	0.0017	0.0002	0.0007	0.0002	0.0009	0.0002	0.0006	0.0002
Eu	0.024		0.008	0.005	0.018		0.013	
Yb	0.0009		0.0015	0.0014	0.0044	0.0025	0.0030	0.0021
Lu	0.0011		0.00037	0.00037	0.00083		0.00009	
Au*	1.1	0.1	0.85	0.08	0.74	0.07	0.57	0.06
Hg	0.011	0.004	0.0057	0.0036	0.011	0.003	0.015	0.004
Th	0.019		0.016		0.002		0.012	
U	0.0023		0.0073	0.0040	0.0084		0.0043	0.0032

* pg/m^3

Elemental Concentrations (ng/m^3) and Filter Blanks (ng/filter) of CIT/MOUDI Aerosol Samples

Date	2/17/96		2/17/96		2/17/96		Blank	
Lower cutsize	0.097 μm		0.056 μm		< 0.056 μm		1.0 μm, 47mm Teflon	
Element	conc.	+/-	conc.	+/-	conc.	+/-	conc.	+/-
Na	4.9	0.7	2.0	0.3	32		17	8
Mg	32		14		17	17	190	
Al	1.5	1.0	21	3	1.4	6.1	100	20
Cl	1.7	0.6	0.5	0.1	21		32	
K	45	10	31		55		420	
Sc	0.0005		0.0005		0.0038		0.02	
Ti	3.3	0.9	4	1	3	6	130	
V	0.080	0.021	0.062		0.15	0.06	0.44	
Cr	11	0.2	9.5	0.9	17	0.9	34	2
Mn	0.86	0.09	0.32	0.02	2.1	0.1	2.8	0.2
Fe	49	7	67	7	81	11	220	80
Zn	1.0	0.4	0.8		3.9		20	4
As	0.018	0.007	0.012	0.005	0.03		0.19	0.06
Se	0.32	0.08	0.005		0.02	0.11	1.2	
Br	0.27	0.07	0.02	0.01	0.031		0.28	
Mo	0.093	0.028	0.054	0.019	0.22	0.06	0.68	
Cd	0.039	0.024	0.037		0.004	0.023	0.20	0.17
In	0.0020		0.0008	0.0006	0.0021	0.0020	0.030	0.030
Sb	0.11	0.01	0.021	0.004	0.37		0.20	0.04
Cs	0.034		0.009	0.007	0.030		0.52	0.18
Ba	0.9	0.6	2.9		0.8		66	
La	0.007	0.001	0.0002		0.028	0.003	0.022	0.012
Ce	0.064		0.039		0.016	0.013	0.36	0.28
Sm	0.0002	0.0002	0.0002	0.0001	0.0006	0.0002	0.002	0.002
Eu	0.006	0.004	0.007	0.003	0.010		0.14	0.07
Yb	0.0037		0.0021		0.0031		0.048	
Lu	0.00037	0.00028	0.00046		0.00009		0.010	
Au*	0.29	0.04	0.14	0.02	4.1	0.3	4.4	0.4
Hg	0.012	0.005	0.0062	0.0025	0.016	0.004	0.052	0.036
Th	0.007	0.005	0.005	0.002	0.003	0.003	0.16	
U	0.012		0.0010	0.0009	0.0070		0.050	0.036

* pg/m^3

Elemental Concentrations (ng/m^3) and Filter Blanks (ng/filter) of CIT/MOUDI Aerosol Samples

Date	Blank		Blank		Blank		Blank	
Lower cutsize	1.0 µm, 47mm Teflon		1.0 µm, 47mm Teflon		1.0 µm, 47mm Teflon		1.0 µm, 37mm Zefluor	
Element	conc.	+/-	conc.	+/-	conc.	+/-	conc.	+/-
Na	7	6	13	6	12	4	660	40
Mg	200		360		360		920	260
Al	100	20	130	20	150	24	660	60
Cl	28		16	4	42		420	60
K	480		320		300		1040	
Sc	0.01	0.01	0.02	0.02	0.01	0.01	0.11	0.03
Ti	52	28	138		122		128	62
V	0.58		0.11		0.76		1.36	0.66
Cr	13	1	20	2	12	1	56	2
Mn	1.3	0.2	2.0	0.2	1.5	0.2	9.0	0.4
Fe	138	68	320	100	186	110	920	180
Zn	24	4	78	8	14	3	90	16
As	0.07		0.10		0.24		0.60	0.12
Se	2.2	1.8	0.8		1.2	1.1	3.6	
Br	0.15		0.09	0.08	0.38		0.44	0.20
Mo	0.54		0.20	0.15	0.60		3.0	0.8
Cd	0.26	0.16	0.10	0.10	0.56	0.20	0.80	0.36
In	0.010		0.034	0.034	0.028		0.062	0.056
Sb	1.00	0.08	0.07	0.02	0.82	0.08	10.2	0.8
Cs	0.20	0.16	0.54	0.26	0.54	0.22	0.74	0.42
Ba	58		52		46		52	22
La	0.030	0.006	0.026		0.052	0.016	1.0	0.1
Ce	0.22	0.18	1.0		1.0		3.4	0.6
Sm	0.002	0.002	0.004		0.004	0.002	0.016	0.004
Eu	0.14	0.06	0.14	0.06	0.32	0.12	0.24	0.14
Yb	0.044		0.052		0.022		0.098	
Lu	0.010		0.014		0.014	0.006	0.024	
Au*	1.1	0.2	1.9	0.4	76	6	240	20
Hg	0.090	0.042	0.090	0.048	0.064	0.042	0.38	0.06
Th	0.19		0.26		0.22		0.17	0.11
U	0.066		0.096		0.14		0.18	

* pg/m^3

Elemental Concentrations (ng/m^3) and Filter Blanks (ng/filter) of CIT/MOUDI Aerosol Samples

Date	Blank		Blank		Blank		Blank	
Lower cutsize	1.0 µm, 37mm Zefluor		1.0 µm, 47mm Teflon		1.0 µm, 47mm Teflon		1.0 µm, 47mm Teflon	
Element	conc.	+/-	conc.	+/-	conc.	+/-	conc.	+/-
Na	720	60	11	5	16		11	
Mg	700	400	144		240		300	
Al	520	200	60	14	52	14	78	14
Cl	480	80	28		20	4	22	
K	820	300	320		320		460	
Sc	0.05	0.02	0.04	0.01	0.02	0.01	0.03	0.01
Ti	144	86	118		28	26	112	
V	3.80		0.72		0.44		0.58	
Cr	64	2	5.2	0.8	6.4	1.0	6.6	1.2
Mn	7.8	0.4	0.7	0.1	0.8	0.1	0.6	0.1
Fe	760	120	260		140	90	180	100
Zn	80	10	26	6	18	4	24	4
As	0.54	0.16	0.09		0.19		0.11	
Se	1.5	1.5	1.1	0.7	0.6		0.6	
Br	0.90	0.32	0.12	0.07	0.34		0.32	0.14
Mo	3.0	0.8	0.42		0.52		1.2	
Cd	0.56	0.28	0.14	0.14	0.40	0.22	1.20	0.54
In	0.030		0.036	0.032	0.024		0.030	
Sb	5.8	0.4	0.56	0.06	0.07	0.02	0.32	0.04
Cs	1.1	0.3	0.78	0.26	1.2	0.3	1.2	0.4
Ba	60		48		44		58	
La	0.24	0.04	0.028		0.036		0.008	0.008
Ce	0.56	0.36	0.34	0.30	0.64	0.32	0.84	0.58
Sm	0.012	0.004	0.002	0.002	0.006		0.008	
Eu	0.17	0.12	0.32	0.12	0.16	0.08	0.28	0.12
Yb	0.058	0.034	0.004		0.048	0.040	0.15	0.07
Lu	0.020	0.008	0.014		0.016		0.008	0.008
Au*	112	8	0.30	0.20	2.4	0.6	0.42	0.18
Hg	0.32	0.08	0.042	0.026	0.12	0.06	0.19	0.09
Th	0.28		0.24		0.22		0.36	
U	0.19		0.088		0.12		0.16	

* pg/m^3

Elemental Concentrations (ng/m^3) and Filter Blanks (ng/filter) of CIT/MOUDI Aerosol Samples

Date	Blank		Blank		Blank	
Lower cutsize	2.0 µm, 47mm Teflon		2.0 µm, 47mm Teflon		2.0 µm, 47mm Teflon	
Element	conc.	+/-	conc.	+/-	conc.	+/-
Na	26	6	20	7	15	6
Mg	560		380		920	
Al	38		40	30	190	
Cl	26	8	20	6	22	
K	420		520		440	
Sc	0.02	0.01	0.02	0.02	0.02	0.01
Ti	10		50	46	260	
V	0.52		0.28		1.1	
Cr	3.2	1.2	4.6	1.2	6.0	1.2
Mn	1.2	0.1	1.1	0.1	1.9	0.2
Fe	64		130	70	110	
Zn	19	5	36	8	56	8
As	0.36		0.19		0.24	
Se	2.4	1.0	4.2	1.4	1.8	1.7
Br	0.44	0.34	0.46		0.58	
Mo	1.8		0.38		1.7	
Cd	0.74	0.58	0.28		1.6	0.8
In	0.050		0.026		0.066	0.056
Sb	0.08	0.04	0.07	0.03	0.07	0.03
Cs	0.64	0.26	0.68	0.34	0.72	0.26
Ba	54		58		60	
La	0.066		0.048		0.058	
Ce	1.9		0.98	0.68	2.0	
Sm	0.014		0.010		0.012	
Eu	0.52	0.14	0.34	0.10	0.24	0.10
Yb	0.066	0.066	0.082	0.054	0.088	
Lu	0.026		0.006		0.006	
Au*	0.04		1.0	0.3	0.58	0.22
Hg	0.14	0.10	0.12	0.06	0.072	0.072
Th	0.32		0.11	0.10	0.34	
U	0.26	0.10	0.20		0.24	

* pg/m^3

Vapor Phase Mercury Concentrations (ng/m^3)

Date	Conc.	±
7/14/95	1.4	0.7
7/15/95	1.8	0.9
7/16/95	1.5	0.7
7/17/95	2.7	1.5
7/23/95	2.5	1.3
7/24/95	1.6	0.8
7/28/95	1.1	0.5
7/29/95	3.0	1.7
7/30/95	1.4	0.6
7/31/95	1.3	0.6
8/6/95	2.2	1.1
8/7/95	1.1	0.5
8/11/95	1.0	0.5
8/12/95	1.7	0.9
8/13/95	1.8	0.8
8/14/95	2.5	1.3
8/18/95	1.6	0.8
8/19/95	2.1	1.1
8/20/95	2.1	1.0
8/21/95	1.6	0.8

Elemental concentrations (ng/m^3) for NPS/IMPROVE Samples

Date	7/15/95		7/16/95		7/17/95		7/18/95	
Element	conc.	+/-	conc.	+/-	conc.	+/-	conc.	+/-
Al	111	16	64	10			104	18
Si	221	20	307	22	265	22	125	14
S	4999	257	4566	234	5491	282	2706	143
K	91	9	87	8	108	10	55	8
Ca	62	7	52	6	39	6	55	7
Fe	49	3	35	2	44	2	29	2
Cu	2.09	0.21	1.08	0.15	2.97	0.28	1.61	0.22
Zn	10.47	0.63	9	0.56	11.59	0.71	8.35	0.55
Pb	4.11	0.26	3.02	0.23	3.64	0.27	3.88	0.3
Se	1.8	0.15	1.2	0.12	1.77	0.16	1.57	0.15
Br	3.04	0.22	1.92	0.16	2.25	0.19	1.97	0.18
SO4	14461	522	15665	565	18039	651	7433	268
NH4	3900	262	3717	249	3817	256	2135	143

Date	7/19/95		7/20/95		7/21/95		7/22/95	
Element	conc.	+/-	conc.	+/-	conc.	+/-	conc.	+/-
Al			80	12	67	11		
Si	240	27	155	15	214	18	122	13
S	2239	119	3972	204	2463	129	1640	89
K	68	8	82	8	67	9	51	7
Ca	55	6	38	6	52	7	20	4
Fe	26	2	44	2	39	2	21	1
Cu	1.53	0.22	1.96	0.21	1.56	0.18	0.62	0.12
Zn	7.45	0.48	9.34	0.57	8.66	0.54	4.11	0.31
Pb	3.33	0.25	3.61	0.26	2.95	0.22	2.32	0.21
Se	1.77	0.15	2.16	0.17	1.44	0.13	0.89	0.1
Br	2.22	0.18	2.83	0.2	2.27	0.17	1.72	0.15
SO4	5838	211	11374	410	6396	231	4391	159
NH4	1766	119	3000	201	2024	136	1078	72

Date	7/23/95		7/24/95		7/25/95		7/26/95	
Element	conc.	+/-	conc.	+/-	conc.	+/-	conc.	+/-
Al	94	17	256	21	968	57	936	57
Si	162	16	522	32	1871	99	1955	105
S	1227	67	1048	58	1287	70	1629	88
K	59	7	74	7	211	15	207	15
Ca	40	6	77	7	213	14	181	14
Fe	26	2	128	7	459	23	443	23
Cu	1.14	0.17	1.29	0.16	0.76	0.14	1.17	0.15
Zn	3.9	0.3	3.61	0.28	5.47	0.38	6	0.41
Pb	1.76	0.18	2.03	0.19	2.52	0.21	2.54	0.22
Se	0.77	0.1	0.82	0.1	0.94	0.1	0.86	0.11
Br	2.04	0.16	1.97	0.16	1.96	0.16	2.06	0.17
SO4	3335	120	2931	106	4162	150	4559	165
NH4	806	54	704	47	966	65	1037	70

Elemental concentrations (ng/m^3) for NPS/IMPROVE Samples

Date	7/27/95		7/28/95		7/29/95		7/30/95	
Element	conc.	+/-	conc.	+/-	conc.	+/-	conc.	+/-
Al	268	23	166	16	205	19	70	13
Si	497	31	354	24	381	25	100	14
S	1353	73	904	52	517	32	1020	57
K	87	8	57	7	82	10	46	6
Ca	60	6	45	5	52	6	21	4
Fe	128	7	81	4	88	5	23	1
Cu	0.95	0.14	0.72	0.13	0.72	0.12	1.06	0.15
Zn	5.64	0.39	1.89	0.19	2.17	0.21	3.01	0.25
Pb	1.79	0.16	1.18	0.15			1.15	0.25
Se	0.76	0.1			0.36	0.15	0.45	0.07
Br	1.82	0.15	1.02	0.11	1.09	0.11	1.54	0.13
SO4	3743	135	2506	91	1691	61	2966	107
NH4	801	54	498	33	371	25	685	46

Date	7/31/95		8/1/05		8/2/95		8/3/95	
Element	conc.	+/-	conc.	+/-	conc.	+/-	conc.	+/-
Al	93	13			82	14	335	25
Si	97	12	137	22	123	14	634	38
S	1027	57	1818	98	1588	85	379	25
K	85	9	65	9	72	7	92	8
Ca	10	4			38	5	108	9
Fe	14	1	17	1	17	1	152	8
Cu	1.43	0.18	0.85	0.13	1.16	0.15	0.8	0.13
Zn	3.04	0.25	3.34	0.27	5.38	0.37	1.92	0.19
Pb	2.39	0.23	2.1	0.2	2.19	0.19	1.14	0.14
Se			0.67	0.09	0.66	0.09	0.13	0.04
Br	1.78	0.15	2.14	0.17	1.6	0.13	0.85	0.1
SO4	2960	107	4844	175	4105	148	1086	39
NH4	700	47	1219	82	908	61	61	4

Date	8/4/95		8/5/95		8/6/95		8/7/95	
Element	conc.	+/-	conc.	+/-	conc.	+/-	conc.	+/-
Al			190	18	91	20	72	11
Si	138	15	355	24	126	16	119	13
S	516	35	836	48	1214	67	1103	61
K	44	7	81	9	30	5	54	7
Ca	38	6	56	6	15	3	33	5
Fe	24	1	75	4	18	1	19	1
Cu	0.46	0.11			0.74	0.15	0.77	0.13
Zn	1.19	0.15	2.15	0.22	3.61	0.28	2.35	0.22
Pb			1.36	0.13	1.8	0.17		
Se			0.43	0.08	0.42	0.07		
Br	0.91	0.11	1.57	0.14	0.94	0.1	1.25	0.13
SO4	1271	46	2480	90	3058	110	3251	117
NH4	125	8	364	24	613	41	661	44

Elemental concentrations (ng/m^3) for NPS/IMPROVE Samples

Date	8/8/95		8/9/95		8/10/95		8/11/95	
Element	conc.	+/-	conc.	+/-	conc.	+/-	conc.	+/-
Al			91	17	41	10	79	13
Si					97	12	114	12
S	914	51	1730	96	3207	166	2625	137
K	44	7	49	7	65	7	74	8
Ca			34	7	28	5	35	5
Fe	7	1	17	1	25	1	30	2
Cu	0.76	0.13	10.59	0.65	1.89	0.2	2.9	0.25
Zn	2.33	0.22	4.69	0.34	6.18	0.41	6.56	0.43
Pb	1.4	0.15	2.3	0.2	2.47	0.2	2.4	0.19
Se			0.7	0.09	1.36	0.13	0.84	0.1
Br	0.52	0.08	1.34	0.13	2.44	0.18	1.89	0.16
SO4	2512	91	4859	175	9277	335	8472	306
NH4	460	31	1135	76	1913	128	1985	133

Date	8/12/95		8/13/95		8/14/95		8/15/95	
Element	conc.	+/-	conc.	+/-	conc.	+/-	conc.	+/-
Al	94	15	302	30	364	30	317	27
Si	258	21	709	46	841	51	757	46
S	3954	205	6353	326	7718	394	5849	299
K	64	8	97	10	150	13	110	11
Ca	109	9	114	11	137	12	118	10
Fe	43	2	159	8	193	10	158	8
Cu	1.72	0.19	1.63	0.19	7.93	0.52	4.47	0.34
Zn	4.43	0.32	5.78	0.4	7.77	0.5	7.01	0.46
Pb	2.85	0.21	2.98	0.24	3.94	0.27	4.04	0.27
Se	1.04	0.11	1.34	0.13	2.52	0.19	1.73	0.15
Br	1.66	0.14	1.76	0.16	2.43	0.19	2.32	0.18
SO4	12166	439	20967	756	23232	838	18486	667
NH4	2436	163	2983	200	3858	259	3456	232

Date	8/16/95		8/17/95		8/18/95		8/19/95	
Element	conc.	+/-	conc.	+/-	conc.	+/-	conc.	+/-
Al	249	22	274	32	244	34	251	28
Si	520	32	698	47	505	40	473	34
S	5451	278	10554	538	12416	633	6325	325
K	101	9	116	14	81	12	79	9
Ca	116	10	100	10	74	10	69	8
Fe	135	7	146	8	93	5	100	5
Cu	3.86	0.32	4.6	0.35	2.42	0.23	3.35	0.28
Zn	7.7	0.49	20.09	1.12	9.43	0.57	7.47	0.48
Pb	4.05	0.3	5.28	0.31	5.07	0.31	4.89	0.29
Se	1.99	0.16	5.81	0.36	4.12	0.27	2.25	0.17
Br	2.82	0.21	4.47	0.29	3.34	0.23	2.35	0.18
SO4	19319	697	30293	1092	42704	1540	19390	699
NH4	3460	232	4040	271	4978	334	3332	224

Elemental concentrations (ng/m^3) for NPS/IMPROVE Samples

Date	8/20/95		8/21/95		8/22/95		8/23/95	
Element	conc.	+/-	conc.	+/-	conc.	+/-	conc.	+/-
Al							69	14
Si	122	19	140	21	224	24	191	21
S	1849	102	2393	128	5895	303	6163	317
K	60	9	72	13	83	9	81	10
Ca	11	4	27	6	42	6	33	6
Fe	13	1	24	1	46	3	33	2
Cu	1.1	0.15	1.09	0.17	2.21	0.22	2.08	0.21
Zn	2.87	0.25	5.34	0.37	12.76	0.75	9.46	0.58
Pb	2.25	0.2	2.23	0.21	5.12	0.29	4.88	0.28
Se	0.67	0.09	0.7	0.09	2.95	0.21	4.04	0.26
Br	1.02	0.11	1.57	0.14	3.21	0.22	3.21	0.22
SO4	5241	189	6320	228	18182	656	20318	733
NH4	1082	73	1381	93	3468	233	2776	186

Date	8/25/95	
Element	conc.	+/-
Al	50	10
Si	101	12
S	1908	101
K	76	8
Ca	25	5
Fe	18	1
Cu	2.34	0.23
Zn	4.38	0.32
Pb	2.37	0.2
Se	0.59	0.08
Br	1.65	0.14
SO4	4705	170
NH4	1014	68

APPENDIX B CALCULATED MASS CONTRIBUTION DATA

These are calculated daily mass contributions from the sources identified by Factor Analysis of the MIT/SU and NPS/IMPROVE data sets. They are the result of the Absolute Factor Score-Multiple Linear Regression method described in Chapter 3 and Equations 3.5 – 3.7. They are presented graphically in Figures 3.6 and 3.7.

Daily mass contributions ($\mu g/m^3$) from sources identified by Factor Analysis of the MIT/SU data set.

Date	Combustion Sources	Crustal Material	Unidentified Sources
7/15/95	28.9	1.3	1.0
7/16/95	28.3	0.9	1.6
7/17/95	37.1	0.9	3.0
7/18/95	20.8	0.8	0.3
7/19/95	19.7	0.6	0.4
7/20/95	29.0	0.7	1.3
7/21/95	18.6	0.6	1.6
7/22/95	13.5	0.5	1.7
7/23/95	9.1	1.1	0.1
7/24/95	11.9	3.2	0.3
7/25/95	14.0	9.3	0.2
7/26/95	11.4	8.3	1.0
7/27/95	10.9	2.2	0.3
7/28/95	5.4	2.0	0.8
7/29/95	7.0	1.9	1.1
7/30/95	7.1	0.8	0.4
7/31/95	5.4	1.0	-0.03
8/1/95	10.8	1.2	1.5
8/2/95	7.9	1.0	0.03
8/3/95	5.3	3.5	0.02
8/4/95	3.9	1.2	0.01
8/5/95	8.8	2.3	0.3
8/6/95	8.8	0.5	0.3
8/7/95	7.2	0.7	0.1
8/8/95	7.1	0.5	0.5
8/9/95	21.0	0.8	-1.9
8/10/95	18.7	1.0	0.4
8/11/95	18.3	0.7	-0.01
8/12/95	22.4	1.7	0.3
8/13/95	35.0	3.2	4.2
8/14/95	46.9	3.2	-0.9
8/15/95	29.2	3.2	-0.4
8/16/95	32.6	3.0	0.1
8/17/95	67.7	2.1	-0.7
8/18/95	66.5	1.7	0.3
8/19/95	33.1	2.1	0.02
8/20/95	10.9	0.6	0.5
8/21/95	10.7	0.7	0.2
8/22/95	39.6	0.6	0.1
8/23/95	35.7	0.7	0.1
8/24/95	12.9	1.1	18.5
8/25/95	8.9	1.0	4.3

Daily mass contributions ($\mu g/m^3$) from sources identified by Factor Analysis of the NPS IMPROVE data set.

Date	Combustion Sources	Crustal Material	Unidentified Sources
7/15/95	43.6	2.1	0.03
7/16/95	36.1	1.9	-0.1
7/17/95	38.8	2.1	1.3
7/18/95	27.7	1.5	-0.2
7/19/95	27.5	1.8	-0.4
7/20/95	37.9	1.6	-0.3
7/21/95	28.5	1.7	-0.3
7/22/95	18.4	1.1	-0.8
7/23/95	15.1	1.6	-0.3
7/24/95	14.5	3.8	-0.1
7/25/95	14.5	13.2	-1.0
7/26/95	14.7	12.7	-0.8
7/27/95	15.6	3.8	-0.6
7/28/95	6.9	2.5	-0.1
7/29/95	8.7	3.1	-0.1
7/30/95	11.3	1.0	0.1
7/31/95	15.8	1.4	0.2
8/1/95	18.8	1.4	-0.5
8/2/95	16.2	1.6	-0.1
8/3/95	3.6	5.1	0.4
8/4/95	9.4	1.3	-0.2
8/5/95	9.2	3.0	-0.2
8/6/95	10.6	0.8	-0.1
8/7/95	11.8	1.3	-0.2
8/8/95	8.6	1.1	0.4
8/9/95	7.6	1.1	11.3
8/10/95	26.6	1.1	0.2
8/11/95	22.3	1.5	1.9
8/12/95	24.6	2.5	1.2
8/13/95	29.4	4.9	0.7
8/14/95	37.3	6.1	7.5
8/15/95	32.8	5.1	3.5
8/16/95	36.8	4.3	2.4
8/17/95	67.4	4.4	0.2
8/18/95	61.9	2.9	0.1
8/19/95	36.6	3.2	1.7
8/20/95	14.5	1.0	0.4
8/21/95	19.3	1.4	-0.1
8/22/95	49.1	1.6	-0.7
8/23/95	48.3	1.4	-0.9
8/24/95	12.9	1.1	18.5
8/25/95	8.9	1.0	4.3

APPENDIX C The INAA results of SRM standards and integrated fine particulate samples

The total number of counts of each isotope was determined by using the interactive peak fitting and analysis software from Canberra Industries (Meriden, CT). Stable isotope ratios are based on the ratios of N listed in Equation 2.1.

INAA results of SRM standards and stable isotope ratios

Toatl area (number of counts) after blank and interference corrections

Isotope	FA001	FA002	FA003	FA004	FA005	FA006	FA007	FA008
Br-79								
Br-81								
Sr-84	1.8E+03	2.1E+03	1.9E+03	1.1E+03	1.1E+03	1.7E+03	1.8E+03	2.1E+03
Sr-86	4.1E+03	3.6E+03	3.7E+03	3.9E+03	4.0E+03	4.0E+03	4.3E+03	3.6E+03
Sb-121	1.6E+04	1.3E+04	1.3E+04	1.1E+04	1.6E+04	1.2E+04	1.6E+04	1.3E+04
Sb-123	7.1E+02	6.3E+02	5.1E+02	5.3E+02	5.9E+02	5.8E+02	7.0E+02	7.2E+02
Ba-130	1.0E+04	9.3E+03	8.4E+03	8.3E+03	9.4E+03	9.4E+03	1.0E+04	8.5E+03
Ba-138	1.3E+04	1.2E+04	1.2E+04	1.1E+04	1.3E+04	1.2E+04	1.3E+04	1.2E+04

Absolute Detector Efficiency

Isotope	FA001	FA002	FA003	FA004	FA005	FA006	FA007	FA008
Br-79	2.39E-03	2.39E-03	2.29E-03	2.29E-03	2.36E-03	2.36E-03	2.41E-03	2.41E-03
Br-81	1.94E-03	1.94E-03	1.84E-03	1.84E-03	1.91E-03	1.91E-03	1.97E-03	1.97E-03
Sr-84	2.84E-03	2.84E-03	2.72E-03	2.72E-03	2.81E-03	2.81E-03	2.86E-03	2.86E-03
Sr-86	3.62E-03	3.62E-03	3.43E-03	3.43E-03	3.59E-03	3.59E-03	3.65E-03	3.65E-03
Sb-121	2.60E-03	2.60E-03	2.50E-03	2.50E-03	2.57E-03	2.57E-03	2.62E-03	2.62E-03
Sb-123	9.02E-04	9.02E-04	8.64E-04	8.64E-04	8.04E-04	8.04E-04	8.63E-04	8.63E-04
Ba-130	2.94E-03	2.94E-03	2.81E-03	2.81E-03	2.90E-03	2.90E-03	2.96E-03	2.96E-03
Ba-138	5.72E-03	5.72E-03	5.31E-03	5.31E-03	5.75E-03	5.75E-03	5.84E-03	5.84E-03

Correct Factor (combine cross section, neutron flux, irradiation time, decay time, detector efficiency and branching ratio)

Isotope	FA001	FA002	FA003	FA004	FA005	FA006	FA007	FA008
Br-79	1.56E-12	1.41E-12	1.56E-12	1.41E-12	1.56E-12	1.41E-12	1.56E-12	1.41E-12
Br-81	3.35E-11	2.42E-11	3.35E-11	2.42E-11	3.35E-11	2.42E-11	3.35E-11	2.42E-11
Sr-84	8.72E-12	8.68E-12	8.72E-12	8.68E-12	8.55E-12	8.68E-12	8.72E-12	8.68E-12
Sr-86	7.43E-13	7.36E-13	7.43E-13	7.36E-13	7.43E-13	7.36E-13	7.43E-13	7.36E-13
Sb-121	1.81E-10	1.52E-10	1.81E-10	1.52E-10	1.81E-10	1.52E-10	1.81E-10	1.52E-10
Sb-123	2.29E-11	2.28E-11	2.29E-11	2.28E-11	2.24E-11	2.28E-11	2.29E-11	2.28E-11
Ba-130	1.98E-10	1.90E-10	1.98E-10	1.90E-10	1.98E-10	1.90E-10	1.98E-10	1.90E-10
Ba-138	1.46E-13	1.43E-13	1.46E-13	1.43E-13	1.46E-13	1.43E-13	1.46E-13	1.43E-13

Stable Isotope Ratios

	FA001	FA002	FA003	FA004	FA005	FA006	FA007	FA008
Br-79/81								
Sr-84/86	0.04645	0.06208	0.05625	0.03050	0.02996	0.04750	0.04504	0.06169
Sb-121/123	0.99126	1.07424	1.08408	1.05117	1.02075	0.98507	0.96974	0.90633
Ba-130/Ba13	0.00112	0.00115	0.00097	0.00107	0.00103	0.00113	0.00110	0.00105

INAA results of SRM standards and stable isotope ratios

Irradiatopn Time (Min)

Isotope	FA001	FA002	FA003	FA004	FA005	FA006	FA007	FA008
Br-79	0.83	0.83	0.83	0.83	0.83	0.83	0.83	0.83
Br-81	360	360	360	360	360	360	360	360
Sr-84	360	360	360	360	360	360	360	360
Sr-86	0.83	0.83	0.83	0.83	0.83	0.83	0.83	0.83
Sb-121	360	360	360	360	360	360	360	360
Sb-123	360	360	360	360	360	360	360	360
Ba-130	360	360	360	360	360	360	360	360
Ba-138	0.83	0.83	0.83	0.83	0.83	0.83	0.83	0.83

Cooling Time (Min)

Isotope	FA001	FA002	FA003	FA004	FA005	FA006	FA007	FA008
Br-79	2.15E+01	2.40E+01	2.15E+01	2.40E+01	2.15E+01	2.40E+01	2.15E+01	2.40E+01
Br-81	1.02E+04	1.12E+04	1.02E+04	1.12E+04	1.02E+04	1.12E+04	1.02E+04	1.12E+04
Sr-84	2.21E+04	2.28E+04	2.21E+04	2.28E+04	2.48E+04	2.28E+04	2.21E+04	2.28E+04
Sr-86	5.40E+01	5.65E+01	5.40E+01	5.65E+01	5.40E+01	5.65E+01	5.40E+01	5.65E+01
Sb-121	1.02E+04	1.12E+04	1.02E+04	1.12E+04	1.02E+04	1.12E+04	1.02E+04	1.12E+04
Sb-123	2.21E+04	2.28E+04	2.21E+04	2.28E+04	2.48E+04	2.28E+04	2.21E+04	2.28E+04
Ba-130	1.02E+04	1.12E+04	1.02E+04	1.12E+04	1.02E+04	1.12E+04	1.02E+04	1.12E+04
Ba-138	5.40E+01	5.65E+01	5.40E+01	5.65E+01	5.40E+01	5.65E+01	5.40E+01	5.65E+01

Counting Time (Min)

Isotope	FA001	FA002	FA003	FA004	FA005	FA006	FA007	FA008
Br-79	3.00E+01	3.00E+01	3.00E+01	3.00E+01	3.00E+01	3.00E+01	3.00E+01	3.00E+01
Br-81	5.40E+02	5.40E+02	5.40E+02	5.40E+02	5.40E+02	5.40E+02	5.40E+02	5.40E+02
Sr-84	6.00E+02	6.00E+02	6.00E+02	6.00E+02	6.00E+02	6.00E+02	6.00E+02	6.00E+02
Sr-86	6.00E+01	6.00E+01	6.00E+01	6.00E+01	6.00E+01	6.00E+01	6.00E+01	6.00E+01
Sb-121	5.40E+02	5.40E+02	5.40E+02	5.40E+02	5.40E+02	5.40E+02	5.40E+02	5.40E+02
Sb-123	6.00E+02	6.00E+02	6.00E+02	6.00E+02	6.00E+02	6.00E+02	6.00E+02	6.00E+02
Ba-130	5.40E+02	5.40E+02	5.40E+02	5.40E+02	5.40E+02	5.40E+02	5.40E+02	5.40E+02
Ba-138	6.00E+01	6.00E+01	6.00E+01	6.00E+01	6.00E+01	6.00E+01	6.00E+01	6.00E+01

Neutron Flux (n/cm2 s)

Isotope	FA001	FA002	FA003	FA004	FA005	FA006	FA007	FA008
Br-79	8.E+12	8.E+12	8.E+12	8.E+12	8.E+12	8.E+12	8.E+12	8.E+12
Br-81	8.E+12	8.E+12	8.E+12	8.E+12	8.E+12	8.E+12	8.E+12	8.E+12
Sr-84	8.E+12	8.E+12	8.E+12	8.E+12	8.E+12	8.E+12	8.E+12	8.E+12
Sr-86	8.E+12	8.E+12	8.E+12	8.E+12	8.E+12	8.E+12	8.E+12	8.E+12
Sb-121	8.E+12	8.E+12	8.E+12	8.E+12	8.E+12	8.E+12	8.E+12	8.E+12
Sb-123	8.E+12	8.E+12	8.E+12	8.E+12	8.E+12	8.E+12	8.E+12	8.E+12
Ba-130	8.E+12	8.E+12	8.E+12	8.E+12	8.E+12	8.E+12	8.E+12	8.E+12
Ba-138	8.E+12	8.E+12	8.E+12	8.E+12	8.E+12	8.E+12	8.E+12	8.E+12

INAA results of SRM standards and stable isotope ratios

Toatl area (number of counts) after blank and interference corrections

Isotope	OL001	OL002	OL003	OL004	OL005	OL006	OL007	OL008
Br-79						3.9E+02	2.1E+02	2.9E+02
Br-81						1.4E+04	2.2E+04	1.5E+04
Sr-84								
Sr-86		3.2E+02						
Sb-121	1.7E+04	1.8E+04	1.5E+04	1.3E+04	1.8E+04	1.5E+04	1.7E+04	1.4E+04
Sb-123	3.0E+02	3.8E+02	3.0E+02	2.6E+02	2.7E+02	2.8E+02	3.1E+02	3.2E+02
Ba-130								
Ba-138		2.9E+02			3.9E+02	3.0E+02		4.7E+02

Absolute Detector Efficiency

Isotope	OL001	OL002	OL003	OL004	OL005	OL006	OL007	OL008
Br-79	2.39E-03	2.39E-03	2.29E-03	2.29E-03	2.36E-03	2.36E-03	2.41E-03	2.41E-03
Br-81	1.94E-03	1.94E-03	1.84E-03	1.84E-03	1.91E-03	1.91E-03	1.97E-03	1.97E-03
Sr-84	2.84E-03	2.84E-03	2.72E-03	2.72E-03	2.81E-03	2.81E-03	2.86E-03	2.86E-03
Sr-86	3.62E-03	3.62E-03	3.43E-03	3.43E-03	3.59E-03	3.59E-03	3.65E-03	3.65E-03
Sb-121	2.60E-03	2.60E-03	2.50E-03	2.50E-03	2.57E-03	2.57E-03	2.62E-03	2.62E-03
Sb-123	9.02E-04	9.02E-04	8.64E-04	8.64E-04	8.04E-04	8.04E-04	8.63E-04	8.63E-04
Ba-130	2.94E-03	2.94E-03	2.81E-03	2.81E-03	2.90E-03	2.90E-03	2.96E-03	2.96E-03
Ba-138	5.72E-03	5.72E-03	5.31E-03	5.31E-03	5.75E-03	5.75E-03	5.84E-03	5.84E-03

Correct Factor (combine cross section, neutron flux, irradiation time, decay time, detector efficiency and branching ratio)

Isotope	OL001	OL002	OL003	OL004	OL005	OL006	OL007	OL008
Br-79	1.79E-12	1.89E-12	1.79E-12	1.89E-12	1.79E-12	1.89E-12	1.79E-12	1.89E-12
Br-81	1.33E-10	1.00E-10	1.33E-10	1.00E-10	1.33E-10	1.00E-10	1.33E-10	1.00E-10
Sr-84	8.55E-12	8.51E-12	8.55E-12	8.51E-12	8.25E-12	8.51E-12	8.55E-12	8.51E-12
Sr-86	7.56E-13	7.61E-13	7.56E-13	7.61E-13	7.56E-13	7.61E-13	7.56E-13	7.61E-13
Sb-121	3.83E-10	3.28E-10	3.83E-10	3.28E-10	3.83E-10	3.28E-10	3.83E-10	3.28E-10
Sb-123	2.24E-11	2.23E-11	2.24E-11	2.23E-11	2.15E-11	2.23E-11	2.24E-11	2.23E-11
Ba-130	2.35E-10	2.27E-10	2.35E-10	2.27E-10	2.35E-10	2.27E-10	2.35E-10	2.27E-10
Ba-138	1.51E-13	1.53E-13	1.51E-13	1.53E-13	1.51E-13	1.53E-13	1.51E-13	1.53E-13

Stable Isotope Ratios

	OL001	OL002	OL003	OL004	OL005	OL006	OL007	OL008
Br-79/81						1.19320	0.59302	0.81180
Sr-84/86								
Sb-121/123	1.14056	1.10668	0.98328	1.15721	1.15456	1.13068	1.06525	0.99780
Ba-130/Ba138								

INAA results of SRM standards and stable isotope ratios

Irradiatopn Time (Min)

Isotope	OL001	OL002	OL003	OL004	OL005	OL006	OL007	OL008
Br-79	0.83	0.83	0.83	0.83	0.83	0.83	0.83	0.83
Br-81	360	360	360	360	360	360	360	360
Sr-84	360	360	360	360	360	360	360	360
Sr-86	0.83	0.83	0.83	0.83	0.83	0.83	0.83	0.83
Sb-121	360	360	360	360	360	360	360	360
Sb-123	360	360	360	360	360	360	360	360
Ba-130	360	360	360	360	360	360	360	360
Ba-138	0.83	0.83	0.83	0.83	0.83	0.83	0.83	0.83

Cooling Time (Min)

Isotope	OL001	OL002	OL003	OL004	OL005	OL006	OL007	OL008
Br-79	1.80E+01	1.66E+01	1.80E+01	1.66E+01	1.80E+01	1.66E+01	1.80E+01	1.66E+01
Br-81	6.02E+03	6.89E+03	6.02E+03	6.89E+03	6.02E+03	6.89E+03	6.02E+03	6.89E+03
Sr-84	2.48E+04	2.55E+04	2.48E+04	2.55E+04	2.97E+04	2.55E+04	2.48E+04	2.55E+04
Sr-86	4.99E+01	4.83E+01	4.99E+01	4.83E+01	4.99E+01	4.83E+01	4.99E+01	4.83E+01
Sb-121	6.02E+03	6.89E+03	6.02E+03	6.89E+03	6.02E+03	6.89E+03	6.02E+03	6.89E+03
Sb-123	2.48E+04	2.55E+04	2.48E+04	2.55E+04	2.97E+04	2.55E+04	2.48E+04	2.55E+04
Ba-130	6.02E+03	6.89E+03	6.02E+03	6.89E+03	6.02E+03	6.89E+03	6.02E+03	6.89E+03
Ba-138	4.99E+01	4.83E+01	4.99E+01	4.83E+01	4.99E+01	4.83E+01	4.99E+01	4.83E+01

Counting Time (Min)

Isotope	OL001	OL002	OL003	OL004	OL005	OL006	OL007	OL008
Br-79	3.00E+01	3.00E+01	3.00E+01	3.00E+01	3.00E+01	3.00E+01	3.00E+01	3.00E+01
Br-81	5.40E+02	5.40E+02	5.40E+02	5.40E+02	5.40E+02	5.40E+02	5.40E+02	5.40E+02
Sr-84	6.00E+02	6.00E+02	6.00E+02	6.00E+02	6.00E+02	6.00E+02	6.00E+02	6.00E+02
Sr-86	6.00E+01	6.00E+01	6.00E+01	6.00E+01	6.00E+01	6.00E+01	6.00E+01	6.00E+01
Sb-121	5.40E+02	5.40E+02	5.40E+02	5.40E+02	5.40E+02	5.40E+02	5.40E+02	5.40E+02
Sb-123	6.00E+02	6.00E+02	6.00E+02	6.00E+02	6.00E+02	6.00E+02	6.00E+02	6.00E+02
Ba-130	5.40E+02	5.40E+02	5.40E+02	5.40E+02	5.40E+02	5.40E+02	5.40E+02	5.40E+02
Ba-138	6.00E+01	6.00E+01	6.00E+01	6.00E+01	6.00E+01	6.00E+01	6.00E+01	6.00E+01

Neutron Flux (n/cm2 s)

Isotope	OL001	OL002	OL003	OL004	OL005	OL006	OL007	OL008
Br-79	8.E+12	8.E+12	8.E+12	8.E+12	8.E+12	8.E+12	8.E+12	8.E+12
Br-81	8.E+12	8.E+12	8.E+12	8.E+12	8.E+12	8.E+12	8.E+12	8.E+12
Sr-84	8.E+12	8.E+12	8.E+12	8.E+12	8.E+12	8.E+12	8.E+12	8.E+12
Sr-86	8.E+12	8.E+12	8.E+12	8.E+12	8.E+12	8.E+12	8.E+12	8.E+12
Sb-121	8.E+12	8.E+12	8.E+12	8.E+12	8.E+12	8.E+12	8.E+12	8.E+12
Sb-123	8.E+12	8.E+12	8.E+12	8.E+12	8.E+12	8.E+12	8.E+12	8.E+12
Ba-130	8.E+12	8.E+12	8.E+12	8.E+12	8.E+12	8.E+12	8.E+12	8.E+12
Ba-138	8.E+12	8.E+12	8.E+12	8.E+12	8.E+12	8.E+12	8.E+12	8.E+12

INAA results of SRM standards and stable isotope ratios

Toatl area (number of counts) after blank and interference corrections

Isotope	AGV001	AGV002	AGV003	AGV004	AGV005	AGV006	AGV007	AGV008
Br-79								
Br-81								
Sr-84	6.4E+02	5.3E+02		5.1E+02	6.1E+02	8.5E+02	5.4E+02	5.6E+02
Sr-86	1.6E+03	1.5E+03	1.0E+03	2.0E+03	1.9E+03	2.1E+03	1.2E+03	1.3E+03
Sb-121	6.8E+03	7.3E+03	4.0E+03	7.3E+03	5.3E+03	7.6E+03	4.6E+03	6.6E+03
Sb-123	4.5E+02	3.9E+02	2.5E+02	3.4E+02	2.8E+02	3.8E+02	2.6E+02	3.4E+02
Ba-130	4.5E+03	3.9E+03	3.1E+03	3.8E+03	3.9E+03	4.2E+03	3.0E+03	3.4E+03
Ba-138	6.3E+03	5.0E+03	4.1E+03	5.2E+03	6.0E+03	5.6E+03	4.5E+03	5.0E+03

Absolute Detector Efficiency

Isotope	AGV001	AGV002	AGV003	AGV004	AGV005	AGV006	AGV007	AGV008
Br-79	2.39E-03	2.39E-03	2.29E-03	2.29E-03	2.36E-03	2.36E-03	2.41E-03	2.41E-03
Br-81	1.94E-03	1.94E-03	1.84E-03	1.84E-03	1.91E-03	1.91E-03	1.97E-03	1.97E-03
Sr-84	2.84E-03	2.84E-03	2.72E-03	2.72E-03	2.81E-03	2.81E-03	2.86E-03	2.86E-03
Sr-86	3.62E-03	3.62E-03	3.43E-03	3.43E-03	3.59E-03	3.59E-03	3.65E-03	3.65E-03
Sb-121	2.60E-03	2.60E-03	2.50E-03	2.50E-03	2.57E-03	2.57E-03	2.62E-03	2.62E-03
Sb-123	9.02E-04	9.02E-04	8.64E-04	8.64E-04	8.04E-04	8.04E-04	8.63E-04	8.63E-04
Ba-130	2.94E-03	2.94E-03	2.81E-03	2.81E-03	2.90E-03	2.90E-03	2.96E-03	2.96E-03
Ba-138	5.72E-03	5.72E-03	5.31E-03	5.31E-03	5.75E-03	5.75E-03	5.84E-03	5.84E-03

Correct Factor (combine cross section, neutron flux, irradiation time, decay time, detector efficiency and branching ratio)

Isotope	AGV001	AGV002	AGV003	AGV004	AGV005	AGV006	AGV007	AGV008
Br-79								
Br-81	1.66E-11	2.22E-11	1.66E-11	2.22E-11	1.66E-11	2.22E-11	1.66E-11	2.22E-11
Sr-84	8.64E-12	8.59E-12	8.64E-12	8.59E-12	8.64E-12	8.59E-12	8.64E-12	8.59E-12
Sr-86	8.15E-13	8.07E-13	8.15E-13	8.07E-13	8.15E-13	8.07E-13	8.15E-13	8.07E-13
Sb-121	1.30E-10	1.51E-10	1.30E-10	1.51E-10	1.30E-10	1.51E-10	1.30E-10	1.51E-10
Sb-123	2.26E-11	2.25E-11	2.26E-11	2.25E-11	2.26E-11	2.25E-11	2.26E-11	2.25E-11
Ba-130	1.99E-10	2.06E-10	1.99E-10	2.06E-10	1.99E-10	2.06E-10	1.99E-10	2.06E-10
Ba-138	1.75E-13	1.72E-13	1.75E-13	1.72E-13	1.75E-13	1.72E-13	1.75E-13	1.72E-13

Stable Isotope Ratios

	AGV001	AGV002	AGV003	AGV004	AGV005	AGV006	AGV007	AGV008
Br-79/81								
Sr-84/86	0.04709	0.04138		0.02989	0.03902	0.04862	0.05352	0.05243
Sb-121/123	0.91800	0.97162	0.97600	1.10248	1.01729	0.93553	1.03370	0.95898
Ba-130/Ba13	0.00124	0.00125	0.00126	0.00114	0.00116	0.00123	0.00118	0.00110

INAA results of SRM standards and stable isotope ratios

Irradiatopn Time (Min)

Isotope	AGV1001	AGV1002	AGV1003	AGV1004	AGV1005	AGV1006	AGV1007	AGV008
Br-79	0.83	0.83	0.83	0.83	0.83	0.83	0.83	0.83
Br-81	360	360	360	360	360	360	360	360
Sr-84	360	360	360	360	360	360	360	360
Sr-86	0.83	0.83	0.83	0.83	0.83	0.83	0.83	0.83
Sb-121	360	360	360	360	360	360	360	360
Sb-123	360	360	360	360	360	360	360	360
Ba-130	360	360	360	360	360	360	360	360
Ba-138	0.83	0.83	0.83	0.83	0.83	0.83	0.83	0.83

Cooling Time (Min)

Isotope	AGV1001	AGV1002	AGV1003	AGV1004	AGV1005	AGV1006	AGV1007	AGV008
Br-79	3.15E+01	3.40E+01	3.15E+01	3.40E+01	3.15E+01	3.40E+01	3.15E+01	3.40E+01
Br-81	1.27E+04	1.18E+04	1.27E+04	1.18E+04	1.27E+04	1.18E+04	1.27E+04	1.18E+04
Sr-84	2.34E+04	2.42E+04	2.34E+04	2.42E+04	2.34E+04	2.42E+04	2.34E+04	2.42E+04
Sr-86	3.15E+01	3.40E+01	3.15E+01	3.40E+01	3.15E+01	3.40E+01	3.15E+01	3.40E+01
Sb-121	1.27E+04	1.18E+04	1.27E+04	1.18E+04	1.27E+04	1.18E+04	1.27E+04	1.18E+04
Sb-123	2.34E+04	2.42E+04	2.34E+04	2.42E+04	2.34E+04	2.42E+04	2.34E+04	2.42E+04
Ba-130	1.27E+04	1.18E+04	1.27E+04	1.18E+04	1.27E+04	1.18E+04	1.27E+04	1.18E+04
Ba-138	3.15E+01	3.40E+01	3.15E+01	3.40E+01	3.15E+01	3.40E+01	3.15E+01	3.40E+01

Counting Time (Min)

Isotope	AGV1001	AGV1002	AGV1003	AGV1004	AGV1005	AGV1006	AGV1007	AGV008
Br-79	3.00E+01	3.00E+01	3.00E+01	3.00E+01	3.00E+01	3.00E+01	3.00E+01	3.00E+01
Br-81	6.00E+02	6.00E+02	6.00E+02	6.00E+02	6.00E+02	6.00E+02	6.00E+02	6.00E+02
Sr-84	6.00E+02	6.00E+02	6.00E+02	6.00E+02	6.00E+02	6.00E+02	6.00E+02	6.00E+02
Sr-86	6.00E+01	6.00E+01	6.00E+01	6.00E+01	6.00E+01	6.00E+01	6.00E+01	6.00E+01
Sb-121	6.00E+02	6.00E+02	6.00E+02	6.00E+02	6.00E+02	6.00E+02	6.00E+02	6.00E+02
Sb-123	6.00E+02	6.00E+02	6.00E+02	6.00E+02	6.00E+02	6.00E+02	6.00E+02	6.00E+02
Ba-130	6.00E+02	6.00E+02	6.00E+02	6.00E+02	6.00E+02	6.00E+02	6.00E+02	6.00E+02
Ba-138	6.00E+01	6.00E+01	6.00E+01	6.00E+01	6.00E+01	6.00E+01	6.00E+01	6.00E+01

Neutron Flux (n/cm2 s)

Isotope	AGV1001	AGV1002	AGV1003	AGV1004	AGV1005	AGV1006	AGV1007	AGV008
Br-79	8.E+12	8.E+12	8.E+12	8.E+12	8.E+12	8.E+12	8.E+12	8.E+12
Br-81	8.E+12	8.E+12	8.E+12	8.E+12	8.E+12	8.E+12	8.E+12	8.E+12
Sr-84	8.E+12	8.E+12	8.E+12	8.E+12	8.E+12	8.E+12	8.E+12	8.E+12
Sr-86	8.E+12	8.E+12	8.E+12	8.E+12	8.E+12	8.E+12	8.E+12	8.E+12
Sb-121	8.E+12	8.E+12	8.E+12	8.E+12	8.E+12	8.E+12	8.E+12	8.E+12
Sb-123	8.E+12	8.E+12	8.E+12	8.E+12	8.E+12	8.E+12	8.E+12	8.E+12
Ba-130	8.E+12	8.E+12	8.E+12	8.E+12	8.E+12	8.E+12	8.E+12	8.E+12
Ba-138	8.E+12	8.E+12	8.E+12	8.E+12	8.E+12	8.E+12	8.E+12	8.E+12

INAA results of SRM standards and stable isotope ratios

Toatl area (number of counts) after blank and interference corrections

Isotope	COAL001	COAL002	COAL003	COAL004	COAL005	COAL006	COAL007	COAL008
Br-79								
Br-81								
Sr-84								
Sr-86	6.4E+02	4.9E+02	3.8E+02	3.5E+02	7.1E+02	5.6E+02	7.5E+02	5.9E+02
Sb-121	1.5E+03	1.3E+03	5.6E+02	4.2E+02		3.5E+02	1.2E+03	6.6E+02
Sb-123								
Ba-130							1.2E+03	4.9E+02
Ba-138	5.3E+02	5.1E+02	4.6E+02	1.2E+03	1.1E+03	4.4E+02	9.6E+02	4.2E+02

Absolute Detector Efficiency

Isotope	COAL001	COAL002	COAL003	COAL004	COAL005	COAL006	COAL007	COAL008
Br-79	2.39E-03	2.39E-03	2.29E-03	2.29E-03	2.36E-03	2.36E-03	2.41E-03	2.41E-03
Br-81	1.94E-03	1.94E-03	1.84E-03	1.84E-03	1.91E-03	1.91E-03	1.97E-03	1.97E-03
Sr-84	2.84E-03	2.84E-03	2.72E-03	2.72E-03	2.81E-03	2.81E-03	2.86E-03	2.86E-03
Sr-86	3.62E-03	3.62E-03	3.43E-03	3.43E-03	3.59E-03	3.59E-03	3.65E-03	3.65E-03
Sb-121	2.60E-03	2.60E-03	2.50E-03	2.50E-03	2.57E-03	2.57E-03	2.62E-03	2.62E-03
Sb-123	9.02E-04	9.02E-04	8.64E-04	8.64E-04	8.04E-04	8.04E-04	8.63E-04	8.63E-04
Ba-130	2.94E-03	2.94E-03	2.81E-03	2.81E-03	2.90E-03	2.90E-03	2.96E-03	2.96E-03
Ba-138	5.72E-03	5.72E-03	5.31E-03	5.31E-03	5.75E-03	5.75E-03	5.84E-03	5.84E-03

Correct Factor (combine cross section, neutron flux, irradiation time, decay time, detector efficiency and branching ratio)

Isotope	COAL001	COAL002	COAL003	COAL004	COAL005	COAL006	COAL007	COAL008
Br-79	1.59E-12	1.93E-12	1.59E-12	1.93E-12	1.59E-12	1.93E-12	1.59E-12	1.93E-12
Br-81	8.32E-11	6.85E-11	8.32E-11	6.92E-11	8.32E-11	6.92E-11	8.32E-11	6.92E-11
Sr-84	8.47E-12	8.42E-12	8.47E-12	8.42E-12	8.47E-12	8.42E-12	8.47E-12	8.42E-12
Sr-86	7.47E-13	7.62E-13	7.47E-13	7.62E-13	7.47E-13	7.62E-13	7.47E-13	7.62E-13
Sb-121	2.97E-10	2.67E-10	2.97E-10	2.68E-10	2.97E-10	2.68E-10	2.97E-10	2.68E-10
Sb-123	2.21E-11	2.20E-11	2.21E-11	2.20E-11	2.21E-11	2.20E-11	2.21E-11	2.20E-11
Ba-130	2.21E-10	2.16E-10	2.21E-10	2.16E-10	2.21E-10	2.16E-10	2.21E-10	2.16E-10
Ba-138	1.47E-13	1.53E-13	1.47E-13	1.53E-13	1.47E-13	1.53E-13	1.47E-13	1.53E-13

Stable Isotope Ratios

	COAL001	COAL002	COAL003	COAL004	COAL005	COAL006	COAL007	COAL008
Br-79/81								
Sr-84/86								
Sb-121/123								
Ba-130/Ba138							0.00163	0.00164

INAA results of SRM standards and stable isotope ratios

Irradiatopn Time (Min)

Isotope	COAL001	COAL002	COAL003	COAL004	COAL005	COAL006	COAL007	COAL008
Br-79	0.83	0.83	0.83	0.83	0.83	0.83	0.83	0.83
Br-81	360	360	360	360	360	360	360	360
Sr-84	360	360	360	360	360	360	360	360
Sr-86	0.83	0.83	0.83	0.83	0.83	0.83	0.83	0.83
Sb-121	360	360	360	360	360	360	360	360
Sb-123	360	360	360	360	360	360	360	360
Ba-130	360	360	360	360	360	360	360	360
Ba-138	0.83	0.83	0.83	0.83	0.83	0.83	0.83	0.83

Cooling Time (Min)

Isotope	COAL001	COAL002	COAL003	COAL004	COAL005	COAL006	COAL007	COAL008
Br-79	2.11E+01	1.61E+01	2.11E+01	1.61E+01	2.11E+01	1.61E+01	2.11E+01	1.61E+01
Br-81	7.45E+03	8.05E+03	7.45E+03	8.02E+03	7.45E+03	8.02E+03	7.45E+03	8.02E+03
Sr-84	2.62E+04	2.69E+04	2.62E+04	2.69E+04	2.62E+04	2.69E+04	2.62E+04	2.69E+04
Sr-86	5.29E+01	4.79E+01	5.29E+01	4.79E+01	5.29E+01	4.79E+01	5.29E+01	4.79E+01
Sb-121	7.45E+03	8.05E+03	7.45E+03	8.02E+03	7.45E+03	8.02E+03	7.45E+03	8.02E+03
Sb-123	2.62E+04	2.69E+04	2.62E+04	2.69E+04	2.62E+04	2.69E+04	2.62E+04	2.69E+04
Ba-130	7.45E+03	8.05E+03	7.45E+03	8.02E+03	7.45E+03	8.02E+03	7.45E+03	8.02E+03
Ba-138	5.29E+01	4.79E+01	5.29E+01	4.79E+01	5.29E+01	4.79E+01	5.29E+01	4.79E+01

Counting Time (Min)

Isotope	COAL001	COAL002	COAL003	COAL004	COAL005	COAL006	COAL007	COAL008
Br-79	3.00E+01	3.00E+01	3.00E+01	3.00E+01	3.00E+01	3.00E+01	3.00E+01	3.00E+01
Br-81	5.40E+02	5.40E+02	5.40E+02	5.40E+02	5.40E+02	5.40E+02	5.40E+02	5.40E+02
Sr-84	6.00E+02	6.00E+02	6.00E+02	6.00E+02	6.00E+02	6.00E+02	6.00E+02	6.00E+02
Sr-86	6.00E+01	6.00E+01	6.00E+01	6.00E+01	6.00E+01	6.00E+01	6.00E+01	6.00E+01
Sb-121	5.40E+02	5.40E+02	5.40E+02	5.40E+02	5.40E+02	5.40E+02	5.40E+02	5.40E+02
Sb-123	6.00E+02	6.00E+02	6.00E+02	6.00E+02	6.00E+02	6.00E+02	6.00E+02	6.00E+02
Ba-130	5.40E+02	5.40E+02	5.40E+02	5.40E+02	5.40E+02	5.40E+02	5.40E+02	5.40E+02
Ba-138	6.00E+01	6.00E+01	6.00E+01	6.00E+01	6.00E+01	6.00E+01	6.00E+01	6.00E+01

Neutron Flux (n/cm2 s)

Isotope	COAL001	COAL002	COAL003	COAL004	COAL005	COAL006	COAL007	COAL008
Br-79	8.E+12	8.E+12	8.E+12	8.E+12	8.E+12	8.E+12	8.E+12	8.E+12
Br-81	8.E+12	8.E+12	8.E+12	8.E+12	8.E+12	8.E+12	8.E+12	8.E+12
Sr-84	8.E+12	8.E+12	8.E+12	8.E+12	8.E+12	8.E+12	8.E+12	8.E+12
Sr-86	8.E+12	8.E+12	8.E+12	8.E+12	8.E+12	8.E+12	8.E+12	8.E+12
Sb-121	8.E+12	8.E+12	8.E+12	8.E+12	8.E+12	8.E+12	8.E+12	8.E+12
Sb-123	8.E+12	8.E+12	8.E+12	8.E+12	8.E+12	8.E+12	8.E+12	8.E+12
Ba-130	8.E+12	8.E+12	8.E+12	8.E+12	8.E+12	8.E+12	8.E+12	8.E+12
Ba-138	8.E+12	8.E+12	8.E+12	8.E+12	8.E+12	8.E+12	8.E+12	8.E+12

INAA results of SRM standards and stable isotope ratios

Toatl area (number of counts) after blank and interference corrections

Isotope	BL001	BL002	BL003	BL004	BL005	BL006	BL007	BL008
Br-79	2.9E+02	1.9E+02				1.8E+02	2.1E+02	
Br-81	5.7E+03	4.9E+03				5.3E+03	6.4E+03	
Sr-84								
Sr-86								
Sb-121	6.5E+02	6.5E+02						
Sb-123								
Ba-130								
Ba-138								

Absolute Detector Efficiency

Isotope	BL001	BL002	BL003	BL004	BL005	BL006	BL007	BL008
Br-79	2.39E-03	2.39E-03	2.29E-03	2.29E-03	2.36E-03	2.36E-03	2.41E-03	2.41E-03
Br-81	1.94E-03	1.94E-03	1.84E-03	1.84E-03	1.91E-03	1.91E-03	1.97E-03	1.97E-03
Sr-84	2.84E-03	2.84E-03	2.72E-03	2.72E-03	2.81E-03	2.81E-03	2.86E-03	2.86E-03
Sr-86	3.62E-03	3.62E-03	3.43E-03	3.43E-03	3.59E-03	3.59E-03	3.65E-03	3.65E-03
Sb-121	2.60E-03	2.60E-03	2.50E-03	2.50E-03	2.57E-03	2.57E-03	2.62E-03	2.62E-03
Sb-123	9.02E-04	9.02E-04	8.64E-04	8.64E-04	8.04E-04	8.04E-04	8.63E-04	8.63E-04
Ba-130	2.94E-03	2.94E-03	2.81E-03	2.81E-03	2.90E-03	2.90E-03	2.96E-03	2.96E-03
Ba-138	5.72E-03	5.72E-03	5.31E-03	5.31E-03	5.75E-03	5.75E-03	5.84E-03	5.84E-03

Correct Factor (combine cross section, neutron flux, irradiation time, decay time, detector efficiency and branching ratio)

Isotope	BL001	BL002	BL003	BL004	BL005	BL006	BL007	BL008
Br-79	1.95E-12	1.67E-12	1.95E-12	1.67E-12	1.95E-12	1.67E-12	1.95E-12	1.67E-12
Br-81	5.32E-11	4.35E-11	5.32E-11	4.35E-11	5.32E-11	4.35E-11	5.32E-11	4.35E-11
Sr-84	8.37E-12	8.28E-12	8.37E-12	8.28E-12	8.37E-12	8.28E-12	8.37E-12	8.28E-12
Sr-86	7.64E-13	6.71E-13	7.64E-13	6.71E-13	7.64E-13	6.71E-13	7.64E-13	6.71E-13
Sb-121	2.33E-10	2.08E-10	2.33E-10	2.08E-10	2.33E-10	2.08E-10	2.33E-10	2.08E-10
Sb-123	2.19E-11	2.16E-11	2.19E-11	2.16E-11	2.19E-11	2.16E-11	2.19E-11	2.16E-11
Ba-130	2.09E-10	2.04E-10	2.09E-10	2.04E-10	2.09E-10	2.04E-10	2.09E-10	2.04E-10
Ba-138	1.54E-13	1.35E-13	1.54E-13	1.35E-13	1.54E-13	1.35E-13	1.54E-13	1.35E-13

Stable Isotope Ratios

	BL001	BL002	BL003	BL004	BL005	BL006	BL007	BL008
Br-79/81	1.13561	0.79958				0.72969	0.74415	
Sr-84/86								
Sb-121/123								
Ba-130/Ba138								

INAA results of SRM standards and stable isotope ratios

Irradiatopn Time (Min)

Isotope	BL001	BL002	BL003	BL004	BL005	BL006	BL007	BL008
Br-79	0.83	0.83	0.83	0.83	0.83	0.83	0.83	0.83
Br-81	360	360	360	360	360	360	360	360
Sr-84	360	360	360	360	360	360	360	360
Sr-86	0.83	0.83	0.83	0.83	0.83	0.83	0.83	0.83
Sb-121	360	360	360	360	360	360	360	360
Sb-123	360	360	360	360	360	360	360	360
Ba-130	360	360	360	360	360	360	360	360
Ba-138	0.83	0.83	0.83	0.83	0.83	0.83	0.83	0.83

Cooling Time (Min)

Isotope	BL001	BL002	BL003	BL004	BL005	BL006	BL007	BL008
Br-79	1.59E+01	1.97E+01	1.59E+01	1.97E+01	1.59E+01	1.97E+01	1.59E+01	1.97E+01
Br-81	8.82E+03	9.44E+03	8.82E+03	9.44E+03	8.82E+03	9.44E+03	8.82E+03	9.44E+03
Sr-84	2.77E+04	2.91E+04	2.77E+04	2.91E+04	2.77E+04	2.91E+04	2.77E+04	2.91E+04
Sr-86	4.74E+01	5.12E+01	4.74E+01	5.12E+01	4.74E+01	5.12E+01	4.74E+01	5.12E+01
Sb-121	8.82E+03	9.44E+03	8.82E+03	9.44E+03	8.82E+03	9.44E+03	8.82E+03	9.44E+03
Sb-123	2.77E+04	2.91E+04	2.77E+04	2.91E+04	2.77E+04	2.91E+04	2.77E+04	2.91E+04
Ba-130	8.82E+03	9.44E+03	8.82E+03	9.44E+03	8.82E+03	9.44E+03	8.82E+03	9.44E+03
Ba-138	4.74E+01	5.12E+01	4.74E+01	5.12E+01	4.74E+01	5.12E+01	4.74E+01	5.12E+01

Counting Time (Min)

Isotope	BL001	BL002	BL003	BL004	BL005	BL006	BL007	BL008
Br-79	3.00E+01	3.00E+01	3.00E+01	3.00E+01	3.00E+01	3.00E+01	3.00E+01	3.00E+01
Br-81	5.40E+02	5.40E+02	5.40E+02	5.40E+02	5.40E+02	5.40E+02	5.40E+02	5.40E+02
Sr-84	6.00E+02	6.00E+02	6.00E+02	6.00E+02	6.00E+02	6.00E+02	6.00E+02	6.00E+02
Sr-86	6.00E+01	5.28E+01	6.00E+01	5.28E+01	6.00E+01	5.28E+01	6.00E+01	5.28E+01
Sb-121	5.40E+02	5.40E+02	5.40E+02	5.40E+02	5.40E+02	5.40E+02	5.40E+02	5.40E+02
Sb-123	6.00E+02	6.00E+02	6.00E+02	6.00E+02	6.00E+02	6.00E+02	6.00E+02	6.00E+02
Ba-130	5.40E+02	5.40E+02	5.40E+02	5.40E+02	5.40E+02	5.40E+02	5.40E+02	5.40E+02
Ba-138	6.00E+01	5.28E+01	6.00E+01	5.28E+01	6.00E+01	5.28E+01	6.00E+01	5.28E+01

Neutron Flux (n/cm2 s)

Isotope	BL001	BL002	BL003	BL004	BL005	BL006	BL007	BL008
Br-79	8.E+12	8.E+12	8.E+12	8.E+12	8.E+12	8.E+12	8.E+12	8.E+12
Br-81	8.E+12	8.E+12	8.E+12	8.E+12	8.E+12	8.E+12	8.E+12	8.E+12
Sr-84	8.E+12	8.E+12	8.E+12	8.E+12	8.E+12	8.E+12	8.E+12	8.E+12
Sr-86	8.E+12	8.E+12	8.E+12	8.E+12	8.E+12	8.E+12	8.E+12	8.E+12
Sb-121	8.E+12	8.E+12	8.E+12	8.E+12	8.E+12	8.E+12	8.E+12	8.E+12
Sb-123	8.E+12	8.E+12	8.E+12	8.E+12	8.E+12	8.E+12	8.E+12	8.E+12
Ba-130	8.E+12	8.E+12	8.E+12	8.E+12	8.E+12	8.E+12	8.E+12	8.E+12
Ba-138	8.E+12	8.E+12	8.E+12	8.E+12	8.E+12	8.E+12	8.E+12	8.E+12

The INAA Results of Integrated Fine Particulate Samples and Stable Isotope Ratios

Toatl Area after correction

Isotope	Half-Life	Energy (Kev)	Dust1	Dust2	Pollution1	Pollution2
Br-79*	17.68m	616.2	5.6E+02	5.6E+02	9.9E+02	9.9E+02
Br-81	35.3 h	776.8	9.8E+03	7.6E+03	2.2E+04	1.7E+04
Sr-84	64.84 d	514				
Sr-86	2.81 h	388.4				
Sb-121	2.7 d	564.1	1.3E+04	1.2E+04	4.1E+04	3.1E+04
Sb-123*	60.2 d	1690.98	3.1E+03	3.1E+03	9.9E+03	9.9E+03
Ba-130*	11.8 d	496.3	1.1E+03	1.1E+03	1.7E+03	1.7E+03
Ba-138	84.63 m	165.8	9.1E+02	7.6E+02	1.2E+03	1.8E+03

* Samples were only counted once due to either long counting time or fast deacy

Absolute Detector Efficiency

Isotope	Energy (Kev)	Dust1	Dust2	Pollution1	Pollution2
Br-79	616.2	4.19E-03	4.19E-03	4.19E-03	4.19E-03
Br-81	776.8	3.33E-03	3.33E-03	3.33E-03	3.33E-03
Sr-84	514	5.08E-03	5.08E-03	5.08E-03	5.08E-03
Sr-86	388.4	6.64E-03	6.64E-03	6.64E-03	6.64E-03
Sb-121	564.1	4.61E-03	4.61E-03	4.61E-03	4.61E-03
Sb-123	1690.98	1.50E-03	1.50E-03	1.50E-03	1.50E-03
Ba-130	496.3	5.27E-03	5.27E-03	5.27E-03	5.27E-03
Ba-138	165.8	1.09E-02	1.09E-02	1.09E-02	1.09E-02

Correct Factor

	Dust1	Dust2	Pollution1	Pollution2
Br-79	5.61E-11	5.61E-11	4.49E-11	4.49E-11
Br-81	3.09E-10	2.43E-10	1.91E-10	1.50E-10
Sr-84				
Sr-86				
Sb-121	1.30E-09	1.14E-09	9.98E-10	8.73E-10
Sb-123	1.62E-09	1.62E-09	1.77E-09	1.77E-09
Ba-130	7.77E-09	7.77E-09	1.26E-08	1.26E-08
Ba-138	4.65E-12	3.58E-12	4.44E-12	7.18E-12

Stable Isotope Ratio

	Dust1	Dust2	Pollution1	Pollution2
Br-79/81	0.251	0.255	0.151	0.149
Sr-84/86				
Sb-121/123	1.66	1.84	2.39	2.10
Ba-130/Ba138	0.00157	0.00145	0.00107	0.00111

The INAA Results of Integrated Fine Particulate Samples and Stable Isotope Ratios

Irraduation Time (Min)

	Dust1	Dust2	Pollution1	Pollution2
Br-79	40	40	40	40
Br-81	1440	1440	1440	1440
Sr-84	1440	1440	1440	1440
Sr-86				
Sb-121	1440	1440	1440	1440
Sb-123	1440	1440	1440	1440
Ba-130	1440	1440	1440	1440
Ba-138	40	40	40	40

Cooling Time (Min)

	Dust1	Dust2	Pollution1	Pollution2
Br-79	11.2	11.2	16.88	16.88
Br-81	7963	8695	9425	10178
Sr-84				
Sr-86				
Sb-121	7963	8695	9425	10178
Sb-123	22841	22841	10978	10978
Ba-130	22841	22841	10978	10978
Ba-138	11.2	43.08	16.88	87.05

Counting Time (Min)

	Dust1	Dust2	Pollution1	Pollution2
Br-79	30	30	30	30
Br-81	720	720	720	720
Sr-84				
Sr-86				
Sb-121	720	720	720	720
Sb-123	11168	11168	11110	11110
Ba-130	11168	11168	11110	11110
Ba-138	30	30	30	120

Neutron Flux (n/cm2 s)

	Dust1	Dust2	Pollution1	Pollution2
Br-79	7.8E+12	7.8E+12	7.8E+12	7.8E+12
Br-81	8E+12	8E+12	8E+12	8E+12
Sr-84				
Sr-86				
Sb-121	8E+12	8E+12	8E+12	8E+12
Sb-123	8E+12	8E+12	8E+12	8E+12
Ba-130	8E+12	8E+12	8E+12	8E+12
Ba-138	7.8E+12	7.8E+12	7.8E+12	7.8E+12